Effect of Martensite-Austenite (MA) on Mechanical Properties of X80 Linepipe Steel

by

Nazmul Huda

A thesis
Presented to the University of Waterloo
In fulfillment of the
Thesis requirement for the degree of
Doctor of Philosophy
In
Mechanical and Mechatronics Engineering

Waterloo, Ontario, Canada, 2018

Examining Committee Membership

The following served on the Examining Committee for this thesis. The decision of the Examining Committee is by majority vote.

External Examiner	NAME: Douglas G Ivey Title: Professor
Supervisor(s)	NAME: Adrian P. Gerlich Title: Associate Professor
Internal Member	NAME: Norman Zhou Title: Professor
Internal Member	NAME: Mary Wells Title: Professor
Internal-external Member	NAME: Scott Walbridge Title: Associate Professor

Author's Declaration

This thesis consists of material all of which I authored or co-authored: see Statement of Contributions included in the thesis. This is a true copy of the thesis, including any required final revisions, as accepted by my examiners.

I understand that my thesis may be made electronically available to the public.

Statement of Contribution

This thesis includes eight chapters. Each chapter starting from chapter 4 up to 7 represents publications. I authored or co-authored, it should be noted that the main work in the lab including sample preparation, welding of the samples, mechanical testing, writing and characterization was done by my own. The following co-authors have contributed to the current work as outlined below:

Professor Adrian Gerlich supervised this PhD thesis.

James Gianetto at Canmet MATERIALS helped me in providing suggestions for different experimental part of the thesis, performing Charpy test and edited Chapter 7.

Robert Lazor from TransCanada edited Chapter 4 and Chapter 7.

Dr. Yuquan Ding at university of waterloo helped in nanoindentation test for Chapter 4, Chapter 5 and Chapter 6.

Dr. Abdelbaset R. H. Midawi at university of waterloo helped me in sample preparation, metallography and performing experiments for Chapter 7.

Dr. Yiyu Wang university of alberta helped me in simulation part of this thesis.

Professor Leijun Li at university of alberta provided his suggestions for simulation part of thesis and edited Chapter 5.

The balance of this work is my own.

Abstract

The aim of the present work is to dispel some of the controversy involving Martensite-Austenite (MA) in pipeline steel welds. The fraction, size, morphology and distribution of Martensite-Austenite can have considerable impact on the properties of the Heat Affected Zone (HAZ) of pipeline welds, where variations in welding parameters can lead to different peak temperatures and cooling rates, which determine the characteristic features of MA. Recently, MA microconstituents have been under scrutiny because of the significance of MA on mechanical properties is ambiguous, particularly in terms of tensile and toughness properties. The role of MA on mechanical properties has become a more active research subject due to a lack of knowledge combined with contradictory evidence.

The first part of the current research focuses on evaluating the role of MA size, fraction, morphology and distribution effect on the strength and ductility of HAZ in API X80 steel Gas Metal Arc Welds (GMAW). Higher fraction of coarse MA leads to increased strength however result in a loss of ductility. A lower fraction of finer MA microconstituents lead to improvements in ductility. The ductility is found severely impaired due to formation of closely spaced voids around the MA, along with debonding of MA from the matrix, which occurs just above the yield stress. MA constituents initiate premature void nucleation during straining, which is explained by a difference in the nanoindentation hardness of the MA (dominant in martensite but small austenite) versus the ferrite matrix.

Further study performed by thermal simulation using a Gleeble system that produces two different microstructures using two different cooling rates. Variation in cooling rate causes a difference in MA size, distribution, and morphology; while the fraction of MA remained comparable. A higher cooling rate exhibited higher tensile strength and ductility compared to a slower cooling rate. The MA microconstituents formed at slower cooling rate are coarser, which tends to initiate voids more readily under tensile strain. These coarser MA microconstituents were also surrounded by ferrite grains which exhibited higher local grain misorientations. This led to inhomogeneous deformation and enhanced dislocation activity during straining, accelerating void formation, and hampering ductility. In contrast, higher cooling rate results a more uniform local strain distribution with finer MA structures, and higher ductility. Numerical simulation confirmed

the detrimental effect of coarser MA is associated with higher local stress concentrations compared to finer MA

In third stage of this research, an optimum heat treating cycle or tempering cycle (300°C,10 min) is developed to decompose detrimental coarser MA ($\geq 1\mu m$) microconstituents in which the difference in hardness between MA and ferrite is reduced. In addition, a tempering cycle reduces the stress concentration around MA. Applying a tempering cycle to GMAW improves tensile strength and ductility by the shifting fracture location from the HAZ to base metal during transverse tensile testing.

Finally, varying cooling rates are used to investigate the influence of MA microconstituent on the mechanical properties after intercritical reheating, in which a higher fraction of coarse MA grains will severely deteriorate toughness. It is shown that MA deteriorates toughness by facilitating debonding, cracking and crack initiation during impact testing.

Acknowledgement

I wish to express my gratitude to Allah for his grace and mercy for my life. I am thankful to him for reaching this point of life.

I wish to render my respect to my Thesis Supervisor Professor Adrian P. Gerlich for giving me opportunity to pursue PhD under his supervision. I am extremely lucky to have a supervisor whose support and guidance help me a very fruitful and happy PhD life. I would also like to express my thanks to James Gianetto, in Canmet MATERIALS for his support and guidance during the journey of PhD life. I am also grateful to Dr. Ding and Mark Whitney for performing experiments for this thesis. I would like to appreciate University of waterloo technical staff Mark Griffett for helping throughout my PhD study.

Finally, my heartfelt gratitude to TransCanada pipeline and NSERC for funding the project. I would like to express my thanks to all CAMJ members who supported me in critical period of my research.

Dedication

This is dedicated to my family and friends back in Bangladesh specially my parents Md. Mostafizur Rahman and Runufa Akhter. I would like to dedicate this to my lovely family, my wife Sanzida Salekin and daughter Nusaiba Taskin.

Table of Contents

List of Figures

Chapter 1 : Introduction

1.1 Back ground

Long distance high pressure pipelines are the most effective way to transport oil and gas [1, 2], and these sources continue to be a primary natural resource for power generation. The Department of Energy for the Unitied States of America reported a consumption of 99 quadrillion BTU in 2008, of which 37 quadtrillion BTU was supplied by petrolimum and 24 quadrillion BTU was supplied by natural gas [3]. The quest for efficient and reliablae enery sources has continued for the last few decades throughout the world, and is more rigorous in the 21st century. However, most of the fossil fuel is remotely located and needs to be transported from the source to consumers. Consequently, pipelines often need to be installed in arctic regions because of oil and gas source locations [4, 5], where the temperature can average between -40 to 0°C, therefore, the demand for pipeline steels with good strength and fracture toughness at low temperature has increased. However, the integrity of a high pressure pipeline is crucial during installation since failure could lead to enviromental disaster. The microstructural features enabling the required mechanical properties for pipeline steel can be achieved by thermo-mechanically controlled processing (TMCP) followed by accelerated controlled cooling, which is cheaper and more effective than competing processes such as quenching and tempering. Pipeline manufacturers now rely on TMCP as the mostly widely used strengthening technique. The TMCP process leads to a finer grain structure along with various carbides and nitrides (or a combination of both), which improves the strength of materials. Large infrastructure requiring a combination of strength and toughness can be fabricated with High Strength Low Alloy (HSLA) steels which rely on the TMCP technology. In the past two decades, the TMCP process have been commonly used in high-pressure pipelines since the excellent low temperature properties of HSLA steel have improved resistance to fracture.

Long distance pipeline cannot be constructed without welding. However, the integrity of the pipeline can be degraded by the formation of a weld zone and Heat Affected Zone (HAZ) if the welding conditions are not carefully controlled. Since the metallurgical characteristics of newly formed zones after welding are different from the base metal. Good weldability (in terms of the ability to join material without defects, or reduced porosity with good mechanical properties) has to be ensured by the pipeline manufacturer when constructing a pipeline, and the HAZ is usually

considered to be most critical zone of the weld [6-8]. This has demanded a firm understanding of the phase transformation mechanisms within the HAZ to ensure good weldability and satisfactory mechanical properties at different temperature, especially at low temperatures [9, 10].

The HAZ can experience different thermal cycle (different peak temperature and cooling rate) which can lead to formation of a variable microstructure. Grain growth, formation of precipitates, and dissolution of carbides can occur during the heating. The chemical composition, microstructure, crystallographic texture, aging, deformation, surface notches can all affect the properties of HAZ. For example, the formation of a HAZ during welding can lead to a loss in strength due to grain growth, or excessive hardening due to rapid cooling rates which lead to poor toughness. Typical specifications for pipeline installation deal with these complexities in the HAZ by imposing limiting hardness values [11]. Therefore, it is necessary to gain a better understanding of the factors that influence the properties of the HAZ in order to avoid fracture, particularly in extreme low temperatures.

Various microstructures in the HAZ have different toughness and tensile properties which are crucial for pipeline safety. It is very important to understand the crack initiation and crack propagation in rapidly cooled HAZ microstructures after welding. A small localized brittle zone may form in the HAZ and cause the weldment to fail qualification. The study of HAZ properties frequently focused on the bulk microstructures of the HAZ. Some features like Martensite-Austenite (MA), and localized carbides can determine the properties of the bulk structure. These may form in specific regions of the HAZ depending on the thermal cycle experienced in different zones of the HAZ, and it depends on the initial microstructures before heating of the steel during welding. The MA islands are localized zones that can form in the HAZ of pipeline weld and drastically change the properties of the entire HAZ. MA is a microconstituent which is generally a combination of two finely intermixed phases (martensite and austenite), and its contribution to mechanical properties is controversial and ambiguous, which consequently warrants further scrutiny in the present research.

1.2 Problem statement

Although some studies have examined the fraction, size, morphology and distribution of MA as these relate to strength, ductility and toughness, the conclusions of many researchers are contradictory. In some research, MA has been referred to as beneficial [12], while others

pinpointed MA as detrimental to properties [8]. However, the reasons leading to these contradictory results are not often investigated. In addition, most of the studies lack comprehensive evaluation of the MA features since these microconstituents can be submicron-sized and difficult to characterize. Therefore, it is difficult to conclude what role MA has on the yield point, tensile strength, ductility and toughness, considering reports have suggested it is both beneficial and detrimental. Most studies considered it as a single phase microconstituent while it is often composed of a fine mixture of austenite plus martensite. In addition, some features of MA such as the locations of martensite-austenite inside the microconstituent, martensite to austenite ratio, and the varying properties of different MA structures have not been considered.

Moreover, the role of MA on mechanical properties, the mechanisms controlling MA formation during a rapid thermal cycle is also perplexing, particularly the effect of cooling rate and peak temperature. According to some literature, there is an increase in MA fraction with increasing cooling rate [12] while some studies also suggested that there is a decrease of MA fraction with increasing cooling rate [13]. The peak temperature of a particular thermal cycle can also have a significant impact on MA formation, since it could affect the prior austenite grain size and austenite fraction, which would also influence the resulting MA fraction, size and morphology. These issues leave a considerable field of inquiry in this area, and require a number of techniques to be applied to clarify these details.

1.3 **Objectives**

The current work is performed to address the lack of knowledge about MA and focuses on a detailed study regarding the MA size, fraction, internal structure, distribution, morphology and its effect in linepipe materials. The goal is to identify the parameters related to MA that could affect material properties, and develop a methodology to study MA in a particular material and its effect on mechanical properties. In the current thesis, the role of MA on tensile strength and impact toughness will be evaluated in the X80 as a case study, however general conclusions may be applicable to the wider range of thermo-mechanically processed HSLA steels.

1.4 Thesis outline

In this research, initially the formation of MA has been studied in real weld thermal cycles, and subsequently its effect on tensile properties has been evaluated. Later, a simulated thermal cycling was applied which will produce microstructures similar to a real weld with the same tensile and toughness properties. In addition, the efficiency of a tempering cycle to improve tensile properties has been also evaluated by decomposing detrimental MA. This thesis contains eight chapters, including the following:

Chapter 2, a literature review of MA formation in steels, including a theoretical background theory related to linepipe alloys.

Chapter 3, provides a description of characterization methodologies that includes details of different instruments and technique, which has been used throughout the different chapters of this thesis.

Chapter 4, investigates the role of MA size, fraction, distribution, and morphology on strength and ductility of X80 linepipe materials in Gas Metal Arc Welding (GMAW) welding. Two GMAW welds were produced using two different consumerable filler wire and the doubly thermal (overlapped) cycle zone properties were compared.

Chapter 5, determines the contribution of MA size, fraction, and distribution in straining behavior of localized microstructure using simulated HAZ (Intercritical Reheated Coarse Grain HAZ) produced in a Gleeble thermal simulator.

Based on knowledge achieved in Chapter 2-5, Chapter 6 showed the development of an optimum tempering thermal cycle that was used to improve tensile properties of GMAW of X80 material.

Chapter 7, evaluates the role of MA size, fraction, distribution, and morphology effect on toughness using heat treatment process.

Chapter 8, reports the main conclusions and provides an outlook for future investigation.

Chapter 2 : Theoretical Background

2.1 High strength low alloy steel for pipeline application

A larger volume of gas and oil can be transported through pipelines over long distance by increasing the operating pressure [4, 5]. However, it is necessary to make sure that the pipeline material is strong, tough and thick enough to sustain this high-pressure transportation. On the other hand, a reduction in wall thickness and diameter can reduce the cost of pipeline construction. Moreover, a decrease in thickness will result in a reduction in construction time due to the lower volume of weld metal deposition [14]. Current HSLA steels are produced to attain better mechanical properties, reduced wall thickness and make pipeline construction economical. A summary of requirements for high strength pipeline development are shown schematically in Figure 2-1

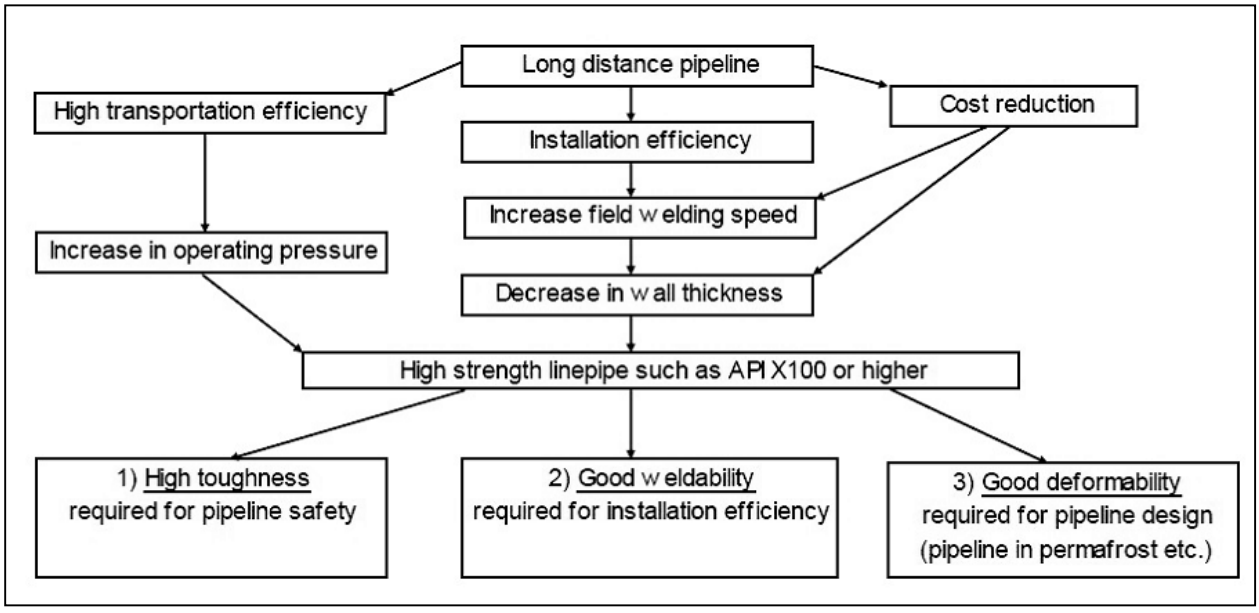

Figure 2-1 : The requirement of high strength steel pipelines [15]

Structural applications like pipeline require high strength and toughness which is achieved with HSLA steel that is produced by TMCP. The yield strength of HSLA can vary from 250 to 590 MPa while its ductile to brittle transition temperature (DBTT) can be as low as -70°C [16, 17]. Specific combinations of alloying elements lead to high strength properties in HSLA steels which

can increase the hardenability by retarding the formation of pearlite and bainite while promoting martensite transformation. Alloy composition greatly affects microstructure of the steel and the microstructure toughness can change dramatically at low temperature. Mechanical properties of HSLA steel can be modified by changing chemical composition and rolling parameters i.e. temperature, rolling passes, finish temperature.

2.2 HSLA classification and composition

Conventional stress based pipeline (design for maximum stress capacity) is used where containment of high-pressure gas is required because it meets the strength requirements. In addition to stress based design, the strain based pipeline design also considered now a days where material deformation ability is more important than the stress that would occur from ground movement associated with frost heaves or setting in areas of unstable permafrost [18]. The pipelines in arctic regions must traverse areas of continuous or discontinuous permafrost; so, a strain based designed is more relevant in such cases. In strain-based design, the strain increases smoothly near the yield stress preventing the occurrence of yield point elongation. The difference between stress and strain based design pipeline steel is shown in Figure 2-2

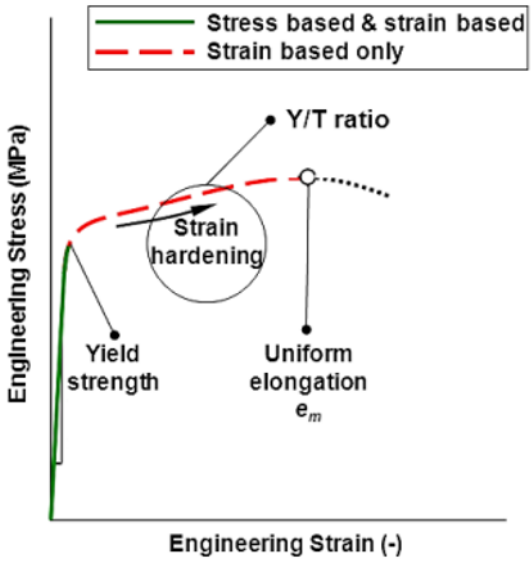

Figure 2-2 Stress based and Strain based pipeline difference [19]

The main specifications for pipeline steels are covered by the American Petroleum Institute (API) standard 5L, in which several HSLA steels such as 5L X52, X70, X80 are distinguished by the specified minimum yield strength, i.e. X52 being at least 52 ksi yield stress or 359 MPa.

Polygonal ferrite and pearlite is the microstructure of initial grades steel such as X52 or X65 [20]. A 550 MPa and an ultimate tensile strength of 620 MPa for X80 steel is reported while X100 line pipe steel shows superior strength of 680 MPa yield strength and 800 MPa tensile strength [21].

The X52 microstructure essentially consists of ferrite and pearlite with varying amounts of interspersed pearlite, while X70 grade linepipe is a ferritic pearlitic structure produced by micro-alloying and TMCP technology [22, 23]. Higher strength and toughness were achieved in X70 linepipe steel that is dominant in ferritic-pearlitic microstructure. Desirable mechanical properties were mainly achieved in X70 material through grain refinement and the promotion of non-polygonal microstructure constituents such as irregular ferrite. In contrast, X80 and higher grades linepipe steels consist of predominantly ferrite and bainitic microstructures. X80 linepipe steel can also be comprised of tempered bainite and tempered martensite. A lower carbon percentage with high manganese content and microalloying elements like niobium, titanium, vanadium, copper, nickel and molybdenum can present in X80 linepipe steel. Fine grained irregular ferrite, including randomly distributed martensite/austenite islands and complex precipitates can resulted through rolling strategy following by accelerated cooling [24]. These microstructures allow for increased operating pressures of large diameter pipelines, while the wall thickness can be decreased for economic reasons. Higher HSLA alloy steels like X100, X120 are currently under development [25, 26] while X100 steel has been used by TransCanada Pipelines Ltd. for purpose of demonstration and test. However, higher hardenability leads to susceptibility to brittle fracture which is a challenging commercial application of X100 steel [27].

The microstructure and properties of HSLA steel are greatly affected by the microalloying elements, where the total amount of alloying elements are kept below 3wt% [28]. Different alloying elements are added for different purposes. Carbon is added to increase the strength of steel; however, the addition of an excess amount of carbon can deteriorate weldability and low temperature toughness because of its tendency to form brittle martensite. Therefore, the carbon content is normally kept low usually below 0.07wt% in pipeline HSLA steels to maintain low temperature ductility, weldability and formability [29, 30]. Manganese can increase hardenability of steels(which is the ability to increase hardness with increased cooling rate) without reduction in toughness and it can also decrease the DBTT [31]. Chromium (Cr), nickel (Ni) and molybdenum (Mo) can also increase the hardenability. Additions of Cr, Ni and Mo can also increase solid solution strengthening where Cr can increase the yield strength and corrosion resistance properties

[28]. Titanium, vanadium and niobium act as grain refinement by preventing the grain growth during austenite transformation and precipitation former elements. They can act as carbide and nitride forming elements and increase strength, ductility and toughness even at low concentrations (below 0.2wt% for example) [32]. Significant grain refinement with moderate precipitation hardening can be attained using niobium. However, vanadium has a weak grain refinement contribution to strengthening. Increased strength through precipitation hardening and grain refinement can be attained using titanium [33]. Silicon is effective in deoxidizing the steel, and will increase the tensile strength but decrease the ductility and increases the impact transition temperature. Nitrogen, sulfur and phosphorus levels should be kept <0.05wt% in steels due to detrimental embrittlement and the potential for weld hot cracking [28].

2.3 **Welding in linepipe steels**

Although, the good strength and toughness of HSLA steels has been ensured through the production procedure and TMCP technology, a drop in properties can occur in the HAZ after welding. Although there is advancement in production of pipeline steel, the thickness of the linepipe for most applications exceeds the range which can be joined by single pass welding. So, multipass welding is needed to join the linepipe, which then leads to reheating of the HAZ. Significant change in HAZ properties can occur from multipass welding. The heating process during welding can transform the base metal microstructure to austenite and on cooling to room temperature this can form ferrite and bainite microstructures which can contain MA microconstituents at prior austenite grain boundaries and inside the grain, depending on the thermal cycle [34].

The welding process used by pipeline manufacturer involved fusion welding which involved arc, generate by electricity. Manual Arc Welding, Gas Metal Arc welding (GMAW), Shield Metal Arc Welding (SMAW) and Submerged Arc Welding (SMAW) are some common welding process used to pipeline steels. Although, different welding processes are currently under investigation by various researchers, GMAW and SAW are still very popular among pipeline manufacturers.

Gas metal arc welding (GMAW)

GMAW involved establishing an arc between the filler wire and base metal where filler wire is melted continuously and deposited in welded joint. Inert gas like argon or helium used during the process to shield the arc and molten pool and hence the terminology, Metal Inert gas (MIG) welding processes. However, non-inert gases like CO_2, lead to the more general term, GMAW, instead of MIG.

Submerged arc welding (SAW)

SAW is used for welding large diameter pipe which is very economical and practical techniques where a faster welding speed can be attained because of higher weld metal deposition rates. It is an automatic or semi-automatic process where electrode and flux are added in weld area. The arc is produced between the wire and the plate to be welded, and the electrode melts under the flux while it is deposited.

Weld structure

The welded structure in pipeline can be divided into weld metal, HAZ and base metal. Weld metal and HAZ (close to fusion line) can undergo different thermal cycles during welding which results different microstructure, however, the base metal away from fusion line remains unaffected. Weld pool can experience a wide range of cooling rate on cooling depending on welding parameters hence a wide range of microstructures can occur. Although the weld metal is very important to weld structure, this region beyond the scope of current research which focuses on the HAZ.

The present research is more focused on the transition section between weld metal and base metal, corresponding to the HAZ metal. The inferior mechanical properties in HAZ have led to a lot of attention to the pipeline manufacture and researcher. The inferior properties often resulted from change in metallurgical factor due to welding thermal cycle. Investigation of HAZ formation and its metallurgical properties required rigorous investigation, where one should be able to distinguish multiple sub regions in a single thermal cycle HAZ. In addition, multipass welding in

pipeline results different zones in HAZ goes undergo multiple thermal cycle. The following section will explain the different sub-region of the weld HAZ, which can result from single and multipass welding processes.

2.3.1 **Single thermal cycle HAZ in welding**

Welding causes the formation of a HAZ. A single pass weld HAZ can be divided into four regions based on peak temperature reached at the regions during the weld thermal cycle. These zones are designated as Coarse Grain Heat Affected Zone (CGHAZ), the Fine Grained HAZ (FGHAZ), the intercritical HAZ (ICHAZ) and the subcritical HAZ (SCHAZ). The resulting zones and microstructures based on different peak temperatures are related to the steel phase diagram is shown Figure 2-3. The temperature at which material starts to transform is called the austenite start temperature (Ac1- where A for austenite and c being derived from the French chauffant). The temperature at which material completely transform into austenite is called austenite finish temperature (Ac3). The zone closesd to the fusion line completely transform into austenite as the temperature in this region reach above Ac3, and is called the CGHAZ. During cooling, the microstructure can transform to different microtsturcture depending on cooling rate. The size of austenite grain size decreases with distance from the fusion line, and this zone is referred as FGHAZ. The temperatures outside the FGHAZ are sufficient to partially transform to austenite during heating since the temperature in this region lies between the Ac1 and Ac3 temperature, and this location is referred as the ICHAZ. Further away from the weld, the temperature in SCHAZ does not exceed Ac1 and the microstructure in this zone is in close proximity with base metal.

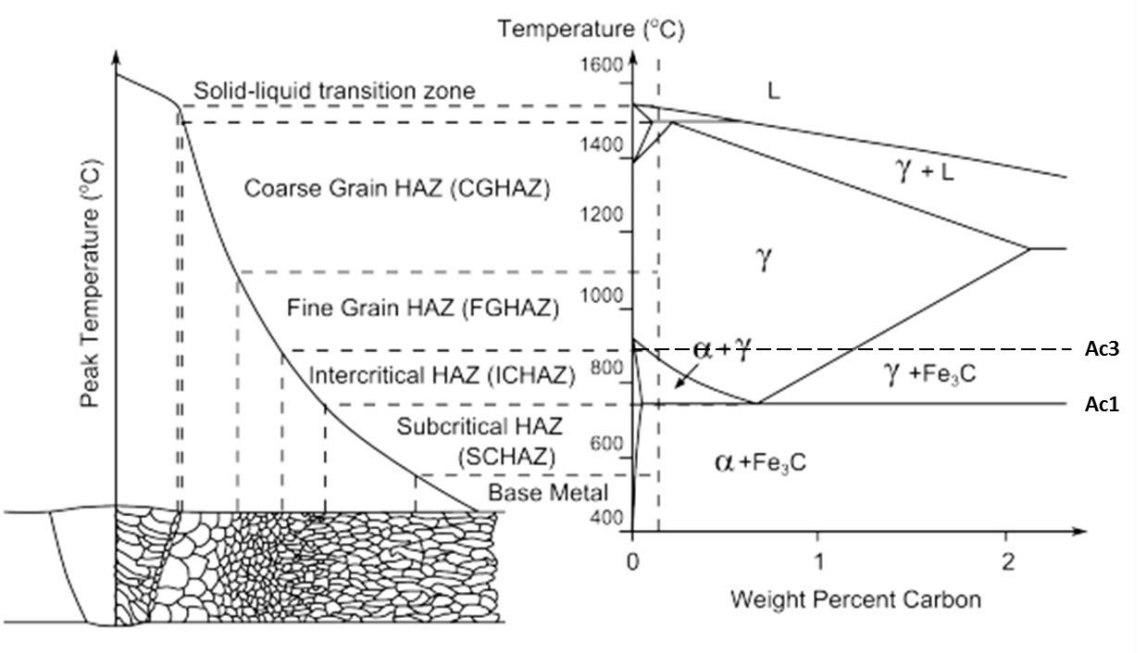

Figure 2-3 : Peak temperature, HAZ position and Fe-C phase diagram for a single torch weld [35]

2.3.2 **Multipass welding**

A series of repeated thermal cycles within the weld during multipass welding results various microstructural areas in the HAZ which make characterization of each region more complex. Toyoda investigated low alloy carbon manganese steel and identified six different zones in the HAZ of a multipass weld (Figure 2-4) [36]. Therefore, a range of microstructures instead of one microstructure will be resulted due to the different heat treatment experience in multipass welding of weld. The temperature in CGHAZ can reach well above Ac3 while the temperature in FGHAZ reaches just above Ac3. However, the temperature in the intercritically reheated zone reaches between Ac1 and Ac3, while the peak temperature in sub critically reheated zone never exceeds Ac1. Locally different cooling histories based on the TTT (time-temperature-transition) results in locally different microstructures that strongly depend on specific position within the weldment.

The HAZ in structural steels has a typical width of 2-5 mm adjacent to the fusion line, and can contain a wide variety of microstructures ranging from martensite and upper bainite near fusion line to ferrite or pearlite near the unaffected part of base metal. The structural integrity of the

weldment can be affected by the properties here since these various microstructures can produce important strength mismatch effects. The application of a wide variety of welding procedures from classical fusion welding to solid state joining (operated at temperature below melting point) makes it difficult to generalize properties about the HAZ. Deformation and fracture behavior vary for different areas of weldment. The capacity for plastic deformation across the joint is described by the by stress-strain curve, which depends on the average microstructure over large area of the weld whereas the tensile strength and fracture toughness for different microstructure is highly localized parameter which primarily depends on the microstructure in the relevant fracture location.

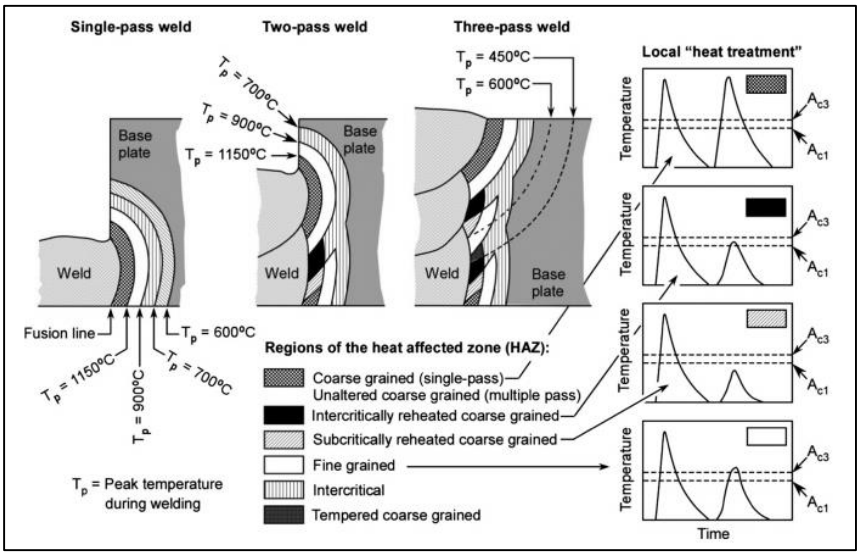

Figure 2-4 : HAZ microstructural zones produced in single-pass and multipass welding [37]

HSLA steel strength and high fracture toughness can deteriorate significantly after a welding thermal cycle, such that it is often the weakest or most brittle part of weld. The CGHAZ in single thermal cycle weld and intercritically reheated coarse grain HAZ (ICRCGHAZ) in multipass welding are often exhibiting the lowest toughness. The fracture toughness degradation is associated to the formation of "local brittle zones" in HAZ which are harder compared to the matrix. Significant embrittlement can be observed in the CGHAZ in particular and in the ICRCGHAZ of multipass weld [10, 38, 39]. However, the lowest toughness may also occur in the intercritical HAZ (ICHAZ) or subcritical HAZ (SCHAZ) [4, 7, 8]. A variety of microstructure can evolve in the HAZ depending on temperature, cooling time. Different metallurgical factors such as microstructure of HAZ, prior austenite grain size, bainite packet size, and the distribution of

second phase (carbide, or MA) can influence the fracture toughness of HAZ. The following section will give a brief description of different microstructures that evolve in HAZ of pipeline welding.

2.3.3 **Microstructure evolution in low carbon steel HAZ**

The time-temperature transformation diagram in Figure 2-5 for steel is showing various microstructure that can form in steel depending on cooling rate. In the following section, different types of microstructure formed in steel will be discussed in detail.

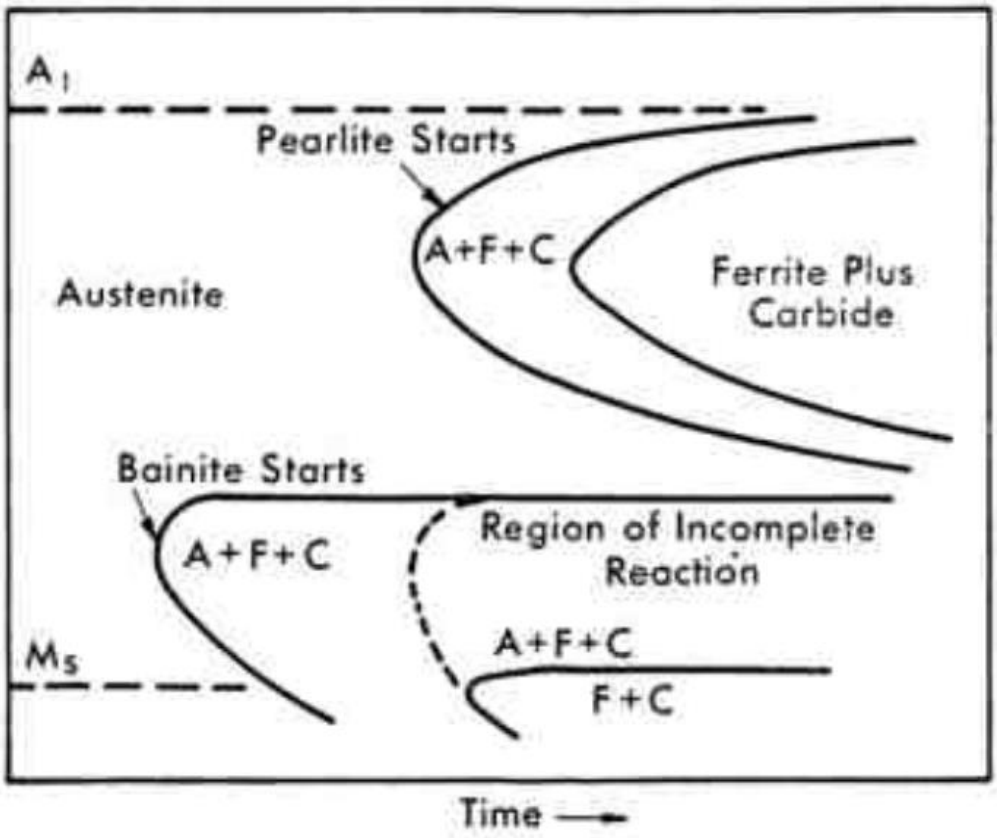

Figure 2-5 Isothermal transformation diagram for steel where A, F, C represent austenite, ferrite and carbide and Ms is martensite transformation start temperature [40]

Polygonal ferrite/pearlite

Polygonal ferrite will form when austenite is cooled at sufficiently slow cooling rates. Nucleation of ferrite will occur at grain boundaries at the Ar3 temperature and grain boundary allotriomorphs will result as ferrite, will continue to grow along austenite grain boundaries, followed by growth into equiaxed grains [41]. The maximum solubility of carbon in ferrite is 0.02wt%, so growing ferrite from austenite rejects carbon to the surrounding austenite. Austenite becomes enriched in carbon and a different concentration in ferrite and austenite will result. Long range diffusion of carbon primarily controls ferrite growth. In low carbon steel the mechanism shift from diffusion controlled to a mixed mode mechanism; in addition to long range carbon diffusion, interface related reactions such as solute drag control the interface propagation occur [41-43].

Pearlite (lamellar structure of ferrite and carbide) microstructures occur when the remaining high carbon austenite transforms at very slow cooling rates. Pearlite consists of alternating colonies of alternation lamella of ferrite and cementite. The rate controlling parameter for pearlite formation is carbon diffusion which requires sufficiently high temperature. Austenite-ferrite interface is the preferred nucleation location for pearlite, which is subsequently followed by lamellar pearlite colony growth into austenite. The driving pressure for the reaction will increase as the transformation temperature is lowered, however diffusivity will decrease such that the pearlite interlamellar spacing is reduced.

Irregular/Quasi polygonal ferrite

Nucleation of irregular ferrite mainly occurs heterogeneously at grain boundaries and the transformation can occur by short range diffusion across the transformation interface. Interstitial or substitutional atoms partitioning can result in an irregular grain boundary and due to competitively migrating interfaces [41, 43, 44]. Entrapped highly dislocated substructures and retained austenite or martensite/austenite constituents can be observed in irregular ferrite by microscopy [45].

Upper and lower bainite

Carbide precipitation in upper and lower bainite is indication of diffusional transformation in bainite. However, the bainite crystallographic orientation relationship with the parent austenite is similar to Kurdjumov-Sachs orientation relationship, suggests it is a diffusion-less transformation product [46]. So the exact transformation mechanism remains a debated issue. Some details of this transformation mode remain controversial i.e., changes in chemical composition during onset of bainite reaction, ferrite component growth mechanism and carbide precipitation source. Researchers continue to be divided regarding the transformation mechanism for bainite, with some believing that bainite is diffusional or reconstructive transformation product, while other arguing bainite forms by a displacive transformation.

Bain and Davenport introduced the term bainite, which was discovered through improved interrupted isothermal transformation tests, and these were the first time temperature transformation diagrams to indicate bainite in 1930 [47]. Zener et al. reported bainite as acicular mixture of ferrite and cementite. Bainite form as super saturated solution by migration of glissile interface [48]. They suggested that supersaturate ferrite will reject carbon to the remaining austenite before the next unit of bainite forms, which can cause carbon enrichment in austenite. Ko and Corrtrell et al. observed surface relief in lower bainite which was attributed to dislocation glide and coordinated atoms movement across the interface, however, a lower transformation rate than martensite suggests that migration at the interface is diffusion controlled [49].

The bainite growth rate is controlled by carbon diffusion, and is reported in several studies [50] while the opinion of displacive theory has also been given [51]. In debate, diffusional grow theory was proposed by Asronson et al. [51]. However, Bhadeshia and Edmonds claimed that bainite grows by displace transformation mechanism based on microstructural observation and thermodynamic analysis. Bainite growth was accompanied by shape deformation. They concluded bainite transformation as diffusion-less, however shortly after arrest of growth carbon partition into residual austenite. Formation of carbide by precipitation is thereby considered as secondary event [52].

Both upper and lower bainite consist of aggregates of plates or sheaves of ferrite; the ferrite could be separated by untransformed austenite, cementite or martensite. Upper bainite form as at higher temperatures consist of parallel ferrite laths series separated by continuous of semi

continuous layer of MA, retained austenite or carbide. Lower bainite formed at a lower temperature and due to limited diffusivity, contains an intra-ferrite distribution of MA, carbide particles and ferrite take the form of laths or plates.

Martensite

Martensitic transformation occurs below the martensite start temperature during rapid cooling and it requires a very high driving force. Transformation to a body centered tetragonal martensite crystal from a face cubic centered austenite crystal occurs by shear. This requires atoms to move less than one interatomic distance. A 3% volume increase can result due to a coordinated movement of atoms. Shape change can induce high elastic tension which can be reduced by slip or twinning, and results in an increase in the hardness of martensite [53].

Martensite morphology is strongly depend on alloy composition mainly on carbon content. Influence of carbon content on the morphology of martensite during cooling is investigated by Stromvinter et al. [54]. They reported a carbon content less than 0.6wt% in lath martensite and more than 1.0wt% carbon in plate martensite.

Martensite/Austenite (M/A)

Apart from the typical microstructures which can occur in the HAZ (martensite, bainite, ferrite), other microconstituents can also play a significant role in mechanical properties of HSLA steel. In particular, the presence of one, the so-called martensite-austenite (MA) grains can have a critical role on the impact fracture toughness, strength and ductility. MA is a small constituent that is a combination of martensite and austenite in what appears to be one grain, which can and forms in the HAZ or weld metal. The martensite transformation is essential for formation of MA constituents, relying on austenite transformed by rapid cooling to room temperature, Martensite forms in hardenable steels (i.e. quenched steel and tempered to improve their strength), and is a supersaturated form of ferrite with a body centered tetragonal crystal structure with very high hardness. Martensite formation occurs at temperatures typically below 500°C, and is diffusion-less rapid process. The martensite start temperature is designated as Ms and referred to the temperature where the diffusion-less transformation starts. The transformation continues in a

displacive mode, until it reaches the martensite finish temperature (M_f). A small amount of austenite can be retained in the MA, with the austenite enriched in carbon thereby stabilized. Hence, some of the parent austenite may be retained to room temperature, and does not transform or only partially transforms below the martensite start temperature remains in the martensite/austenite constituent [55, 56]. Pipeline steels may reach thickness over 25 mm, which may result in rapid cooling due to significant heat sink effects due to surrounding material and the environment. In such cases, formation of MA in the HAZ might be inevitable depending on thermal cycles, and may vary from material to material depending on grain size, cooling rate, carbon equivalent (meaning the combined effects of different alloying elements to calculate an equivalent amount of carbon in steel) and hardenability [57].

2.4 Formation of Martensite-Austenite (MA)

The HSLA steel base metals used in pipelines will endure complex changes and transformations during welding. The peak temperature in ICHAZ of HSLA steels can be in the intercritical temperature range (between Ac1 and Ac3 or approximately 750 to 850ºC), and on cooling to room temperature, the MA constituents can form in this zone (Figure 2-6a). In addition, the CGHAZ is reheated into the mixed austenite and ferrite region (between the so-called Ac1 and Ac3 temperatures) when multipass welding is performed (Figure 2-6b&c). Austenite grows preferentially in prior austenite grain boundaries of the CGHAZ in second thermal cycle during heating. With rapid heating rates and shorter holding times between Ac1 and Ac3, only carbon is partitioned between ferrite and austenite. In the process, austenite islands are enriched in carbon. During cooling stage austenite transform to martensite with some austenite remaining which is called MA (Figure 2-6d) [7, 39, 56, 58]. It has been reported that the toughness of the ICHAZ and ICRCGHAZ is mainly controlled by the size and volume fraction of MA constituents [59]. However, the MA fraction, distribution, morphology of MA is also important to toughness [58]. MA can form as a grain boundary network, inside the grain and triple junctions of grain boundaries. Depending on their morphology and location, MA grains can change the properties of the material at low temperature.

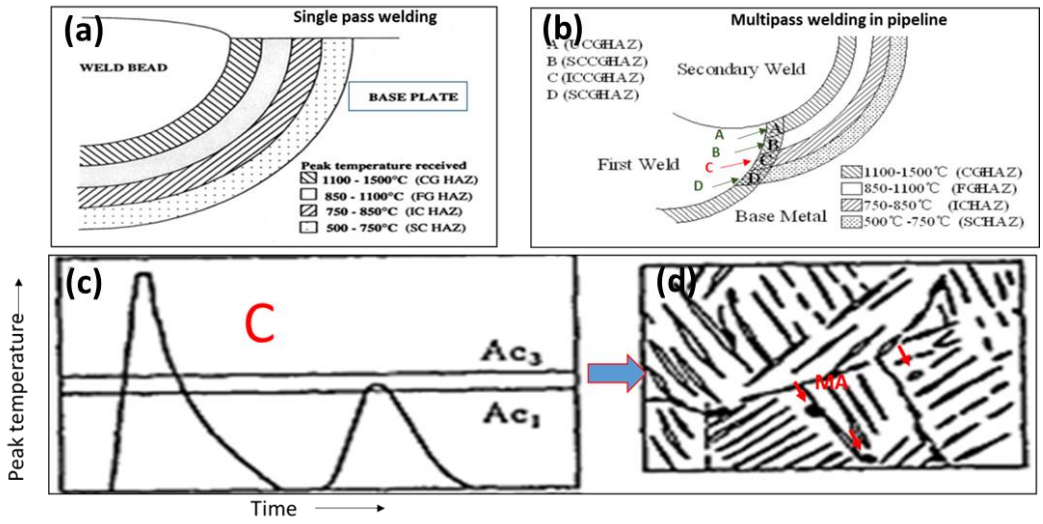

Figure 2-6 : Schematic of HAZ (a) single thermal cycle (b) multipass welding (c) temperature profile in ICRHAZ (d) MA appearance [56]

Several different mechanism of MA formation has been proposed. According to Davis and King [8], the CGHAZ of HSLA steel comprised of upper bainite and is reheated to intercritical temperature in second thermal cycle. During the second thermal cycle heating, austenite nucleates and grows along the prior austenite grain boundaries. In addition, austenite also grows along bainite lath boundaries. On cooling the austenite transforms into MA and located in grain boundary. Davis and King [8] explained the MA formation from reheating of upper bainite structure. Austenite nucleates from prior austenite grain boundaries and bainite lath boundaries. Austenite becomes rich carbon and there will be insufficient time for carbon diffusion. On cooling, this carbon rich austenite will transform into MA.

However, Matsuda et al. [60] in his review paper have explained the MA formation mechanism proposed by Nakao et al. [61] which is slightly different from that proposed by Davis and King [8]. Nakao et al. [62] proposed two MA formation mechanisms based on peak temperature in second thermal cycle. In the first mechanism, reheat temperature is above Ac3 while reheat temperature is between Ac1 and Ac3 in the second mechanism. According to Nakao et al. [62] the austenite grows in high carbon region (prior austenite grain boundary-such as B and C) when temperature reaches above Ac3, as indicated in Figure 2-7. At high temperature, a high carbon region can exist since temperature is not high enough to diffuse carbon uniformly. The subsequent

cooling led formation of ferrite and bainitic ferrite in low carbon region (E and F) while MA constituents form in high carbon austenite region (G).

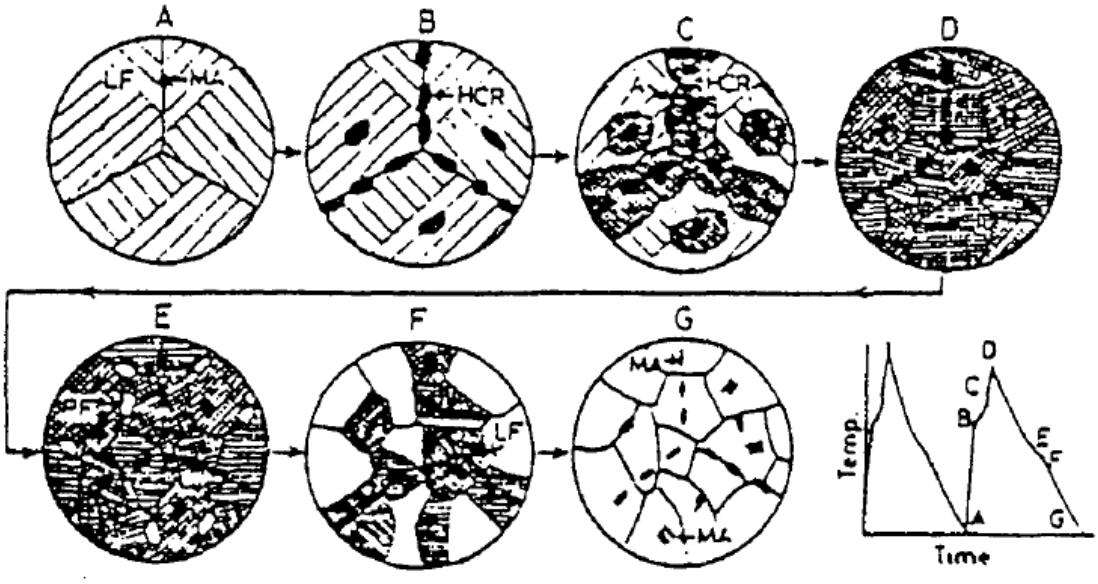

Figure 2-7 Formation mechanism of MA in low hardenability region [62]

The second mechanism suggested that, there could be precipitation of carbides on the coarse prior austenite grain boundaries after first thermal cycle. The second thermal cycle results a temperature peak between Ac1 and Ac3 in the microstructure, and Figure 2-8 indicates that austenite grows along the grain boundaries (B) and the carbides dissolve into austenite regions (C). On cooling, the austenite fraction decreases and remaining austenite become enriched in carbon (D). Finally, part of the austenite will transform into MA [63].

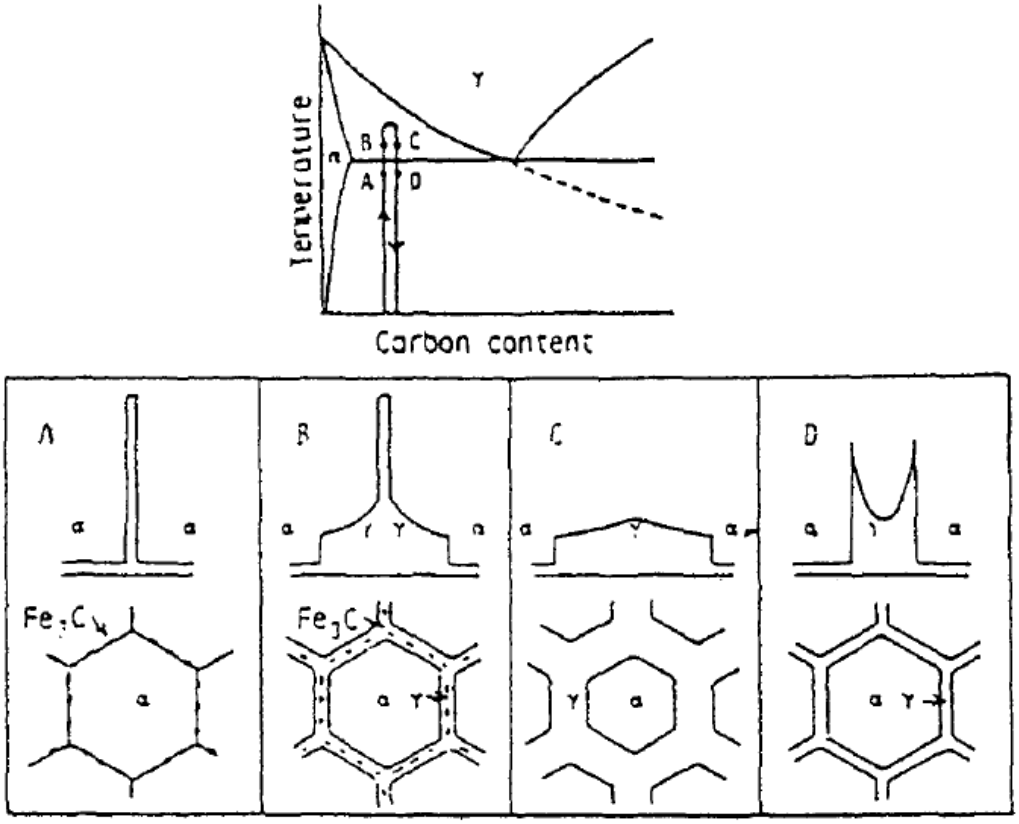

Figure 2-8 Schematic illustration of the formation of MA from ferrite-austenite region [63]

The key difference is that the steel used by Davis and King [8] is produced by thermo-mechanical process and the base metal microstructure is ferrite and tempered bainite. The steel investigated by Nakao et al. [62] did not utilize the TMCP processed steel and the first thermal cycle steel microstructure was ferrite instead of bainite.

2.5 **MA morphology**

The morphology of MA constituents during welding is dependent on the cooling time [58, 64]. Two distinct morphologies of MA have been reported in several studies [8, 58, 65, 66].

1. Blocky particles are usually 3 to 5 μm in diameter [8]. These form at prior austenite grain boundaries, often referred to as MA islands [58], which are formed at longer cooling times.

2. Elongated stringer or lath-type MA constituents form between bainite or martensite laths. Stringer MA are 0.2 to 1 μm wide and several microns in length [8] and the aspect ratio is 3:1 or more. The shape of MA is strongly affected by the crystallography of the surrounding bainite.

Elongated MA grows along the growth direction or habit plane of surrounding bainitic ferrite which has been shown by three dimensional analyses. In contrast, bainitic ferrite which surround MA with different habit planes or elongation directions produce blocky MA [67]. They are formed at short cooling times; however, the thickness of stringer MA will increase with increasing cooling times.

In addition to blocky and elongated MA, Li and Baker et al. [58] reported MA-C particles consisting of MA mixed with other phases i.e. carbide and ferrite. Moreover, Qiu et al. [68] and Luo et al. [69] reported another type of MA which is designated as "Dot" type MA.

Terasaksi and Komizo et al. [70] considered the shape and composition of MA relative to the amount of low angle grain boundaries within a given Bain group. MA constituent were found to be elongated with more retained austenite and less residual martensite in structures with a low density of low angle grain boundaries (LAGB). High densities of LAGB in the Bain group will result in blocky MA and contain a higher fraction of martensite. It is suggested that the MA formation process is governed by the morphology of bainitic ferrite which influences the stability of austenite. Blocky MA islands will form with sizes between 0.5 and 5 μm while elongated MA were reported with a length of 10 μm and a width between 0.2 to 2 μm.

2.6 **Appearance and internal structure of MA**

The MA formation location, and its surrounding structure can have significant effect on its structure. Since MA is very small, it is hard to distinguish MA from carbide by optical microscopy, particularly "dot type". SEM investigation is required to confirm the presence of MA microconstiuents. However, LePera etchant has been produced to distinguish MA via optical microscopy. It has been reported that the MA constituents appear white in color under microscope when LePera etchant is performed [71]. However, it is not possible to distinguish martensite or austenite individually as both of them appear white in colour using an optical microscope when using LePera etchant [72]. An example of MA with a white appearance is shown in Figure 2-9a. However, several other methods have been used to study internal structure of MA. These include EBSD (Electron backscatter diffraction) to map internal structural of MA, and Li et al. [73] has shown that the high band contrast of MA provides good contrast versus the ferrite matrix using EBSD (Figure 2-9b). Reichert et al. [74] successfully index the internal structure of MA using

EBSD (Figure 2-9c), and it has been found that the MA constituents in prior austenite grain boundaries are predominantly martensitic, while MA inside the prior austenite grains are mainly retained austenite.

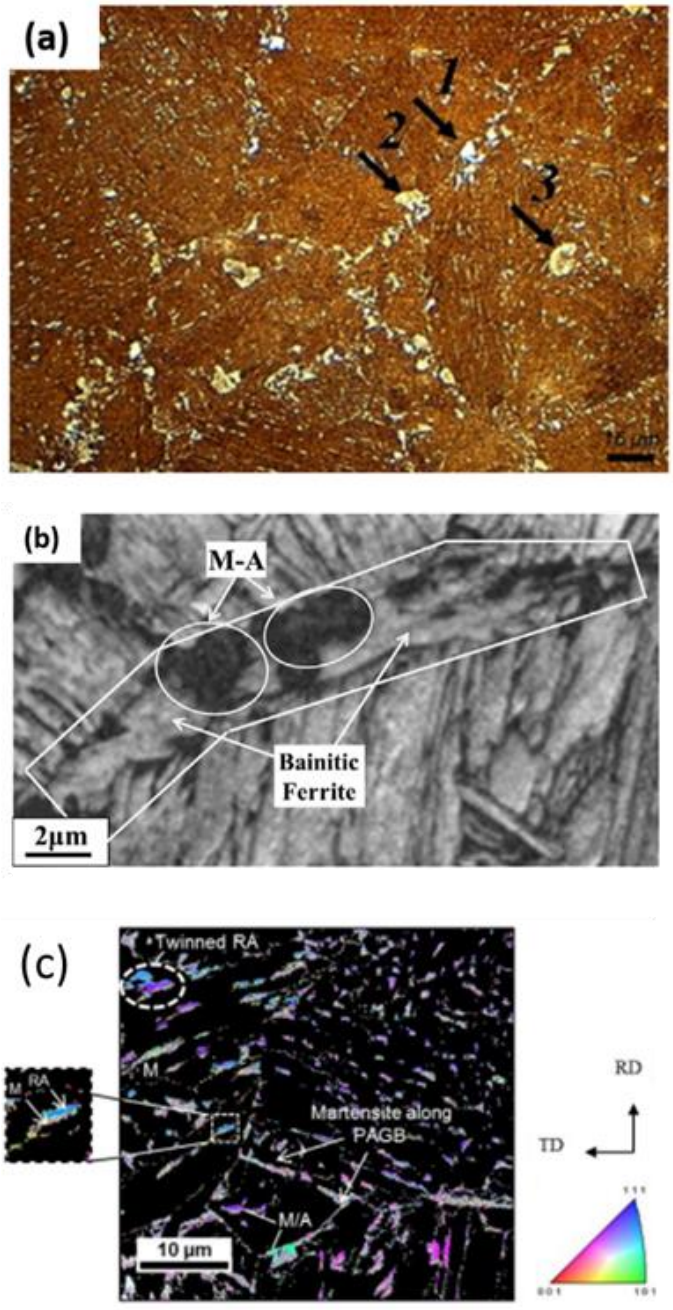

Figure 2-9 : (a) Appearance of MA in LePera etchant [71] (b) EBSD Euler slope map of MA [73] (c) indexing MA using EBSD [74]

Although MA constituents are defined as a combination of martensite and austenite, the relative position of martensite and austenite inside MA can vary. Lambert et al. [75] showed that austenite can be found in the periphery and the martensite in middle of the MA by observation of SEM using Villela etchant reagent (ethyl alcohol 95 ml, hydrochloric acid 5 ml and picric acid 1 g) (Figure 2-10a). The internal structure of MA constituent was investigated further by Shanmugam et al. [76] in a Nb-microalloyed steel and found alternating layers of ferrite, martensite and retained austenite inside MA constituents (Figure 2-10b). In contrast, Wang et al. [77] showed that MA is actually a combination of islands of martensite and austenite when examined by TEM (Figure 2-10b&d).

Hrivnak et al. [78] reported that in addition to martensite and austenite, carbide could exist inside MA. The carbide could precipitate from austenite or self-tempering of martensite and classified into two types; coarser globular cementite particles precipitates from austenite and usually located inside austenite or boundary of austenite. In contrast, one can find needle-like or dendritic cementite precipitates inside martensite following self-tempering. It was also reported that there could be two types of martensite inside MA (dislocation-rich lath martensite when carbon contents are low, and plate martensite with higher carbon contents above 1wt%). The lath martensite contains a high dislocations density and very fine needle like cementite particles, which could precipitate during self-tempering. In the plate martensite, the laths are internally twinned and there are no cementite particles. Like Wang et al. [77], Hrivnak et al. [78] also reported that the austenite form as islands inside MA. Li and Baker et al. [58] observed carbides in MA, though a carbide structure is different from the observation of Hrivnak et al. [78].

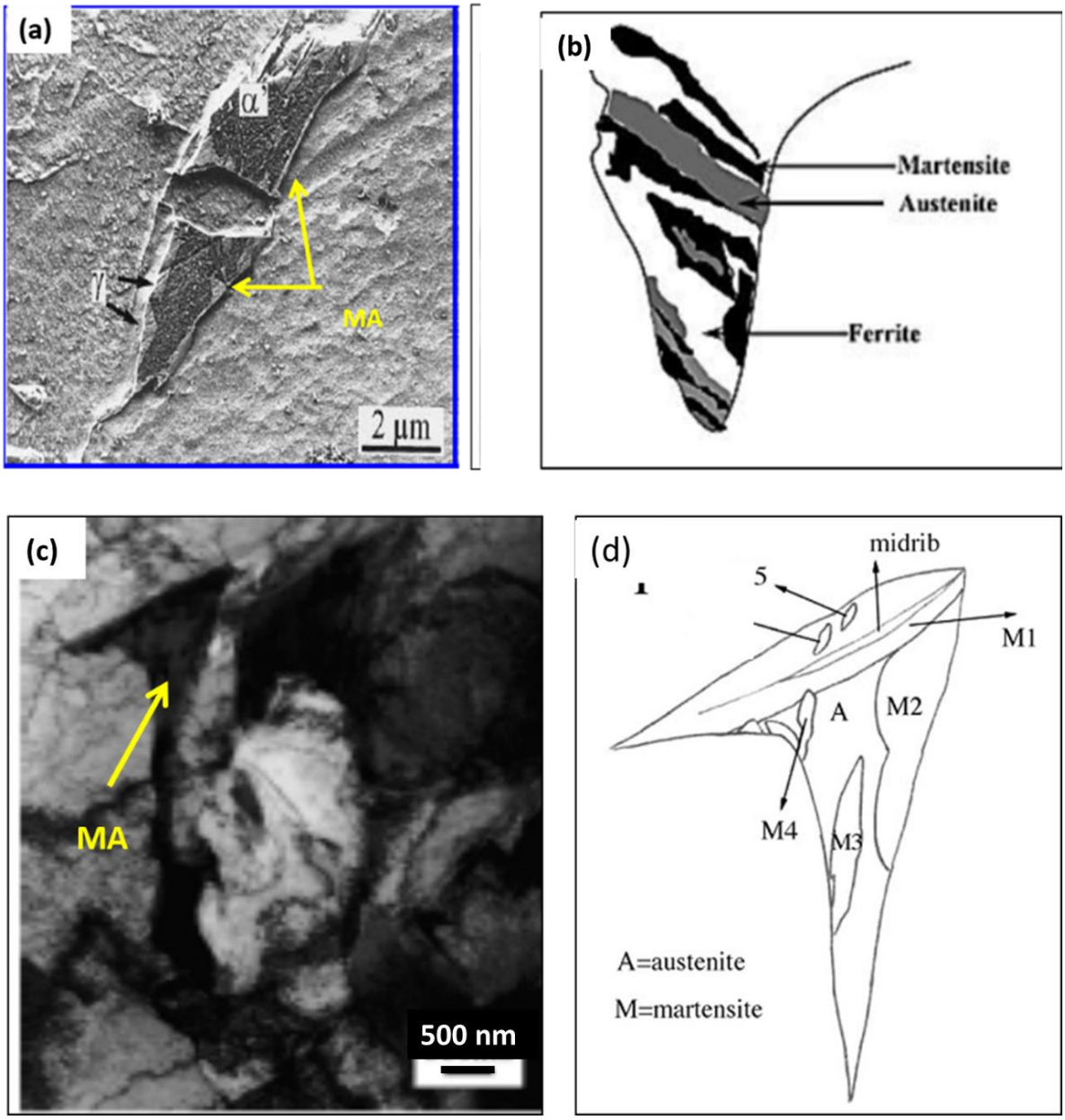

Figure 2-10 : Micrographs obtained by (a) SEM and (b) alternate layer of martensite and austenite inside MA [76] (c,d) TEM, showing the substructure contained within an MA region [77]

Luo et al. [69] observe dot type MA, martensite dominant slender type of MA and massive MA with shell of martensite and core austenite while using TEM analysis when a heat input of 15 KJ/cm, 30 KJ/cm and 50 KJ/cm respectively was applied in second thermal cycle (Figure 2-11). MA constituents with "round dot shape" are not harmful to toughness test [69]. MA constituents

with a slender shape (Figure 2-11b) contain almost entirely martensite, leading to lowest toughness. While the massive ones (Figure 2-11c) have a core-shell structure with martensite forming the "shell" and austenite forming the "core", which provides better toughness compared with structures with slender MA [69].

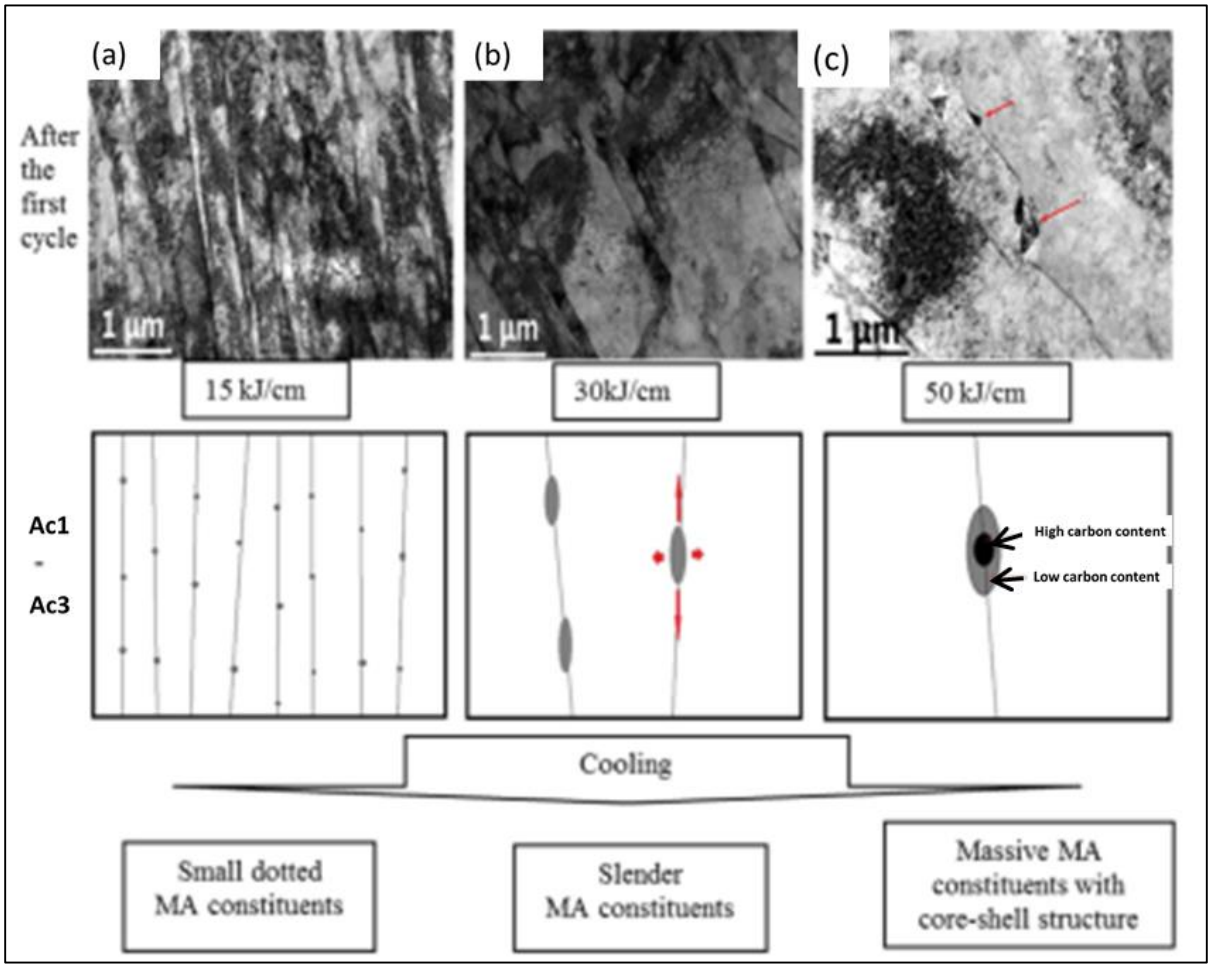

Figure 2-11 : Illustration of formation of MA constituents with different morphologies (a) "Dot" type MA (b) slender MA (c) blocky MA with core shell austenite [69]

2.7 **Properties of MA**

MA properties can vary based on their morphology, carbon content and relative martensite-austenite percentage. The MA usually contains a higher percentage of carbon because carbon does not get the chance to diffuse. Lambert et al. [38] found that the MA contain 0.6 to 1.1wt% carbon.

However, the difference in carbon concentration between austenite and martensite inside MA has not been investigated in any works. The strength and hardness of MA is correlated to carbon content in nearly linear manner [79]. The hardness of blocky MA is reported to be 800 to 1200 HV while for elongated MA it is 600 to 800 HV [78, 80], and the hardness of MA maybe predicted as follows [78]:

$$HV_{M\text{-}A} = 575C + 15 \quad \text{Equation 2-1}$$

where, C is the carbon content in wt%.

2.8 Factors affecting MA constituents formation

2.8.1 Chemical composition of steel effect on MA formation

Numerous alloying elements could facilitate the formation of MA, as reported by several researchers. Carbon, boron and nitrogen has been reported to be strong MA formation elements while niobium, vanadium, molybdenum and chromium carbide forming elements also can assist MA formation in some extent [63, 81, 82]. Manganese, nickel and phosphorus segregation during solidification and carbon, nitrogen, boron segregation during transformation can facilitate the formation of MA [63]. The following sections will summarize the observed role of various elements on MA.

Carbon

An increase in MA fraction with the increase of carbon content of steel is commonly reported. However, the carbon content in steel has little effect in the carbon content of MA. Harrison and Webster et al. [83] proposed an alloying factor to predict the MA fraction in steel. An equation is proposed (as follows) for steel, which contains carbon between 0.06 to 0.11wt%. MA fraction in steel will be lower than 6% if the alloying factor (AlF) value is less than 0.32wt%,

$$\boldsymbol{AlF = \frac{Si+Mn}{6} + \frac{Cr+Mo+V}{5} + \frac{Ni+Cu}{15}, 0.06 < C < 0.11wt\%} \quad \text{Equation 2-2}$$

Relatively high carbon content for MA in comparison matrix is reported in several studies. It is reported that the carbon enrichment in MA could reach 6at% which is equal to 1.4wt% for a

typical steel [84]. Li et al. [85] reported contents of 0.49wt% carbon and 2.32wt% Mn inside MA. Contents of 7at% carbon and 5at% manganese were measured due to the effect of segregation at the MA/matrix interface (Figure 2-12). The segregation of C, Mn, Mo, Ni and Cr in MA/Quasi Polygonal Ferrite (QPF) at the interface has been also reported by Lee et al. [86] which further supports that segregation of carbon at the MA/matrix interface can regularly occur.

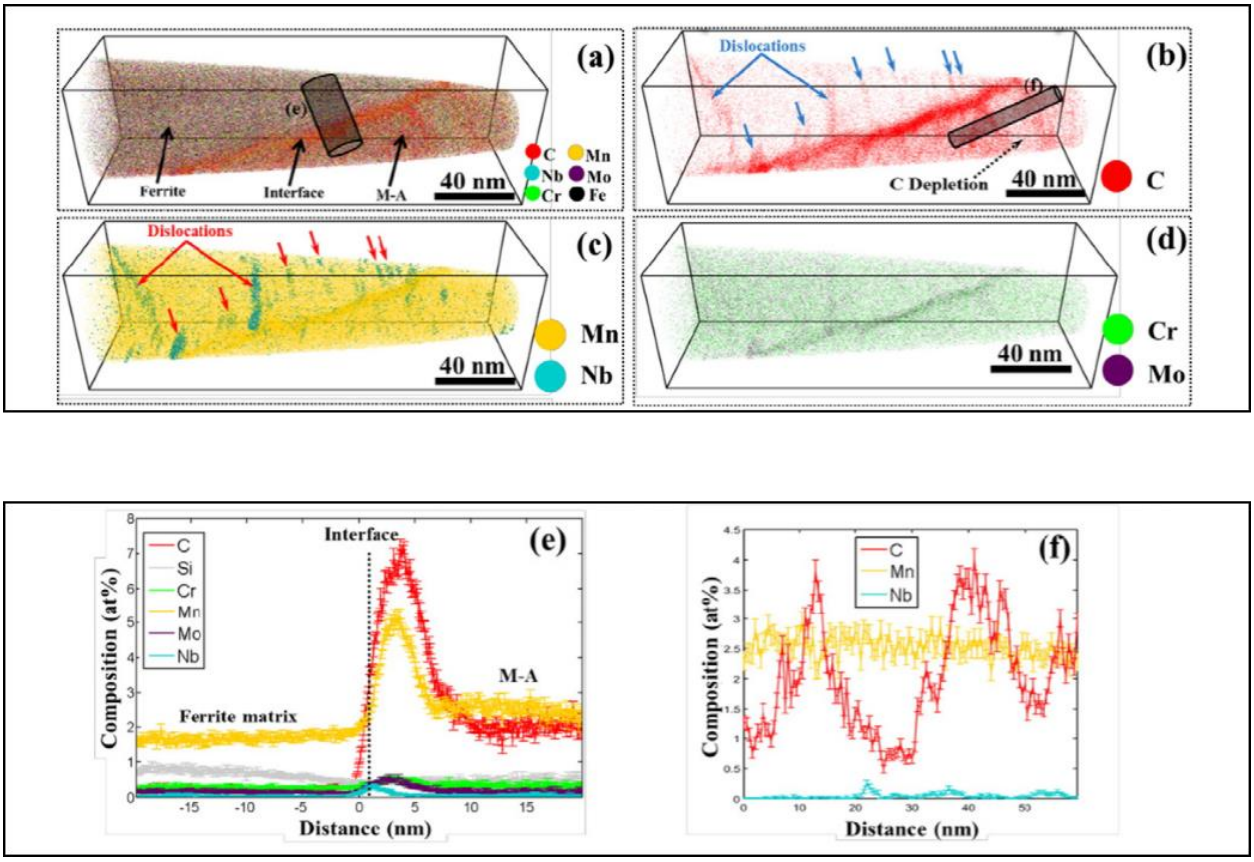

Figure 2-12 : (a–d) APT reconstruction maps of carbon and alloying elements, (e) composition profile of carbon and alloying elements across ferrite, interface and M-A constituent, and (f) variation in C, MN, Nb composition within the M-A constituent [85]

Niobium and vanadium

The hardenability of the re-austenitized regions could be increased due to some carbide forming elements during a second thermal cycle, which can promote formation of MA constituents. It is reported that Nb segregates easily to prior austenite grain boundary and decreases the activation energy and diffusion rate in carbon because of its high affinity for carbon [87]. In addition, a small addition of carbon can suppress the nucleation of ferrite from prior austenite grain boundaries and increase the volume fraction of martensite and austenite [88]. These all decrease the nucleation rate of ferrite and increase the fraction of MA. Moreover, retardation of MA decomposition is reported during the second thermal cycle because of presence of this carbide forming elements [63, 81]. A higher volume fraction and an increased size of MA are reported when the vanadium weight percentage is increased from 0.05 to 0.11%. Moreover, an increase in the size of MA is reported when 0.031 wt% Nb was added to steel [58].

Chromium, Molybdenum and Manganese

Mn, Cr and Mo can reduce the bainite start temperature, which can help to promote MA formation by extending the stability of austenite of lower temperatures. This will allow regions of austenite to remain and increase their chance to reach the martensite start temperature. In addition, the hardenability of re-austenized regions during the second thermal cycle could be increased by adding Cr and Mo which can promote MA formation [38].

Nickel and Copper

Hardenability and upper bainite content can decrease by adding copper and nickel which could results in reduced MA fraction [89]. Furthermore, the Al-Ni chemical attraction force can prevent carbon enrichment in austenite which will form between bainite ferrite plates during weld cycle [89]. Since nickel is also an austenite stabilizer, it will promote formation of more austenite within the MA versus martensite.

Aluminium and Silicon

Aluminum prevents carbon diffusion and carbide precipitation from austenite, thereby facilitate MA formation [63]. Silicon is also reported to retard the cementite precipitation and facilitate MA formation. Moreover, silicon can promote twinned martensite and formation of MA constituents [63, 90]. There is evidence that silicon will also segregate to MA, as a high silicon content in MA was reported by Lan et al. [91] when using electron probe micro-analysis (EPMA).

2.8.2 Peak temperature effect on MA formation during welding

In addition to chemical composition, the peak temperature during thermal cycle can contribute to MA size, fraction and distribution. The peak temperature in the HAZ during a weld thermal cycle determines the prior austenite grain size and the percentage of structure austenized, hence can have significant effect on MA formation. The cooling from the peak temperature in the first thermal cycle could facilitate formation of MA in the ICHAZ region (Figure 2-4). A second thermal cycle with an intercritical peak temperature can then have a more significant effect on MA fraction. The volume fraction of MA increases in the ICCGHAZ with an increase in intercritical peak temperature, as reported by Davis and King [56]. King et al. also showed that low temperature intercritical heating can cause more grain boundary MA formation while higher intercritical temperature causes intergranular MA formation [8].

Peak temperatures have significant effect on prior austenite grain size which can affect the MA formation. Studies have been performed to correlate the prior austenite grain size effect to MA formation. Li et al. [73] reported that coarser MA size is associated with larger prior austenite grain size. A prior austenite grain size more than 30 μm and MA grain size more than 2μm is proposed to be detrimental for toughness.

2.8.3 Cooling rate effect on MA formation

In addition to chemical composition and peak temperature, cooling rate can also be very influential for MA formation. Although MA has been widely studied in recent decades, the effect of cooling rate on its volume fraction remains ambiguous [28]; where some researchers have shown that increased cooling rate will increase the fraction of MA [92, 93], while other work

suggests a decrease in MA fraction occurs with slower cooling rate [55, 77, 94]. Gonzalez et al. reported an increase in MA percentage with increased cooling rate for X80 pipeline during heat treatment [95]. In contrast, Moeifar et al. [94] examined the HAZ of tandem submerged arc welded X80 pipeline using Gleeble simulation (heat treatment) and reported a decrease in MA percentage with increase of cooling rate. The review paper on MA, by Matsuda et al. [60] has shown that there is an increase in MA fraction with increase of cooling time (slower cooling rate) for different steels which as shown in Figure 2-13a. In contrast, Han et al. [12] has shown that there is an increase in MA fraction with an increase in cooling rate (Figure 2-13b).

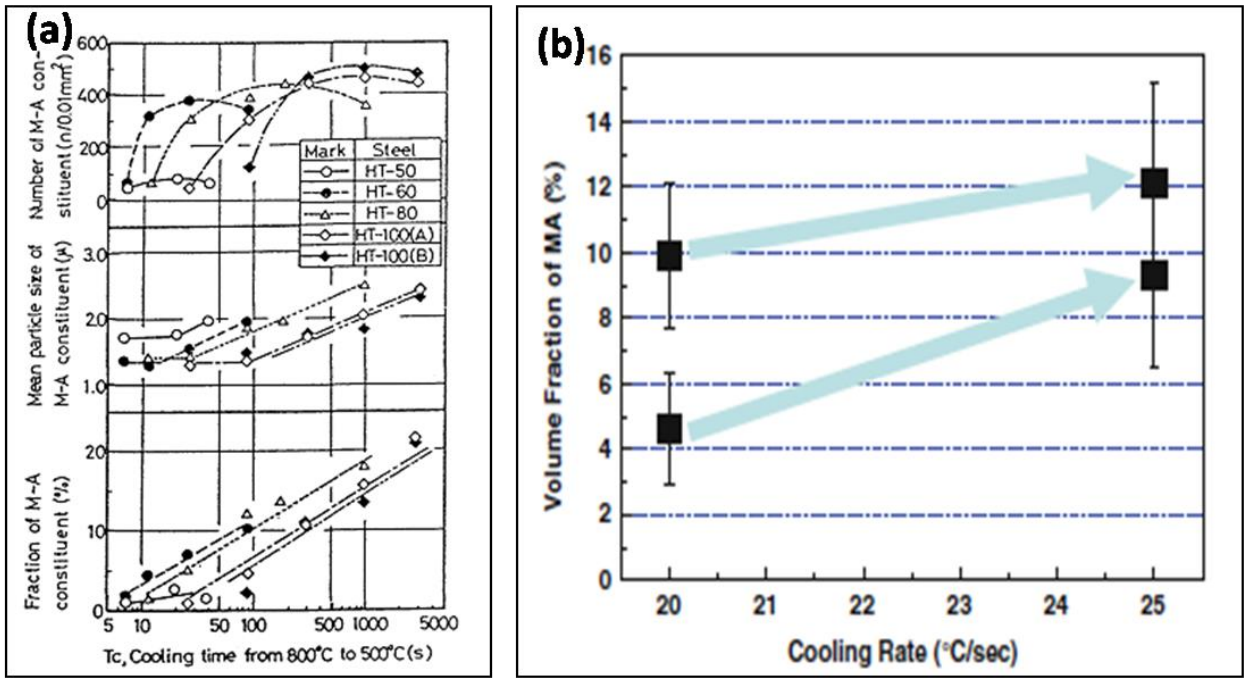

Figure 2-13 : Effect of cooling rate from 800 to 500°C on MA fraction (a) increase in MA fraction with decrease in cooling rate [63] where HT-50, HT-60, HT100 is TS 490MPa, TS590, TS980MPa steel respectively (b) increase in MA fraction with increase in cooling rate in X80 steel [12]

2.9 Effect of MA on mechanical properties

2.9.1 MA effect on tensile strength and ductility

The study of MA and its effect in strength has been seldom reported; however the impact of MA on strength and ductility could be immense. Han et al. [12] reported that there is an increase in tensile strength with an increase of MA fraction in X80 linepipe materials. Increased tensile strength with increase of MA fraction can be explained by the results obtained by Yong et al. [96] who have shown that the formation of MA in the grain boundary can change the direction of crack propagation by 90º in ultra-fine acicular ferrite structures, as confirmed by TEM characterization. They concluded that the combination of MA and low angle grain boundaries could have a similar impact of high angle grain boundary for crack direction change in tensile tests. This suggests that the presence of MA in a structure can provide better strength. An increase in tensile strength because of MA is reported by other researchers as well [97].

In contrast, using the acoustic emission technique, Lambert et al. [98]. has shown that MA is the crack initiation point by performing tensile testing at different temperature (20 and -30°C). It was shown that some high-energy acoustic events occur in the plastic zone before fracture in the tensile test, at which point the loading was halted. Performing metallography from those samples they concluded that high energy acoustic events are related to cleavage initiation, and it was shown that cleavage initiates inside of MA grain. Therefore, this unique work suggests that MA will deteriorate the strength of steel by initiating cracks. Moreover, Davis and King [8] also attributed crack initiation points to MA during tensile tests (at -100°C) in HSLA steel. It should be noted that the findings of above authors are contradictory, since Han et al. [12] and Yong et al. [96] work have shown MA can improve tensile strength while Davis and King [8] and Lambert et al. [98] found MA is deleterious to tensile strength.

2.9.2 Fracture mechanism in tensile test

Researchers also studied the mechanism of failure during tensile tests in the presence of MA. Chen et al. [99] reported that at room temperature MA could break into several parts and create voids. An increase of strain could transform the voids in to larger pores and finally coalescence of these pores leads to failure (Figure 2-14a&b) [99]. They also showed evidence that

MA debonding occurs in room temperature tensile tests by matching the fractured surface features on both sides of the failed specimen. Some of the MA was reported to form large holes or dimples on the fracture surface by coalescence of several smaller holes [99]. Though Chen et al. [99] reported that MA does not have any ductility at room temperature, Hrivnak et al. [80] contradicted this and suggested that MA has good strain capacity. The difference in strain capacity for the MA might relate to the relative percentage of austenite inside the MA regions and the surrounding structure which was not considered in those studies.

In the case of lower temperature tensile tests conducted by Chen et al., it was found that there would be a rise in the stress intensity and triaxiality near the interface of the MA and ferrite on the side of ferrite [99]. At low temperatures, it is difficult for ferrite to deform and finally cleave at higher stress. However, the MA does not break or debond at low temperature. At low temperatures (near that of liquid nitrogen) the tensile failure mechanism reported by Chen et al. [99] indicated that voids formation occurs in the ferrite and the MA interface instead of inside of the MA regions (at room temperature). The reason for this may be that the stiffer MA causes a rise in stress triaxility in the interface of MA and ferrite matrix resulting from volume expansion during austenite to martensitic transformation [100]. At low temperature, it is hard to deform the ferrite and subsequently any strain will cause cleavage fracture [99].

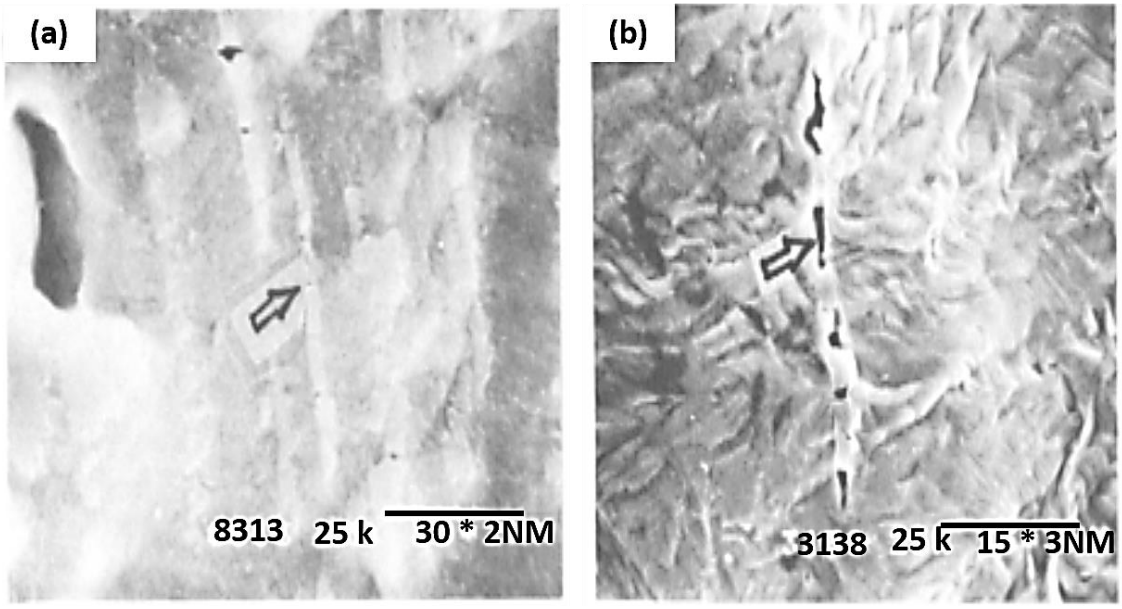

Figure 2-14 : (a) MA fragmentation at lower strain (b) void formation at higher strain [99]

Kim et al. [59] also studied the fracture mechanism during tensile test in the presence of MA. The ductile and cleavage fracture mechanism is schematically presented (see Figure 2-15a&b). In the ductile fracture mechanism, void formation is noted at the interface of MA and ferrite due to ferrite deformation. Higher strain causes those voids to grow in to dimples and due to significant plastic deformation in the ferrite the MA fracture and coalescence of dimples at 45 degrees leads to fracture (Figure 2-15a) [59]. In the brittle facture mechanism, voids initiate in the manner as in ductile fracture, however the void grows in the MA/ferrite interface and nucleates a cleavage crack. This cleavage crack rapidly propagates to reach a prior austenite grain boundary and links up with shear cracks. However, instead of coalescence the void formed travels quickly through the grain to the prior austenite grain boundary and then follows a zig-zag path to fracture (Figure 2-15b).

However, the study regarding the effect of voids formation and spacing between voids on ductility is quite rare. Megnusen et al. [101] showed that ductility and strength has been greatly reduced for random array of voids when spacing between the voids was decreased in low carbon steel (Figure 2-16). In addition, formation of larger void in the structure can reduce the ductility [101].

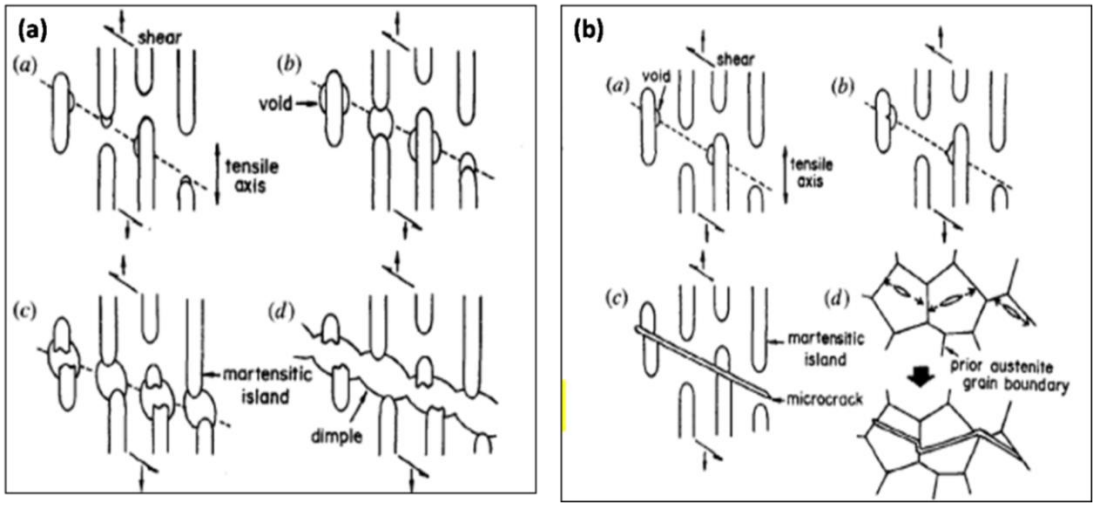

Figure 2-15 : Fracture mechanism in tensile test (a) ductile (b) brittle [59]

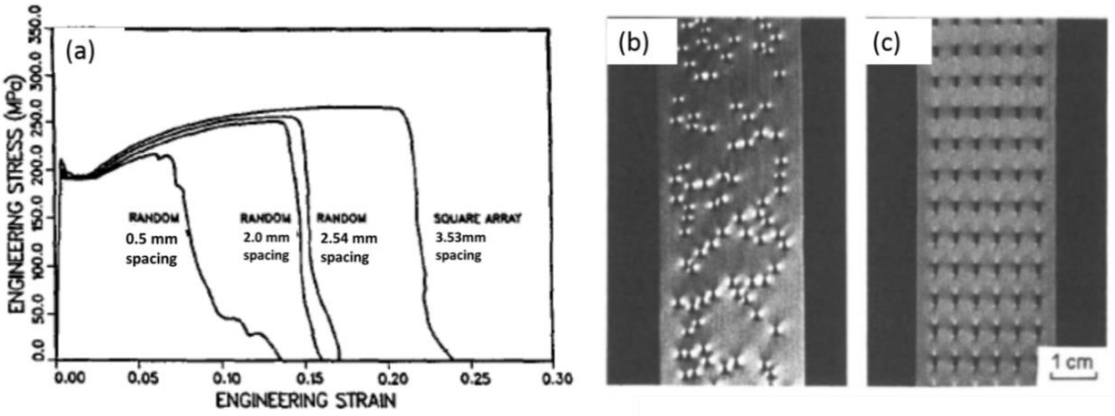

Figure 2-16 : (a) Engineering stress-strain behavior as a function of the hole array for low carbon steel specimen. Macro photographs of specimens containing (b) random (c) regular arrays of holes just prior to failure [101]

2.9.3 MA effect on toughness

MA has a deleterious effect on toughness, as reported by most of the studies. It can be seen from Figure 2-17a that there is a decrease in toughness with increasing MA fraction [60]. Lan et al. [91] observed a difference in MA fraction between weld metal and HAZ. However, the HAZ contains a higher fraction along with larger MA regions than in the weld metal, which led to a lower crack initiation energy for the HAZ than in the weld metal [91].

In contrast, it has also been reported that there is a lower transition temperature in ICCGHAZ and ICHAZ for titanium microalloyed steel (B) and vanadium microalloyed steel (C) (which would be beneficial) compared to niobium microalloyed steel (A), in terms of toughness tests with increased MA fraction. This was attributed to a more uniform and benign MA distribution (Figure 2-17b) [102]. It has been also reported that the amount of secondary phase and the difference in hardness between matrix and MA have a dominant effect on toughness when cooling rate is fast (Figure 2-18). In the slower cooling rate, increased differences in hardness between MA and the matrix may play more dominant role on toughness as a result of matrix softening from tempering and hardening of MA constituents due to carbon accumulation [103].

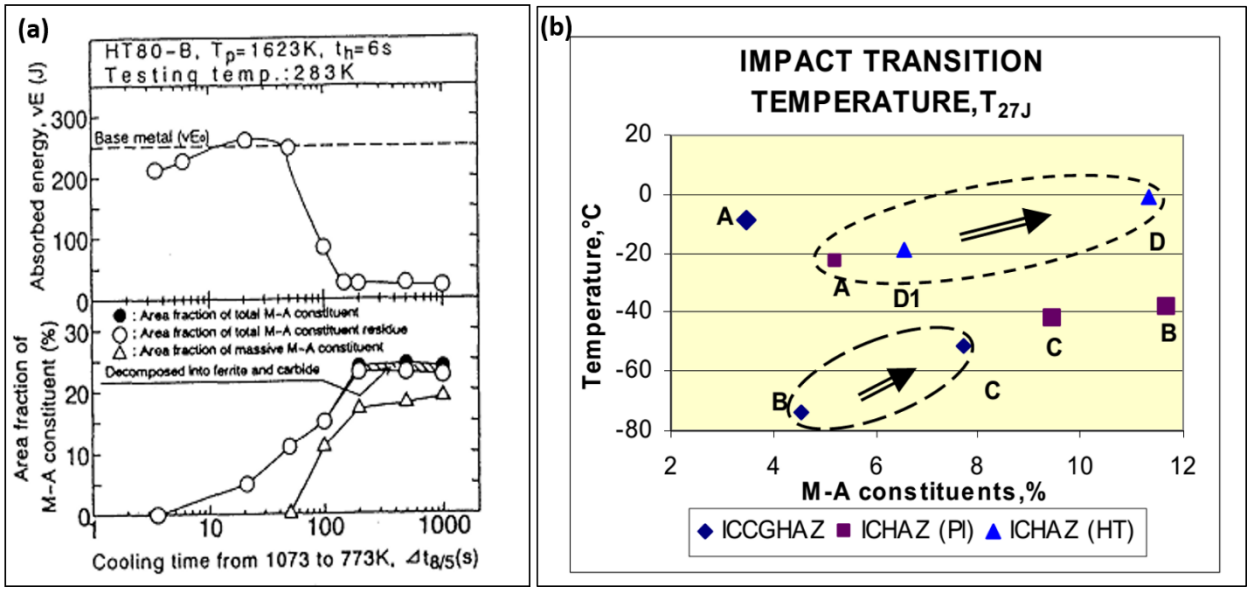

Figure 2-17 : MA fraction effect on toughness (a) toughness decrease with increase of MA fraction [60] (b) imporved toughness for sample B (titanium microalloyed steel) and C (vanadium microalloyed steel) in comparison to sample A (niobium microalloyed steel) [102]

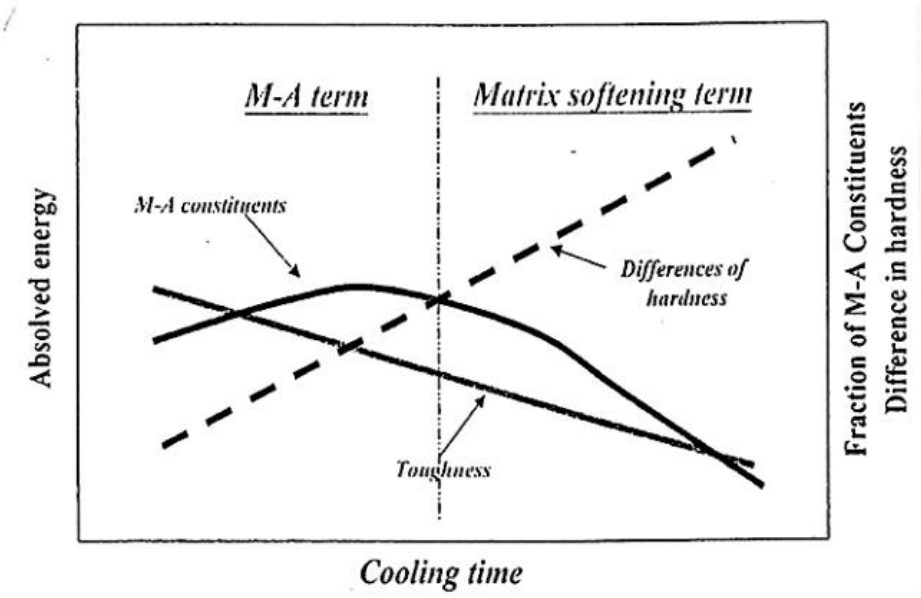

Figure 2-18 : MA-matrix hardness difference, MA fraction and cooling time relation to touhness [103]

The above contradictory results can be explained in terms of MA morphology and formation location. Zhang et al. [104] reported that improved toughness can occur due to the formation of blocky MA. Moeifar et al. [39] simulated supercritical CGHAZ, Intercritical HAZ and subcritical CGHAZ in X80 linepipe steels. The ICCGHAZ exhibited the lowest impact toughness because of a grain boundary network of MA grains. However, the supercritical and subcritical CGHAZ are reported to have improved toughness even though MA was present in these HAZ. They found that smaller and more finely distributed MA can improve toughness [39]. It is interesting to find that Far et al. [105] also reported an improvement in toughness in the CGHAZ for X80 linepipe with the same chemical composition, which was related to the formation of stringer MA. An increase in MA diameter and length led to poor toughness in X80 steels, as reported by Moeinifar et al. [94].

Though it is commonly accepted that MA deteriorates impact toughness of pipeline steel [60, 94], some studies have also claimed an improvement in toughness attributed to the presence of MA in the CGHAZ microstructure of X80 steel produced using thermal simulation [105]. This contradictory result has been explained by pinpointing MA as a crack initiator or crack deflector. Xiaomei et al. [106] clearly showed that MA was the source of crack initiation in X80 linepipe materials (Figure 2-19a). Lambert et al. [75] also showed MA as a crack initiation point in impact toughness test. Hrivnak et al. [80] reported more precisely that carbides inside the MA provide a crack initiation point. In contrast, Baker et al. [58] has shown crack deflection and crack arrest can occur in MA (Figure 2-19 b&c). Improved toughness was also attributed to MA formation in X70, X80, and X120 pipeline steels, possibly due to these latter mechanisms [104, 107]. These competing roles in fracture may explain the contradictory may results based on the fracture mechanism during toughness tests.

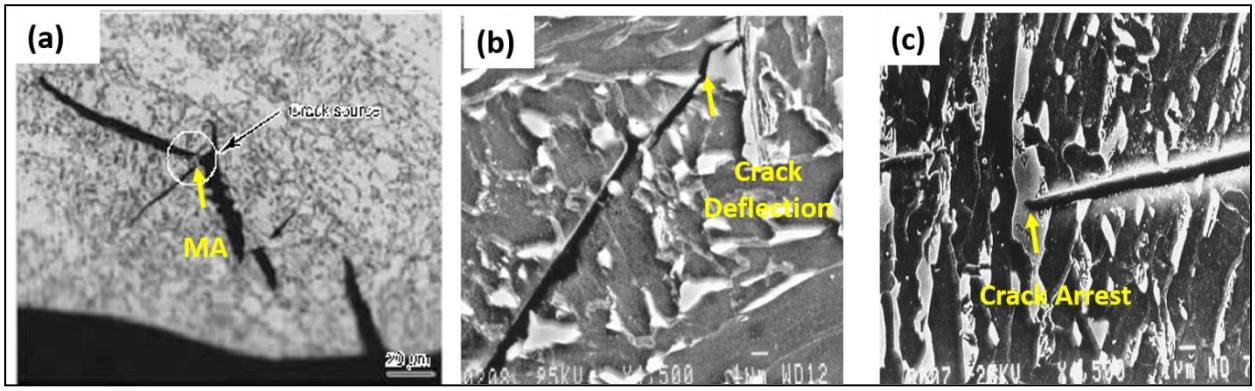

Figure 2-19 : Effect of MA in (a) crack initiation [106] and (b&c) crack deflection and arrest [58]

2.9.4 Fracture mechanism in toughness test

Davis and King proposed four mechanisms by which MA can deteriorate the toughness (which are summarized using schematics in Figure 2-20 [8]) as follows:

1. MA introduce micro cracks easily as it is a brittle phase which can initiates cleavage in the ferrite matrix during brittle fracture (Figure 2-20a).
2. Transformation induced residual tensile stress is produced in the surrounding ferrite can assists cleavage fracture (Figure 2-20b).
3. Higher hardness of MA creates stress concentration in surrounding soft matrix. Stress concentrations can assist cleavage (Figure 2-20c).
4. There could be formation of microcrack at boundary of MA and ferrite matrix. This microcrack can initiate cleavage (Figure 2-20d).

However, Han et al. [12] reported that there is a higher transition temperature for specimens which contain low volume fraction and finer MA, because any cracks are deviated by high angle boundaries (Figure 2-21a). However, a specimen with a high volume fraction and coarser MA enhanced the crack propagation path and thereby results in a lower the transition temperature during impact toughness test (Figure 2-21b).

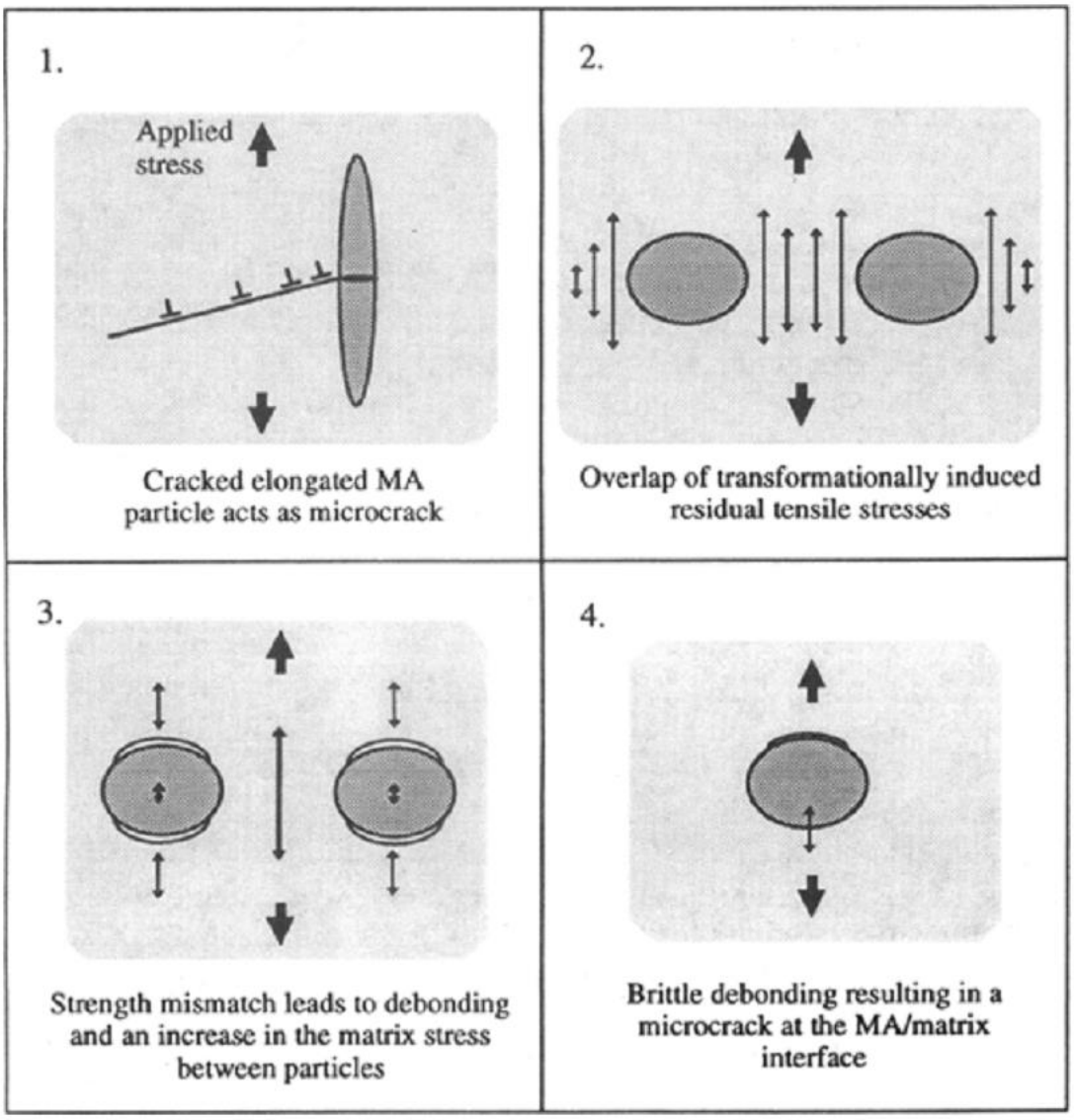

Figure 2-20 : Schematic representation of the four proposed crack initiation from MA in toughness test [8]

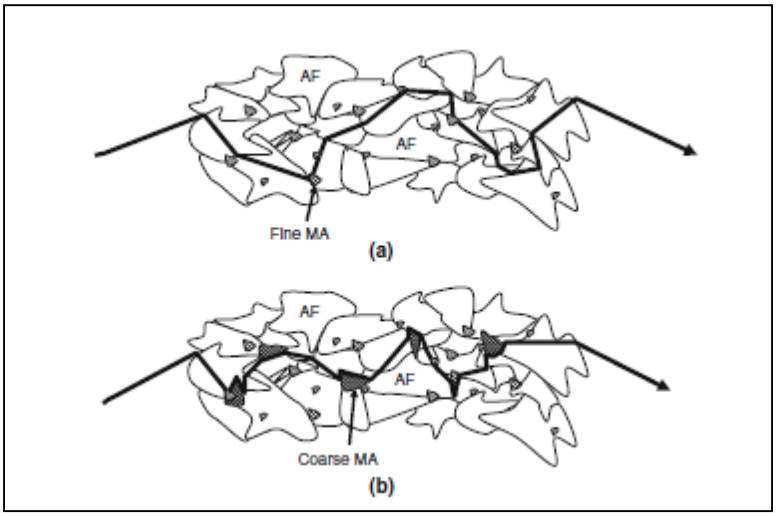

Figure 2-21 : (a) Crack path in acicular ferrite microstructure showing crack propagation bend at high angle grain boundaries (b) Reduced unit crack path in acicular ferrite and coarser MA structure showing MA improvement effect on toughness [12]

2.9.5 MA internal structure contribution to mechanical properties

Although, it is reasonable to think that the toughness is more dependent on the microstructure and grain size, some works have concluded that size of the MA could have effect on toughness. However, most prior work did not investigate whether it is possible to have a different microstructure inside MA other than martensite-austenite, since it is difficult to resolve the sub-micron sized internal structure of MA. Although, it can be clearly observed from Figure 2-10 that various internal structures could form base on the heat treatment and this can have a significant effect on mechanical properties. Davis and King [56] reported an observation of the internal structure regarding MA (Figure 2-22) and related this to mechanical properties [56]. At higher cooling rates, they identified the internal structure of MA as being entirely a combination of martensite and austenite (Figure 2-22a). At intermediate cooling rates, the internal structure of MA is a mixture of martensite and austenite, combined with a secondary microconstituent (presumed to be bainite/pearlite) (Figure 2-22b). Moreover, it has been reported that the internal structure of MA will be bainite instead of martensite-austenite if there is insufficient carbon to stabilize the austenite [73]. At very slow cooling rates, the internal structure is pearlite, although it was still referred to as MA (Figure 2-22c). They found that the MA phase with an internal

structure corresponding to pearlite does not have a deleterious effect on toughness (Figure 2-22d) [56]. Moreover, MA with martensite in middle and austenite in periphery (Figure 2-10a) is reported to be detrimental for toughness properties. However, MA with mixture of martensite and austenite islands has been reported to be beneficial to toughness [77].

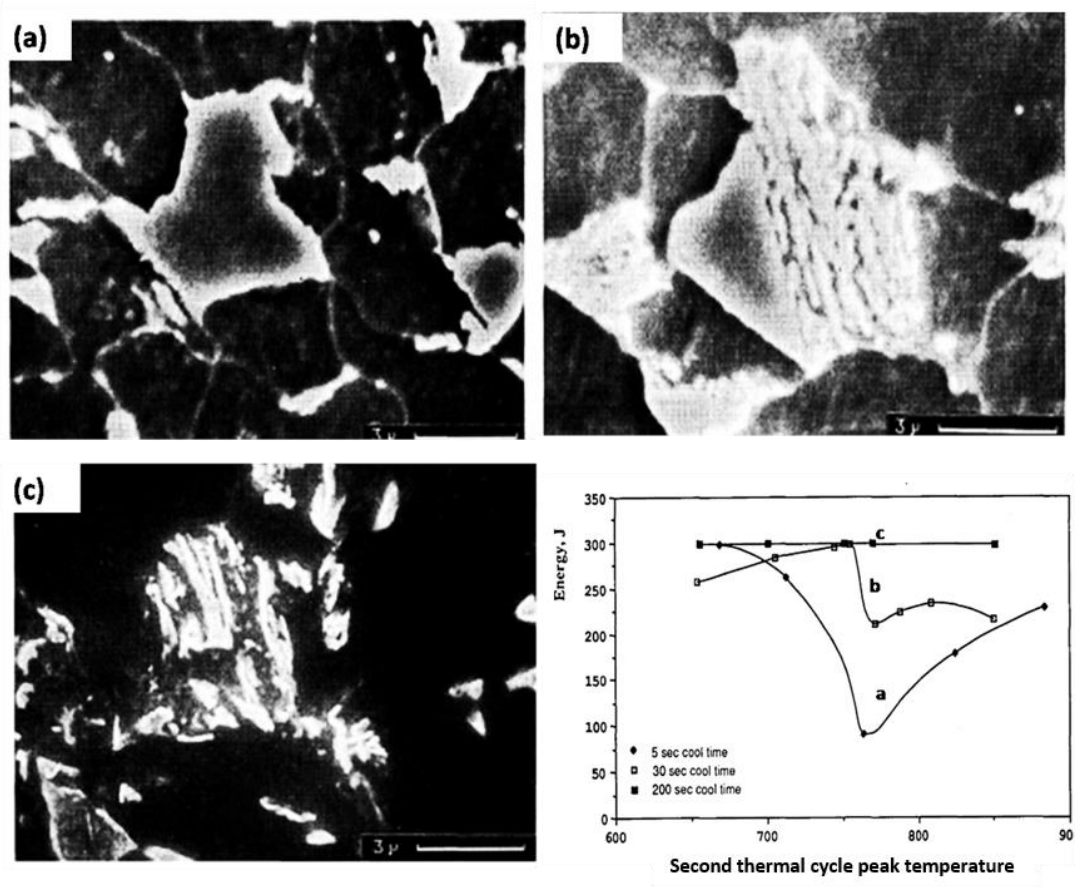

Figure 2-22 : Different MA internal structure with different cooling rate and its effect on toughness properties (a) martensite dominant MA (b) MA with mixture of martensite-bainite (c) MA dominant in pearlite (d) MA internal structure effect on toughness [56]

2.10 Tempering (PWHT) effect on mechanical properties by MA decomposition

It has been reported that properties of material can be improved by post-weld heat treatment (PWHT) [108, 109] which is also referred as tempering cycle. Conversely, tempering embrittlement can occur if the PWHT cycle is not chosen properly [109]. However, selection of an optimum PWHT is vital to obtain good mechanical properties [108]. Although PWHT studies have been performed to observe the change of MA internal structure and its effect on mechanical properties, there is little new information about PWHT parameters (i.e. time and temperature) [110] to decompose detrimental MA while retaining an beneficial MA [108, 109]. Liao et al. [108] showed that a 300°C PWHT temperature with tempering time between 3.6-28.8ks can remarkably improve the ICCGHAZ toughness. In addition to PWHT temperature, the tempering time could have significant effect on mechanical properties, and excessive values will increase costs. Magula et al. [111] used 550°C and 650°C with a 1hr PWHT cycle to improve the toughness of two different grade HSLA steels. Liao et al. [109] used a PWHT temperature range of 250-620°C with a PWHT time of 3.6-28.8ks to study the PWHT cycle effect in presence of MA. It had been reported that toughness was always higher for a tempering temperature of 250-550°C with a cooling time of 80s [109]. Zhuang et al. [112] examined PWHT temperatures of 450-750°C and found increased in toughness for two different X100 grade steels.

Improvement in toughness was reported by Janovece et al. [113] in SQV-2A HSLA steels when tempering cycle (PWHT) temperature range was between 200-300°C with a holding time of 6s. It has been reported that higher tempering temperature reduces the difference in hardness between the MA and ferrite while toughness only improved with tempering temperatures up to 460°C. It was observed that tempering temperature more than 460°C degraded toughness due to growth of carbides like M_3C, and M_2C, which act as crack initiation points during impact toughness testing [109]. Hrivnak et al. [78] also reported carbides as the crack initiation source. These results suggest that a higher temperature and longer tempering time does not ensure improved properties. Magula et al. [111] studied different PWHT temperatures and times in three different grade HSLA steels, and observed that for a certain tempering cycle (300°C, 10 min) there was a significant amount of MA which decomposed. Ikeuchi et al. [110] also concluded that 300°C was the optimum temperature for decomposition of MA in SQV-2A steel. That does suggest that

tempering cycle can change the internal microstructure of MA and it is possible to attain improved properties.

Chapter 3 : Characterization Methodologies

This chapter presents the brief description of the materials preparation for microstructure sample extraction and preparation, mechanical testing, and different methodologies which was used to characterize the materials. However, individual chapter will contain particular methodologies that was used to prepare the relevant specimen and characterize the materials.

3.1 Welding procedure and equipment

The weld was produced using robotic multipass GMAW for current thesis. The welds were produced using constant voltage program. A combination of Ar-15% CO_2 shielding gas was used to shield the weld pool. A data acquisition system (DAQ) was incorporated with robotic welder to collect the instantaneous current signal. The voltage and current output from DAQ was used to calculate heat input in each pass. Four passes of welding were performed to join the material. An interpass temperature of 100°C was applied prior to each pass to control the cooling rate and remove the moisture from the samples. In the current work, an API X80 linepipe material with a 15 mm wall thickness was joined by robotic welding of a V grooved joint with a 40° included angle using single GMAW torch.

3.2 Gleeble thermo mechanical simulator

The various microstructures with different mechanical properties can be resulted in the HAZ of real weld. The deformation behavior of weld HAZ in stress strain curve usually depends on wide range of microstructure over larger area of weld. However, the observed properties during tensile and fracture toughness tests are controlled by localized microstructures in the HAZ. Fracture can occur in Coarser Grain Heat Affected Zone (CGHAZ), Fine Grain Heat Affected zone (FGHAZ), Intercritical Heat Affected Zone (ICHAZ) depending on the properties of each zone.

Heat treatments can be carried out using the Gleeble thermo-mechanical simulator allowing design of complex thermal cycles to create localized microstructures in bulk HAZ microstructure and hence help to study particular microstructure (CGHAZ, FGHAZ, ICHAZ) properties. To study localized microstructure properties in current study, the localized HAZ microstructures which produced during GMAW welding was simulated using Gleeble 3500 (Figure 3-1) and properties

of these microstructure were studied. K-type thermocouples were spot welded to the sample where temperature and cooling rate was monitored and controlled. Thermocouples were attached in different locations along the length of the sample to identify the area of uniform temperature and cooling rate. The programmed thermal cycle was used as the set point to control the heating based on the temperature and cooling rate feedback from the thermocouple. A C-gauge clamp was used to monitor the thermal expansion during heating and cooling at midpoint of the sample. In the current study, a preheat of 100°C is maintained before applying the actual thermal cycle. However, it should be noted that significant residual stress can be developed in the HAZ during welding which can play a role in microstructure development. The residual stress contribution is difficult to determine via Gleeble simulation, and hence it was not considered.

Figure 3-1 : Overall view of Gleeble thermomechanical simulator

3.3 Digital image correlation (DIC)

Tensile specimen produced from weld structure contains base metal, weld metal and HAZ. Each of these zones has different properties. In addition, the HAZ itself can contain different zone as shown in Figure 2-4. Measuring strain using conventional mechanical extensometer does not allow measurement of localized microstructure strain of the weld. However, non-contact Digital image correlation (DIC) measurement facilitates to monitor local deformation properties and thereby provide more information about straining, fracture and deformation.

DIC is an optical technique of non-contact strain and displacement measurement. It involves comparing digital photographs of a test piece at different stages of deformation by tracking block of pixels. DIC is simple to use and more accurate than manual strain gauge measurement methods. It allows local strain observation and measurement than the global strain measurement. It requires painting on surface to produce contrast on the surface which is monitored during deformation. Two cameras monitor the speckle on surface during deformation with the help of lighting that is projected on the surface. The captured images are fed into software for analysis of strain. In the current study, digital image correlation (DIC) based strain monitoring was utilized to measure the localized and global strains. Image processing settings were applied within VIC-3D software using a step size of 29 and sub-size 7 to extract strain data using VIC-3D software. The step size controls the number of points analyzed during correlation while the sub-size controls the area of image. Those areas are used to track displacement between images. Stress values from tensile machine and strain values from DIC were synchronized to develop stress-strain curve.

3.4 Auger electrom spectroscopy (AES)

Auger Electron Spectroscopy (AES) facilitate quantitative elemental analysis from a solid materials surface. Finely focused electron beam is used to excite a sample surface which force to emits auger electrons. The elemental identity and quantity of a detected element is determined by analyzing the kinetic energy and intensity of auger peak. AES analysis technique is suitable for compositional analysis of thin layers which allow analysis depth of less than 5 nm. However, Energy Dispersive Spectroscopy (EDS) allow typical depth analysis of 1-3 μm. In current study, AES was used to map the carbon distribution of different microconstituents of the samples using a JEOL 9500F system. Characterization involved a Zeiss LEO Scanning Electron Microscope (SEM) to investigate internal structure of MA. A JEOL 9500F was used to map carbon distribution inside the MA using AES.

3.5 Sample preparation for microscopic examination

Sample preparation for macro and micro observation

Metallographic samples were prepared using standard polishing techniques with final polishing using 1 micron diamond particles. Nital solution (2%) was used for a 10 to 15 second etching time to reveal the microstructure, the time varying in order for the reheated zone to appear clearly in the stereoscope. Lepera's reagent (equal parts of 25 ml distilled water + 25ml Picric acid with 0.25g $Na_2S_2O_5$) was used to reveal the MA in the microstructure. The MA appeared white in colour when the surface appears uniform gold using Lepera etchant. When using LePera etchant, the sample surface turns to a uniform gold colour and MA appears white [114, 115]. To ensure successful etching by the LePera solution, it was found that the best results were obtained by first etching with a 2% nital solution and subsequently removing the excess etching byproduct using light diamond polishing pad with 1 μm diamond media before using Lepera. The LePera etchant does not work if some nital etching byproduct remains on the surface. Villela etchant (95 mL ethanol + 5 mL HCl + 1 mL picric acid) for 5-7 second was used to characterized martensite and austenite inside MA microconstituents.

Optical Microscope and Scanning Electron Microscope (SEM)

An Olympus BX51 microscope was used to observe the microstructure. A Zeiss LEO 1530 Scanning Electron Microscope (SEM) was used to investigate the MA structure at higher magnification. A 7 kV voltage and 9-11 mm working distance was used for imaging. A 20 kV voltage was used for EDS analysis. MA quantification was performed in optical microscope and SEM images using image-processing software Photoshop 6 and the average MA fraction was reported based on quantification from three images.

Electron Backscatter Diffraction (EBSD)

EBSD technique facilitates to observe the misorientation difference in MA and ferrite. A JEOL JSM-7000F SEM with HKL EBSD (Electron backscatter diffraction) software was used to map

KAM (Kernel Average Misorientation). Markers were used to clearly identify the reheated zone at the macro scale, and images were taken solely from that zone.

EBSD analysis was performed using a Zeiss Sigma FESEM, equipped with an Oxford AZtecSynergy system for collecting electron backscattered diffraction patterns, and was operated at 20 kV accelerating voltage and a step size of 3 μm. Prior to mapping, samples surfaces were milled using Ar ion milling for approximately 1 minute to improve Kikuchi pattern indexing quality. Post processing of the EBSD data was conducted by using AZtecHKL, with a mean angular deviation acceptance criteria of 0.6, and step sizes from 0.23 to 0.29 μm.

TEM sample preparation

TEM analysis was also performed to characterize the microstructure using JEOL 2010F at 200 kV. Martensite-Austenite internal structure was analyzed using TEM to identify the relative position of martensite, austenite and any presence of carbide. Moreover, dislocation density difference was also observed which solely qualitative observation. In-situ heating and cooling was performed inside TEM to study tempering effect. Each chapter will contain a description of the sample preparation procedure.

X-ray diffraction

The XRD was conducted using a Bruker D8, operated at a 2 deg / scan rate. X-ray diffraction was used to confirm the presence of martensite and austenite. A Cu-K_{alpha} radiation source was used to determine the peak of ferrite and austenite. The relative intensity peak was used to calculate the percentage of austenite in the structure.

Vickers Hardness and Nano indentation

The Vickers hardness was measured using a load of 300 g and 15 s dwell time. A cross-check was performed in stereoscope and microscope to ensure that the indentations were made in the reheated zone. The Vickers hardness was measured using a load of 300 g and 15 second dwell time. Nanoindentation was performed using a Hysitron TriboIndenter with a Berkovich indenter,

a 2000 μN load, where the indentation location and phase in contact was ensured by observation in SEM.

Tensile Test

The tensile samples were prepared according to ASTM sub-size standard (ASTM E8/E8M-09). Both a mechanical extensometer and DIC were used during tensile tests to monitor strain behavior. DIC facilitated measurement of strain distribution and gradients, with a gauge length of 32 mm used for the measurement, with a subset size 29 and step size 7 being applied. Load from the tensile frame load cell was used to calculate stress and strain from the DIC were combined and the stress-strain curve was plotted. The yield strength was calculated using the 0.2% offset method.

Tensile tests were performed using a Tinius Olsen HK10T servo-mechanical tensile frame with maximum load capacity of 10 kN. The specimens were loaded at a 1 mm/min strain rate. The chemical composition of X80 linepipe material was analyzed by inductively coupled plasma emission, as reported in Table 1. The last parameter listed in the Table, Ceq, is the carbon equivalent calculated based on the following equation 3-1 [116]:

Table 3-1: Chemical composition of the X80 line pipe steel

Elements	C	Mn	Si	Cr	Ni	Cu	Mo	Al	Ti	Nb	N	O	Ceq
Wt.%	0.051	1.73	0.18	0.03	0.13	0.12	0.21	0.03	0.01	0.04	0.0004	0.0011	0.405

$$\mathbf{Ceq} = \mathbf{C} + \frac{\mathbf{Si}}{\mathbf{25}} + \frac{\mathbf{Mn+Cu}}{\mathbf{16}} + \frac{\mathbf{Cr}}{\mathbf{10}} + \frac{\mathbf{Ni}}{\mathbf{40}} + \frac{\mathbf{Mo}}{\mathbf{15}} + \frac{\mathbf{V}}{\mathbf{10}} \quad \text{...Equation 3-1}$$

Chapter 4 : Study of MA Effect on Yield Strength and Ductility of X80 Linepipe Steels Weld[1]

4.1 Overview and background

Differences in MA fraction, size and morphology can lead to a significant variation in tensile strength and ductility. However, few studies have considered the effect of MA on quasi-static strength and ductility [59, 98, 99]. This is of particular interest for strain based pipeline design applications, and particularly during pipeline construction where there is a potential for strain localization in the weld HAZ when the welded pipe is lowered below the ground during construction.

Several researchers studied the effect of MA on tensile behaviour. Lanzillotto et al. reported an increase in all strength parameters contributed by the presence of MA in dual phase steel [100]. An increase in tensile strength attributed to MA has been reported by other researchers [97, 117]. Han et al. reported that there could be an increase in ultimate tensile strength, with low transition temperatures with higher MA area fraction [12]. In contrast, Lambert et al. have used acoustic emission technique to show that MA is a crack initiation point during tensile tests [38, 98]. Moreover, Davis and King also pinpointed MA as the crack initiation point in HSLA steel [8].

Although there are a few investigations reported about the effect of MA on tensile strength and fracture mechanisms, the study of its effect on ductility is not common. Coldren et al. reported that although there is an increase in strength, often there is a deterioration of ductility even with a 1% increase in the fraction of MA [118]. Hrivnak et al. reported that MA could increase the strength; however, MA could decrease its ductility by facilitating dimple fracture initiation, and they concluded that MA impairs ductility [80].

Considering these various claims and the gap in conclusive opinions, the current chapter is focused on bridging the gaps regarding MA study and its effect on tensile strength and ductility. Moreover, fracture mechanism was correlated to ductility. The present study on X80 linepipe material examines two different weld metals which experienced slightly different cooling rate

1 This chapter is published Manuscript in Metallurgical and Materials Transactions A on June 20, 2017, available online: DOI: 10.1007/s11661-017-4171-1, Nazmul Huda, Robert Lazor, and Adrian P. Gerlich, Study of MA Effect on Yield Strength and Ductility of X80 Linepipe Steels Weld.

resulting in a different MA size, fraction and distribution in the doubly-reheated HAZ. Tensile tests were carried out on the samples that are produced from the reheated zone of both welds. Performing tensile tests in this kind of samples will help to determine the role of MA size, fraction and distribution effect on mechanical properties. In addition to the effect on tensile strength, the fracture mechanisms are also investigated for both welds.

4.2 Materials and experimental procedure

Two different metal wires with slightly different chemical compositions were used to join the X80 linepipe material, where sections pieces of pipe were extracted for weld tests. The base metal chemical composition is given in Table 3-1. Weld A was produced with a 0.984 mm diameter wire and weld B with 0.909 mm diameter wire. The chemical composition of wires (A and B) were analyzed using inductively coupled plasma emission method, (see in Table 4-1). Welding current 178 to 185 A, with a voltage of 20 to 22 V, wire feed speeds between 8.4 to 10.9 m/min and travel speeds from 0.3 to 1.2 m/min for the various passes. The heat input for root and hot pass was maintained 0.18-0.29 kJ/mm while for fill and cap pass the heat input was maintained between 0.51-0.78 kJ/mm.

Markers were used to clearly identify the reheated zone at the macro scale, and images were taken solely from reheated zone. A cross-check was performed in stereoscope and microscope to ensure that images were taken and hardness indentations were performed in from the reheated zone. The tensile samples were prepared according to ASTM sub-size standard (ASTM E8/E8M-09). The welding design with tensile samples were produced from direction orientation as shown in Figure 4-1

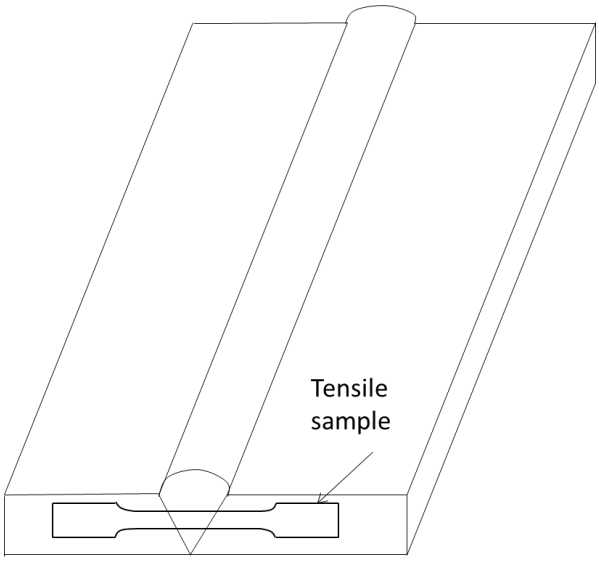

Figure 4-1 Welding design and tensile specimen

Both a mechanical extensometer and DIC were used during tensile tests to monitor strain behavior. DIC facilitated measurement of strain distribution and gradients, with a gauge length of 32 mm used for the measurement. Force data from the tensile frame load cell was used to calculate stress and strain from the DIC were combined and the stress-strain curve was plotted. The yield strength was calculated using the 0.2% offset method.

A 10 x 10 mm sample was cut from welded sample including the fusion line. The sample was grinded to 0.15 mm using 800 grit paper. Punching of a 3 mm disc was performed from the fusion line to a distance around ICRHAZ, with twin jet electropolising used to thin the foil. Ion milling was performed to reduce the thickness to 100 nm.

Table 4-1: Chemical composition of wires

Elements	C	Mn	Si	Ni	Cu	Mo	Ti	Nb	N	Ceq
Wire A	0.08	1.26	0.48	0.80	0.12	0.30	0.031	0.012	0.005	0.41
Wire B	0.06	1.28	0.40	0.03	0.16	0.34	0.002	0.011	0.004	0.35

4.3 Macrostructure and Microstructure

The base metal microstructure contains ferrite and bainite, as shown in Figure 4-2, the volume fraction being measured to be 83% ferrite and 17% is bainite. The macrograph for each of the welds is shown in Figure 4-3. It can be seen that weld B contains traces of micro-porosity (although within acceptable levels based on qualification standards), whereas weld A is free of

porosity. Both weld metals consisted of an acicular ferrite microstructure, with weld A having a finer microstructure than weld B. The hardness of weld metal A for single and multipass welding was higher than that of weld metal B [119]. It is believed that the higher hardness of weld metal A is associated with the higher alloying composition of wire A. Regardless, the current work is focused on the reheated HAZ rather than the weld metal. It can be noticed that the etching is performed in such a way that the reheated HAZ can be clearly identified (Figure 4-3). The microstructure from the reheated zone for both welds is shown in Figure 4-4. While the microstructure of both reheated zones is mostly ferrite, at higher magnification the reheated zone of weld A contains more black colored zones (indicated by arrow) than the weld B reheated zone (Figure 4-4a&b).

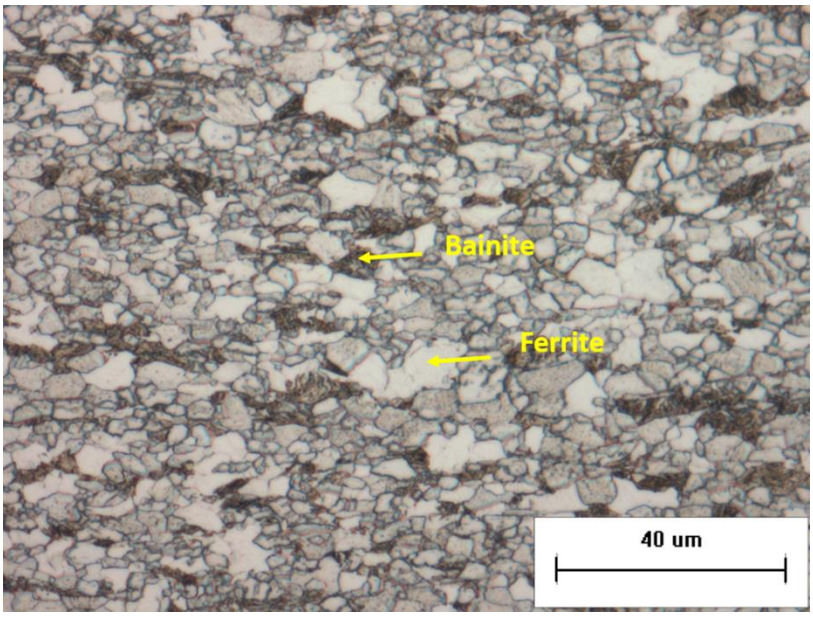

Figure 4-2 : Base metal microstructure, consisting of 83% ferrite and 17% bainite (2% Nital)

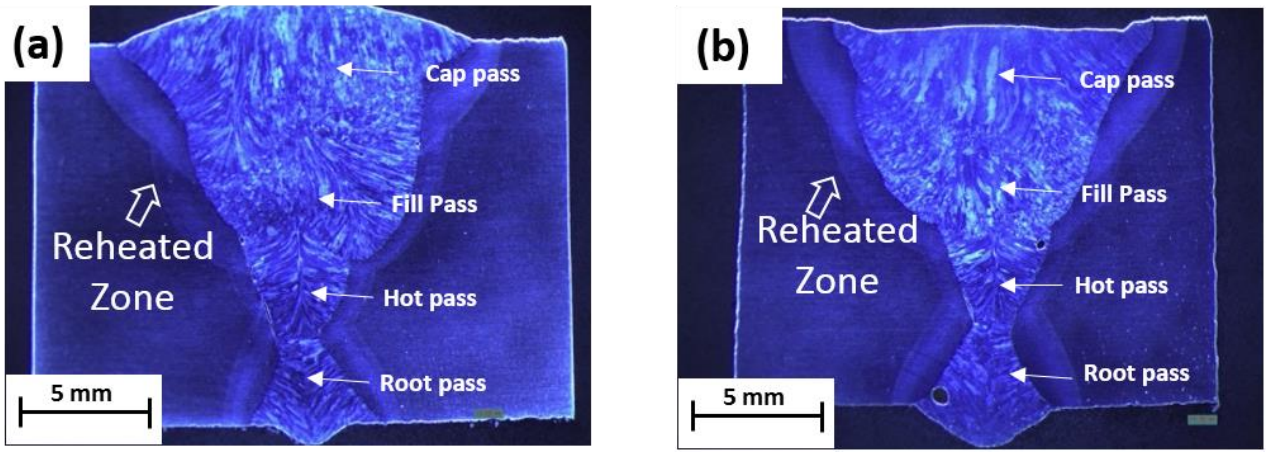

Figure 4-3 : Macrograph of a) weld A and b) weld B produced by wire A and wire B respectively (2% Nital etchant)

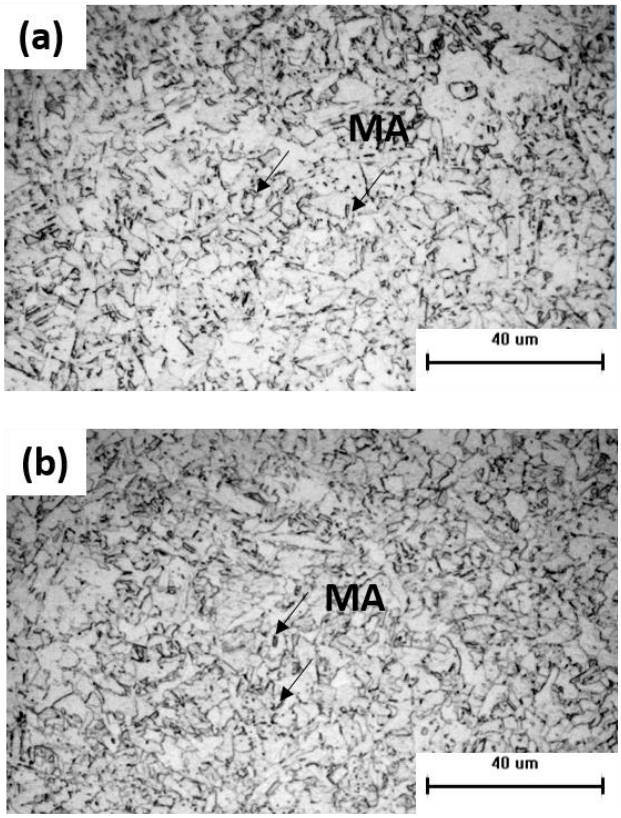

Figure 4-4 : Microstructure in the reheated zone (2%-Nital etchant) for (a) weld A and (b) weld B

4.4 Hardness in reheated zone

The base metal average hardness is 230 ±10 HV. Multiple hardness line profiles are produced in the reheated zone for both welds at an equal spacing of 150 μm between the indents for each line. The comparison of average hardness profile along those lines for both welds is shown in Figure 4-5 along with an image of the HAZ location with the indents. Further away from the fusion line the hardness decreases for both of the welds. However, the hardness for the weld A reheated zone is consistently higher than that of weld B.

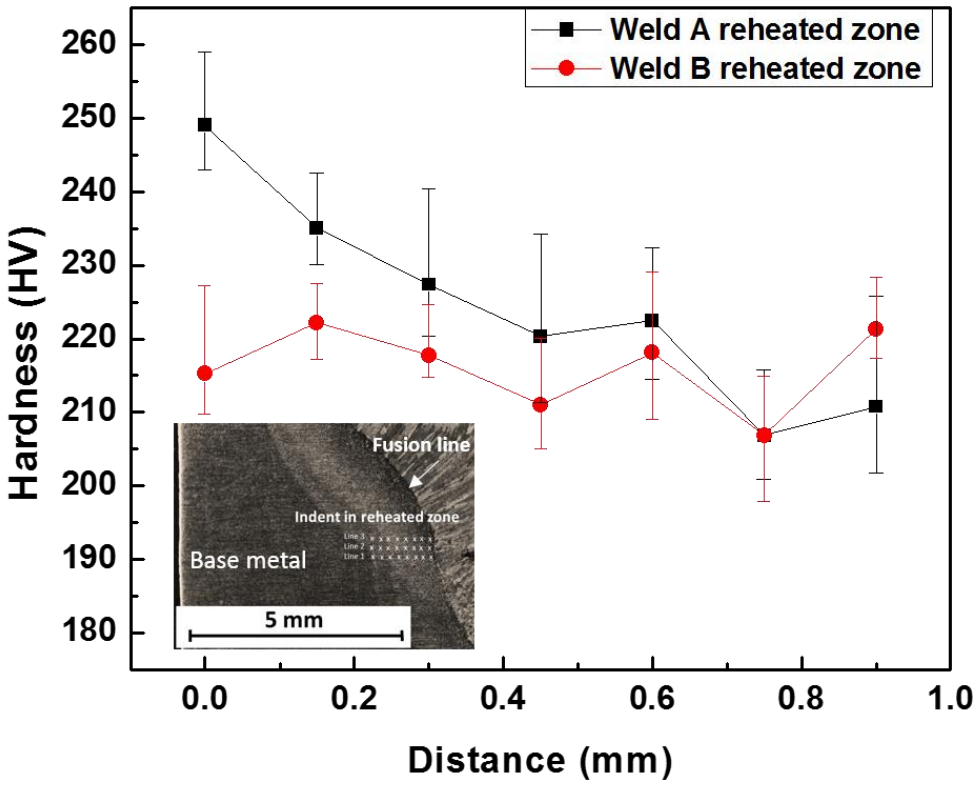

Figure 4-5 : Average (three lines) hardness comparison in reheated zone between weld A and weld B, where "0" distance represent the fusion line

The microstructure adjacent to hardness indent between 0.4-0.6 mm for both welds shows a similar ferrite grain size but only differing in the fraction of black phases which are indicated by

arrows in Figure 4-4a&b. LePera etchant is used in both of the welds keeping the above hardness indents in the reheated zone to ensure a similar location comparison (Figure 4-6). LePera etchant showed that there are numerous white particles around those indents whose size vary between 0.2 to 4.0 μm. The MA particles of the weld A reheated zone are coarser than for weld B (Figure 4-6). Three images (120 μm x 120 μm) were used to average the volume fraction of MA. Image analysis quantification revealed that the reheated structure in weld A contains 5% MA while that of weld B contains 3% MA. This indicates that a higher fraction of MA leads to higher hardness in the reheated zone of weld A, which agrees with an increase in hardness stemming from MA as reported elsewhere [56]. Akselen et al. reported critical MA fraction (minimum 6%) [120] had an influence on mechanical properties while Li et al. define the effect of MA based on critical diameter (~2 μm) [73].

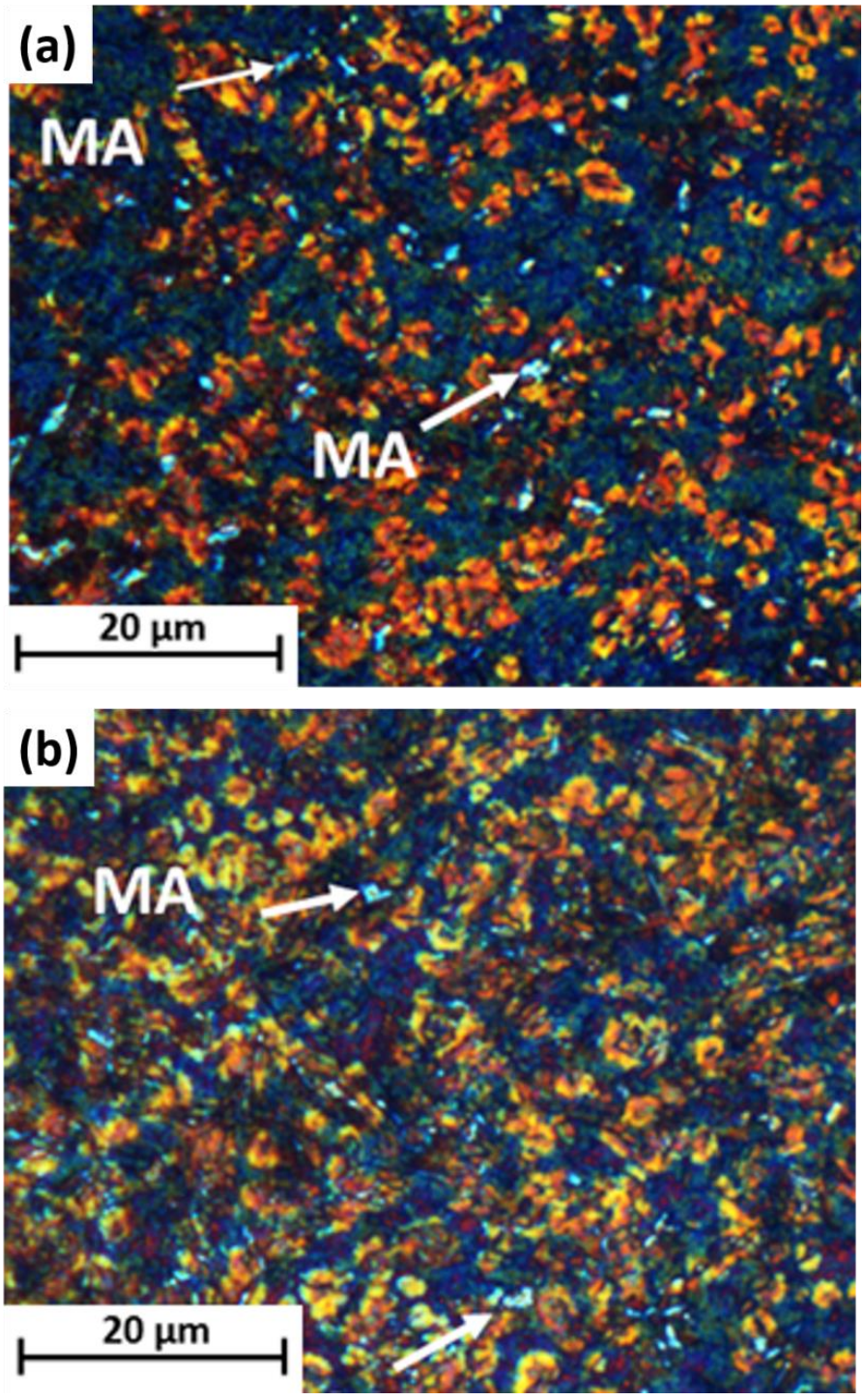

Figure 4-6 : Microstructure observed following application of LePera etchant for weld A and weld B (a) weld A reheated zone (b) weld B reheated zone

4.5 **SEM investigation of MA**

SEM observation in the reheated zone microconstituents indicated presence of two different structures of MA. One of the MA microconstituents shows uniform solid structure inside which is presumed as untempered MA (Figure 4-7a). Villela etchant on this untempered MA shows contrast inside the MA microconstituents (Figure 4-7b). The black smooth regions inside the microconstituents are presumed as austenite while the other regions are martensite. Lambert et al. was successful in distinguishing martensite and austenite inside MA using Villela etchant [75]. The other MA structure (see Figure 4-7c) might contain some carbides inside the grain, which would correspond to tempered martensite. It had been reported that tempered martensite can occur in the reheated zone when multipass welding is performed [78], related to the existence of MA in the single thermal cycle HAZ.

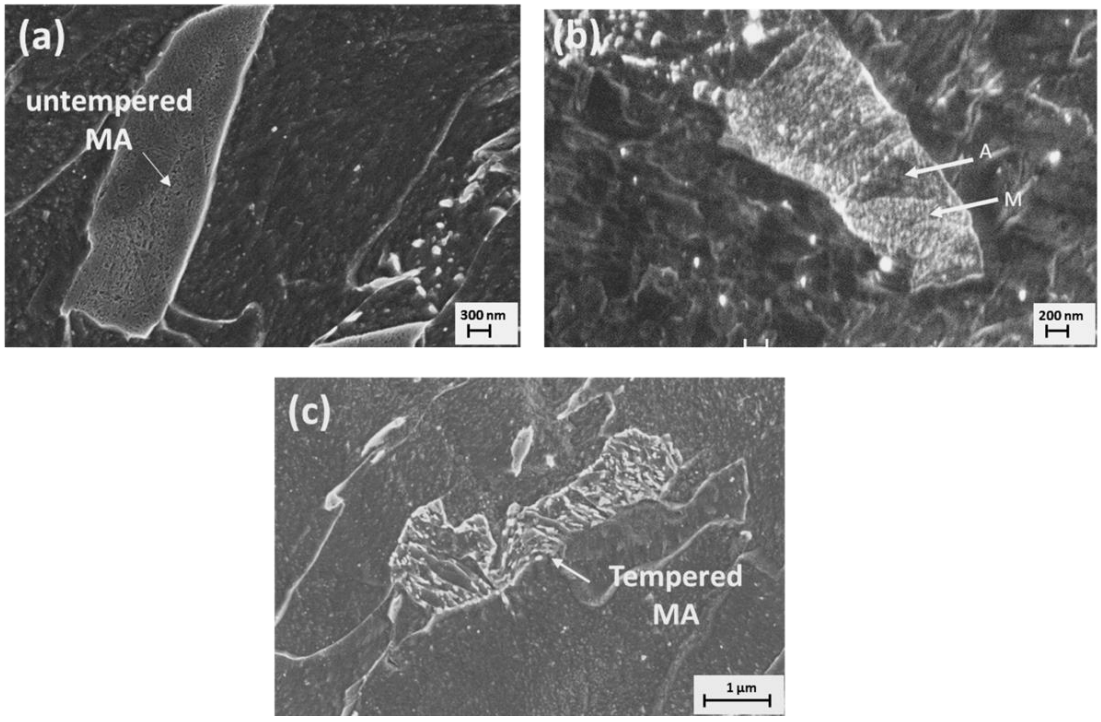

Figure 4-7 : SEM observation of MA in the reheated zone of weld A and weld B (a) untempered MA (2% Nital etchant) (b) untempered MA appearance after performing Villela etchant (c) tempered MA (2% Nital etchant)

LePera etchant on the single thermal cycle sample showed the existence of MA particles in the CGHAZ, which was also reported in other work [75]. Formation of MA during the first thermal cycle had also been reported [60], and during a single thermal cycle with different finish rolling temperature as well [55]. It was found that the formation of MA may occur during the austenite to bainite transformation. The mechanism by which MA form was explained as involving carbon rejection from the bainite to the austenite during transformation, thereby enriching austenite in carbon and stabilizing it to lower temperatures. Subsequently, carbon enriched austenite transforms into MA due to fast cooling in the first thermal cycle. The percentage of MA can vary from 0 to 4% depending on bainite transformation temperature [55]. Super saturated ferrite theory and carbide precipitation mechanisms can also explain the formation of MA [121], however, carbon diffusion and carbide precipitation theory are more commonly suggested [121]. This mechanism might lead to the formation of MA in the CGHAZ of weld A and weld B. Moreover, there could be formation of MA in the ICHAZ during single thermal cycle because of intercritical heating. Subsequently, the MA in the CGHAZ and ICHAZ may get tempered when another pass of welding is performed. The presence of tempered MA in ICRCGHAZ had been reported by Hrivnak et al. [78]. However, it is suggested that the white particles in the reheated zone in Figure 4-6 essentially represent untempered MA rather than tempered MA, since the tempered MA does appear white in colour using LePera etchant.

4.6 EBSD of reheated zone

The band contrast which represents the average intensity of Kikuchi bands with respect to overall intensity within the EBSP (Electron backscattering pattern) was determined for reheated zone. EBSD results show very high EBSD band contrast between the MA and ferrite for both weld A and weld B (Figure 4-8a&d) reheated zone. The EBSD software was unable to index the interior of the MA regions (appearing as a black phase), likely because of the fine structure with high misorientations and lattice strains of the martensite. The KAM (Kernel Average Misorientation) profile in reheated zone showed that there is considerable misorientation (based on 15° criteria for high angle misorientation observation) in the structure (Figure 4-8b&e). The 15-degree was used since 2-degree map did not show difference of misorientation difference between MA and ferrite, and 15 degrees is the widely accepted limit for most alloys as the maximum misorientation that a

boundary can still be easily represented as an array of dislocations. High band contrast between MA and the ferrite matrix was also reported by Li et al. [73].

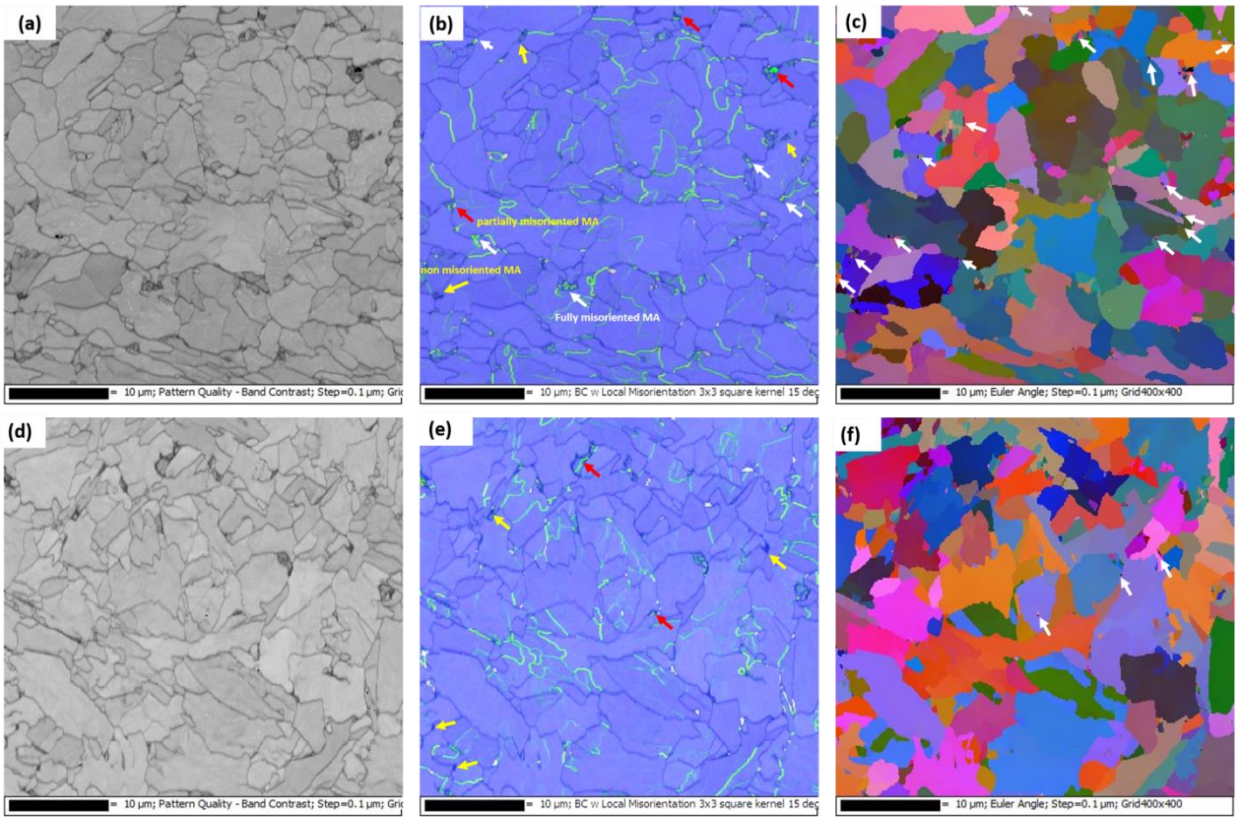

Figure 4-8 : EBSD band contrast maps for ferrite and MA (a) weld A reheated zone and (d) weld B reheated zone; EBSD KAM misorientation (15°) maps inside MA and surrounding matrix (b) Weld A and (e) weld B; Euler orientation maps for (c) weld A and (f) Weld B

It is notable that not all of the MA exhibits misorientations with more than 15° (Figure 4-8b&e). It can be also observed that some MA grains contain (mostly in boundaries) entirely with more than 15° misorientation (white arrow), while for some MA regions, where fraction of an MA area have misorientation greater than >15° mixed with fraction MA area have less than misorientations 15° (red arrow). In addition to the observation that some MA does not have any 15° misorientation regions, there is also a lower band contrast with ferrite in most of the cases (yellow arrow). The difference in misorientation distribution inside the MA might relate to a difference in martensite versus austenite fraction. MA with a martensite dominant structure

contains primarily more than 15° misorientation boundaries. Mixed misorientation might relate to combination of martensite and austenite as in Figure 4-7b, where austenite is presumed to have lower misorientation boundaries than martensite. Likewise, the tempered MA (Figure 4-7c) does not have misorientation more than 15° inside it. It is found that the percentage of untempered, mixed MA and tempered MA grain are 11%, 58% and 31% respectively for weld A reheated zone (Figure 4-8b), while for weld B the percentages are 15%, 45% and 40% respectively. From the Euler map, it can be seen that there are regions which appear black area because of the high angle misorientations (Figure 4-8c&f). However, it is noticeable that not all MA regions are necessarily plotted in black in the Euler map (which illustrate crystal orientations across the area), with some boundaries appearing black. These dark areas within the MA indicate high angle misorientations, as also reported by Han et al. for X80 steels [12]. In addition, it was reported that there are high dislocation densities inside MA [41, 122].

Moreover, when the MA constituents are closer together, the adjacent misorientations in the ferrite are locally increased. The 2° KAM misorientation mapping indicates that numerous ferrite grains go under significant misorientation when the MA regions are closely spaced (0.5-1 μm). Okada et al. showed that high strain fields are found in the ferrite around MA, and showed using finite element analysis that this could lead to crack initiation or debonding [123]. Stresses induced in the ferrite because of the close spacing of MA were found to be important for the crack initiation and debonding mechanisms [8]. The spacing of MA was also important for void formation which can promote fracture, as reported by Kim et al. [59]. Davis and King also proposed that the mechanism of debonding occurs when two MA regions of MA are close to each other [56].

4.7 TEM analysis of MA

A sample carefully prepared from the reheated zone of weld A allowed investigation of the internal structure of MA. The bright field image from one of the small MA grains is shown Figure 4-9a. Electron diffraction patterns from the MA grain suggest the presence of a BCT structure (martensite) with $(0\bar{2}0)$, $(1\bar{1}0)$, $(2\bar{2}0)$ reflections and FCC structure with $(11\bar{1})$ and $\bar{1}1\bar{1}$ reflections (Figure 4-9b). Existence of martensite and austenite has been also observed in another

area of MA (Figure 4-9c). Both blocky (0.5-2 μm in length, 0.5-1.00 μm width) and slender MA (1-5 μm length, 0.3 μm width) is observed in TEM (Figure 4-9d).

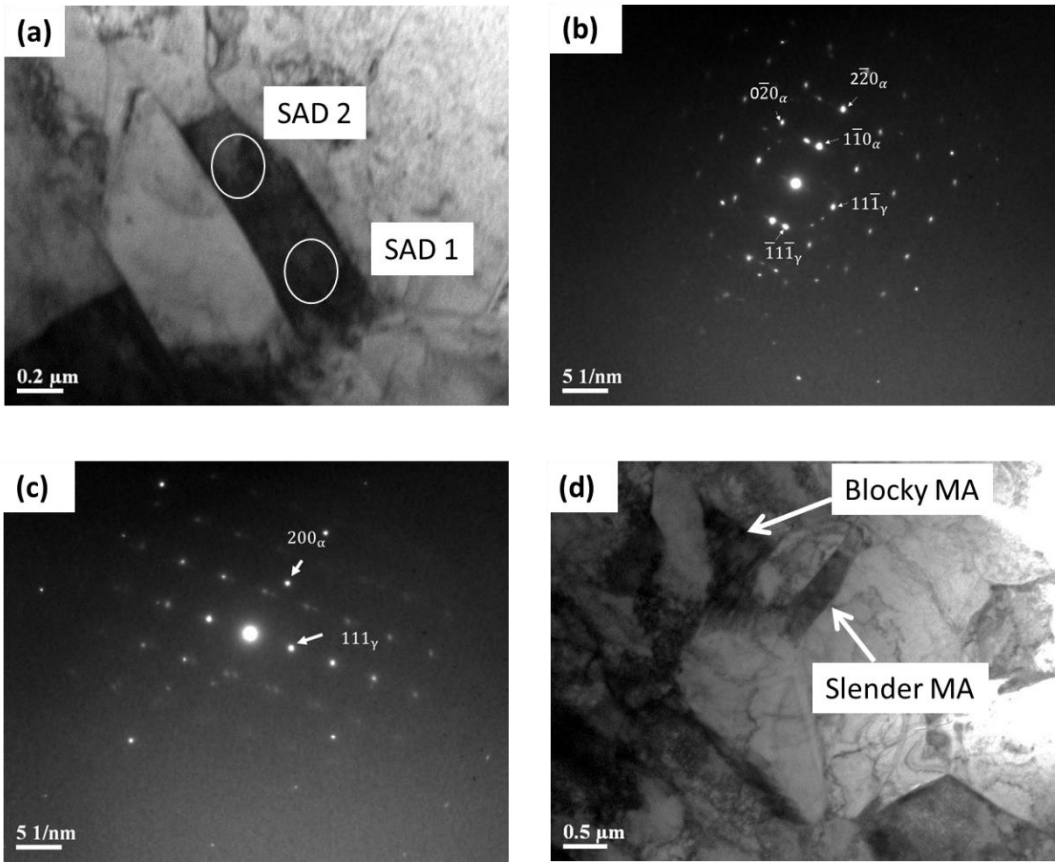

Figure 4-9 : TEM of MA a) bright field image b) diffraction pattern form MA (SAD 1) c) martensite and austenite inside MA of weld A (SAD 2) d) blocky and slender MA

4.8 Nanoindentation

The load-displacement curve from nanoindentation is shown in Figure 4-10. It is found that the untempered MA hardness is 6.10 GPa, whereas, the ferrite hardness is 2.86 GPa, indicating that the hardness of MA is almost twice the hardness of the ferrite matrix. The hardness value of MA is significantly higher than the hardness value of MA (~510 MPa) reported by Xu et al. using nanoindentation [124]. The high hardness of MA in comparison to matrix had been also reported by Janovec et al. [113], which can create a significant internal stress in the ferrite matrix.

In addition, when two MA constituents are close to each other, the overlapping stress on the ferrite matrix can cause debonding of MA and void formation at the MA/ferrite interface. Li et al. and King et al. concluded that the higher hardness of MA [124] induces stress on the softer ferrite matrix which was due to volume expansion during austenite to martensitic transformation [8, 58]. This difference in hardness can lead to debonding or void formation during the application of strains under load.

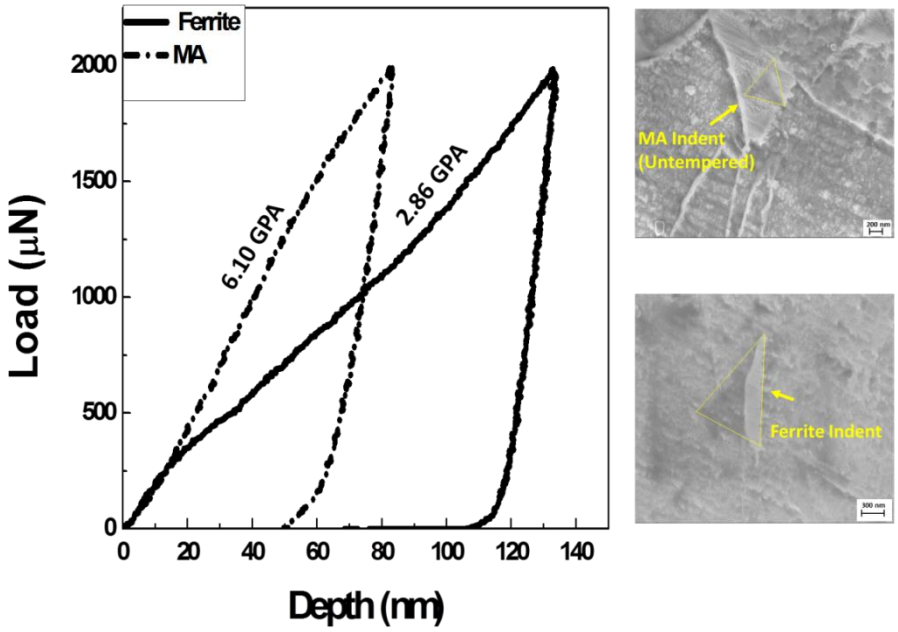

Figure 4-10 : Comparison of hardness between MA and ferrite matrix using nanoindentation

4.9 Tensile test comparison

Tensile response is evaluated for base metal and welded samples. Strain is measured by using both a mechanical extensometer and DIC. The tensile sample for welded is produced from the reheated zone in such a way that the reheated zone remained approximately in the middle part of the tensile specimens. Moreover, the total area of weld metal within the tensile specimens gauge length is kept similar for both welds. The tensile specimens HAZ width for weld A varied from 1.36 to 2.35 mm, while for weld B, it varied from 1.36 to 1.74 mm. It had been reported that the higher diameter wire of weld A will increase the weld bead width in comparison to smaller wire diameter if the chemical composition is kept constant (wire A had 0.075 mm greater diameter than

wire B) [125]. This suggests that the larger diameter of wire A will promote more heat to flow in the transverse direction of the plate which causes a higher HAZ width in weld A. Moreover, it is suggested that the higher weld metal deposition in cap pass of weld A than weld B might subject the CGHAZ of weld A to higher temperature than Ac1 which might lead to more MA formation in the reheated zone of weld A than weld B. A higher area fraction of MA with higher heat input and higher second thermal cycle peak temperature were reported [126].

4.9.1 Tensile test using mechanical extensometer

The average base metal yield and tensile strength in hoop direction is 662 ±23 MPa and 770 ±4 MPa with elongation of 21%. The average yield and tensile strength for weld A is 575 ±10 MPa and 664 ±24 MPa respectively, while it is 507 ±66 MPa, 592 ±60 MPa for weld B. The overall elongation across the gauge length of the transverse weld sample is 10.2% for weld A while it is 19.2% for weld B based on the mechanical extensometer. However, these values do not reflect the local strain accumulation that occurs near the fracture locations

4.9.2 Tensile test using DIC

The DIC virtual extensometer tools indicate an elongation along the gauge length of 10.7% for weld A while for weld B it is 13.0%. However, the most important feature observed via DIC is that it provides local strain field measurements. It is observed that during the tensile tests, the CGHAZ near the cap pass started to yield first for both welds. Then the strain gradually transmitted to the HAZ of fill passes. Due to the high heat input in the cap pass, the HAZ near cap pass will soften more readily than the HAZ of the reheated zone due to the presence of more upper transformation products. However, strain accumulation is not significant in base metal and weld metal in comparison to HAZ. The local strain measurement in the base and weld metal indicated that there is maximum 2% accumulation of strain in the weld metals and a maximum 2% strain accumulation in base metal during tensile tests. In tensile tests, the force applied is initially distributed uniformly across the whole gauge length. However, as testing continues, the accumulation of strain occurs in the HAZ on both sides of the weld. Finally, stress is localized in one HAZ, at which point failure occurred. Therefore, it is more appropriate to correlate the stress of tensile machine with strain in the failed HAZ points. It is to be noted that DIC virtual

extensometer strain measurement is different from local strain measurement due to the non-uniform properties and elongations across the gauge length. So, the strain from five points along the fractured HAZ is calculated and plotted against stress, shown in Figure 4-11. It can be noted that there is a difference in yield strength, tensile strength and elongation between the two welds.

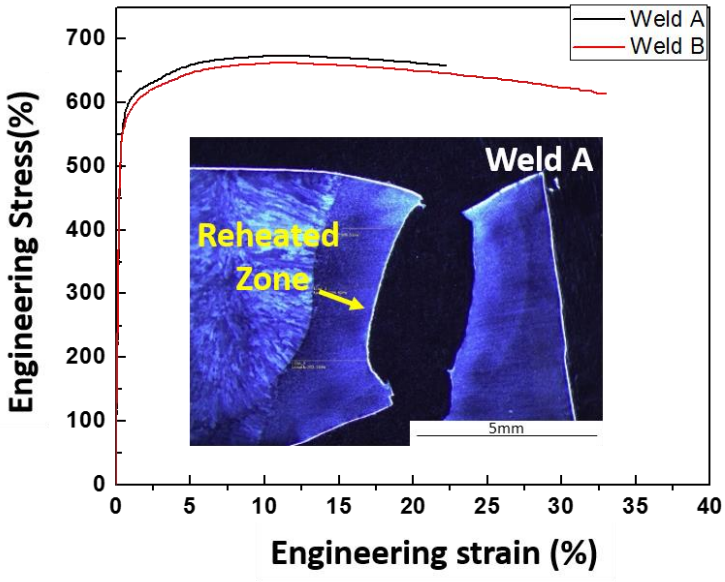

Figure 4-11 : Stress–Strain curve comparison between weld A and weld B using DIC (averaging strains at 5 points along fracture location).

The strain distribution along a line (line AB-connected dot, in this case as shown in Figure 4-12) of HAZ in the fracture zone for the two welds is shown in Figure 4-12; where index along X-axis represents number of points (in this case 10 points) in line AB for which strain was monitored. It can be seen that the total strain at those points of weld B is higher than weld A. This might mean that throughout the tensile tests weld B was undergoing more deformation than weld A with the same loading condition. That suggests a higher fraction of MA in weld A HAZ can provide higher strength. However, a lower fraction of MA in weld B HAZ might gave less strengthening to its HAZ, which can result in low tensile and yield strength, but provides higher elongation. Increasing strength with the presence of MA has been reported by several researchers from a standpoint of composite reinforcement in terms of the rule of mixtures [12, 97, 117]. Hence, it might be concluded that the higher fraction of MA in the weld A HAZ might provide higher

tensile strength, at the expense of lower elongation, which agrees with the suggestion by Hrivnak et al. who reported that MA could impair ductility [80].

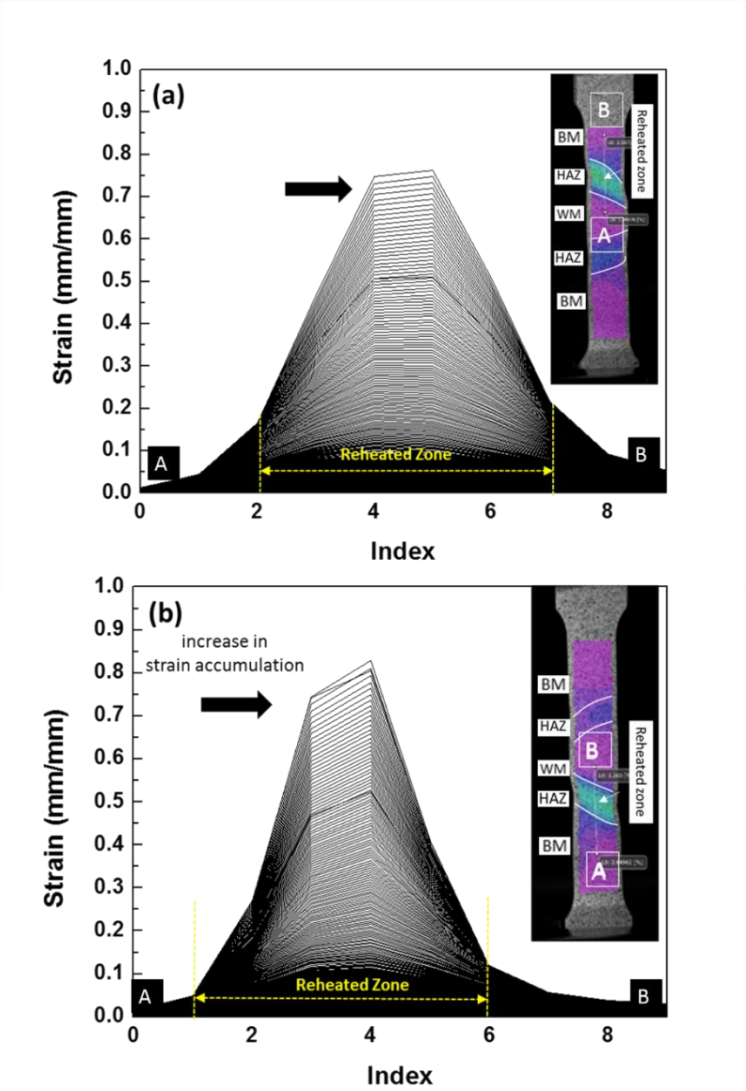

Figure 4-12 : Comparison of strain distribution across HAZ fracture location for a) weld A and b) weld B

To investigate the deformation of the reheated zones, one of the tensile test samples for both welds were stopped intentionally just before failure. It can be clearly seen that the weld B reheated HAZ underwent significant deformation while deformation in weld A reheated zone is not significant as observed using a stereoscope (Figure 4-13a&b). The microscopy from the reheated zone of tensile fractured specimen for both of the weld samples is shown in Figure

4-13a&b. SEM observation from the reheated zone of weld B suggests that exhibits more strain than the reheated zone of weld A (Figure 4-13c&d). Since the grains in this region are initially equiaxed before deformation, to determine the differences in localized strain in the reheated zone for both welds, the values were calculated based on the ratio of horizontal to vertical linear intercept lengths of the grains, L_h/L_v. L_h is the measurement of grain length along straining direction whereas L_v is the grain size measurement in the transverse direction of straining direction. At least three images were used to determine L_h/L_v, and the calculated average is reported. The average value of L_h/L_v ratio for weld A reheated is 1.22, in comparison to weld B which is 1.54. This results also showed that weld B reheated HAZ underwent more deformation than weld A HAZ. It can also be observed that MA takes on the directionality along the tensile test axis in weld B HAZ (Figure 4-13b).

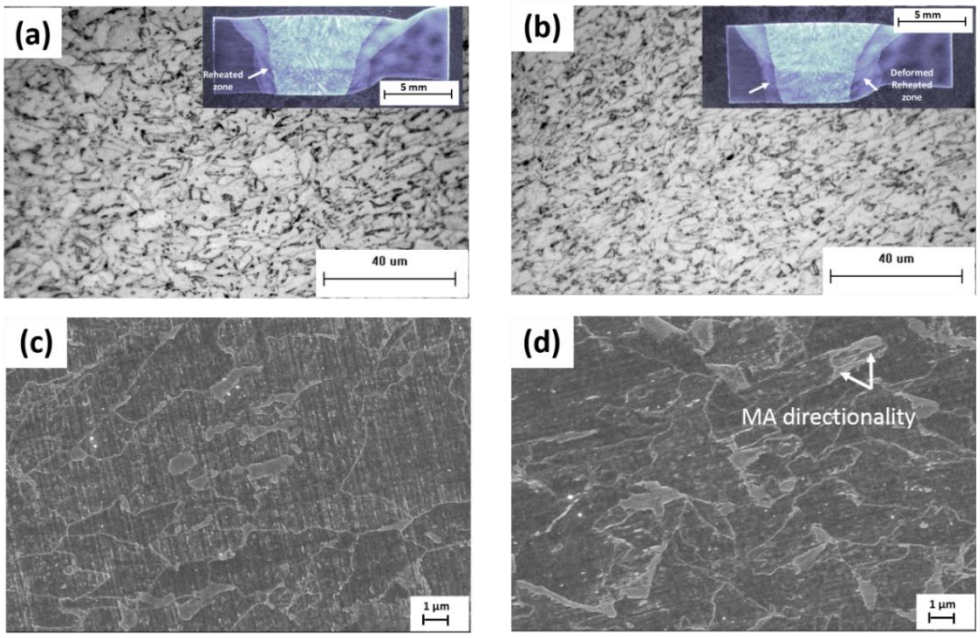

Figure 4-13 : Optical and SEM micrographs (2% Nital etchant) showing evidence of strain accumulation in reheated zone of weld A (a&c) and weld B (b&d)

Hardness is measured near the fractured zone for both welds. It is seen that the hardness of weld B near the fracture is higher than in weld A. The average hardness for weld A is 265.8 ±5 HV while it is 280.2 ±5 HV for weld B. The greater hardness near the fracture might suggest that weld B HAZ experienced more deformation during tensile test. This might suggest that the degree

of strain hardening in the weld B reheated zone is more significant than in weld A. Hardness is also measured across reheated HAZ zone on both sides of the welds. The result is shown in Figure 4-14. The comparison of Figure 4-5 hardness and Figure 4-14, indicates that the hardness is higher in Figure 4-14 for both welds. This indicates that straining of both welds leads to a hardness increase in the HAZ after tensile testing. One can also see that the hardness in the fractured side of weld A is higher than the unfractured side. From the DIC measurements, it is observed that stress accumulation occurs in both sides of weld with the start of tensile test. However, after certain strain, the stress started to concentrate in particular HAZ and failure occurred in that HAZ. This implies that the HAZ near the fractured surface underwent more strain than the HAZ on the other side of the weld. Higher strain leads to higher hardness near the fractured surface than the other side of HAZ. A similar phenomenon has been observed for weld B HAZ (Figure 4-14b).

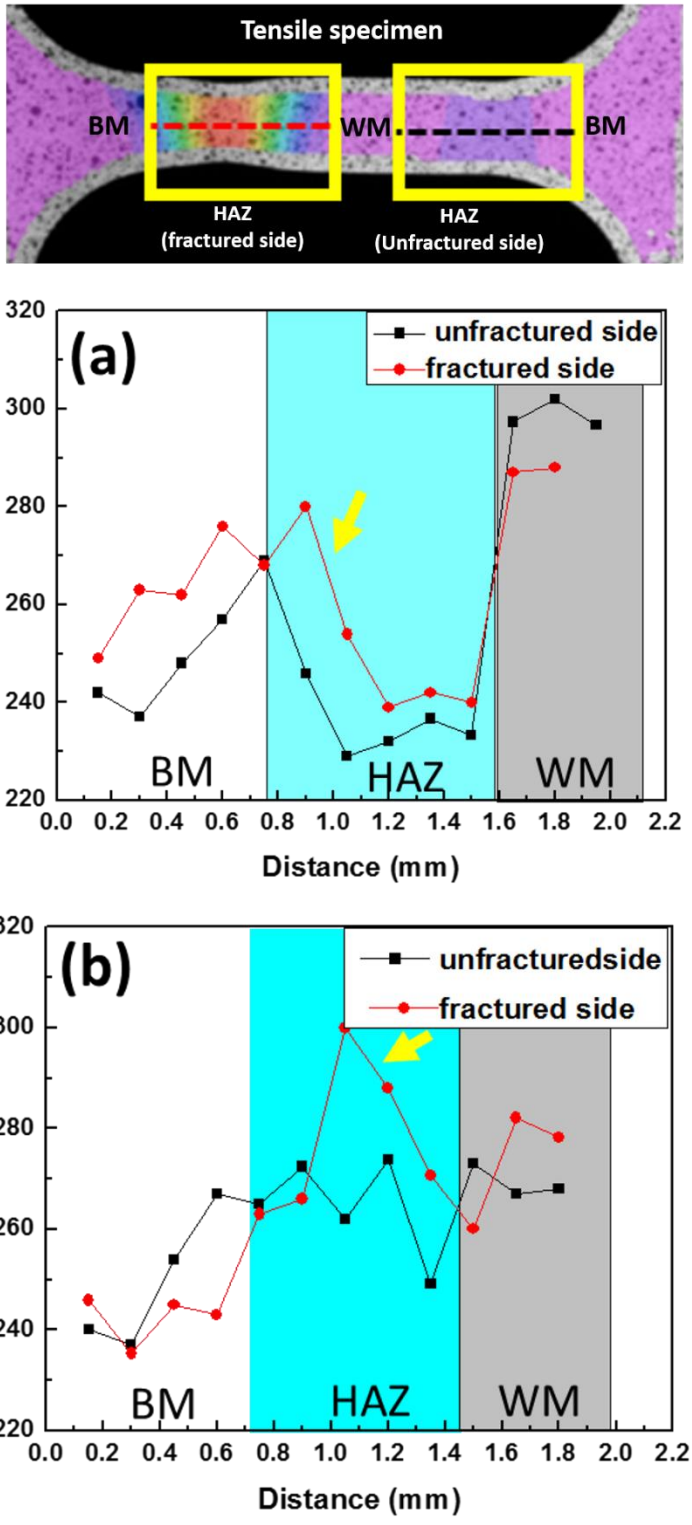

Figure 4-14 : Hardness comparison of reheated zone in both side of weld a) weld A b) weld B (arrow mark in the graph represents the fractured location)

Figure 4-14a&b revealed that the hardness of reheated zone in both side of the weld B is higher than in weld A reheated zone. However, from Figure 4-5 it can be seen that the hardness of reheated zone of weld B is lower than weld A before tensile test; this does suggest that the hardness of the reheated zone of weld B after tensile test increased more significantly than weld A. All these results suggest that weld B reheated HAZ has undergone more deformation during tensile test than the reheated HAZ of weld B. LePera etchant showed numerous white particles close to the fracture of weld A, however there are few MA close to the weld B fracture.

A higher fraction of MA provides better strength but prevent deformation in the HAZ. Increases in the tensile strength with increase of MA fraction is reported by Han et al. [12]. Coldren et al. reported an increase of 6.86 to 11.77 MPa in tensile strength with increase of 1% MA fraction [127]. It has been reported that grain boundaries or MA are more influential than the grain size for increasing strength [128]. Increased MA fraction can generate mobile dislocation between the interface of MA/ferrite interface which can essentially increase the tensile strength [128]. In addition, Tian et al. reported that MA will prevent dislocation movement and thereby increase tensile strength, and concluded that MA provides dispersion strengthening [107].

The microstructure of the fractured samples reheated zone close to the fracture exhibit that all the regions of weld A contained a higher fraction of MA than weld B. The quantification comparison for both welds is shown in Figure 4-15. It can be observed that weld A contains a higher fraction of MA in comparison to weld B. Moreover, a higher fraction of MA is associated with larger MA (Figure 4-15). However, the MA size in weld A reheated zone is higher than in the weld B reheated zone. The existence of larger MA was associated with a high volume fraction of MA, as reported by Li et al. when studying high niobium (0.031%) steel [129].

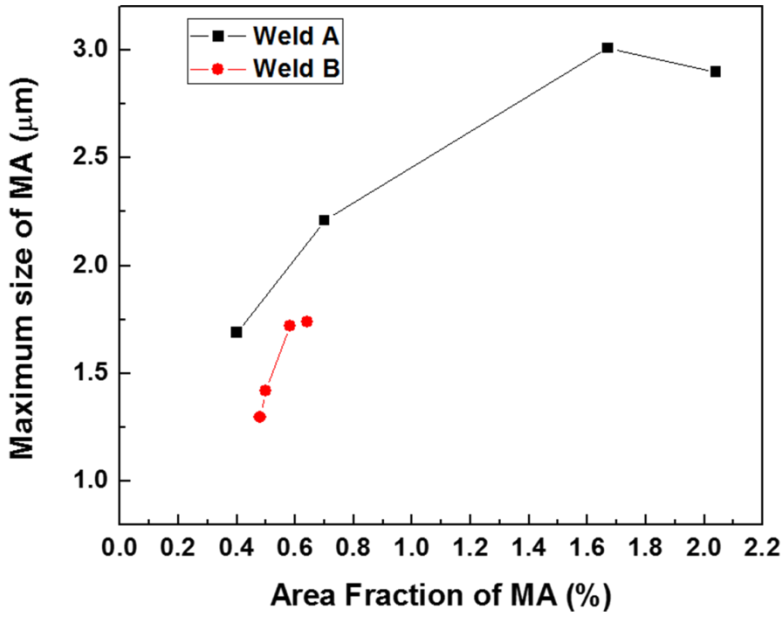

Figure 4-15 : Relationship between MA fraction and size for weld A and weld B

The high volume fraction of MA in the HAZ of weld A might also mean that this reheated zone might have experienced higher intercritical peak temperature which caused more CGHAZ area to be reaustenitized, and the subsequent cooling caused a high volume fraction of MA. A higher volume fraction of MA with higher intercritical peak temperature has also been reported by other researchers [75]. Moreover, the higher peak temperature can lead to larger prior austenite grain size and it had been reported that the higher the prior austenite grain size, the size of MA is coarser [73].

4.10 Fractography of tensile specimens

To investigate the failure mechanism, SEM observations are performed close to the fractured tensile surface, in reheated zone for both of the welds. Numerous large voids are found close to the fracture surface in the HAZ of weld B (Figure 4-16a) which are quite large, and it is not possible to identify the source of voids from Figure 4-16a. A slender morphology MA is also observed to be fragmented due to significant straining which was also reported by Chen et al. [99]. SEM

observation away from the fracture surface showed that the source of those voids is between the intersections of two MA (Figure 4-16b&c).

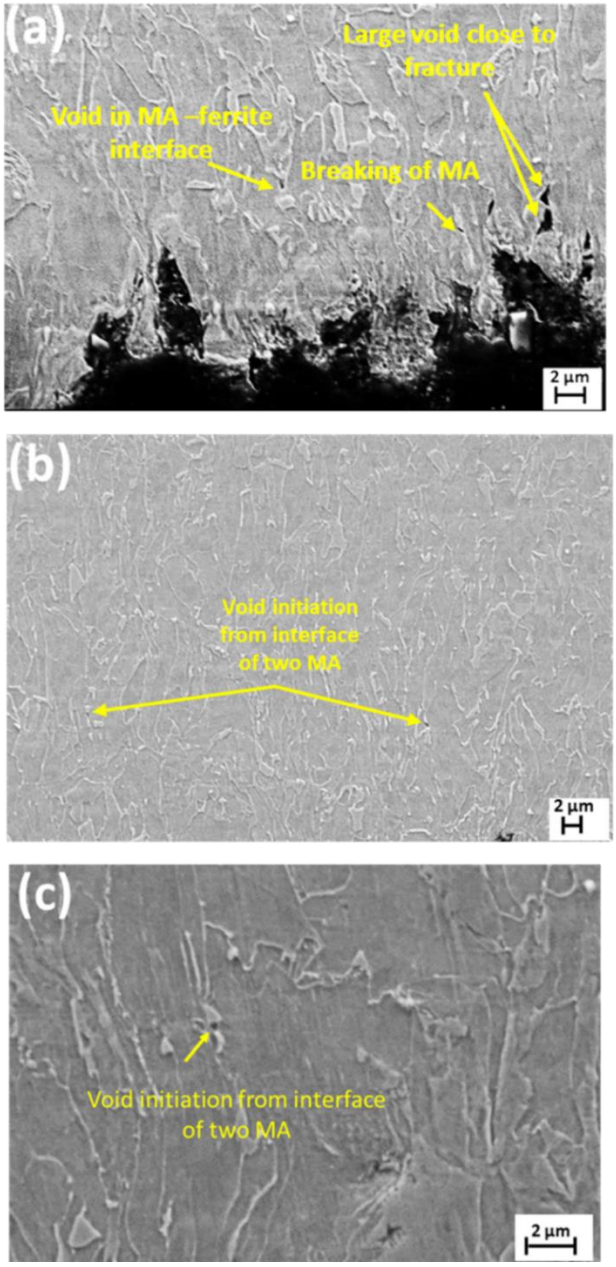

Figure 4-16 : a) Voids near fractured tensile specimen of weld B (b) voids away from fractured surface (2% Nital) (c) voids at the interface of two MA (2% Nital)

More extensive void formation is observed close to the weld A fractured surface, since the percentage of MA is high and they are closely spaced (Figure 4-17a). Residual overlapping stress on the matrix due to the high hardness of closely spaced MA might lead to the formation of observed holes or pits. Moreover, some slender MA is found debonded and fragmented but within the matrix (Figure 4-17b). Kim et al. also reported the fragmentation of slender MA due to high deformation surrounding the matrix [59].

Some of the MA is found completely debonded from structure (Figure 4-17c). In some case, part of some MA is found missing and created pits opposite to the MA microconstituent, while the other half is found retaining the grain in its position in the matrix. Now, it can be seen that the debonded MA is fragmented (Figure 4-17b). Therefore, it suggests that during tensile test, hard MA becomes fragmented and a partial or entire MA microconstituent is pulled out from the matrix.

The observation of base metal fracture surface is found to be significantly different from the samples that fractured in HAZ (Figure 4-17d&e). A significant amount of large voids are found in the HAZ fractured sample. The depth and width of voids is higher than the dimples of the base metal fractured surface. Hrivnak et al. also reported that they found particles inside the tensile fractured surface dimples which was presumably MA or part of MA [80].

It is found that there are no particles in the base metal fractured surface dimples while most of the voids in HAZ fractured sample contain particles inside it (Figure 4-17f). The particles inside large dimples are believed to be MA or fragment of MA, which suggests that MA is acting as sources for void formation, which could lead to premature fracture and impair ductility. This finding supports the mechanism proposed by Kim and Chen et al. who observed fragmentation of MA and void formation during tensile testing [59, 99].

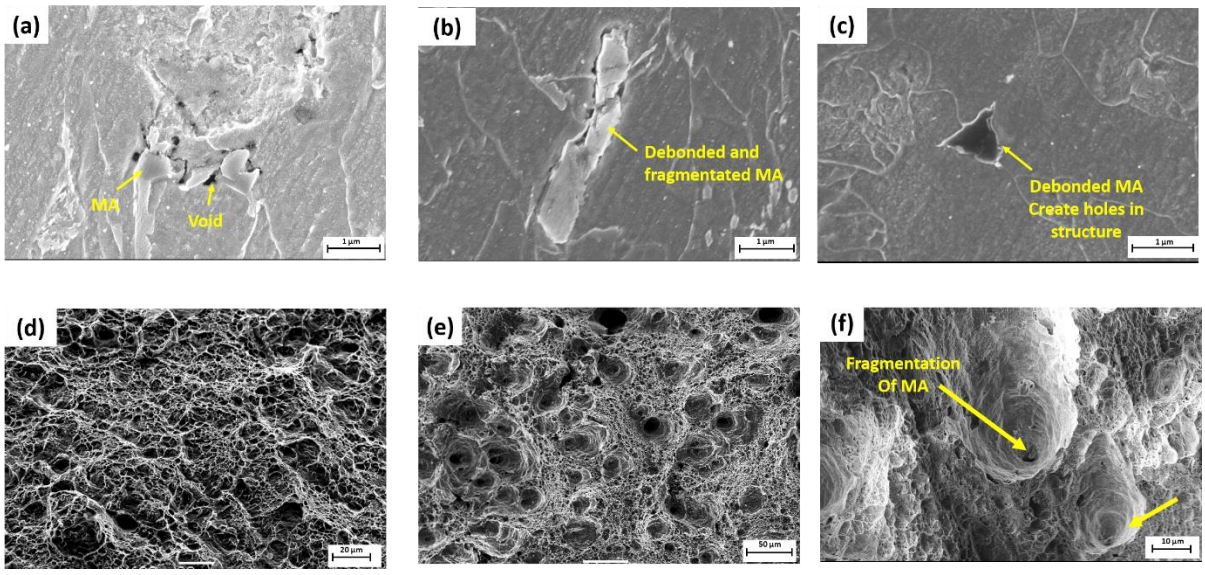

Figure 4-17 : Void formation in weld A (a) voids in closely spaced MA (2% Nital) (b) debonding and fragmentation of slender MA (2% Nital) (c) formation of voids from debonded MA (2% Nital) (d) base metal fracture surface (e) HAZ fracture surface with significant amount of voids (f) particles inside voids

4.11 Voids and debonding initiation stage

It is found that the weld A contain more voids and debonding close to fractured surface than weld B. It is worthwhile investigating void initiation and coalescence stage. To do this, quasi-static tensile tests are performed where the tensile test is stopped just after yield strength and ultimate tensile strength (UTS) for weld A (Figure 4-18a). Initially, the strain localization was determined by observing the video. Five points were chosen across the localization zone and average peak strain was determined. The average peak strain was plotted again stress. It can be seen that there is 5% strain at the yield point while at the ultimate tensile stress the strain is 15%. Investigation in the reheated zone of yield and UTS stopped sample shows numerous voids in MA/ferrite interface and debonding of MA. It is found that debonding is even observed at quasi-static yield point sample (Figure 4-18b). According to Chen et al. [99] and Kim et al. [59], crack initiation or void formation inside MA or the MA/matrix interface occurred at lower strain while an increase of strain causes these voids to grow until at higher strains and the voids coalescence

cause failure. This does suggest that it is probable that crack initiation and coalescence would occur at different stages of the tensile test.

It can be observed that there is higher strain accumulation in the end period of the tensile test (Figure 4-12a&b) as the strain increases at the end of tensile test. However, due to large numbers of voids growing in weld A associated with a higher percentage MA, this led to early fracture by coalescence of voids. However, lower amounts of voids in weld B delayed fracture by void coalescence. The authors believe that the large increase in strain at the end of the tensile test relates to the void coalescence stage which can be confirmed by observation of Figure 4-16a where large voids are found close to fracture. This confirms that void coalescence takes place at the end of test which is also supported by Kim et al. [59] and Chen et al. [99] who concluded that voids or cracks can initiate even at lower strain and coalescence would occur at higher strain.

Lambert et al. used an acoustic emission technique and showed MA as the crack initiation source in the plastic zone by observing high level acoustic events at the end of tensile test [98]. It can be noted in this prior work that there were some low level acoustic events (just after yield point), while high level acoustic events occurred at the end of tensile test [98]. When the tensile was stopped at the high acoustic level event, MA was found as crack initiator. However, details of the metallography used to investigate crack initiation of MA was not given [98] like the position of the crack on tensile specimen. In the current investigation, it is observed that there could be variations in the number of voids or crack initiation from surface to surface based on 3 observations of 0.1 mm at the failure location.

It is observed that coarser and larger MA is mainly responsible for void formation and debonding (Figure 4-18b). It can be also noted that slender MA debond more frequently (Figure 4-17b and Figure 4-18b). King et al. reported that MA and ferrite deform elastically initially in tensile test [8]. At a certain point the ferrite will start to deform plastically and will lead to stress development in MA/ferrite interface which will lead to debonding [8]. Stress development in MA/ferrite interface can occur due to austenite to martensite transformation. It was reported that there is a 4% increase in volume during austenite to martensite transformation which could lead to triaxiality stress in the matrix [8]. Chen et al. [99] observed void formation inside MA at room temperature tensile test, however Kim et al. [59] observed void formation always at the MA/ferrite interface.

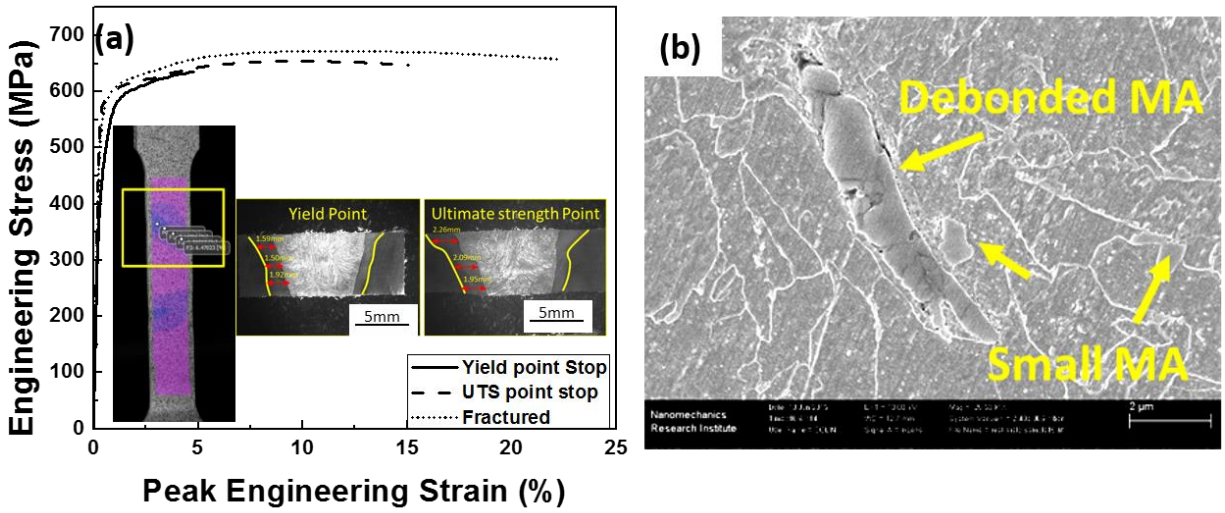

Figure 4-18 : a) Quasi static tensile test of weld A at fracture, yield strength and ultimate tensile point b) debonding of slender MA in the reheating zone at the quasi static tensile test (yield point stop).

In the current investigation, MA is found mostly debonded from the structure instead of breaking, which might suggest that segregation and volume expansion of martensite might weaken the MA/ferrite interface. Lambert et al. had reported that the interface of ferrite/austenite phase of MA (austenite in periphery) was enriched in carbon using convergent beam electron diffraction measurement [75]. Subramanina et al. also showed the carbon enrichment in MA/matrix interface using atom probe characterization [130]. It had been reported that carbon diffusion is slow in austenite during cooling [131, 132] which could lead to carbon enrichment in MA/ferrite interface. Moreover, volume constraints can stabilize the austenite in periphery of MA which could lead to carbon enrichment in MA/ferrite interface. It had been also shown that slender MA contains high carbon using Auger spectroscopy [133]. Moreover, Matsuda et al. reported that elongated MA decomposed more quickly than the blocky MA during tempering [134]. In current study, elongated MA has observed to contain lath of martensite, which is shown in Figure 4-19.

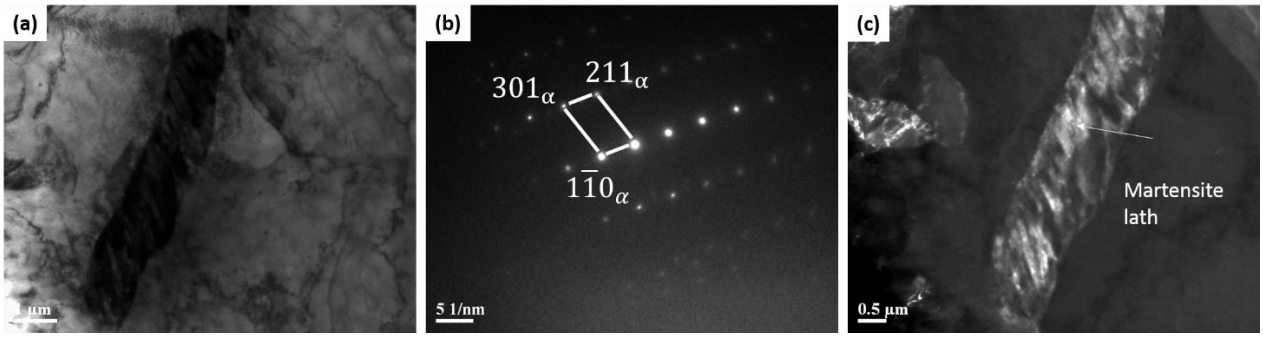

Figure 4-19 : (a) Bright field image of slender MA (b) SAD pattern from MA (c) martensite lath in slender MA(using $1\bar{1}0_\alpha$ spot)

These results all suggest that the elongated MA and ferrite interface is enriched in carbon. The MA/matrix interface might weaken by carbon segregation as previously reported [135], and moreover the interfacial energy of stringer MA is significantly lower than blocky MA which could lead to debonding [58]. King et al. observed debonding even in a tensile test which was performed at 196°C [8]. Stevenson et al. reported that MA interface might weaken by carbon segregation [136]. Hence, these suggest that MA could debond easily from the matrix.

It is also important to notice the orientation of slender MA to the tensile axis. The stringer MA in Figure 4-18b was found almost 45° to the tensile axis which is the preferred shear direction. The orientation of slender MA to the tensile axis could also affect the tensile strength and ductility. Kim et al. [59] and Tian et al. [107] reported that micro-voids can form more easily in stringer MA/ferrite interface than blocky MA/ferrite interface. These all suggest that the presence of MA in the reheated zone could impair the ductility severely, which is consistent with a high fraction of MA in the weld A reheated zone which exhibited lower elongation to failure.

4.12 Summary

1. A higher fraction and coarser MA in the weld A reheated zone was associated with the higher tensile and yield strength than weld B which contain low fraction of MA. However, weld A exhibited lower elongation then weld B.

2. Voids formation from MA/ferrite interface and MA debonding deteriorate ductility. Higher fraction of MA and coarser MA in weld A HAZ causes more voids formation and

debonding, which leads to more deleterious effect on ductility. Coalescence of those voids lead to early failure in weld A HAZ and causes poor ductility. MA was found to have more significant effect on ductility by formation of voids and debonding.

3. Voids and debonding due to MA was found to occur at the quasi-static yield point in tensile tests, which suggest MA can deteriorate the ductility significantly.

Chapter 5 : Effect of Martensite-Austenite (MA) Distribution on Mechanical Properties of ICRCGHAZ of X80 Linepipe Steel[2]

5.1 Overview and background

Chapter 4 showed the difference in MA fraction and size lead to difference in strength and ductility. However, which parameter between MA fraction and size is more contributing to the detrimental properties was not clear. Moreover, heat input, hardness of the weld metal, HAZ size between two welds can have contribution to variation in results. Hence, the goal of current study was to determine most contributing factor among MA fraction, size and morphology on tensile properties of localized ICRHAZ microstructure in X80 linepipe material subjected to Gleeble testing (thermal cycling heat treatments). Two different distributions of MA with varying sizes were produced by double heating cycle with two final cooling rates, while the same peak temperature is maintained for both first and second heating periods. This allows one to maintain a similar total fraction of MA, allowing study the effect of MA size on tensile properties (along with void formation phenomena).

5.2 Experimental procedure:

Rectangular sections with dimensions of 100 mm x 10 mm x 1mm were produced from the transverse direction of an X80 linepipe steel with a 15 mm wall thickness. The rectangular middle section was subjected to a first thermal cycle with a peak temperature of 1350°C at a heating rate of 300°C/s and cooled at 14.4°C/s to room temperature to simulate the coarse grain heat affected zone (CGHAZ) of joints produced by either GMAW or SAW. A 100°C preheat was applied before performing the first thermal cycle. The corresponding heat input for the thermal cycle was 0.78 kJ/mm. The cooling rate was measured across the length of the rectangular section to ensure a uniform 300°C/s heating rate and 14.4°C/s cooling rate zone along the length of the controlled

2 This chapter will be submitted soon for publication by Nazmul Huda, Yiyu Wang, a Leijun Li and Adrian P. Gerlich. The simulation part was performed by Yiyu Wang, University of Alberta

zone by attaching K-type thermocouples at different locations. These heating and cooling rates were maintained across a 12 mm gauge length of the section. A second thermal cycle was then applied to a peak temperature of 850°C at a 300°C/s heating rate, followed by cooling at 2°C/s and 10°C/s to simulate the inter-critical reheated CGHAZ (ICRHAZ). Dog-bone shaped samples were produced from the uniform thermal region as a rectangular section with 12 mm gauge length and 6 mm width in middle. The specimens were loaded at a 1 mm/min crosshead movement, while a digital image correlation (DIC) based strain monitoring system was utilized to measure the localized and global strains.

In order to determine the local stresses produced in the microstructures observed, numerical simulation of the actual grain structures under tensile testing was performed using the Comsol Multiphysics software. A 2D microstructure-based model was generated from the observed structure in SEM images. Two components, including the ferrite matrix and MA constituents, were considered in the model. The mechanical properties (elastic modulus and yield strength) of the two components were taken as 210 GPa for ferrite and 203 for martensite based on recent reports [137].. Free triangular elements were used of meshing. The tensile testing simulation was conducted under the plane strain condition. For the boundary condition, the left edge of the model was constrained and fixed. A symmetry boundary condition was applied for both the top and bottom edges. A boundary load of 417 MPa was applied on the right edge.

5.3 Results

5.3.1 Microstructure

The X80 base metal average hardness is 230 ±10 HV, and contains a mixture of ferrite (83%) and bainite (17%) Figure 5-1a. The microstructures of the CGHAZ microstructure which was cooled at 14.4°C/s cooling rate to room temperature from a peak temperature of 1350°C is shown in Figure 5-1(b). The second thermal cycle microstructures produced from the CGHAZ, following a cooling rate of 2 and 10°C/s from an intercritical peak temperature (between Ac1 and Ac3) of 850°C are shown in (Figure 5-1c&d). A ferrite-plus MA microstructure occurred for both cooling rates, however the size of ferrite and MA is finer for 10°C/s. A higher magnification observation in SEM from both of the microstructures are shown in (Figure 5-1e&f).

A coarser microstructure is produced with a slower cooling rate (2°C/s) while a finer microstructure dominates after a higher cooling rate (10°C/s) is applied during the second thermal cycle. Ferrite grains size were measured in both the second thermal cycle microstructures using three SEM images, and these were quantified using ASTM E112 based on the planimetric method. The average ferrite grain size in the specimen cooled at 2°C/s (7.02 µm) is 2 µm larger than the specimen cooled at 10°C/s. In addition to coarser ferrite grain in specimens cooled at 2°C/s, the MA microconstituent size (3.47 ±2.49µm) is also coarser in the specimen cooled at 2°C/s, versus at 10°C/s which averaged (2.87 ±1.49µm). The average volume fraction for 2°C/s and 10°C/s was 5.7 ±1.4% and 5.8 ±0.7% respectively. Although the total MA fraction is similar in microstructures cooled at either rate (~5.8%), approximately half (~2.7%) area fraction of MA was tempered in 2°C/s while no significant tempering was observed in 10°C/s based on SEM image quantification. The average spacing between MA was determined using the linear line intercept method, revealing a larger spacing of 10 µm when a cooling rate of 2°C/s is applied, versus a spacing of 5 µm when 10°C/s is applied. The fraction of grain boundary MA and MA inside of ferrite grains has been quantified for both microstructures. Only a small percentage of MA was formed inside the ferrite grain in both microstructures, where 85.1% of MA microconstituents formed along grain boundary and triple junctions in the specimen cooled at 2°C/s, which was comparable to 82.4% observed after cooling at 10°C/s.

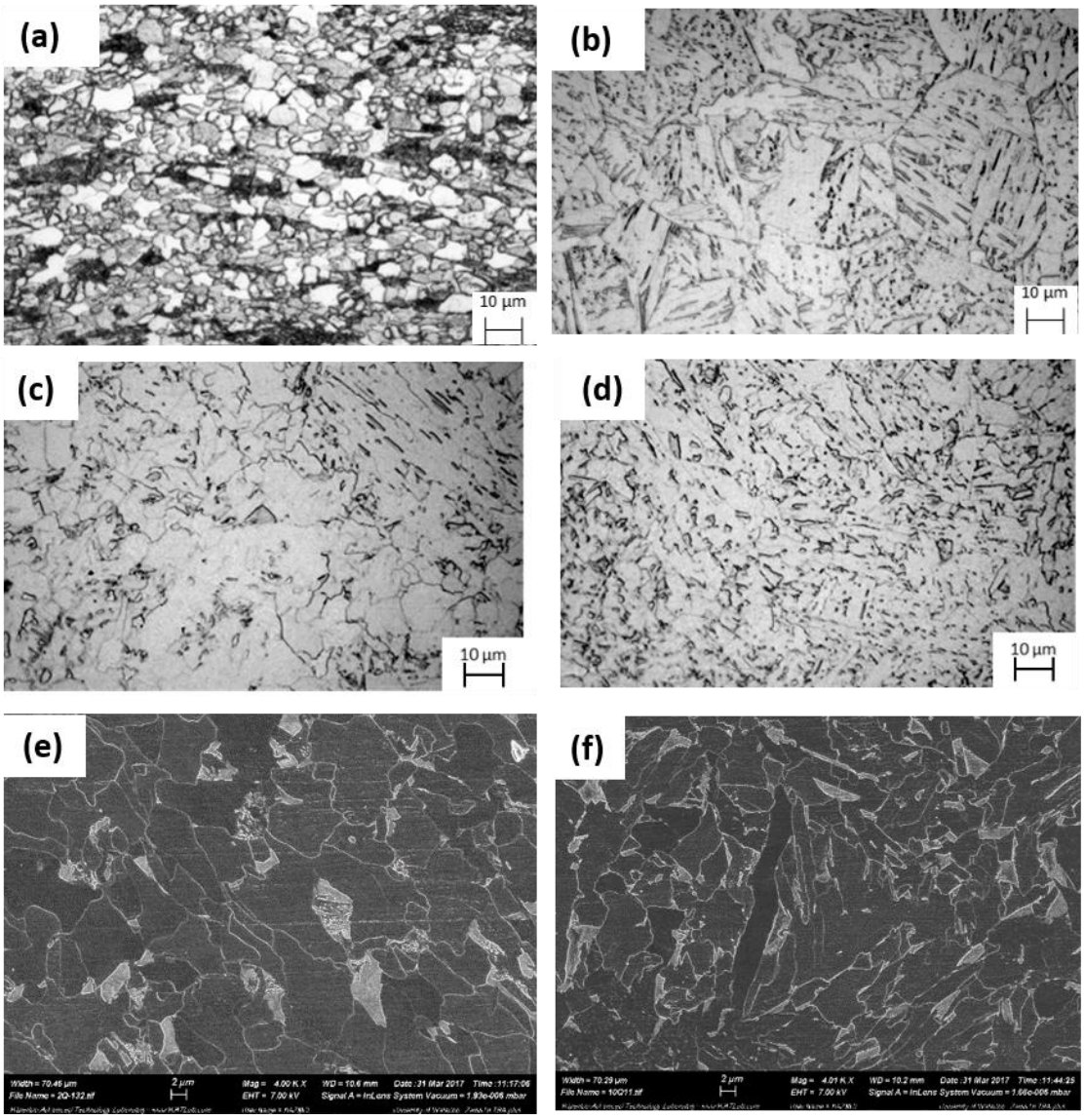

Figure 5-1 : (a) Base metal (b) 14.4°C/s microstructure (c) 2°C/s microstructure (d) 10°C/s. SEM observation (e) 2°C/s (f) 10°C/s (all the image was produced using 2% Nital)

5.3.2 Microconstituents (MA and ferrite) hardness in nanoindentation

Nanoindentation was performed in for specimens produced with both 2 and 10°C/s cooling rates and the force-displacement curves from the tests are shown in Figure 5-2 for locations confirmed to be MA microconstituents. At least 10 indentations were performed and the average hardness has been reported, and SEM was used to verify the locations coincide with MA. The average hardness of MA microconstituents in the 10°C/s specimen (9.49 ±1.47 GPa) is higher than

the specimen produced using 2°C/s (8.51 ±1.32 GPa). However, average ferrite hardness was 3.63 GPa for both specimens.

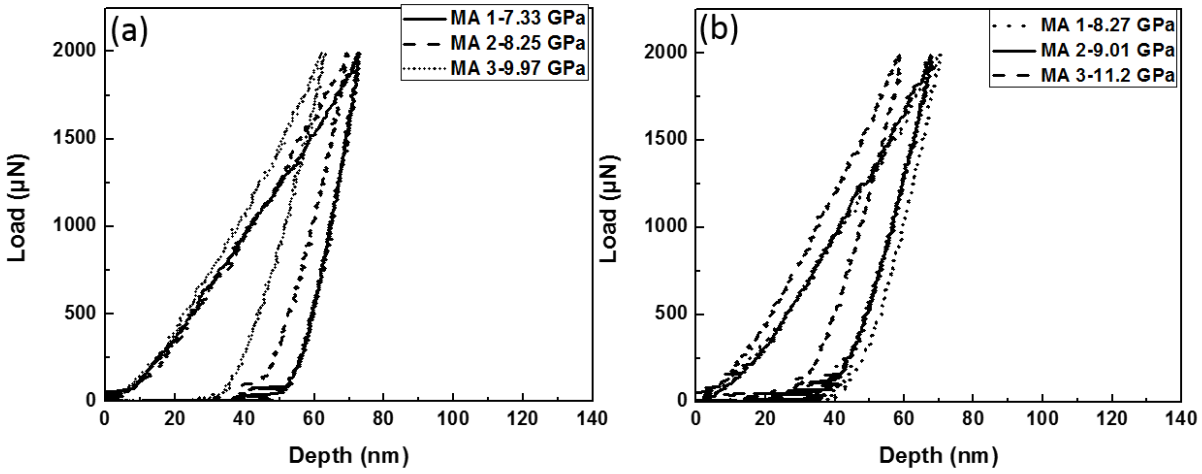

Figure 5-2 : Load-depth curves in nanoindentation for MA microconstituents (a) 2°C/s (b) 10°C/s

5.3.3 Tensile properties

The average base metal yield and tensile strength in the hoop direction is 662 ±23 MPa and 770 ±4 MPa with elongation of 21%. The stress-strain plots for 2 and 10°C/s are shown in Figure 5-3a. The specimen produced using 2°C/s exhibits a yield and tensile strength of 417 ±10, 529 ±15 MPa respectively with 23.4% ductility. The yield and tensile strength for 10°C/s are 494.5 ±13 and 574.67 ±17 MPa respectively with 26.9% ductility. Both the yield and tensile strength in the specimen produced at 10°C/s are higher than that in the specimen produced using 2°C/s. Moreover, a cooling rate of 10°C/s also provided slightly better ductility when 2°C/s is imposed. The localized strain distribution across the gauge length is shown in Figure 5-3b&c. It is interesting to note that the local ductility around the failure location also improved to 51% when a cooling rate of 10°C/s versus a peak of 40% ductility when 2°C/s was applied. In addition, the strain distribution is more dispersed for 2°C/s specimen while the strain distribution is more concentrated in 10°C/s specimen. The 10°C/s specimen exhibited a cup cone fracture surface while shear failure is observed in 2°C/s, which is also consistent with the difference in observed ductility (Figure 5-3a).

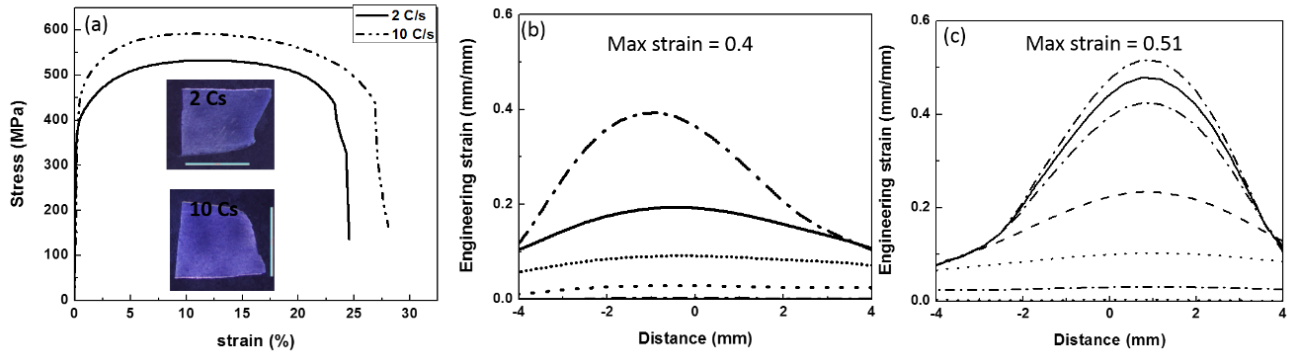

Figure 5-3: (a) Stress-strain plot for specimens cooled at 2 and 10°C/s, (b&c) localized strain distribution in 2 and 10 °C/s across the gauge length in different stages of tensile test

5.3.4 **Fracture surface observation**

Observations of the tensile fracture surface indicate significant deformation and numerous voids close to fracture close to fracture for the both microstructures (Figure 5-4a&b). The features were dominated by dimple structures in both specimens, indicating ductile fracture (Figure 5-4 c&d). It can be also observed that the specimen cooled at 10°C/s contained fracture surface dimples which were finer than those observed in the 2°C/s specimen. In addition, most of the dimples are accompanied by particles at the centers of dimples (similar to Figure 4-17f in Chapter 4), which may correspond to fragments of MA microconstituents, or partially broken MA microconstituents [10].

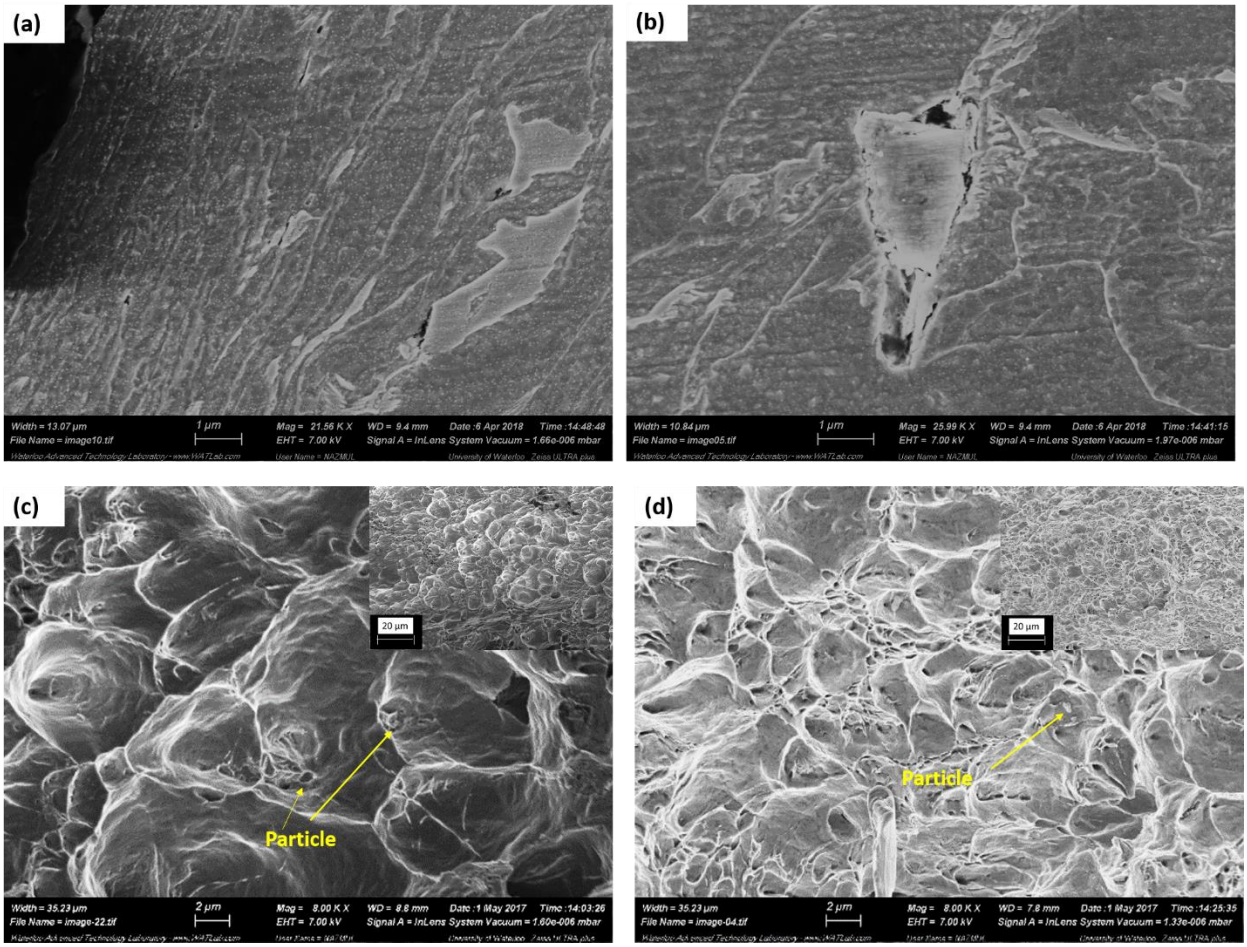

Figure 5-4 : (a) Voids formation from coarser MA of 2°C/s structure (2% Nital) (b) completely debonded coarse MA structure. Tensile fractured specimen (2% Nital) (c) 2°C/s (d) 10°C/s

5.3.5 EBSD analysis of microstructure

The crystallographic orientations of the grains produced at cooling rates of 2 and 10°C/s have been examined with the EBSD technique. The local kernel average misorientation (KAM) distribution for a 15-degree threshold in both specimens have been explored and compared to band contrast maps, as shown in Figure 5-5, Figure 5-6 and Figure 5-7. A high band contrast between MA and ferrite is evident for 2 and 10°C/s before any deformation in the structures (Figure 5-5a&b). A similar trend has been observed for the tensile strained (1mm away from tensile fractured surface) 2 and 10°C/s specimen (Figure 5-6a&b). Higher lattice misorientations are noted within the MA microconstituents, which results in a darker appearance due to low band contrast,

indicating that the interior of the MA microconstituents could not be indexed reliably due to the fine scale of the microstructures present. A similar result was obtained in Chapter 4.

The KAM distribution in both structures (as-treated) is shown using 15-degree misorientation map (Figure 5-5c&d). The MA microconstituents have high misorientations immediately surrounding ferrite, while the bulk of the ferrite exhibits rather low KAM misorientation values for both the 2 and 10°C/s specimens in as-treated condition. In addition, coarser MA in the 2°C/s is associated with higher surrounding KAM values in comparison to the KAM values around finer MA microconstituents observed in the specimen cooled at 10°C/s. Moreover, coarser MA in the 2°C/s specimen (as-treated) appear to contain more severe KAM misorientation values in the surrounding ferrite (Figure 5-5c) while finer MA microsconstituents in the 10°C/s specimen (as-treated) produce lower KAM values (Figure 5-5d). The coarser MA in the 2°C/s (as-treated) exhibits larger islands of more concentrated 15-degree misorientations, while the misorientation is more uniformly dispersed in the specimen cooled at 10°C/s (Figure 5-5d). Some grain boundaries and ferrite also have 15-degree KAM misorientations, which may correspond to subgrain boundaries and local dislocation arrays within the ferrite grains.

As expected, the KAM misorientation maps for near the fracture surfaces of tensile specimens indicate that the tensile strained materials exhibit much higher fraction of high angle misorientation compared to the as-treated samples (Figure 5-6c&d). In addition, the tensile strained specimen which was cooled at 2°C/s exhibits a much larger area of high angle misorientations than the tensile strained specimen, cooled at 10°C/s (Figure 5-6c&d). This is also noted by the EBSD statistics for misorientation angle fraction, as shown in the Figure 5-7a&b. It is observed from Figure 5-7a (for the as-treated specimens) that the material cooled at 10°C/s contains a slightly lower fraction of low angle misorientation (1 to 4 degrees), while the specimen cooled at 2°C/s contains a higher fraction of medium angle boundaries (4 to 15 degree). Quantitative EBSD measurement of misorientation angle fraction are compared between both cooling rates are shown in Figure 5-7b (after tensile strain). The specimen cooled at 2°C/s reveals a significant reduction in the fraction of low angle misorientations (1 to 4 degrees) after deformation and increase in medium angle misorientations (4 to 15 degree), see Figure 5-7a&b. Meanwhile, the fraction of low angle misorientation (1 to 4 degree) and medium angle misorientation (5 to 15 degree) in the 10°C/s specimen did not change significantly (Figure 5-7a&b). A higher fraction of high angle misorientation (4 to 15 degree) in the tensile strained

specimen cooled at 2°C/s suggest that strains and dislocation motion occurred more readily during tensile testing compared to the 10°C/s specimen.

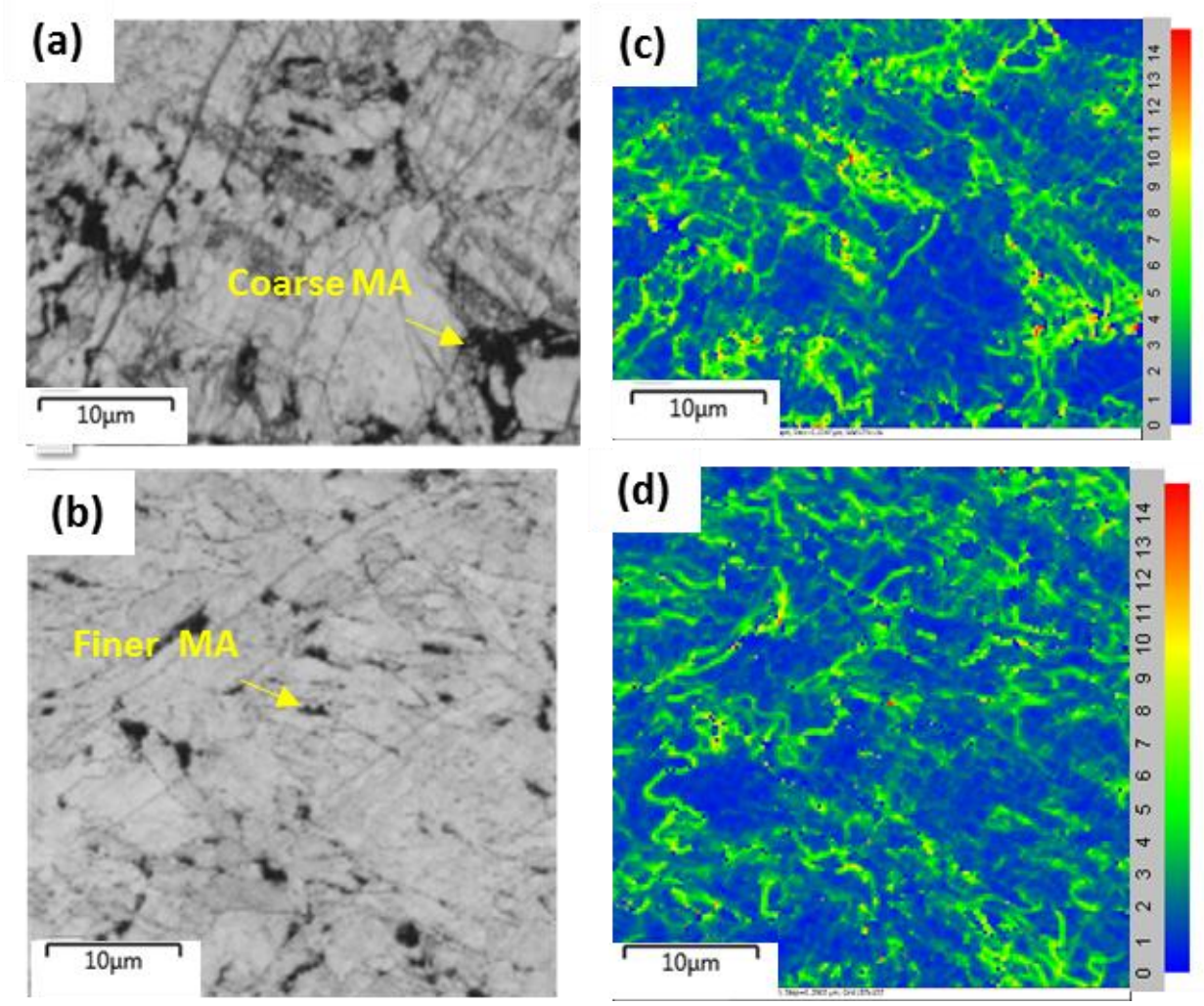

Figure 5-5 : Band contrast in as-treated condition (a) 2°C/s (b) 10°C/s. 15-degree (blue to red represent low to high angle) misorientation map as-treated specimen (c) 2°C/s (d) 10°C/s.

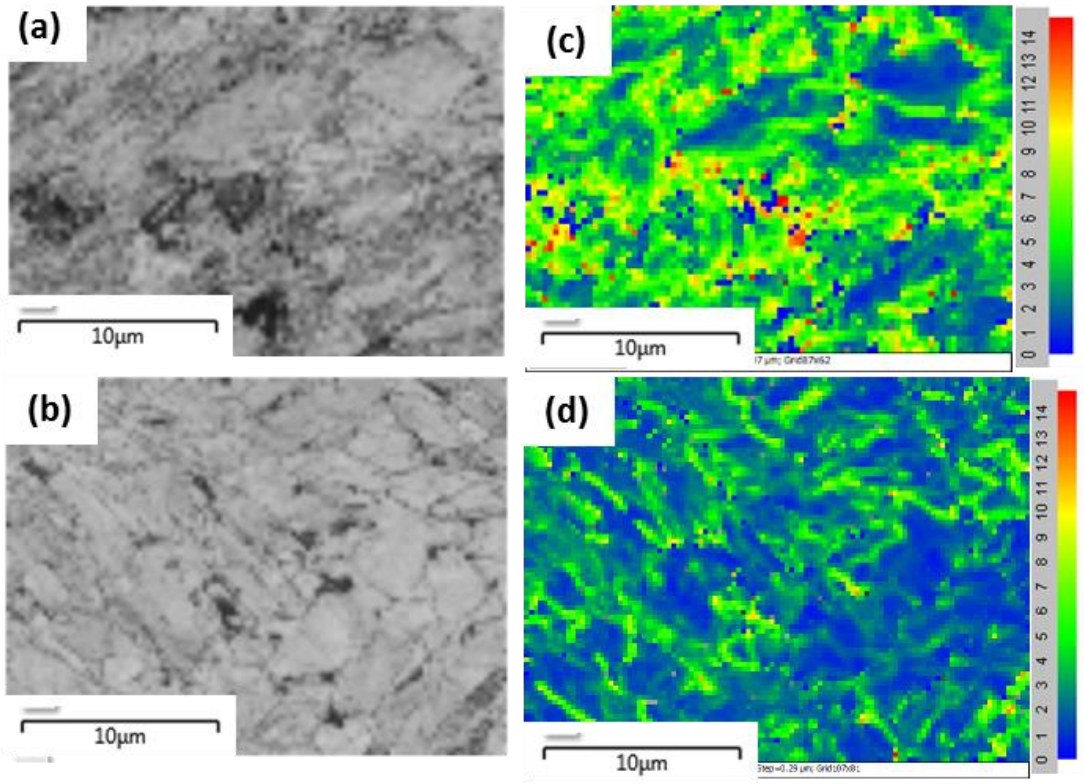

Figure 5-6 : Band contrast 1 mm away from tensile fractured surface (tensile strained) (a) 2°C/s (b) 10°C/s. 15-degree misorientation (blue to red represent low to high angle) map in strained specimen (c) 2°C/s (d) 10°C/s.

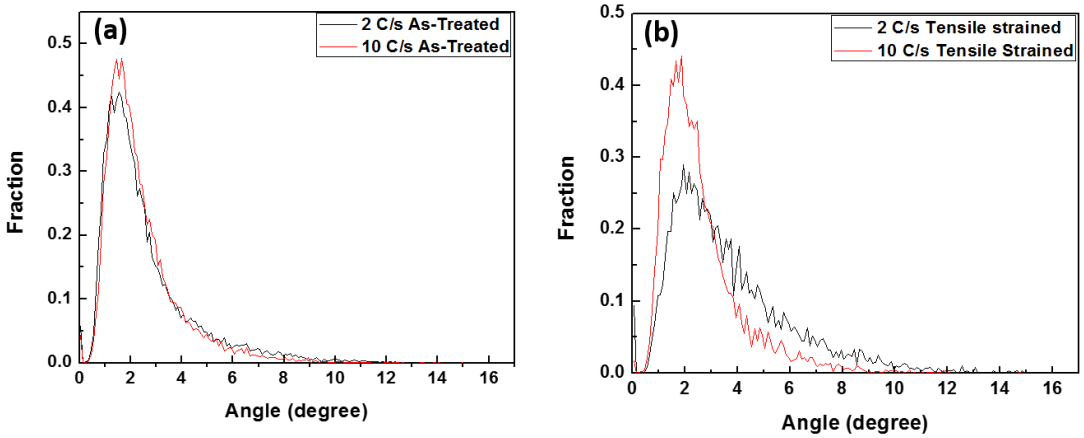

Figure 5-7 : Misorientation fraction comparison (a) as treated specimen (b) tensile strained specimen.

5.3.6 **Tensile test simulation**

To correlate and validate void nucleation from coarser MA/ferrite interface, tensile loading was simulated for the microstructure observed in the specimen cooled at 2°C/s. The results from simulation for the 2°C/s structure are shown in Figure 5-8. The mesh configuration, generated model and locations of ferrite versus MA constituents were developed based on the actual microstructure observed in the specimen cooled at 2°C/s, shown in Figure 5-8a,b&c. The stress distribution was calculated based on a uniform stress of 417 MPa (corresponding to the actual yield strength of the 2°C/s specimen) applied in the transverse direction of material, as indicated by the arrow. The von Mises stress distribution is shown in Figure 5-8d in response to this loading scenario, with the left side of the structure under a fixed boundary condition. An acute stress concentration is observed at the interfaces of MA/ferrite. Stress localization is more severe around the coarser MA/ferrite grain interfaces than compared to finer MA regions. The maximum local stress concentration reached 3.7 GPa at the interface, while the typical stress level in ferrite was between 100-500 MPa. The MA microconstituents with an average size of 1 μm or below do not introduce significant stress concentrations in the structure. Moreover, MA microconstituents which are inside of ferrite grains (particularly those smaller than 1 μm), do not present any severe stress concentrations, suggesting these are mainly benign to the fracture properties.

Another interesting observation is that the stress concentration locations around MA microconstituents were most severe at sharp corners. In addition, the probability of a high stress concentration at sharp edges will be higher when it coincides with a grain boundary. Moreover, the angle of those sharp edges to the applied stress direction could also have a significant role in stress concentration. It can be observed that when several sharp edges are close to each other and are approximately 90 degrees to the applied stress, this leads to the most significant stress concentration. It is also interesting to observe that some of the large MA grains has plastic deformation capacity. In Figure 5-8d some of the MA sustains strain in a similar way to the ferrite grains.

The principal stress is distribution is shown in Figure 5-9. The resulting distribution of stress was nearly the same for both, meaning it is mostly uniaxial, with only some increased multi-axial at the locations with more elongated holes which lead to a higher von Mises in those locations.

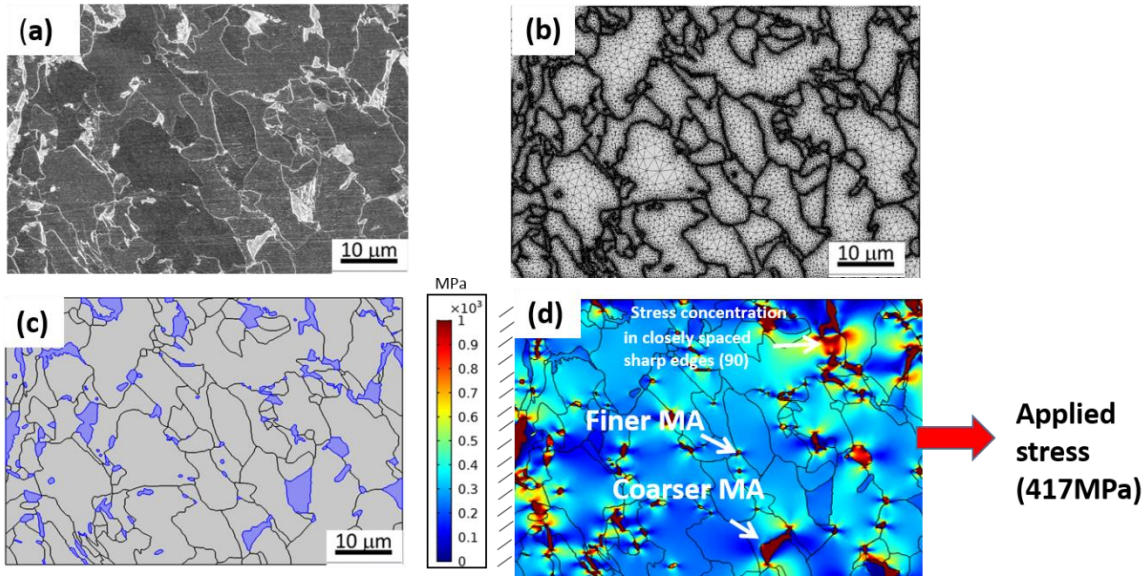

Figure 5-8 : (a) 2°C/s microstructure used for model generation (b) meshed figure (c) generated model with highlighted MA (d) von Mises stress distribution at 417 MPa applied stress.

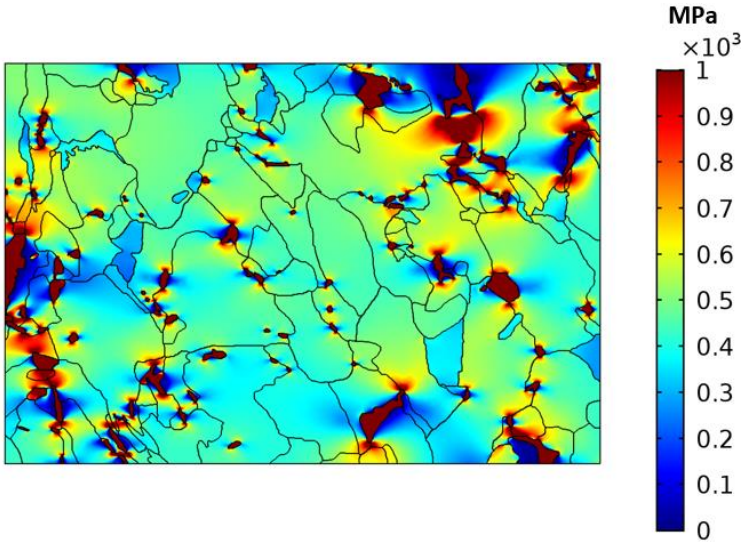

Figure 5-9 : Principal stress distribution at 417 MPa applied stress

5.4 Discussion

The ferrite and MA microconstituents are coarser in the 2°C/s than 10°C/s due to the slower cooling rate which contributes more to grain growth, leading to lower hardness as well. The difference in MA size and distribution may relate to carbon diffusion time. Davis and King [8] explained the MA formation from reheating of upper bainite structure. Austenite nucleates from prior austenite grain boundaries and bainite lath boundaries. Austenite becomes rich carbon and there will be insufficient time for carbon diffusion. On cooling, this carbon rich austenite will transform into MA. Nakao et al. [62] proposed two MA formation mechanisms based on peak temperature in second thermal cycle. In first mechanism, reheat temperature is above Ac3 while reheat temperature is between Ac1 and Ac3 in second mechanism. According to Nakao et al. [62] the austenite grows in high carbon region (prior austenite grain boundary) when temperature reach above Ac3. The subsequent cooling led formation of ferrite and bainitic ferrite in low carbon region while MA constituents form in high carbon austenite region. While the second mechanism suggested that, there could be precipitation of carbides on the coarse prior austenite grain boundaries after first thermal cycle. Second thermal cycle results a temperature peak between Ac1 and Ac3 in the microstructure. Austenite grows along the grain boundaries and the carbides dissolve into austenite regions during second thermal cycle heating. On cooling the austenite transforms and part of austenite transform into MA [63]. That suggest MA preferentially grow in high carbon region and its formation highly depends on carbon diffusion time. Now in current study, the very slow cooling rate 2°C/s will provide sufficient time for growth of ferrite grain and diffusion of carbon from ferrite. This will also allow the growth of coarser MA structure in 2°C/s. However, faster cooling rate may not provide sufficient time grain growth and carbon diffusion in 10°C/s thereby a more disperse distribution of MA occurred from lack of carbon diffusion time.

The MA microconstituents exhibited a lower hardness in the 2°C/s specimen compared to the specimen cooled at 10°C/s which likely results from diffusion of carbon and auto-tempering of the MA at lower cooling rates. Higher cooling rates will might prevent carbon diffusing from the MA microconstituents, and any martensite formed will likely remain untempered as the cooling rates increase.

Figure 5-3a reveals that the specimen cooled at 10°C/s exhibits a higher yield and tensile strength with combination of higher ductility than the 2°C/s. In the present work, one can note that coarser ferrite and MA microconstituents produced at a cooling rate of 2°C/s leads to inferior

strength compared to the 10°C/s cooling rate. The difference in strength between 2 and 10°C/s relate to ferrite grain size and MA distribution. The ferrite grain size contribution to yield strength was calculated using the Hall–Petch equation [138]. According to this, the ferrite grain size (7 μm) of 2°C/s specimen have 209 MPa contribution towards yield strength while it is 247 MPa for 5 μm ferrite grain size of 10°C/s specimen. Consequently, one can note a difference of 37 MPa (overall 77 MPa) value was accuounted for by ferrite grain sizes between two microstructures. However, there is a difference in yield strength of 40 MPa between the 2 and 10°C/s specimens which is contributed by factors other than ferrite grain size. That suggests, this 40 MPa difference is mainly contributed from a secondary phase, or solid solution strengthening within the ferrite grains. Moreover, it should be noted that the MA distribution is more uniform in the 10°C/s specimen, which enhances strengthening of the ferrite as form of dispersion strengthening.

It is commonly accepted that an increase in strength will generally result in reduced ductility for the same alloy composition. In Chapter 4, it has been shown that a higher MA fraction will reduce ductility in X80 linepipe material GMAW weld. However, despite higher strength in 10°C/s specimen, it exhibits better ductility. The MA/ferrite interface had been shown to be the source of void formation in Chapter 4 during tensile testing, and so it was suggested that the higher MA fraction will produce more voids and coalescence of those voids lead to loss of ductility. In the current investigation both the microstructures have a similar fraction of MA, but differ in terms of size, density, morphology and distribution. Since, the density of MA is higher in the 10°C/s specimen with a shorter spacing between them; this is likely to produce a higher density of voids prior to fracture along with poor ductility. However, the opposite trend has been observed in Figure 5-3a, meriting further discussion to explain this phenomenon.

It can be observed that MA constituents are coarser in the 2°C/s specimen compared to the 10°C/s. The coarser MA in the 2°C/s structure may easily initiate voids, leading to loss in ductility. The observation of larger voids close to the main tensile fracture path, and the observation of coarser dimple on the fracture surface of the 2°C/s specimen support this explanation. Furthermore, the finer MA constituents in the 10°C/s specimen might contribute to more uniform straining during tensile test. A finer dimple structure on the fracture surface and lower number of large voids near the fracture path in the 10°C/s also suggests higher ductility, especially locally around the fracture as evident in Figure 5-3c. The finer distribution of MA microconstituents will have a more benign stress concentration distribution as shown in Figure 5-8d, which will delay the onset of

grain decohesion and fracture, thus enhancing ductility. In current study, the simulation results suggest that the stress at MA/ferrite interface could reach 3.7 GPa when yield stress was applied; which is higher than the martensite-ferrite interface strength (2.4-2.5 GPa) determined by Poruks et al. [139]. So it suggest that void formation can occur when yield point is reached which was also shown in Chapter 4 study.

The second important observation is the trends in misorientation angles, which may closely correlated to dislocation density around the coarser MA. Kamaya et al. correlated as-treated and plastic strained specimen strain to dislocation accumulation in austenitic stainless steel using EBSD and the method is independent of step size, number of data and EBSD system [140]. The EBSD data plotted for 15-degree misorientation maps from the 2 and 10°C/s specimens before deformation suggest that misorientation distribution is more uniform in the 10°C/s structure while some areas of the 2°C/s specimen have inhomogeneous and locally high misorientations. Most of the highly misoriented area of the 2°C/s also contain coarser MA. This suggests that the coarser MA creates more misorientation gradients which might associated with higher dislocation density. The presence of dislocations around MA has been confirmed using TEM and high misorientation around MA have been shown around MA in Chapter 4.

High densities of dislocations at the MA/ferrite interface can have a significant contribution in tensile properties. Kang et al. [141] suggested that the interface of MA constituents and ferrite is the source of stress concentration, as demonstrated by tensile testing using local strain monitoring facilities. Chen et al. [99] reported that the critical fracture stress is reduced when MA grows larger than a critical size. Okada et al. [60] used finite element analysis to show that the strain field around massive MA was much larger than elongated ones, and thereby massive MA was more detrimental as a factor for crack initiation. Kadkhodapour et al. [142] also showed that coarser MA causes void formation in dual phase steel. Okada et al. suggested that the strain field around MA might be a controlling factor for crack initiation. Micro-voids and micro-cracks can form in coarser MA surrounding ferrite matrix easily which may related to lower critical fracture toughness around it [60, 99]. The simulation results also suggest that coarser MA/ferrite interface subjected to more stress than finer MA (Figure 5-8d). Deformation of the coarser MA and high dislocation around MA in the 2°C/s specimen support above explanation (Figure 5-6a). Moreover, void formation in the MA/ferrite interface and debonding of MA from the structure suggests a weakness interface (Figure 5-4a&b). That is evident in 15-degree misorientation map of the 2°C/s

specimen (Figure 5-6b). Dislocation pile up in that location creates a significant fraction medium angle misorientation (4 to 15 degree). In contrast, the 10°C/s specimen contains lower dislocation densities around finer MA and the number of grain boundaries is higher, which may make dislocation movement difficult (Figure 5-6d).

The distribution of MA constituents can also have role in differentiating the two specimens here versus ductility. It is believed that the 2°C/s specimen contains ferrite which deformed easily considering the lower density of MA with a wider spacing between them, compared to the 10°C/s specimen. In support of this, high degrees of ferrite deformation are suggested by the 15-degree misorientation maps of the deformed 2°C/s specimen. However, deformation in the 10°C/s specimen is more uniform and less severe than the 2°C/s. Okada el al. [13] reported void formation in the early stage of ductile fracture as a result of internal stress which was due to a difference in plastic strain between the hard secondary phase and matrix.

It was observed that void sizes close to the main fracture of the 2°C/s samples are significantly higher than the 10°C/s samples, which is likely related to the size of MA. In addition to size and distribution, the morphology of MA constituents is also important. It has been shown in research that sharper edges of MA are often a source of stress concentration. The distribution of von Mises stress concentration based on simulation suggest that the sharper edges which are at 90 degrees to the applied stress is the most severe source of stress concentration, promoting voids to form first, and hamper ductility. In addition, when the sharper edges (at 90 degrees to the applied stress) are close to each other, the stress concentration is more severe (Figure 5-8d). Kang et al. [141] results suggested that intercritical annealed specimens contain MA microconstituents and stress concentrated in sharper edges of MA, while even small MA microconstituents with sharper edges can be source of stress concentration. Kadkhodapour et al. [142] also showed that void formation occurs at the sharper edges of MA in dual phase steels.

It is also interesting to observe that some of the large MA microconstituentss exhibit low stress concentrations throughout and around them. This is against the report by Chen et al. [99] who suggest MA itself does not have any ductility at room temperature, while support Hrivnak et al. [80] the view that MA has good strain capacity. However, the simulation results suggest that some of the MA sustains strain a similar way to ferrite grain, which may be due to a favorable orientation of MA and the microstructure around the MA.

5.5 Summary

1. The 2°C/s microstructure contains coarser ferrite and MA than 10°C/s. While the distribution of MA is more benign in 10°C/s than 2°C/s.

2. Void formation from MA/ferrite interface led to failure during tensile test in 2 and 10°C/s microstructures. Hardness difference between MA and ferrite lead to stress concentration in MA/ferrite interface which causes void formation.

3. Coarser MA is found more prone to form early void formation in the structure. Coarser size MA in 2°C/s causes premature void formation which led to loss in ductility.

4. Dispersed distribution and finer size of MA lead to improved tensile properties (strength and ductility) in 10°C/s than 2°C/s.

Chapter 6 : Temper-Treatment Development to Decompose Detrimental Martensite-Austenite and its Effect on Linepipe Welds[3]

6.1 Overview and background

The results from prior Chapter 4 and 5 suggest that the interface of coarse MA and ferrite is primarily responsible for premature void formation. The difference in hardness between MA and ferrite, along with a strain field around the MA readily promotes void formation. The goal of the current chapter work to develop a heat treatment procedure to temper detrimental coarser MA and make the strain field around MA more benign, and potentially improve mechanical properties.

6.2 Experiemtal procedure

Weld A from Chapter 4 which was produced by wire A with a diameter 0.984 mm was used for the present study. Transformation temperatures Ac1 (709°C) and Ac3 (871°C) of the X80 base metal are calculated using equations 6-1 to 6-3 provided by Andrews [143] and Ishida et al. [144] where chemical composition of elements are in weight percentage. Numerous experiments were performed using a furnace with different temperatures and holding times to confirm the Ac1 temperature of the material in second thermal cycle. It was found that a temperature of 709°C with a hold time of 20 min was the threshold for the start of austenization (Ac1) of the X80 material. It is reported that the maximum MA formation occurs when reheating just above the Ac1 temperature [145]. Thus, a second thermal cycle at a temperature of 710°C was selected to observe the MA formation and its effect on tensile strength and ductility.

3 This chapter is published Manuscript in Materials Science and Technology, 2017 on 9 May 2017, available online: https://doi.org/10.1080/02670836.2017.1342019 Nazmul Huda, Yuquan Ding and Adrian P. Gerlich, Temper-treatment development to decompose detrimental martensite‐austenite and its effect on linepipe welds.

Ac1 (°C) = 723-10.7Mn-3.9Ni+29Si+16.7Cr+290As+6.38W……Equation 6-1

Ac3 (°C) = 910-230 C0.5 -15.2Ni+44.7Si+104V+31.5Mo+13.1W……Equation 6-2

Ms (°C) = 545-330C+2Al+7Co-14Cr-13Cu-23Mn-5Mo-4Nb-13Ni-7Si+3Ti+4V…..Equation 6-3

Here, elemental composition is in wt%.

The heat treatment cycles were performed using an electric furnace preheated to the desired temperature and then samples were put inside the furnace in open air. A heat treatment schedule with a first thermal cycle temperature of 1000°C and 20 min holding time was applied and followed by cooling in air. A second thermal cycle was applied to the pre heat-treated specimen at a temperature of 710°C and 20 min holding time to investigate the MA structures after cooling in water. The post-weld heat treatment (PWHT) thermal cycle was imposed at temperatures of 200°C and 300°C, which were selected with different tempering times from 1 minute to 1 hour for comparison, and samples were cooled in water.

XRD analysis (with Cu-Kα radiation) was conducted using a Bruker D8 at a scan rate of 2 deg/min to quantify the percentage of austenite in the structure. A JEOL 9500F was used to map carbon distribution inside the MA using Auger electron spectroscopy (AES). Tensile tests were performed using standard sub-sized tensile sample (in the hoop direction with a 100 mm total length, with a 32 mm gauge length, 6 mm width, 2 mm thickness). Yield strength was calculated based on 0.2% offset method. The welding design with tensile samples were produced from direction orientation as shown in Figure 4-1. A precision cutter was used to extract 10 x 10 mm specimen. The specimen was grinded to 0.15 mm using 800 grit paper. Ion milling was performed to reduce the thickness to <100 nm in the middle of 3 mm discs punched from the specimen.

6.3 Microstructure and hardness in weld reheated zone

The X80 base metal contains a mixture of bainite (17%) and ferrite (83%), with an average hardness of 230 ±10 HV, with a microstructure shown in Figure 6-1a. A macrograph of the four pass weld is shown in Figure 6-1b. Etching is performed in such a way that the reheated HAZ zone between cap pass and fill pass can be clearly identified. Hardness of this zone varied from 240 HV to 220 HV (based on an average of three lines) moving from fusion line to base metal. The microstructure of the reheated zone is shown in Figure 6-1c, which is mostly granular bainite, and

it has been reported that it is easy to form MA along with this microstructure [146]. LePera etchant reveals the existence of MA (corresponding to a white appearance) in the reheated zone (Figure 6-1d). There are white structures (untempered MA) observed in the reheated zone which amount to 5% of the structure in this region, with sizes varying from 0.2 to 4 μm. The presence of MA in the ICCGHAZ and ICHAZ is well known to result from intercritical heating [8]. Both untempered MA and tempered MA are found in the reheated zone (Figure 6-1e&f). It has been suggested that tempered MA could occur in the reheated HAZ zone because the second bead is performed in top of first bead [108] and in the process any untempered MA in the first bead ICHAZ can be decomposed.

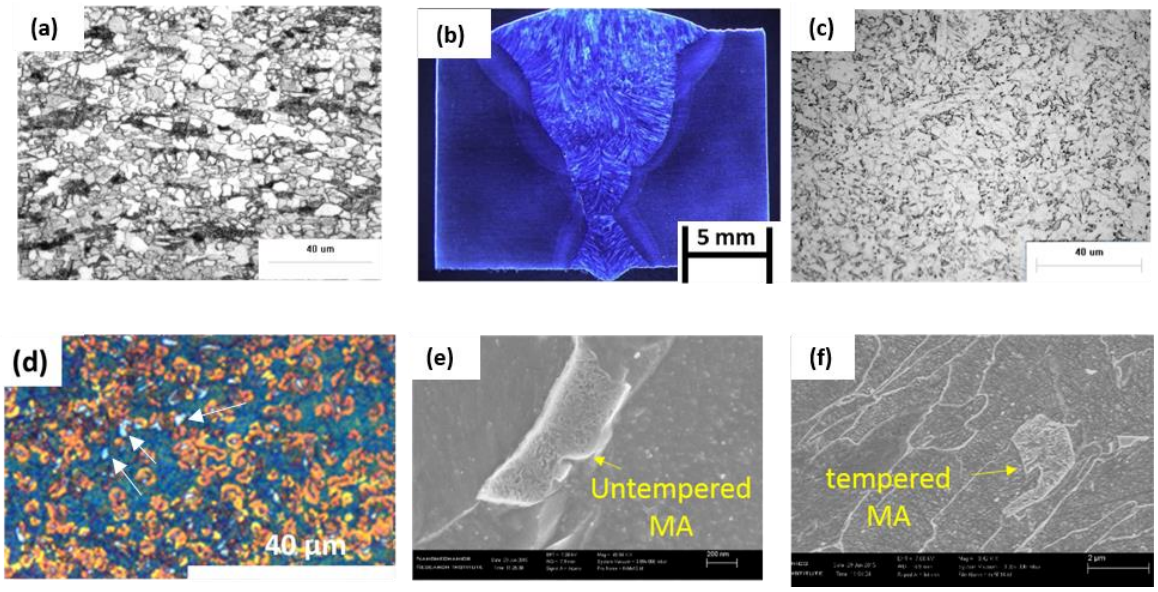

Figure 6-1 : (a) Base metal microstructure (2% Nital) (b) weld macrograph (2% Nital) (c) reheated zone microstructure (2% Nital) (d) LePera etching of MA in reheated zone (e) untempered MA in reheated zone (2% Nital) (f) tempered MA in reheated zone (2% Nital)

6.4 Tensile test investigation in welded sample

The base metal yield strength and tensile strength are 662 ±23 MPa and 770 ±4 MPa respectively, with an elongation of 21%, while for welded sample it is 575 ±10 MPa, 605 ±24 MPa respectively with 10.2% elongation. Tensile tests were performed on the welded sample with the

reheated HAZ between the fill and cap passes positioned in the mid-section of the tensile sample. Tensile results indicated the fracture occurred in the HAZ (as shown in Figure 6-2a).

Numerous voids with average sizes ranging from 0.3 to 30 μm are observed in vicinity to main fracture path. It is observed that 94% of the voids initiated from large MA/ferrite interfaces (Figure 6-2b). Example of more voids initiation from MA/ferrite interface and MA debonding can be found in Chapter 4. It can be observed from Figure 6-2b that one of the slender MA regions can be observed and debonded from the structure; however it is retained in the matrix. Moreover, the slender MA is fragmented in the middle. However, small MA (less than 1 μm in size) do not become debonded or initiate voids in the structure (Figure 6-2b), which might indicate smaller size MA is not as detrimental to mechanical properties as larger MA. It can be also observed that tempered MA does not initiate voids or debond from a matrix structure, which suggests that tempered MA is not as detrimental (Figure 6-2b). Davis and King suggested that MA with pearlite dominant MA microstructure is beneficial to impact toughness [56].

A difference in the yield strength and plastic strain capacity between ferrite and MA can have significant effect which is discussed in Chapter 5. Kadkhodapour et al. showed using simulation that strain localization occurs in the sharper ends of MA, and the two sharp ends of slender MA are more prone to stress-strain concentration in dual phase steel [142] which is also observed in Chapter 5. In addition, Li et al. suggested slender MA has a greater likelihood to debond from the structure due to low dihedral angle [58].

In addition to stress-strain and angle, the austenite percentage in MA can also play a significant role in straining ability of MA. The presence of more austenite in the MA might provide more strain capacity, thereby reducing the probability of fragmentation or debonding. Hrivnak et al. also suggested MA has a strain capacity [78] which depends on the austenite percentage. In the current investigation, it is believed that straining causes fragmentation of MA and more strain leads to debonding of fragmented MA. During polishing this specimen, fragmented parts of the MA may dislodge out of the structure.

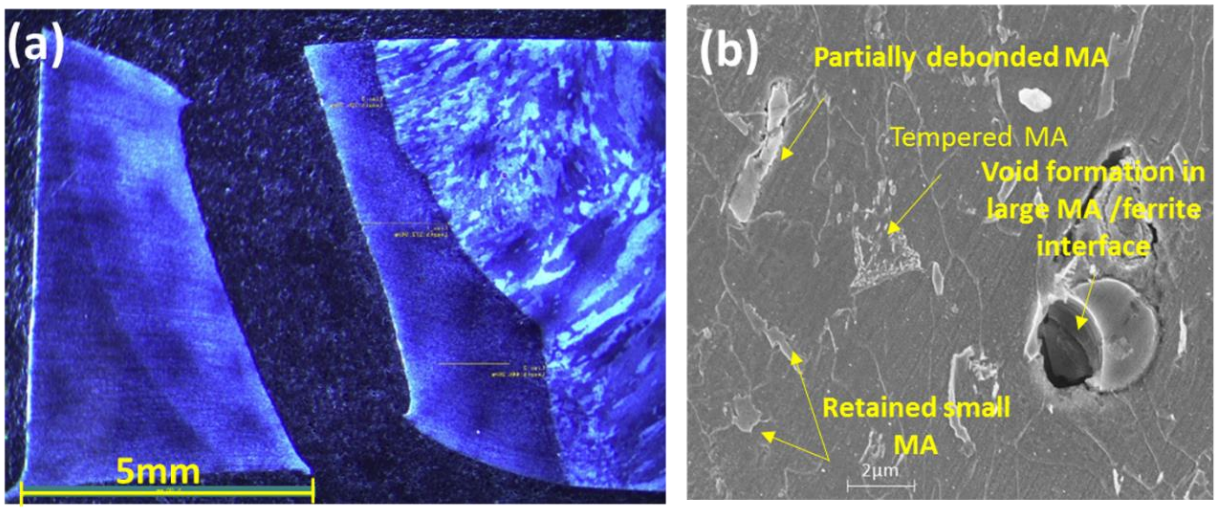

Figure 6-2 : (a) Fracture in HAZ for as welded sample in tensile test (2% Nital) (b) debonding of MA and void formation in MA/ferrite interface, tempered MA is not debonded, small MA does not get debonded (2% Nital)

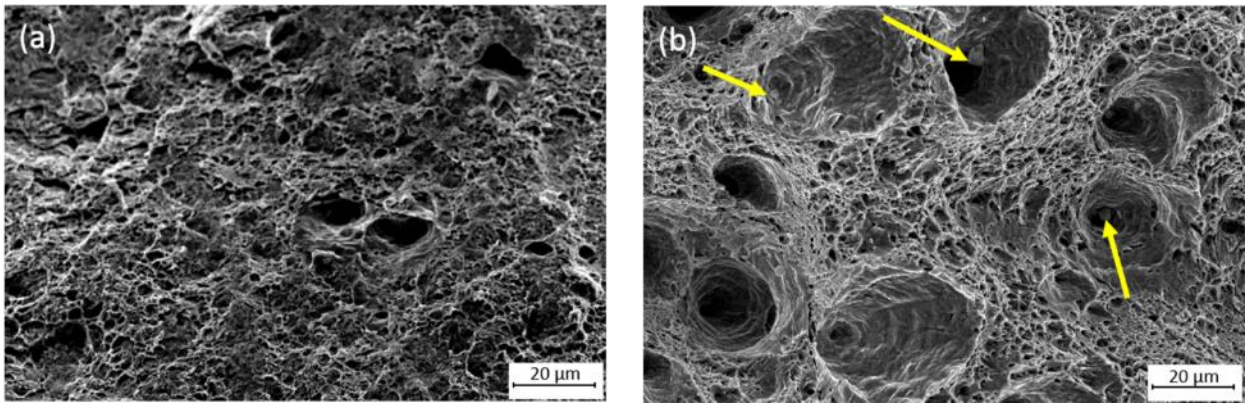

Figure 6-3 : (a) Base metal fracture surface of dimples dominant structure (b) HAZ fractured surface of large voids dominant structure with particles inside voids

To investigate further the debonding reported earlier in more detail, SEM observations of the tensile fracture surfaces in the base metal and the weld HAZ are compared, which exhibit a significant difference in appearance (Figure 6-3a&b). The fracture surface of the base metal is dominated by small dimples, while the fracture surface of HAZ fracture sample is mostly large voids. Some of the voids in the HAZ fractured sample are associated with particles in their centre, which presumably corresponds to MA or fragmented portions of MA (Figure 6-3b). Since Kim et

al. proposed that ferrite deforms more significantly than MA during the room temperature tensile test [59], this is consistent with the fragments inside the dimples.

6.5 Optimum PWHT cycle determination for weld by heat treatment study

According to the characterization of the welded sample and its corresponding tensile fracture surface, larger MA (≥1μm) appears to deteriorate the properties of the HAZ during tensile tests by initiating voids and debonding these from the ferrite structure. It is possible an optimum PWHT cycle with different temperatures and tempering times can improve the tensile properties by decomposing the mainly detrimental large (≥1μm) MA, without significantly deteriorating grain structures or impact toughness. However, the reheated zone in weld is rather small, and exhibits significant variation in MA type (comprising either untempered or tempered structures), which complicates an analysis of the role of tempering. So, a heat treatment schedule has been developed as per Figure 6-4 to determine an optimum PWHT cycle and subsequently apply it to the weld. A single thermal cycle sample with a 1000°C peak temperature is used to heat the sample and cooled in still air. Subsequently the sample is heated to 710°C (above Ac1) and cooled in water. Two tempering temperatures of 200°C and 300°C are chosen with tempering times of 1 hr, 30 min, 10 min, 5 min, 2 min, 1 min followed by water quenching to determine a useful tempering cycle in order to identify a minimum tempering time to be practical in the field.

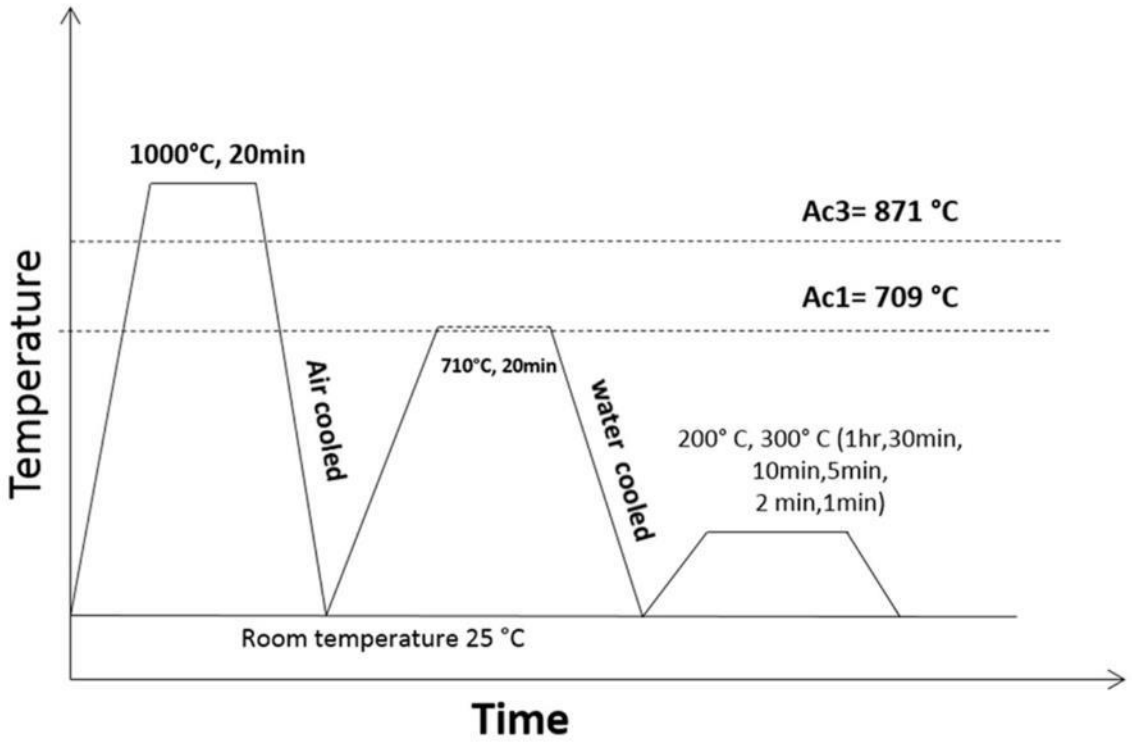

Figure 6-4 : Heat treatment cycle schedule in furnace for heat treatment study to determine optimum PWHT cycle

6.5.1 Microstructure in heat treated sample

After the first thermal cycle (at 1000°C), the microstructure is mostly ferrite and degenerated pearlite (Figure 6-5a&b), as confirmed by SEM. EDS analysis showed the manganese percentage is 2.0% which is higher than the base metal manganese content (1.73%). Measurements were performed based on standard-less method and repeated for several MA points, with scatter of 0.1%. The quantitative microscopy revealed that 11% of the structure is degenerated pearlite and the remainder is ferrite. After a second thermal cycle (at 710°C), MA is found in triple junctions of ferrite grain, at grain boundary regions and inside ferrite grain (Figure 6-5c), while use of LePera reveals white structures which are MA (Figure 6-5d). The quantification based on area analysis indicates that 20% of the structure is MA. SEM observation confirms the absence of a tempered MA in the structure (Figure 6-5e), with a heterogeneity of phases internally (Figure 6-5f). Villela etchant reveals a variation in austenite-martensite percentage from one MA grain to another (Figure 6-6). The MA grain in Figure 6-6a indicates a high percentage of austenite while

Figure 6-6b MA contains a low percentage austenite. Lambert et al. have also used similar methods to characterize martensite austenite inside MA microconstituents using Villela etchant [75].

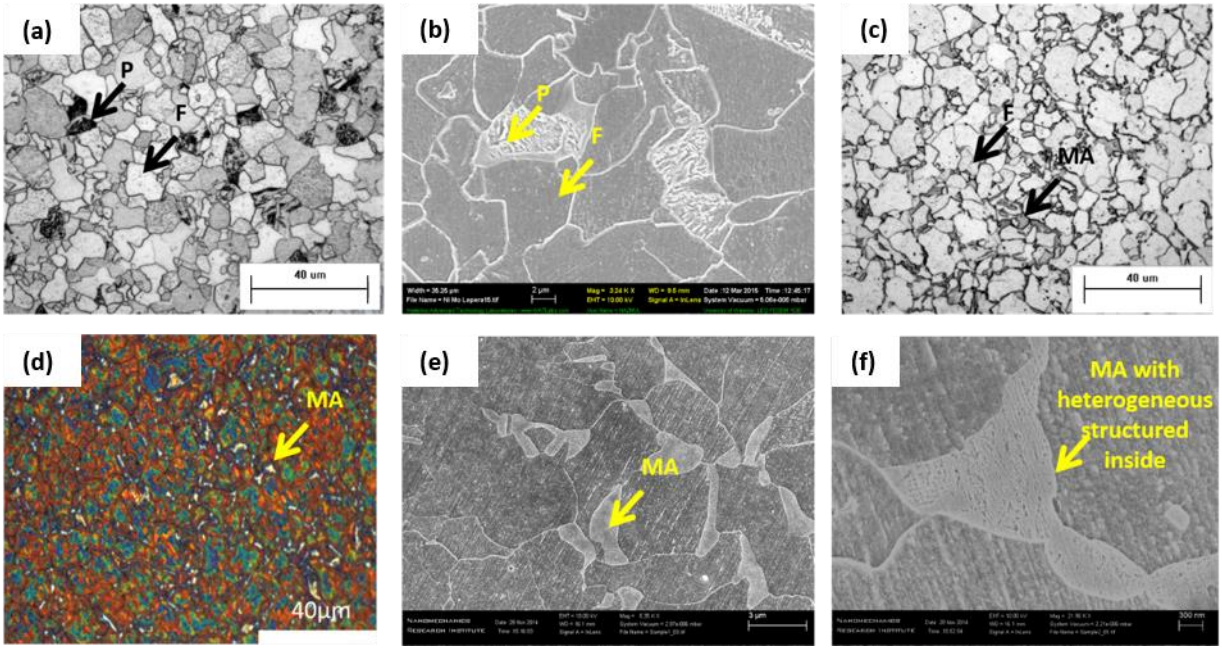

Figure 6-5 : (a) First thermal cycle microstructure (1000°C)- 2% Nital (b) First thermal cycle SEM (1000°C) - 2% Nital (c) Second thermal cycle microstructure (710°C) - 2% Nital (d) Lepera etching of second thermal cycle microstructure (710°C), (e) SEM image from the second thermal cycle specimen (710°C) - 2% Nital, (f) Higher magnification image of MA (2% Nital)

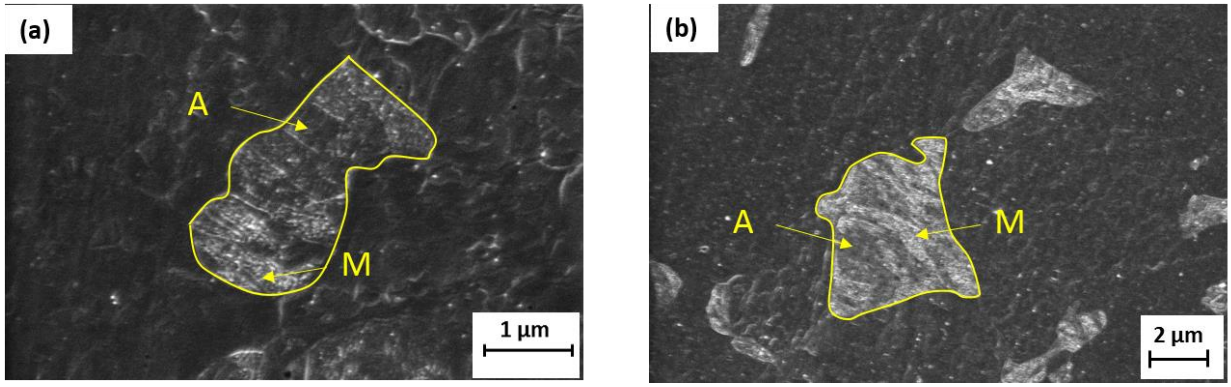

Figure 6-6 : (a) Untempered MA with high percentage austenite (6% of MA) of austenite (Villela etchant) (b) untempered MA with low percentage austenite (2.8% of MA) austenite (Villela etchant)

A tempering cycle with a temperature of 200°C for times of 1 hr and 10 min respectively showed that MA does not decompose, considering that the MA retains the white appearance (Figure 6-7a-b). This is confirmed by SEM observation (Figure 6-7c-d). However, when applying a temperature of 300°C for 1 hr during the tempering cycle, a significant fraction of MA is decomposed (Figure 6-7e), with the exception of a small MA (<1µm) which do not decompose. Likewise, applying a tempering temperature of 300°C for 10 min also promoted most of the MA fraction to decompose, however small sized (<1 µm) MA does not decompose (Figure 6-7f), which is confirmed by SEM observation (Figure 6-7g-h).

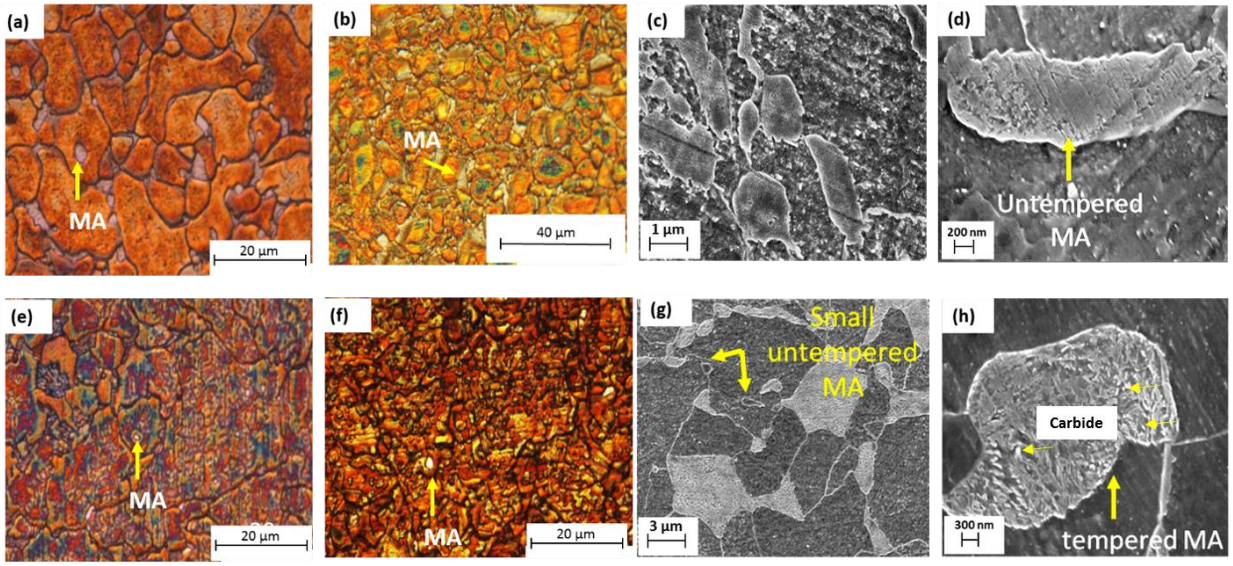

Figure 6-7 : Lepera etching and SEM image (a) 200°C, 1 hr tempering (Lepera etching) (b) 200°C, 10 min tempering (Lepera etching) (c) 200°C, 10 min tempering (2% Nital) (d) untempered MA (2% Nital) (e) 300°C, 1 hr tempering (Lepera etching) (f) 300°C, 10 min tempering (Lepera etching) (g) temper microstructure at 300°C, 10 min (2% Nital) (h) tempered MA (2% Nital)

X-ray diffraction is used to investigate the austenite percentage in water cooled (710°C) and water cooled tempered (300°C, 10 min) sample. XRD analysis of the water cooled sample confirmed the presence of austenite (Figure 6-8), where the graph is normalized based on the highest peak measured. The retained austenite percentage is calculated in the air and water cooled samples relative to ferrite based on the equations below, based on the prior work outlined by Zhou et al. [147]:

Austenite percentage, $\gamma\ \% = \frac{100}{1+\frac{R_\gamma}{R\alpha}*\frac{I\alpha}{I\gamma}}$ ... ...Equation 6-4

where I is the x-ray intensity peak count of a respective phase, and:

$$\frac{R_\gamma}{R\alpha} = \frac{V\alpha^2}{V_\gamma{}^2}\ \frac{F_\gamma{}^2}{F_\alpha{}^2}\frac{P_\gamma}{P_\alpha}\left(\frac{1+Cos^2 2\theta}{1+Cos^2 2\theta_\alpha}\right)\left(\frac{Sin^2\theta_\alpha\ Cos\theta_\alpha}{Sin^2\theta_\gamma\ Cos\theta_\gamma}\right)$$ ……Equation 6-5

Here, R is crystal correction factor accounting for volume of unit cell, structural factor, multiplication factor and brag angle, V is the volume of unit cell ($V\alpha$ =2.86 Å and V_γ =3.81 Å.), F is the crystal structural factor ($F_\alpha = 4\ f_\alpha^2$, $F_\gamma = 16\ f_\gamma^2$; for steel $f_\alpha = f_\gamma$), and P is the multiplicity factor for the lattice. The calculation showed that the austenite is 0.2% in water cooled sample (710°C) which is 0.9% of only the MA regions. However, after tempering at 300°C the austenite percentage is 0.14% overall, which corresponds to a 17.3% portion of only the MA regions. It can be observed that there is a slight decrease in total austenite after PWHT, however the austenite fraction within only MA slightly increases (i.e.: since the martensite portion has decomposed while austenite does not change). The decrease in austenite with PWHT was reported in other work [148]. It had been also reported that the austenite percentage decreases with an increase of MA size [100].

It has been previously suggested the smaller MA contains more austenite than larger MA, based on SEM and Auger spectroscopy [133]. A similar phenomenon can be observed by comparing Figure 6-6a&b. The MA grains with an average size of 1.7 µm contain 6% austenite while MA with a size of 4 µm contains 2.8% austenite. The current tempering cycle is designed in such a way that most of the larger MA (containing low amounts of austenite) will decompose while the smaller MA containing more austenite does not. The larger MA only decomposed after tempering, the austenite inside larger MA may transforms to ferrite and carbides. However, the austenite in small MA was retained after tempering, which may account for the remaining large austenite even after tempering. The larger MA is predominantly martensite and contains higher carbon than smaller MA. Thus, larger MA is more prone being tempered than smaller MA. The higher carbon in the larger MA provides a driving force to complete the transformation to ferrite and carbide. It has been reported that small austenite (<1µm) will remain as austenite even with faster cooling rates [7, 100]. It had been reported that the austenite transforms into ferrite and carbide at a PWHT temperature of 620°C.

However, at temperatures of 300°C and 200°C with short tempering times of 1 to 5 min, there was no evidence of MA decomposition. This observation is also confirmed by SEM. These results suggest that both tempering temperature and tempering time have effect on decomposition of MA, while temperature has more significant effect. Liao et al. reported partial decomposition of MA at tempering temperature of 200-250°C, however 300-400°C causes necklace-like MA

constituents to decompose, associated with an improvement in toughness at this PWHT temperature range [108].

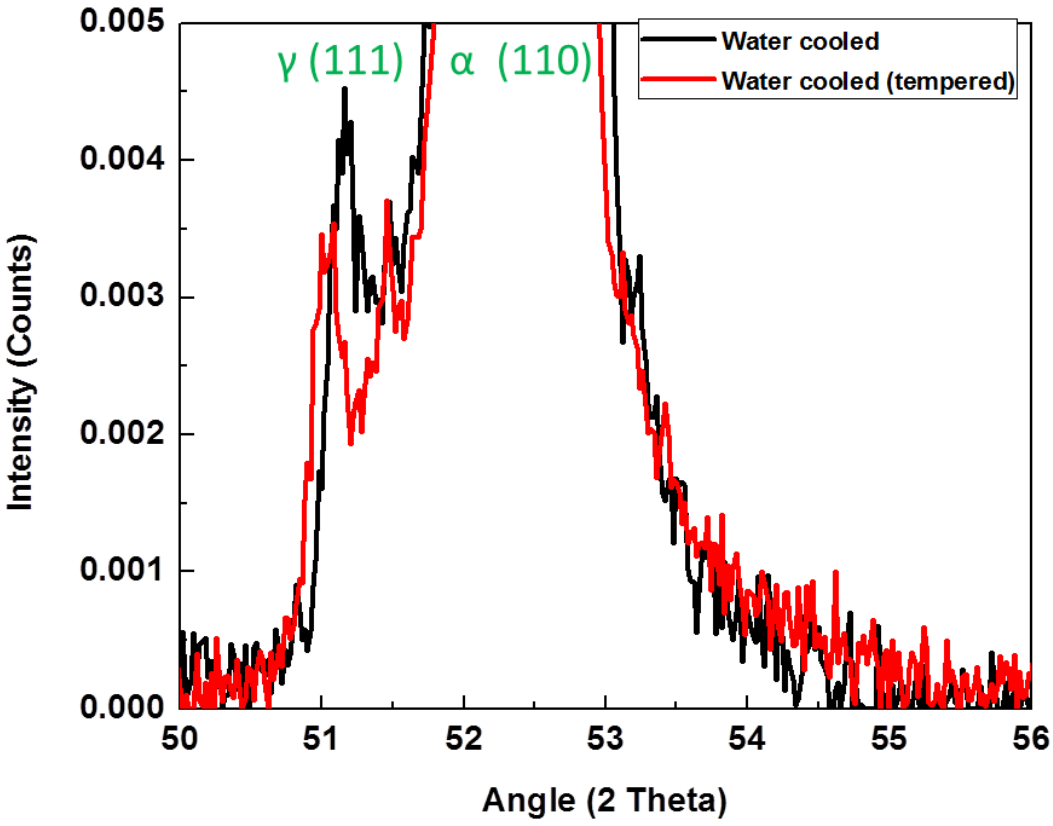

Figure 6-8 : XRD analysis before and after tempering in water cooled sample at 300°C

6.5.2 Hardness Investigation in heat treated sample

The base metal average hardness is 230 ±10 HV, while the hardness following the first thermal cycle (1000°C) is 168.2 ±6 HV. After the second thermal cycle (710°C), hardness increased to 189.7 ±3 HV, where this increase may be due to a higher percentage of MA. After tempering treatments at 300°C and 200°C for 1 hr, the hardness decreased to 160.3 ±2 and 178.4 ±8 HV respectively. However, when the tempering time is reduced to 10 min, the hardness is 170.8 ±3.5 and 186.9 ±7.7 HV respectively. It can be also observed that there is a decrease in hardness with increases of tempering temperature (200°C to 300°C) and time (10 min to 1hr). The drop in

hardness with increase of tempering temperature and time had been reported by Janovec et al. and Liao et al. due to MA decomposition [108, 109, 113].

6.5.3 In-Situ TEM analysis of MA tempering

In-situ tempering is performed in a TEM to investigate the structure inside and around MA before and after PWHT. The bright field and dark field images of several MA microconstituents were compared before applying a tempering cycle (300°C for 10 min). Diffraction is performed in several MA constituents before tempering, confirming the presence of both austenite and martensite. One of the bright filed images of a larger MA (3 μm in length, 2 μm in width) is shown in Figure 6-9a. It is found that the MA contains mostly martensite as revealed by indexing selected area electron diffraction spots (Figure 6-9b). Though this larger MA does not reveal the presence of austenite, the smaller MA contains more austenite. However, this larger MA is selected to observe the effect of tempering in-situ (since during the optimum tempering cycle only the larger MA is decomposed). Then a heat treatment schedule (300°C for 10 min) is performed in-situ during TEM observation, while a video is captured. After heat treatment, the diffraction is performed in the same location of same MA constituents. A bright field image of MA after tempering is shown in Figure 6-9d The presence of cementite is also confirmed after the tempering cycle by indexing the (111) family of reflections (Figure 6-9e) [149]. Dark field imaging was not performed in TEM, since the formation of fine precipitates corresponding to carbides were observed by SEM microscopy (Figure 6-7h) and Auger Electron Spectroscopy (Figure 6-11 a&b).

The dislocation distribution around the MA was observed before and after tempering from same location as shown in Figure 6-9 c&f. There are some dislocations (based on contrast difference performed by different tilting angle) in the ferrite surrounding the MA (Figure 6-9c) which may have resulted from the large hardness difference between MA and ferrite. It can be observed from Figure 6-9f that there is a change in dislocation density around MA (in the ferrite matrix) after the tempering cycle which might suggest a rearrangement in dislocation density, thereby a reduction in residual stress. This suggests that tempering at 300°C for 10 min may relieve stress at the MA/ferrite interfaces. It is also observed that some of the dislocations annihilated around the MA after tempering, which can indicate a high strain distribution in the ferrite around the MA, which might be relieved after in-situ tempering (Figure 6-9c&f). It has been also observed that there is a structural difference within MA after the tempering cycle which might be due to a

reduction in dislocation density. However, the thin specimen may subjected to bending during heating which can affect the observation on dislocation since the contrast can change due to bending. Therefore, there is uncertainty about dislocation distribution observation before and after tempering could be resulted.

Liao et al. observed precipitation of carbide after tempering at a temperature 250°C in a martensite structure, where carbide precipitation was more significant at higher temperature and carbides spheroidized at 620°C [109]. However, they reported that MA was partially decomposed at 250°C in a bainite structure, and MA was completely decomposed at a temperature 350°C [109]. In addition, generation of internal stresses inside martensite caused a significant loss in ductility [148]. Liao et al. suggested heat treatment can eliminate the residual stress [108]. The PWHT process can permit rearrangement of atoms, and thereby relieve internal stresses [150]. Tsuyama et al. reported an improved toughness properties due to uniform strain around MA [151]. The MA constituent may undergo transformation to cementite and ferrite after heat treatment, which will lead to more uniform plastic deformation according to the Ashby model, and thereby will improve toughness [111]. Okada et al. suggested an improvement of toughness due to MA decomposition and matrix softening [149]. Liao et al. showed more conclusive results by differentiating the individual contributions of MA decomposition and matrix softening on toughness after PWHT. There was improvement in toughness only because of MA decomposition at a PWHT temperature range of 250-623°C with a 28.8ks holding time [149], and it can be expected that a lower dislocation density in the matrix is produced after PWHT [109].

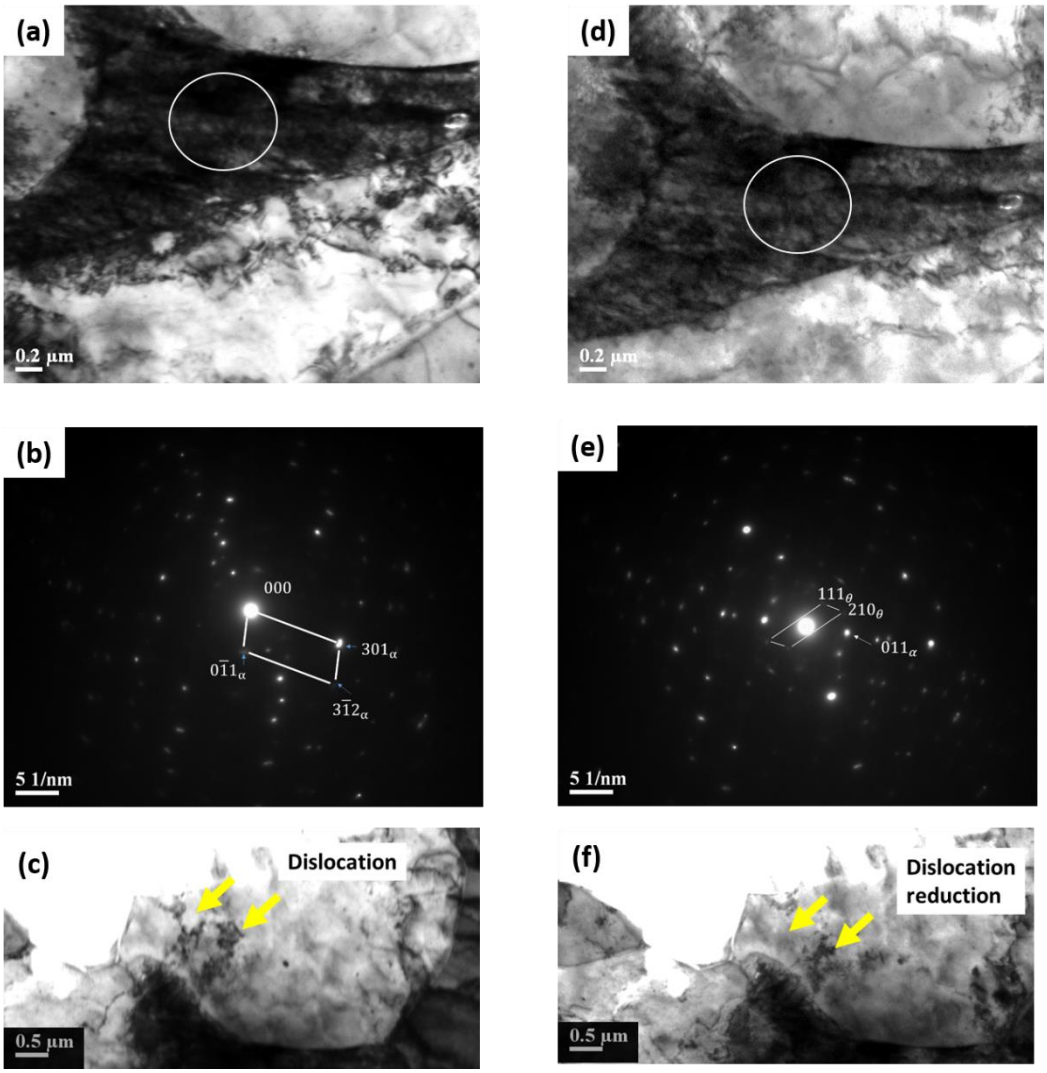

Figure 6-9 : (a) Bright field image of MA before tempering (circle showing SAD pattern location) (b) SAD pattern from MA before tempering cycle (c) dislocation around MA before tempering (d) MA after tempering with circle showing SAD pattern location(e) SAD pattern of MA after tempering (f) dislocation reduction around MA after tempering (300°C, 10 min) in the same location as figure 6-9c.

6.5.4 Auger Electron Spectroscopy of MA

Auger analysis was performed on both water cooled and tempered water cooled samples quenched from a temperature of 300˚C. A uniform carbon distribution was observed inside untempered MA and the ferrite matrix in the water cooled sample Figure 6-10 [133]. It has been observed that the MA contains a high fraction of carbon in comparison to the ferrite matrix. The

presence of high carbon in comparison to the ferrite matrix is reported in other research [63, 152]. However, after tempering the MA internal structure is found to differ from untempered MA (Figure 6-11a&b). Instead of a uniform carbon distribution inside the MA region, a high percentage carbon is observed in several locations within the MA which corresponds to carbides (Figure 6-11b). The presence of cementite carbide was confirmed previously using the TEM analysis in section 6.5.3.

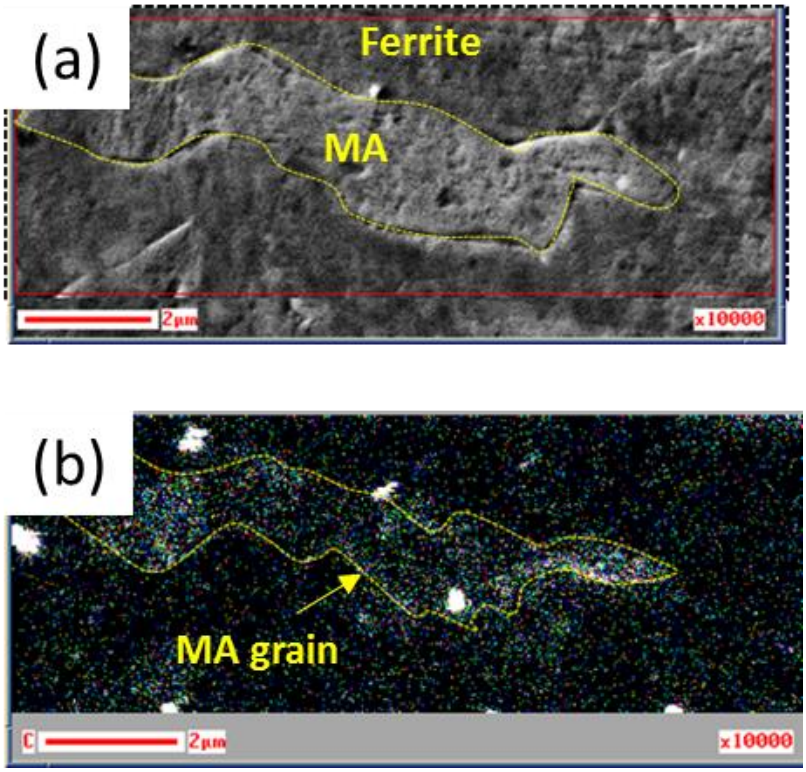

Figure 6-10 Auger Electron Spectroscopy carbon mapping (a) SEM image of untempered MA (b) carbon mapping of untempered MA

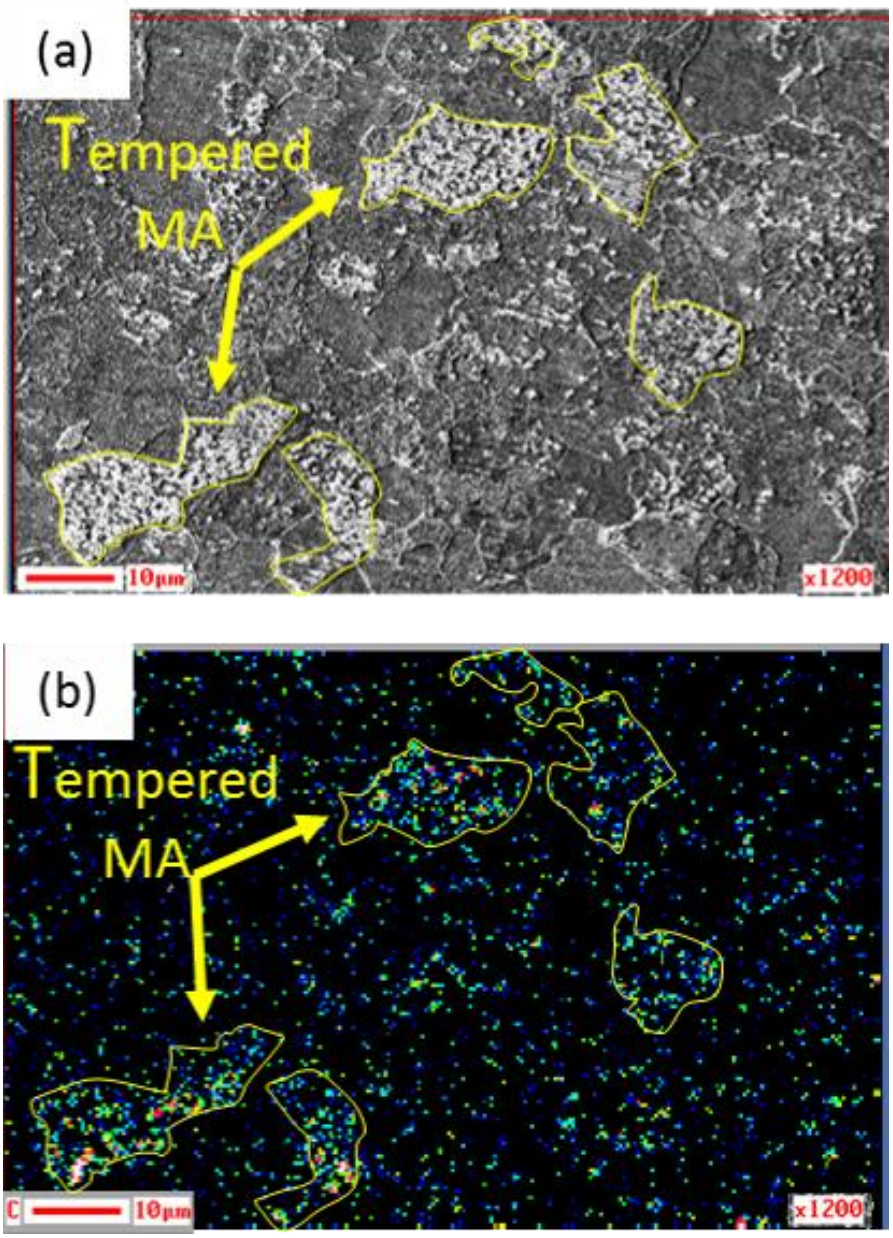

Figure 6-11 : Auger Electron Spectroscopy carbon mapping (a) SEM image of tempered MA with carbide inside after 300°C, 10 min tempering (b) carbon mapping of tempered MA with carbide (high carbon concentration) after 300°C, 10 min tempering

6.5.5 **Nanoindentation**

Nanoindentation is used to investigate properties of isolated grains, first for the water cooled sample containing MA with no tempering imposed. The hardness of MA is found to be 5.09 ±0.5 GPa while ferrite grains exhibit a hardness of 2.82 ±0.3 GPa (Figure 6-12a). The high hardness of MA in comparison to ferrite can be explained by the contribution of a high carbon martensite phase. However, the hardness of tempered MA is 3.7 ±0.75 GPa while the ferrite hardness is 3.5 ±0.68GPa (Figure 6-12b). It had been reported that there was drop in MA hardness after PWHT which results from MA decomposition [113]. The average hardness increase in ferrite coupled with MA softening can be explained by carbon diffusion out of the MA and into the ferrite, resulting in a more uniform hardness distribution throughout the phases, and has also been explained as a secondary hardening effect by Liao et al. [109].

It can be also observed that the load-displacement curve during nanoindentation for the untempered MA exhibits continuous deformation behavior. However, there is evidence of discontinuous deformation behavior in the tempered MA loading curve which is consistent with pop-in behavior [153]. It had been reported that such pop-in behavior is associated with a reduced dislocation density [154], and a similar phenomenon is also observed by Ohmura et al. when nanoindentation is performed in tempered martensite related to dislocation reduction [153].

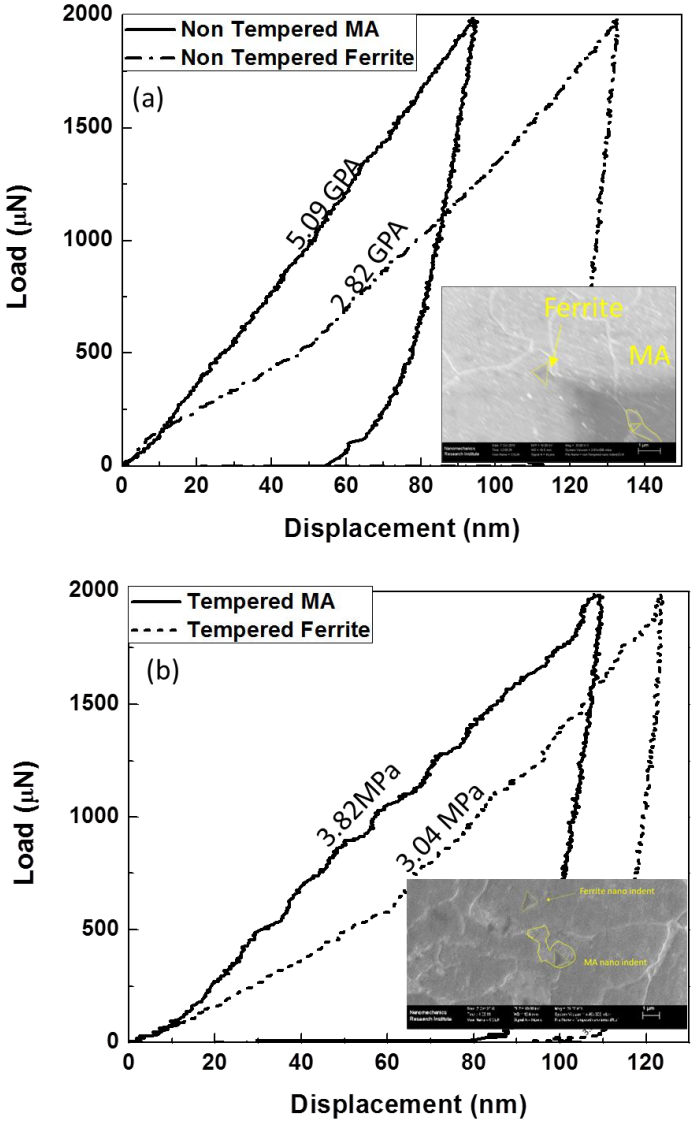

Figure 6-12 : Comparison of nanoindentation loading curves for MA and ferrite hardness (a) before and (b) after tempering (300°C, 10 min).

6.5.6 Tensile testing

The yield, tensile strengths and fracture strains are also compared on water cooled samples with and without tempering. The measured yield and ultimate strength values were 385 ±10 MPa and 552 ±15 MPa for the as-cooled specimen, with a 21.1% elongation observed. However, these values are 419 ±12MPa and 560 ±11MPa respectively for the PWHT water cooled sample, with an elongation of 21.9%. An example for stress-strain curve is shown in Figure 6-13. It can be

observed that there is slight improvement in ductility and yield strength after tempering while the tensile strength remains similar. The bulk strength increase may be attributed to fine carbide formation. It is interesting to find that despite this strength increase, the average hardness decreases from 189 HV to 170 HV after tempering. It can be observed from Figure 6-9c&f that some of the dislocations may disappear around MA after tempering; indicating that some residual stress is relieved. Okada et al. suggested strain field around MA might be a controlling factor for crack initiation [60].

Li et al. observed a drop in hardness with an increase in tempering temperature [148], while simultaneously finding an increase in yield strength and ductility after applying a 300°C tempering temperature. However, tempering temperatures of more than 300°C led to a decrease in tempered martensite and increase in ferrite and carbides due to diffusion of carbon, resulting in an overall decrease in strength, along with an increase in ductility [148]. In addition to residual stress, formation of carbides can affect the ductility and yield strength. For example, Zhao et al. observed a drop in hardness at tempering temperatures in the range of 210-560°C, however the yield strength and ductility was improved [155]. It was noted that ε-carbide formation was observed when tempering at 210°C while acicular cementite formation occurred in the temperature of 310-560°C.

Moreover, it can be observed in Figure 6-8 that there is a decrease in austenite percentage after tempering. The TEM diffraction patterns also reveal the presence of carbide and an BCC structure. That might suggest austenite is transforming at 300°C during a 10 min tempering time, which could indicate that austenite is detrimental to the mechanical properties. It has been suggested that formation of retained austenite can promote migration of impurities to grain boundaries which may facilitate crack initiation [156], by increasing boundary energy. Li et al. also reported a significant amount of austenite decomposed at a temperature of 300°C and this led to an improvement in yield strength and ductility in AISI6150 steel [148].

In addition, Davis and King suggest that there will be debonding of MA from matrix due to a difference in hardness between MA and the matrix during tensile tests [8], along with debonding of MA in elevated temperature tensile testing at 196°C. Now it can be observed from Figure 6-12 that the hardness difference between the MA and ferrite matrix is reduced after tempering. The reduced hardness might also prevent early debonding and thereby improve yield strength and ductility. Moreover, a reduction of dislocation density inside MA (observed by TEM and based on nanoindentation results), which would provide more straining capacity in the

tempered MA, and improve ductility. Fracture surface observation showed that the fracture dimples are finer when tempering is applied (Figure 6-14a&b) which is consistent with higher strength and ductility. In addition, some large holes can be observed in Figure 6-14a which might correspond to larger MA, while holes in tempered water cooled sample are smaller. This would suggest that the larger MA deteriorates the mechanical properties more significantly by forming larger voids during tensile tests.

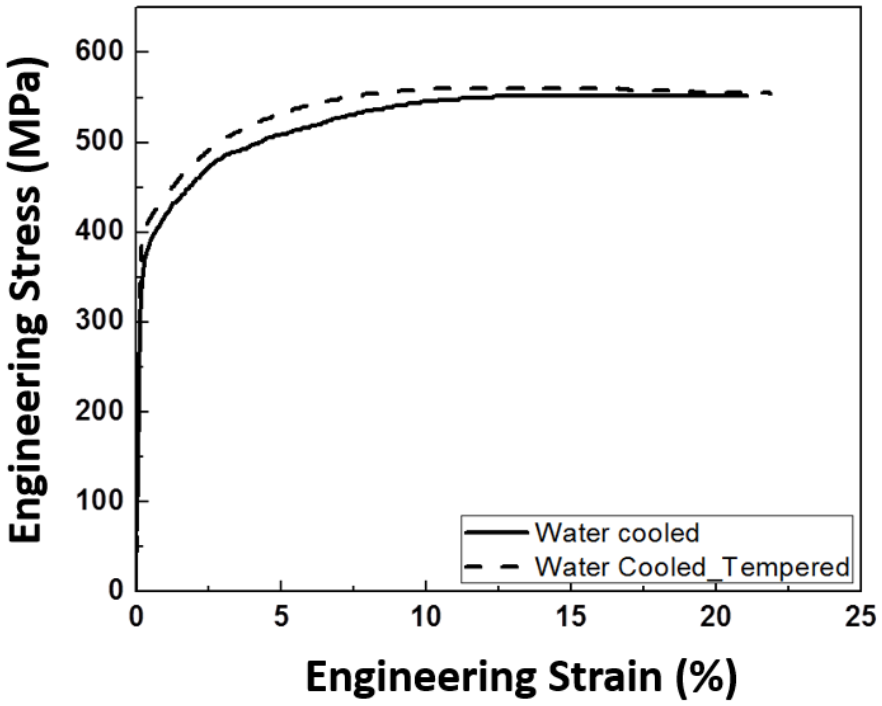

Figure 6-13 : Stress-strain curve for water cooled and water cooled tempered sample

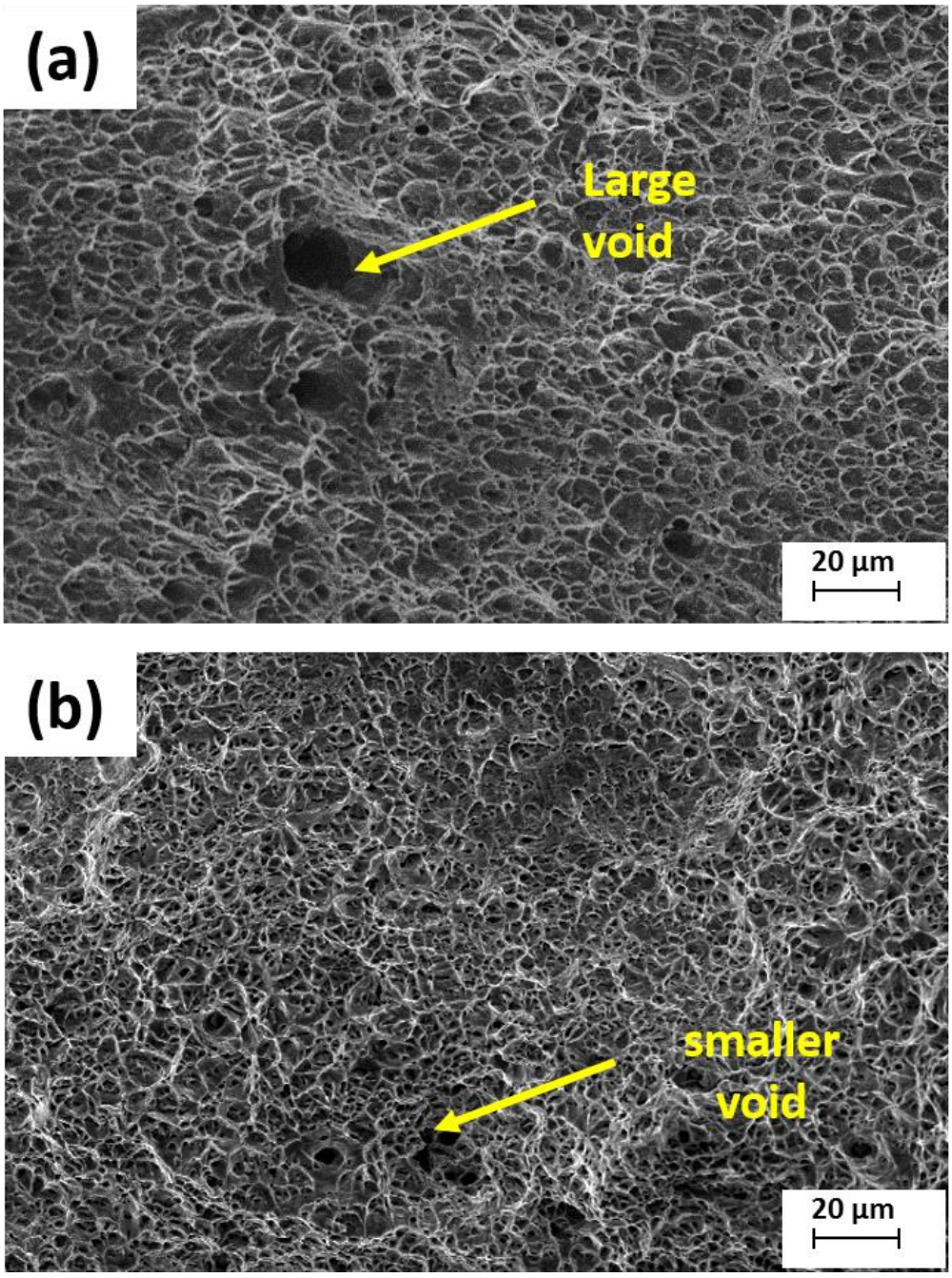

Figure 6-14 : Tensile fractured surface (a) water cooled sample with coarser dimple structure (b) tempered water cooled sample with finer dimple structure

6.6 Welding joint mechanical properties evaluation at tempering cycle

It has been reported by most of the work that massive MA is more detrimental than small MA. According to the results above, a tempering cycle of 300°C applied for 10 min is effective in selectively tempering larger MA, and this schedule is applied to welds for further study to confirm the effect on mechanical properties.

A total of 6 hardness profiles were measured on both sides of weld reheated zone before and after tempering. The average hardness of those lines are shown in Figure 6-15. It can be observed that hardness decreases for both welded and PWHT welded sample, moving from fusion line to base metal direction, over which a gradual grain size decrease can be noted. However, the hardness for PWHT welded sample is lower than the water cooled sample. The drop in hardness might be due to some larger MA decomposing, which is consistent with the heat treatment hardness study. It is observed that there is no change in grain size after PWHT, and hence the drop in hardness appears mainly related to MA decomposition. SEM observation is performed in the reheated zone of PWHT samples. It is observed that most of the large MA ($\geq 1\mu m$) is decomposed, while small MA ($<1\mu m$) are not decomposed (Figure 6-16), which is also consistent with the heat treatment study. The presence of some particles inside decomposed MA is also observed which appear to be carbides (Figure 6-16b). The decomposition of larger MA might lead to a drop in hardness in the reheated zone of the weld after PWHT.

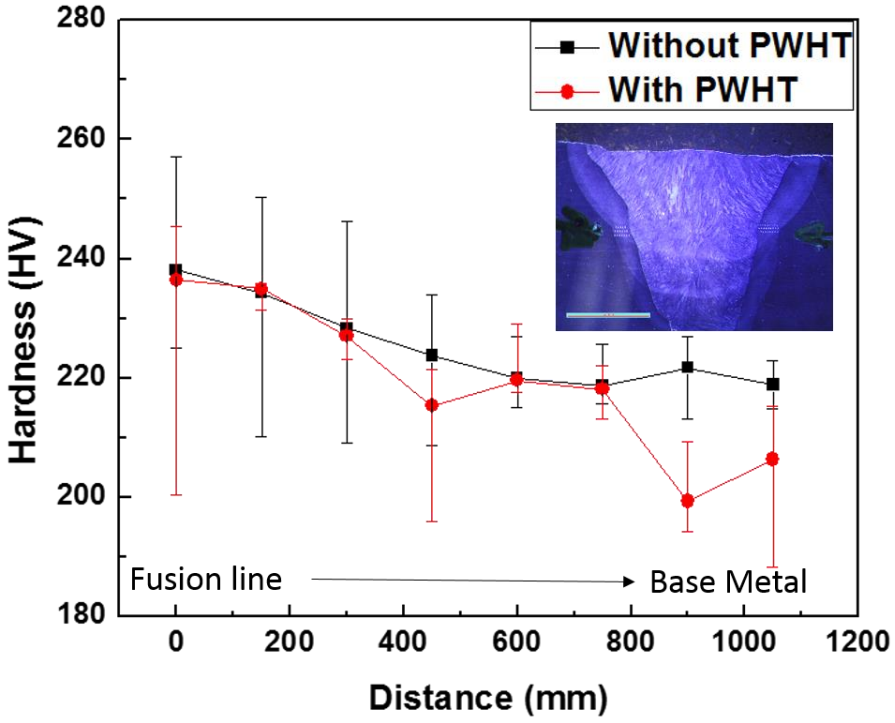

Figure 6-15 : Hardness comparison in reheated zone of welded sample before and after tempering (points are an average of 6 lines on both side of weld)

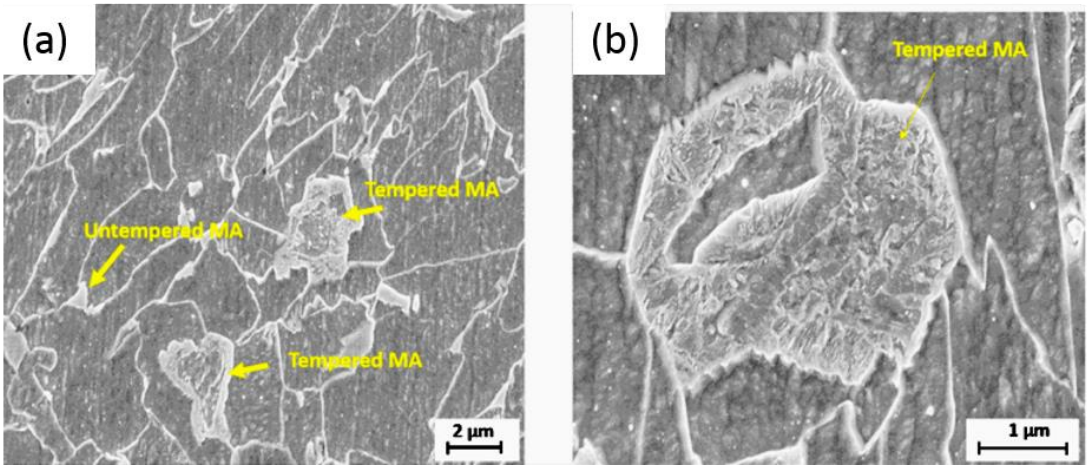

Figure 6-16 : (a) SEM image in reheated zone of welded sample after tempering for 300°C, 10 min (2% Nital) (b) higher magnification image of MA after tempering (2% Nital)

In order to compare the influence of PWHT on the strength and ductility, three tensile tests are performed in same condition as in section 6.4. A higher stress and strain is recorded in tensile test for PWHT welded sample than the as-welded sample. It was found that a 617 ±14 MPa yield strength and 641 ±15 MPa tensile strength with maximum 43% elongation is attained. A stress-strain curve comparison before and after PWHT weld is shown in Figure 6-17. Metallography reveals that the fracture goes through the base metal for PWHT sample instead of HAZ (before PWHT). It is found that fracture occurred at a distance of 0.33 mm in the water cooled sample from fusion line which is inside the HAZ. However, for the PWHT welded sample fracture occurred at a distance of 2.15 mm away from the fusion line, which is in base metal. Observation of the fractured surface revealed that dimples dominate the structure similar to Figure 6-3a, consistent with base metal fracture. Strain measurements using image correlation showed that there is a 23% contraction (ratio of fracture surface width after tensile test versus the width of tensile sample before tensile test) for the HAZ fractured sample while it is 52% for base metal fractured sample. That result suggests that base metal fractured sample sustains higher strain than the HAZ fractured sample which can also be noted in Figure 6-17.

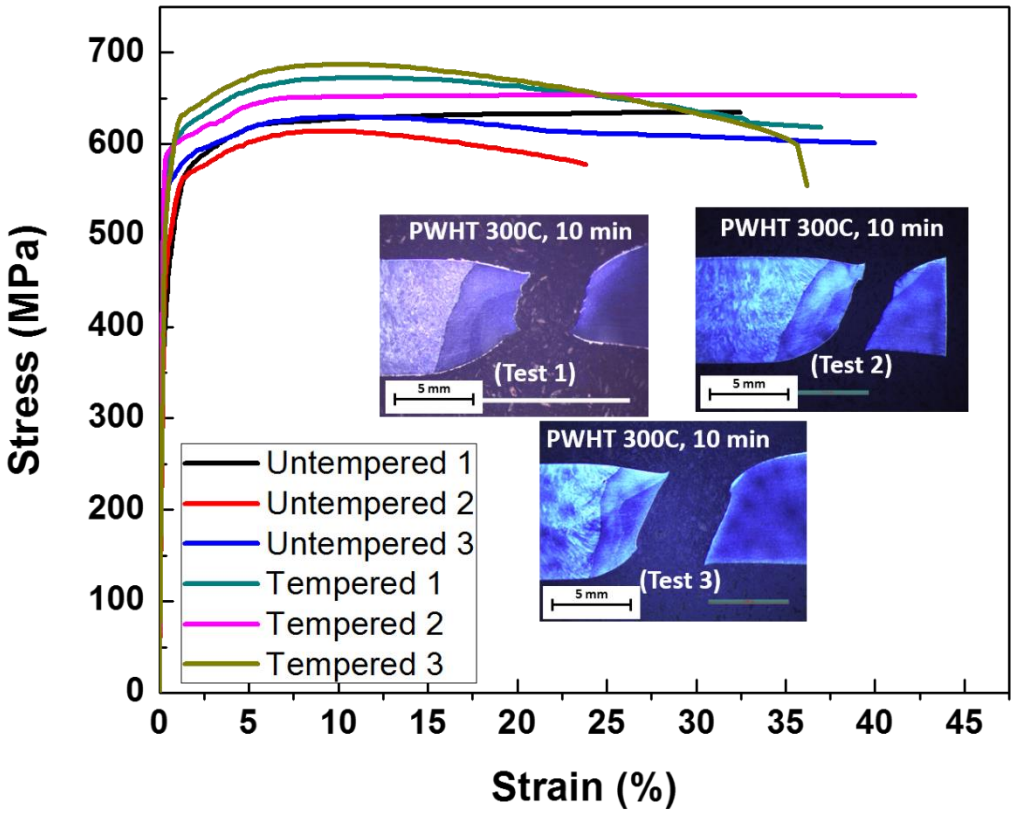

Figure 6-17 : Stress-Strain curve comparison (based on point based strain analysis) before and after PWHT (300°C, 10 min)

The results presented here suggest that a tempering cycle will improve the properties of the weld. Tempering is effective in decomposing detrimental MA and may relieve some residual stress around the MA regions. These remedial effects can strengthen the HAZ and thereby restrict void formation upon plastic deformation, and help suppress fracture in the HAZ. Charpy impact tests conducted in the welded and PWHT welded samples involved making the notch in HAZ, similar to the method proposed by Lan et al. [91]. Metallography showed that primary fracture went through the weld metal instead of the HAZ, though it is difficult to isolate the contribution of PWHT exclusively on the stress-strain performance of the HAZ.

6.7 Summary

A potential Post Weld Heat Treatment (PWHT) cycle has been determined by evaluating the microstructures and mechanical properties for various tempering times at 200 and 300ºC respectively. Fracture occurred in the HAZ before applying a PWHT to a weld. Subsequently, a potential PWHT cycle has been applied to the welded sample. The following conclusions have been reached:

1. Fracture occurred in the HAZ of the welded sample, which is dominated by void nucleation from the MA/ferrite interface and debonding of MA. The MA regions with sizes over 1μm were found detrimental to mechanical properties.

2. Performing tempering at 300°C, for 10 min was found to decompose detrimental coarse MA and provide a more benign size distribution of MA. The hardness of untempered MA regions was found to be twice the hardness of the ferrite matrix before heat treatment. However, after PWHT the hardness difference between MA and ferrite matrix was decreased. After the PWHT cycle the yield strength and ductility was slightly improved, which might relate to decomposition of detrimental MA and reduction in dislocation around MA.

3. Applying the PWHT cycle in the welded sample, fracture during transverse weld tensile testing shifted from the HAZ to the base metal. This was explained by decomposition of detrimental MA and a reduction in dislocation around MA. This prevents premature void formation and coalescence, resulting in an improvement in yield strength and ductility when the fracture location shifted towards the base metal.

Chapter 7 : MA Distribution, Fraction and Size Effect on Toughness [4]

7.1 Overview and background

The objective of the current work is to study the MA fraction, size and distribution effect on toughness properties. This will require one to investigate the effect of MA in pipeline materials, and the results from the specific pipeline alloy studied will provide insights into other similar alloys. Varying cooling rates will be used to investigate the influence of the martensite-austenite (MA) microconstituent on the toughness properties of X80 linepipe steel after intercritical reheating. The effect of MA on toughness will be evaluated and subsequently MA role in fracture mechanism will be investigated.

7.2 Materials and experimental procedure

An X80 linepipe steel was used to investigate the role of thermal cycles on MA formation and the corresponding effect on properties. Based on these temperatures attain from the calculation in Chapter 6 section 6-2, an experimental heat treating schedule was developed as shown in Figure 7-1. In first thermal cycle, three samples with dimensions of 40 x 20 x 15 mm were heated to a temperature of 1000°C (above Ac3) using a furnace, held for 20 min and then air cooled to room temperature. A temperature of 1000°C and 20 min holding was applied to ensure uniform austenization throughout the specimen. In a second thermal cycle, all three samples were heated to a temperature at 710°C (just up to Ac1), for a holding time of 20 mins to achieve the austenization start temperature and subsequently cooled down from that microstructure to observe the change in microstructure. The samples were then subjected to different cooling rates (furnace, air, and water cooling). Three more samples are also heat treated in the same procedure except to a second thermal cycle peak temperature of 750°C (between Ac1 and Ac3) to compare how this higher temperature affects the fraction of MA.

4 This chapter is published Manuscript in Materials Science And Engineering A, 2016 on 22 March 2016, available online: https://doi.org/10.1016/j.msea.2016.03.095, Nazmul Huda, Abdelbaset R.H. Midawi, James Gianetto, Robert Lazor,Adrian P. Gerlich, Influence of martensite-austenite (MA) on impact toughness of X80 line pipe steels

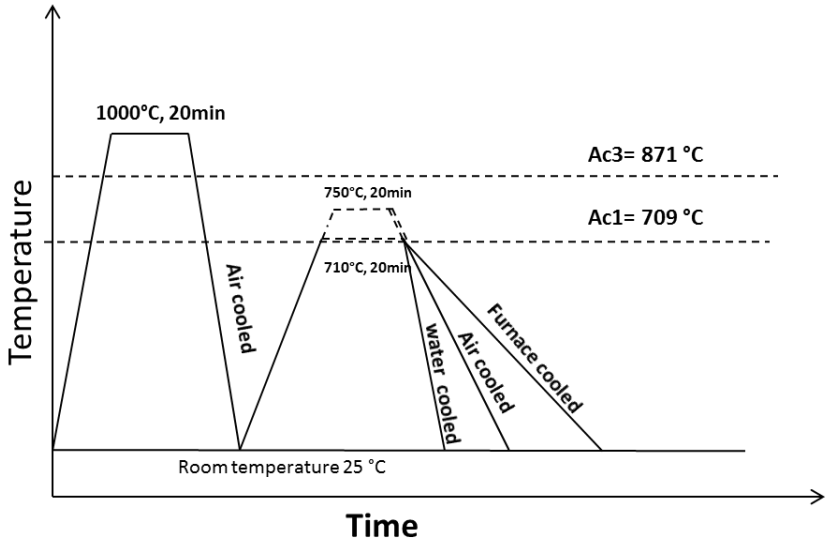

Figure 7-1 : Double thermal cycles developed with initial air cooling followed by intercritical reheating and different cooling conditions

XRD analysis (with Cu-Kα radiation using a Buker D8 instrument) was used to quantify the percentage of austenite in the structure. Auger electron spectroscopy (AES) was used to map the carbon distribution at different microconstituents of the samples using a JEOL 9500F system. Charpy impact testing was performed by cooling full size impact specimens (10 x 10 x 55 mm) to -100°C and -45°C using a mixture of ethanol, dry ice, and liquid nitrogen. At least three tests were performed at this temperature and the average was calculated.

7.3 Results and discussion

7.3.1 Microstructure

The as-received X80 base material microstructure is shown in Figure 7-2a. After the first thermal cycle (1000°C), the ferrite and bainite microstructure transforms into ferrite and degenerated pearlite (DP) (Figure 7-2b&c).

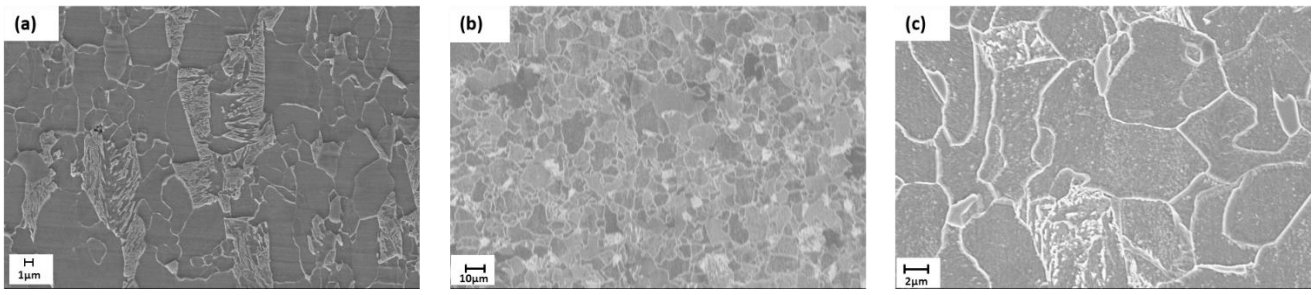

Figure 7-2 : SEM (a) X80 base metal (2% Nital) (b) after first thermal cycle (low magnification) - 2% Nital (c) after first single thermal cycle (higher magnification) - 2% Nital

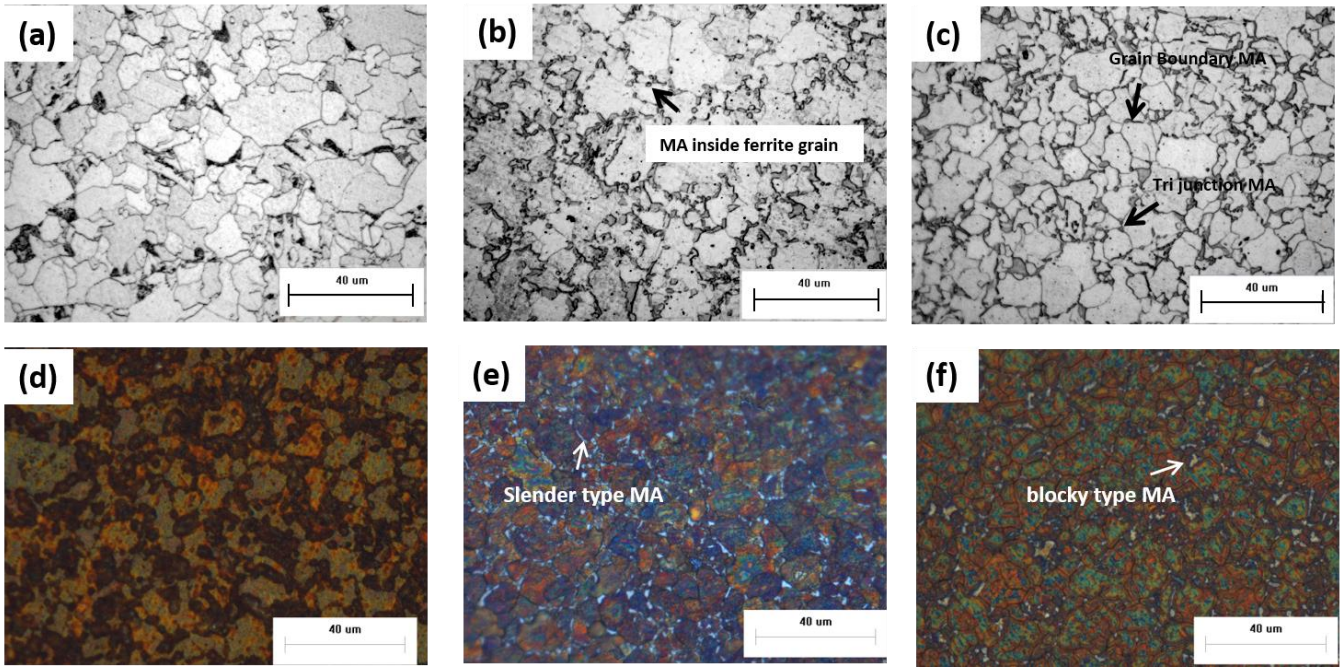

Figure 7-3 : Microstructure after second thermal cycle (710°C) (a, d) furnace cooled (b,e) air cooled (c,f) water cooled revealed using 2% nital and LePera etchants, respectively

The transformation of the ferrite and bainite base metal microstructure into ferrite and DP is confirmed by observations using SEM. The use of EDS analysis shows that the DP contains 2.0% manganese, which is slightly higher than the manganese content in the base metal (1.73%). Measurements were performed based on standard-less method and repeated for several MA points, with scatter of 0.1%. Moreover, it is a generally accepted that DP contains a higher amount of carbon than surrounding ferrite [152]. Based on image area analysis, quantitative microscopy reveals that 11% of the structure is DP and the remaining is ferrite.

After the second heating cycle, the furnace cooled sample exhibits a ferrite and DP structure Figure 7-3a. However, the air and water cooled samples (from a peak of 710ºC) contain fine islands of MA at the triple junctions of ferrite grains, at their grain boundary regions and even inside the ferrite grains Figure 7-3b&c. The use of LePera etchant on the furnace cooled sample does not reveal any white structures, meaning there is no MA in the structure. However, the air and water cooled samples containing numerous white islands in their structure (Figure 7-3e&f).

Both samples exhibit slender (with a length to width ratio of 4:1) and blocky type structures. However, the water cooled sample microstructure is predominantly a blocky type MA. This indicates that increasing the sample cooling rate promotes MA formation along with a transition in MA morphology from slender to blocky. Moeinifar et al. observed the formation of blocky and slender type MA in an X80 steel; however, it has been suggested that only blocky type MA forms along the prior austenite grain boundaries [94]. In contrast, the current work indicates that formation of MA occurs inside the grain as well as along the grain boundary. It is possible the prior observation of blocky MA forming exclusively at austenite grain boundaries is related to the higher peak temperatures used by Moeinifar et al. [94].

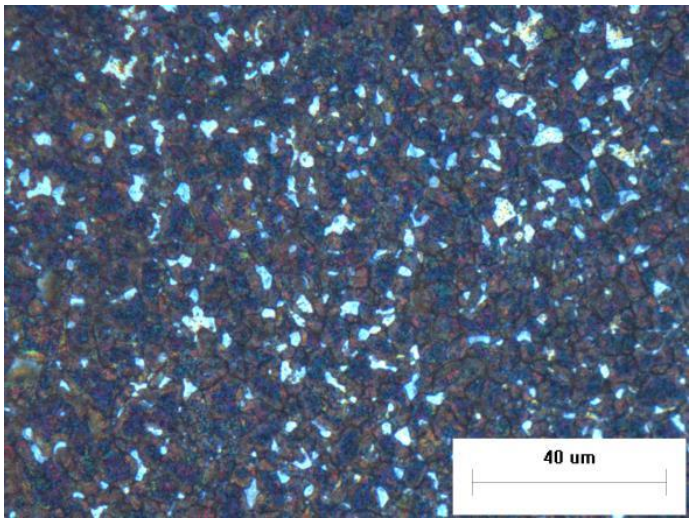

Figure 7-4 : Optical micrograph showing a higher area fraction of mainly blocky MA in a 1.3 mm thick sample exposed to increased cooling rate following reheating to 710ºC and water quenching (LePera etchant)

A small and thin sample (with dimensions of 10 x 10 x 1.3mm) was prepared from a specimen exposed to only the 1st thermal cycle, and reheated to achieve a higher second cooling rate. The specimen was subjected to a temperature of 710°C in the second thermal cycle and quenched in water. The LePera etchant revealed a higher percentage of MA (Figure 7-4) in the structure than the water cooled sample, along with a more blocky appearance.

Quantification of the microstructure following nital etching reveals that the air cooled samples (cooled from 710 and 750°C) with a 15 mm sample thickness contain 16% and 19% fractions of MA respectively. On the other hand, the water cooled sample of similar thickness contains a 20% fraction of MA when reheated to 710°C, versus a 25% fraction when it is reheated to 750°C. The area fraction of MA is greater in the water cooled sample (experiencing the higher cooling rate) than in the air cooled sample (lower cooling rate), regardless of the same peak temperature applied before cooling, suggesting a MA formation depends on the time allowed for transformation and diffusion. It can also be observed that for both air and water cooled samples, increasing the second thermal cycle temperature, also increases the area fraction of MA; which is consistent with literature [75, 100, 157]. By increasing the temperature above Ac1, more of the microstructure will transform into austenite, and so a greater volume fraction of austenite will have an opportunity to transform into MA.

SEM observation was performed on the MA structures appearing white in the air and water cooled samples following LePera etching. (Figure 7-5a&b) shows the air cooled and water cooled samples, in which the MA exhibits a two phase heterogeneity inside the MA grains. It has been reported that almost 96-97% structures are martensite phase in the MA structure [158]. The presence of small amounts of retained austenite in MA is also reported by other authors [59, 60, 159]. The formation of carbide inside MA is also reported in some prior work [78, 159]. However, SEM microscopy does not indicate the presence of carbide inside the MA, since only one heating and cooling cycle is applied without any holding time to cause tempering.

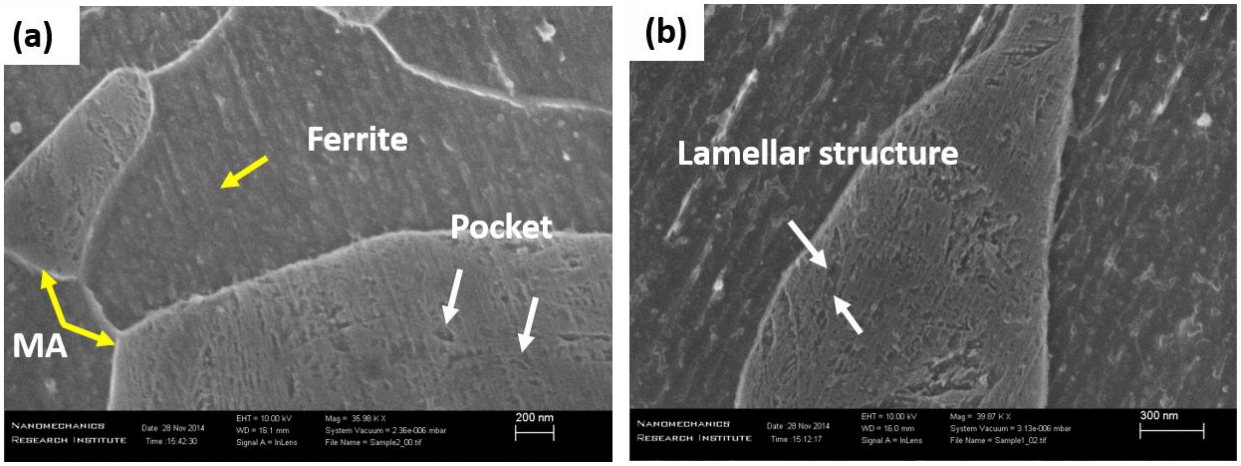

Figure 7-5 : SEM observation of MA (a) air cooled (2% Nital) (b) water cooled (2% Nital). (white arrow indicates a secondary phase inside an MA grain)

The average hardness value of the base metal is 230 ±10 HV. The hardness of the ferrite and DP structure after the 1st thermal cycle is 168.2 ±6 HV. For the second thermal cycle furnace cooled sample there was nearly identical micro hardness obtained 168.5 ±8 HV. In contrast, for the air and water cooled samples there was an increase in hardness, from 168.2 to 182.2 ±6 HV, to 189.7 ±3 HV respectively. The water cooled sample MA fraction (20%) is higher than in the air cooled sample (16%). Based on this it can be noted that with increased cooling rate the hardness increases, which is expected consider on the increased fraction of high hardness MA regions in the water cooled specimen [114].

7.3.2 Tensile testing

The base metal yield and tensile strength in transverse direction was found 662 ±23 and 770 ±4 MPa respectively with an elongation to failure of 21%. Tensile testing was also performed on furnace and water cooled samples to observe the effect of MA on mechanical properties. The furnace cooled samples had a yield strength of 370 MPa (at 0.2% offset) and tensile strength of 483 MPa (Figure 7-6). The water cooled samples had yield and tensile strengths of 404 and 525 MPa, respectively, while the elongation to failure slightly decreased from 15 to 12%. Both the furnace and water cooled samples exhibited yield point elongation (YPE), though the YPE was smaller in the case of the water cooled sample. However, YPE does not occur in base metal, which

may relate to dislocation-carbon interactions. Heat treatment may result in the diffusion free carbon atoms to the dislocations, resulting in the pronounced lower yield point behaviour. However, there may few free carbon atoms decorating dislocations in the base metal, and hence no lower yield point was observed.

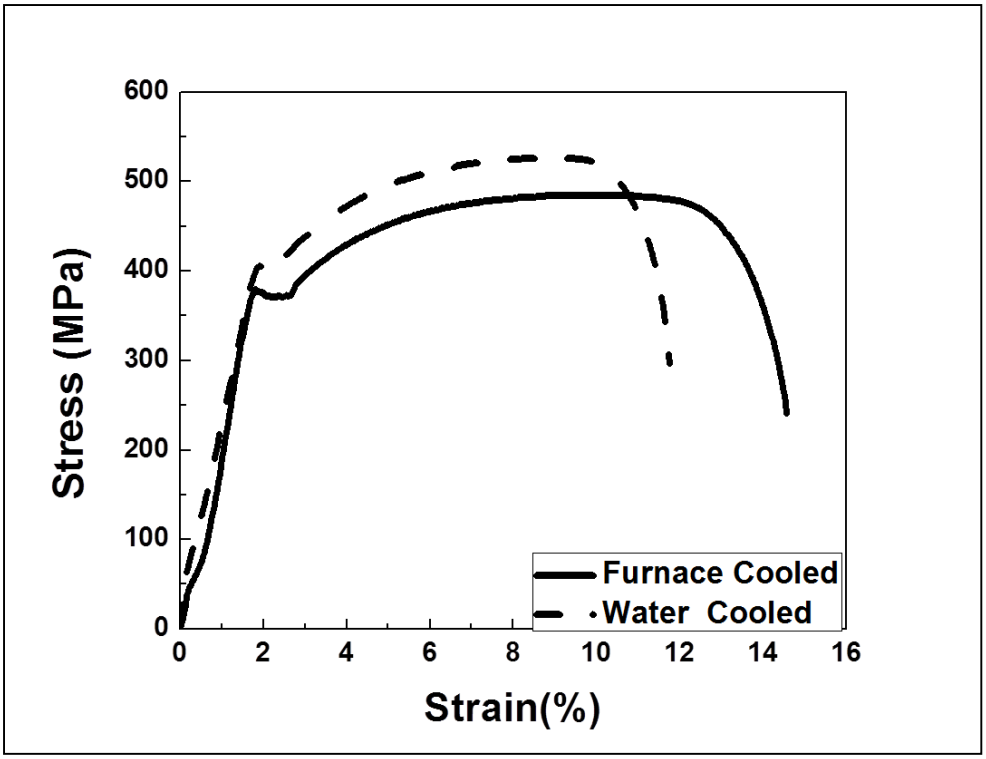

Figure 7-6 : Stress-Strain curves for thermally cycled specimens.

7.3.3 XRD analysis

X-ray diffraction analysis was used to investigate the presence of austenite in furnace, air and water (710°C) cooled samples (Figure 7-7a). The intensity of the counts is normalized based on the highest peak measured, where each sample had peaks measured to approximately 10,000 counts. The graph shows that the furnace cooled sample does not contain austenite. However, a peak for the austenite phase is found in the air and water cooled samples, though the percentage is rather small. The formation of austenite is believed to be due to the high carbon content providing a stabilizing effect for austenite, along with the lack of martensite nucleation and the volume constraint from the surrounding matrix [100]. The austenite percentage was determined using XRD

analysis by comparing the relative peak intensity of the austenite crystal reflection to the ferrite peak as shown in Chapter 6.

According to calculation, the air cooled sample contains slightly more austenite (0.183%) than the water cooled sample (0.179%). Narasimha et al. reported that the austenite percentage decreased in the water cooled sample compared to air cooled sample due to difference in carbon diffusion [160]. Although, the difference of austenite fraction is low between air and water cooled specimen, the high intensity counts of ferrite (400000) may suggest that the difference is significant. Hrivnak and Lambert et al. also reported a decrease of austenite percentage in MA with an increase of cooling time because of a variation in carbon diffusion [75, 80]. Matsuda et al. concluded that blocky type MA contains more austenite than elongated MA [60]. It has also been reported that retained austenite can cause crack initiation and propagation as impurities move to the periphery of austenite during its growth. It should be noted that a 15ºC increase in notch toughness transition temperature can be found with the presence of 1% retained austenite [80].

Research has shown that precipitation of carbide and ferrite could occur from MA when a third thermal cycle is used with a peak temperature between 300 to 600°C, and there could be improvement in toughness [60, 78, 157, 161]. A third thermal cycle could also transform part of the retained austenite into martensite [80, 159]. To investigate this phenomena, the samples which were air and water cooled from 710°C were then subjected to tempering for 1 hour at 300°C and cooled in liquid nitrogen. The motivation behind this third cycle was to temper any martensite contained within the MA phase regions, and also to fully transform any of the retained austenite within the MA phase into martensite, carbide or ferrite structures. XRD analysis was used to investigate the change in austenite percentage in the tempered samples, and this is shown in Figure 7-7b with the intensity peak of the counts normalized. The graph illustrates that although austenite is present, the fraction in both air (0.09%) and water cooled samples (0.14%) are reduced. It has been reported that austenite islands smaller than 1 μm will remain as austenite even at fast cooling rates [7, 162] and thus part of the MA regions in the air and water cooled samples might transform into martensite, cementite or ferrite [80]. XRD results confirmed carbide (Θ) formation in water cooled specimen (Figure 7-7b), although this was not evident in air cooled specimen. However, SEM investigation of the tempered air cooled sample shows the precipitation of carbide inside the MA grain, as shown in Figure 7-8. However, it is difficult to confirm the presence of martensite and austenite inside the MA; and so the hardness of the air cooled sample was measured for before

and after tempering the air cooled sample. The tempered air cooled sample (186.8 to 192.8 HV) was found to be harder than the air cooled sample (177.6 to 186.9 HV) with a 95% confidence level, suggesting that part of the austenite transforms into martensite.

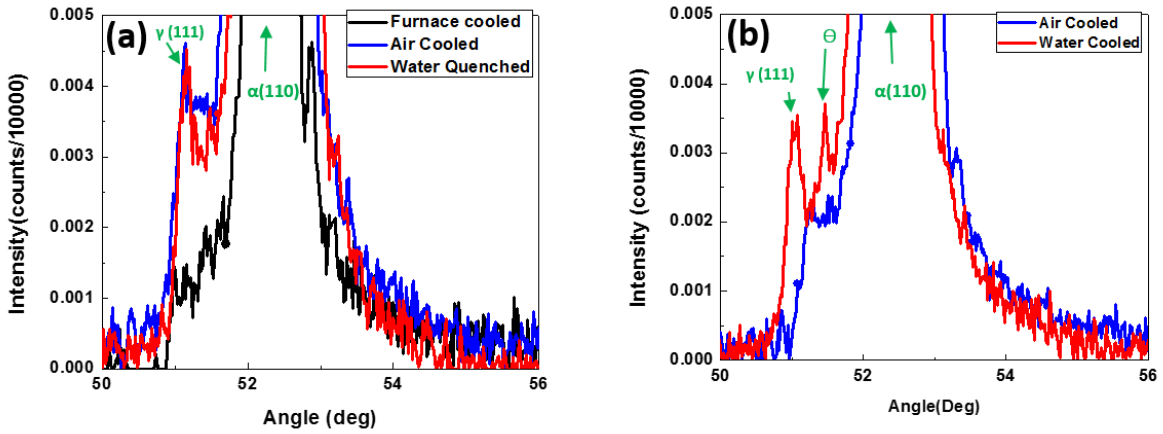

Figure 7-7 : XRD analysis a) after 2nd thermal cycle b) after a 3rd thermal cycle

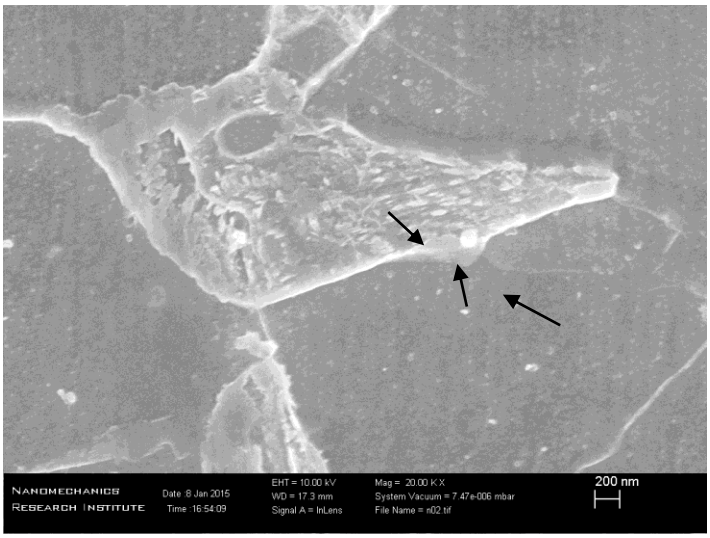

Figure 7-8 : Evidence of tempered MA after 3rd thermal cycle, arrows indicating the presence of carbides within the MA region (2% Nital).

7.3.4 **Carbon mapping within MA regions**

Carbon mapping confirmed a higher carbon content in the MA regions than in the surrounding ferrite matrix for both air and water cooled samples (Figure 7-9b&d). Josefsson and Okada et al. both reported that MA contains a higher percentage of carbon (1.14 & 1.5wt% respectively) than the surrounding ferrite matrix and this carbon percentage increases in MA with an increase in cooling rate [60, 152]. High concentrations of carbon in the MA are also reported by others [38, 71]. The air cooled sample carbon mapping also revealed that the MA regions can be connected to each other (Figure 7-9a), a fact also observed in other work [129]. This connected structure can lead to poor toughness, since it can provide a path for easy crack propagation. Several small and medium sized MA grains (1 to 4 μm in length, 0.5 to 2 μm in width) were also observed in the air cooled sample (Figure 7-9a). The MA grains in the water cooled sample are much larger (8.5 μm in length, 1.7 μm in width) (Figure 7-9c). It can be noted in Figure 7-9b that the finer MA grains in the air cooled sample contain scattered pockets with a high carbon concentration within the MA, along with the appearance of the small islands observed inside the MA in Figure 7-5. It is suggested that these relate to austenite since it has been reported that austenite usually contains a high percentage of carbon, which is greater than in the martensite portion [75, 77, 163].

Based on the mapping results, it appears that the enriched carbon locations are not detected within the larger MA grains (Figure 7-9d), and this is consistent with reports that the austenite is enriched in carbon, and the portion of austenite will decrease when MA size increases [100]. The presence of packets of austenite inside the MA was investigated further using TEM considering this observation. Although some studies argue that silicon and niobium might facilitate the formation of MA, enrichment of these elements in the MA was not observed in this study [91, 129, 157, 159].

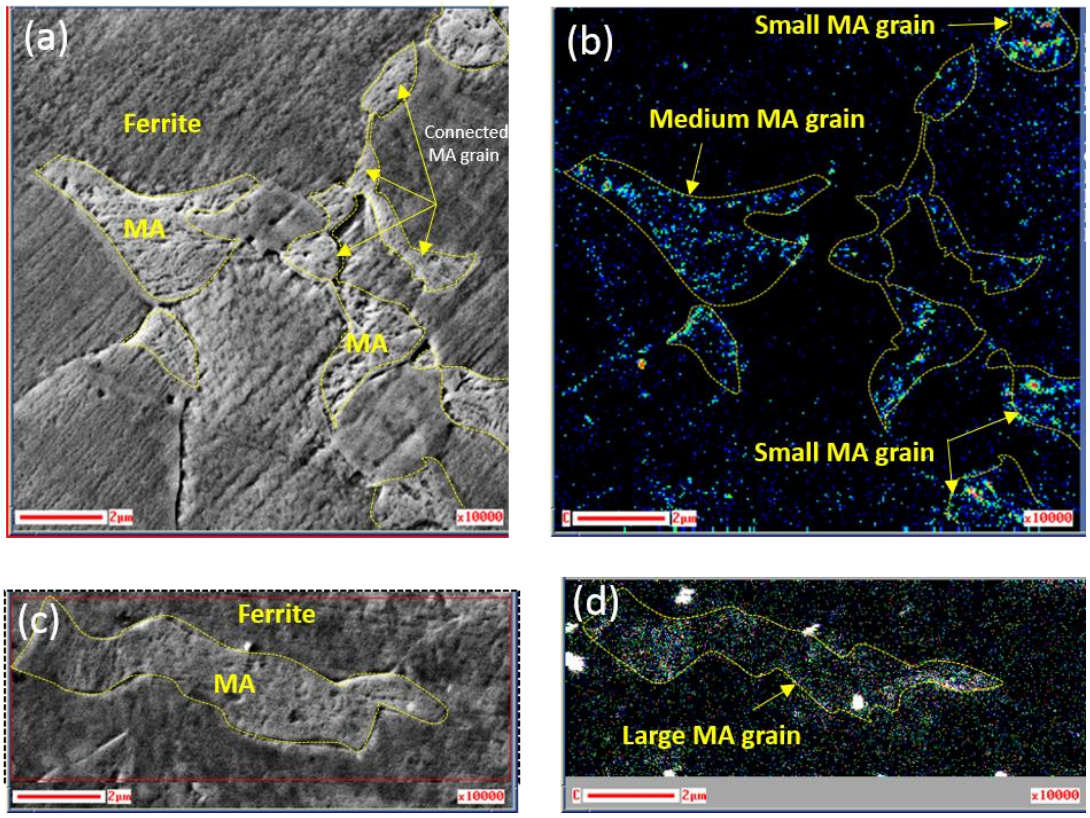

Figure 7-9 : (a&b) SEM images and Auger carbon mapping in air cooled MA (c&d) SEM image and Auger carbon mapping in water cooled MA (Blue to green and red is increasing order of carbon)

7.3.5 TEM analysis of MA

TEM analysis was performed to further characterize the martensite and austenite regions inside the MA. Formation of retained austenite along the periphery of the MA grain with martensite at its centre has been reported [75], however small austenite islands within [78] and scattered throughout the MA grain have also been observed [77].

In the present investigation, all furnace, air and water cooled samples were investigated using TEM. The results confirm that the furnace cooled sample does not contain any MA, while multiple MA structures were identified in air and water cooled samples. Figure 7-10 showed slender and blocky MA formation in water cooled sample. The bright field image from one of the small blocky MA grains in the water cooled sample is shown in Figure 7-11a. Electron diffraction patterns from the MA grain in Figure 7-11a suggest the presence of a BCC structure (martensite)

with (211) and (310) reflections (Figure 7-11b). From the dark field image (Figure 7-11c), it can be clearly seen that there are multiple martensite laths with a high dislocation density inside the MA. Retained austenite typically has lower dislocation density than ferrite or martensite or bainite [78, 98]. The presence of a high fraction of martensite is also supported by the SEM observation, XRD patterns, and carbon mapping. Twinning was also observed by TEM inside some MA grains, and this characteristic is associated with plate martensite [78].

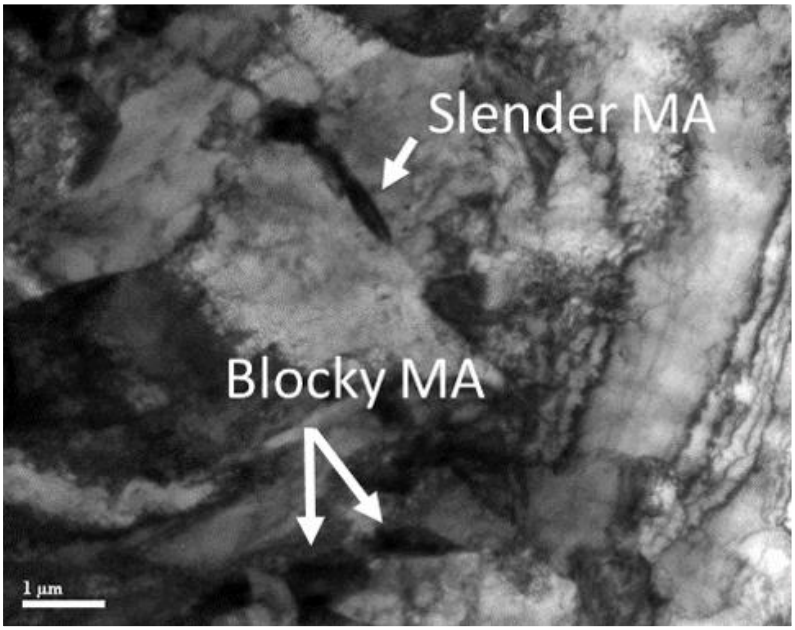

Figure 7-10 : TEM analysis of MA structure in water cooled sample

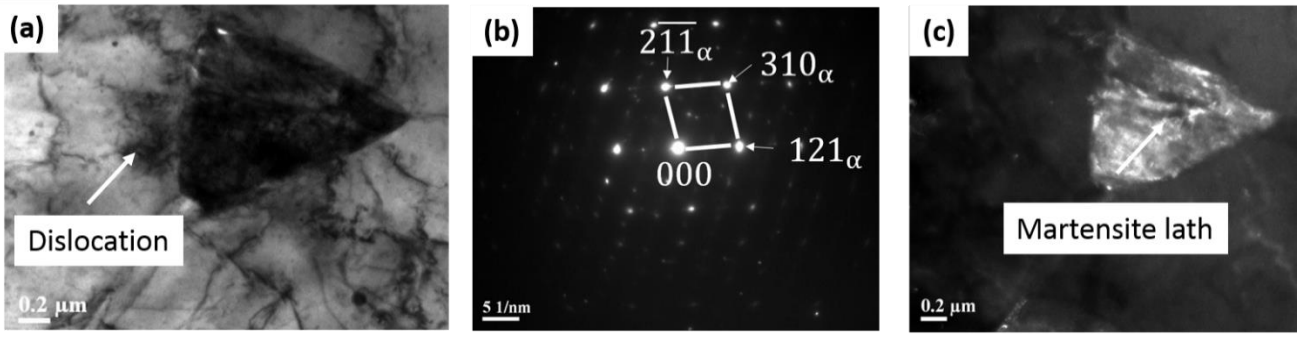

Figure 7-11 : (a) Bright field image of MA (b) SAD pattern from MA (c) dark field image (using 121 spot)

7.3.6 **Charpy impact toughness**

The Charpy impact testing was performed at -100°C and -45°C for the as-received base metal, and heat treated samples (furnace, air and water cooled) in order to evaluate their fracture behavior, as shown in Figure 7-12a. The as-received base metal has an average impact toughness energy of 250 J at -100°C. The furnace cooled samples showed an average impact toughness of 42 J, whereas the air and water cooled samples exhibited 12 J and 6 J, respectively at -100°C. The presence of MA has a significant effect on lower temperature (brittle fracture) toughness. The small difference in the MA fraction between the air and water cooled samples might lead to the difference in lower temperature toughness. At -45°C the base metal showed an average impact toughness of 313 J. However at –45°C, the furnace and air cooled samples exhibited a similar average impact energy (approx. 410 J) while the water cooled sample had a lower average impact energy (349 J). A high percentage of MA and blocky MA might lead to deterioration of toughness in the water cooled sample at -45°C.

It is interesting to find that the average impact energy of all the heat treated (furnace, air, and water cooled) samples at -100°C is much lower than the base metal. However, at -45°C, the heat treated samples showed a much better toughness energy than the base metal. Moreover, there is a significant improvement in toughness for heat treated samples when the test temperature increases from -100°C to -45°C. This explained by a difference in the DBTT (Ductile to Brittle Transition Temperature) for the base metal versus heat treated samples. When considering a test temperature of -100°C, the heat treated samples exhibited very low toughness, since they comprise coarse grains of mainly ferrite with small fraction of MA. However, at a temperature of -45°C the softer heat treated samples dominated by the coarse and ductile ferrite grains provide better toughness since this is likely above the DBTT (compared to the brittle results at -100ºC). This indicates that at lower temperatures (-100°C) MA plays a more significant role in toughness.

As MA has a significant effect in low temperature toughness, only the -100°C impact toughness specimens were selected to further assess the fracture behavior. For example, it can be noted in Figure 7-12b that at -100°C the furnace cooled sample deformed more during the impact toughness test compared to the air and water cooled samples. This is consistent with higher impact energy, while there is negligible bending in the air and water cooled samples since their impact energy values are comparably low.

It is widely recognized that finer grain size can lead to improved toughness at low temperatures [39, 59, 164, 165]. However, the presence of MA can have a deleterious influence on impact toughness [59, 157]. For comparison, the ferrite grain size of the furnace, air and water cooled samples were an average of 14, 12 and 11 μm respectively. Despite the finer grain size in the water cooled sample, it produced the lowest impact toughness energy, which confirms that the MA plays a more significant role than the grain size variation observed here, and this is consistent with other recent findings [157].

The MA regions are considered to be a brittle structure compared to the ferrite grains [80] and their influence on the toughness of a weld inter-critical coarse-grained HAZ depends highly on the size and volume fraction of MA in either a bainite or ferrite matrix [71, 129]. An increase of MA volume fraction, has been associated with a toughness decrease [134]. It has been also concluded that blocky type MA impairs the toughness more severely than the slender type [80, 114, 129, 157]. Other researchers also find that higher hardness occurs with larger MA, which is the main factor for inter-critical coarse-grained HAZ brittleness observed in Gleeble thermal simulations of submerged arc weld metal [91, 166]. Crack initiation energy and crack propagation energy for blocky type MA is significantly lower than slender MA [167]. Moreover Chen et al. reported that the larger the size of MA, the less load is required to form a crack by the ferrite surrounding the MA grain [99].

In addition, formation of MA along the grain boundary has a deleterious effect on impact toughness [129] since cleavage cracks do not deflect at the ferrite-MA interfaces or within the MA [59]. It has been also reported that MA and ferrite can have the same crystallographic orientation, which can facilitate cleavage crack propagation [168]. All these factors indicate that the presence of MA in air and water cooled samples leads to poor toughness at low temperatures. The higher percentage of MA and blocky MA in the water cooled sample leads to lowest toughness.

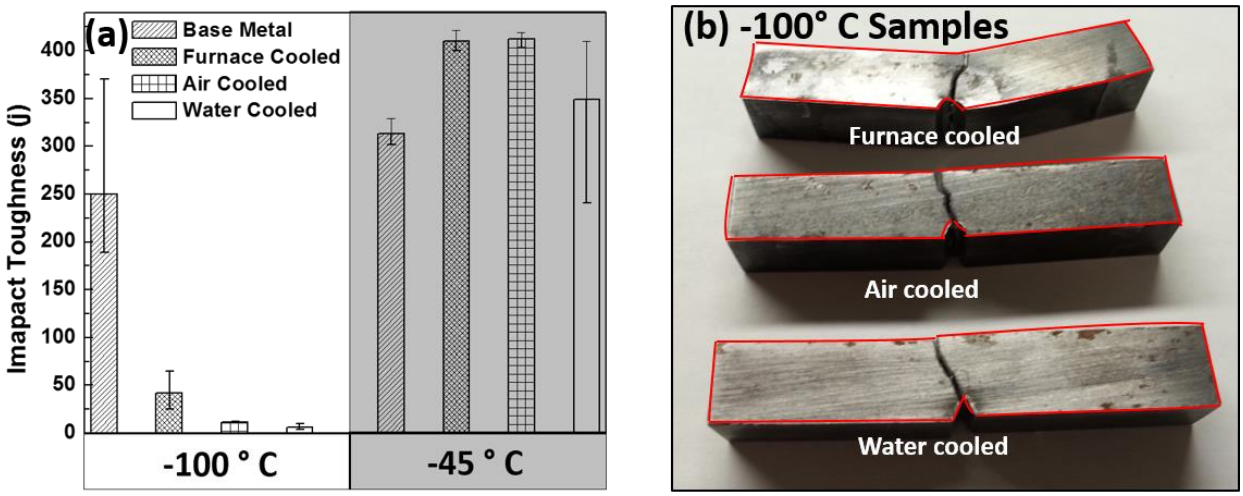

Figure 7-12 : (a) Charpy Impact energy comparison at -100°C and -45°C. (b) fractured samples at -100°C.

7.3.7 **Fracture surface observation**

The Charpy impact specimen fracture surfaces for all specimens revealed brittle fracture in all cases (Figure 7-13). For example, SEM observation of the fractured furnace cooled sample indicates cleavage fracture (Figure 7-13a&b). The air and water cooled samples also show cleavage fracture; the presence of small particles with sizes 0.2 to 5 µm could be noted on these surfaces (Figure 7-13c&e). These features are similar in size to the MA grains observed in these air and water cooled microstructures. A larger number of small particles was observed on the fracture surface of the water cooled specimen compared to the air cooled sample. The air and water cooled fracture surfaces also contained small cavities in the size range of 0.2 to 5 µm (Figure 7-13d&f). The number of these cavities is also higher in the water cooled sample. Moreover, river-like patterns Figure 7-13e are observed to be radiating from one single point, and there are number of particles around this point which are similar to the size of MA regions. This feature has been reported by several researchers as a crack initiation point attributed to MA phases [8, 71, 114].

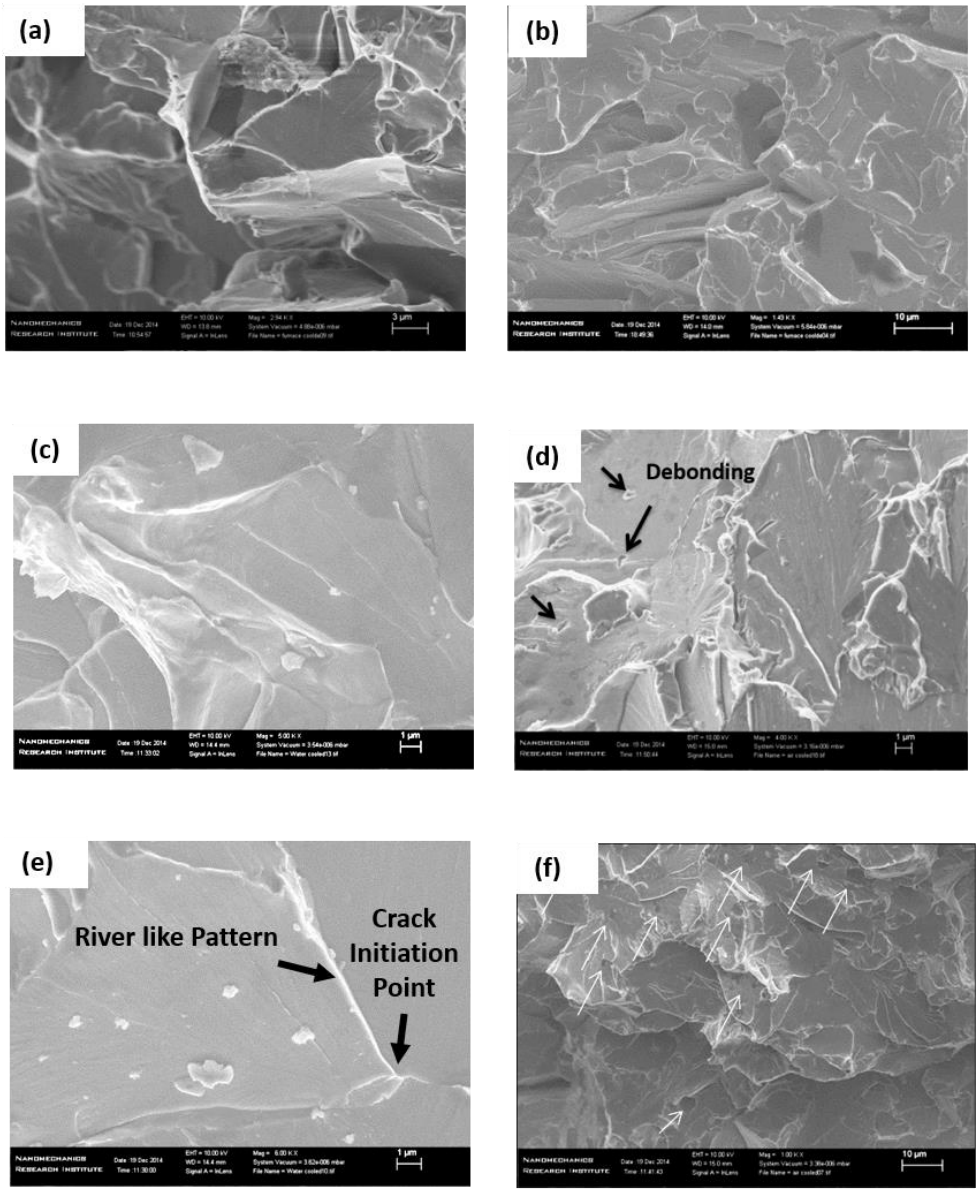

Figure 7-13 : Fracture surface observations using SEM, showing (a,b) furnace cooled sample, (c, d) air cooled sample, and (e,f) water cooled sample.

It is suggested that the particles and cavities observed in Figure 7-13c-f, relate to debonding of MA, and the area fraction of these features can be compared to the MA fraction observed by LePera etching. Based on the image analysis of the fracture surfaces, the debonding features covered areas of 0.22% and 1.73% for air and water cooled sample respectively. Note these percentage values are rather low, however of course not all MA regions will necessarily undergo debonding. The relative rate of this mechanism is consistent with the lower facture toughness in

the water cooled sample. Considering all these phenomena, it can be said that the MA is likely debonding from the microstructure and contributing to low toughness, particularly in the water cooled sample. This debonding mechanism has been shown schematically and described in other works involving fracture surface analysis [8, 114].

It should also be noted that the water cooled sample contains a higher percentage of total MA, especially that of the blocky morphology, which would account for the lower impact energy [169]. Chen et al. [99] observed high stress concentrations in the ferrite matrix surrounding MA and noted only a small load was required initiate microcracks at the MA/ferrite interface. Montermarano also observed crack nucleation in MA/ferrite matrix interface [170], which was also schematically explained by Davis and King [8]. Furthermore, in cleavage fracture, it has been observed that tri-axial stresses may promote interlinking and void formation around MA, and lead to propagation of cleavage cracks [99]. Yoneda and Nakanshi et al. also reported that MA was a crack initiation point and would also propagate the crack [99, 167]. To evaluate these mechanisms, the water cooled fracture specimens were cross-sectioned and metallographically examined around the crack surface. Numerous small cracks were observed close to the fractured surface in optical microscope and SEM (Figure 7-14a&b).

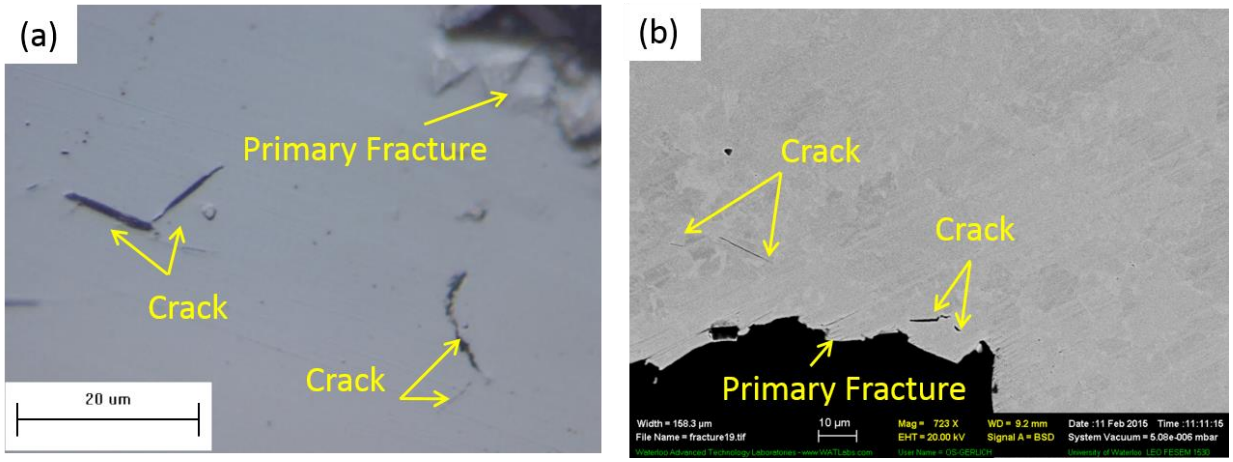

Figure 7-14 : Cross-sections near Charpy fracture surfaces in a water cooled sample, observed using (a) optical, and (b) SEM microscopy.

The use of LePera etchant reveals that cracks initiate from the MA in the ferrite matrix (Figure 7-15a). Moreover, the blocky type MA seems to initiate the crack rather than the slender

MA. Some cracks have also been observed going through blocky and slender MA, which indicates that this MA phase is very brittle and can break easily (Figure 7-15b). Davis et al. schematically showed that MA brittleness and determined it to be a source of crack nucleation [8]. Hence, a combination all of above mechanisms (debonding, brittleness & crack initiation) for MA lead to poor toughness in the air and water cooled sample. Therefore, the higher percentage of blocky MA in the water cooled sample is correlated with the lowest impact toughness.

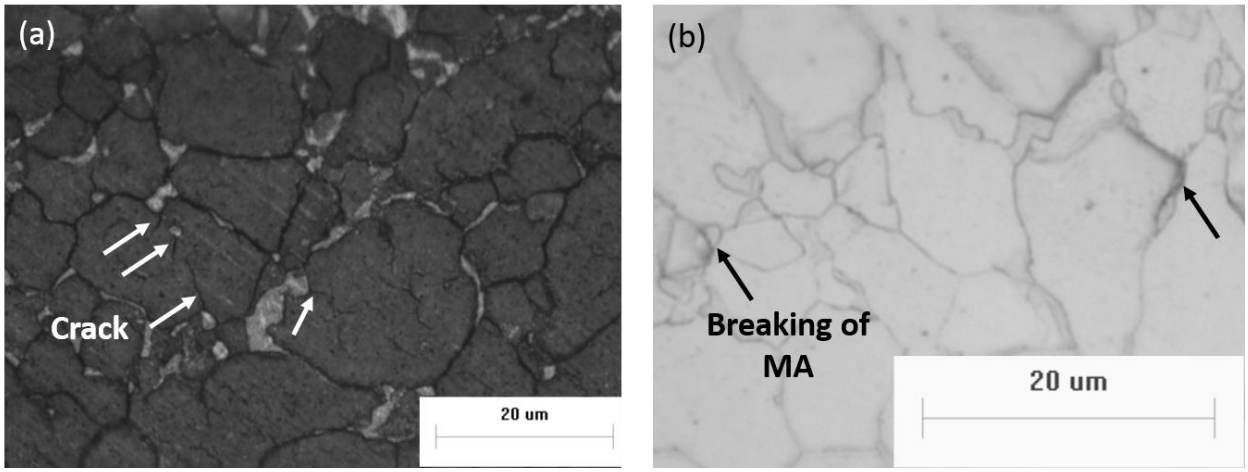

Figure 7-15 : (a) Crack initiation from MA/ferrite interface and partially through a ferrite grain (LePera etchant) , and (b) fracture through MA constituents (2% Nital)

7.4 Summary

Controlled thermal cycling of an X80 pipe steel was used to establish the influence of varying cooling rates on the fraction and morphology of MA and its effect on mechanical properties. Double thermal cycles consisting of the same initial Tp =1000°C and air cooling were then intercritically reheated and subjected to different cooling conditions (water, air and furnace). It was found that:

1. Furnace cooled samples do not lead to MA formation. However, with the increase of cooling rate the MA fraction increase and change its morphology from slender to blocky (coarser). Grain boundary MA, intergranular MA as well as inter connected MA is found in the structure.

2. The water cooled sample exhibited a high hardness and tensile strength compared to the furnace cooled sample due to contribution of a high fraction of MA.

3. Quantification showed the percentage of austenite is very small in MA structure compared to martensite in both air and water cooled sample. However, the furnace cooled sample does not contain austenite.

4. The higher cooling rate restricts the carbon diffusion and leads to MA formation. Carbon mapping showed the MA contains higher carbon content than surrounding ferrite matrix.

5. The furnace cooled sample showed better impact toughness than the air and water cooled samples at -100°C. Water cooled sample provided the lowest toughness at both temperature (-100°C and -45°C). MA has deleterious impact in the air and water cooled sample by affecting the structures debonding, brittleness and crack initiation mechanism at -100°C. The higher MA fraction and blocky (coarser) MA in water cooled sample resulted in the lowest toughness.

This results in this chapter clearly reveal that a higher MA fraction and coarser MA lead to detrimental toughness properties. However, the reasons for contradictory results in literature were not clear. Hence, an effort has been performed to combine different results of toughness from numerous study on MA which is focused to analyze MA impact on toughness. The toughness which was performed at temperature -20°C was taken for compiling the information [12, 73, 126, 128, 171-173]. An impact toughness lower than 20 J at test temperature -20°C considered "Failure" while more than 20 J is consider "Pass". The data was collected from recent publication which used HSLA steel (X70, X80, X100) for study. Figure 7-16 represents the summarization the data that was compiled.

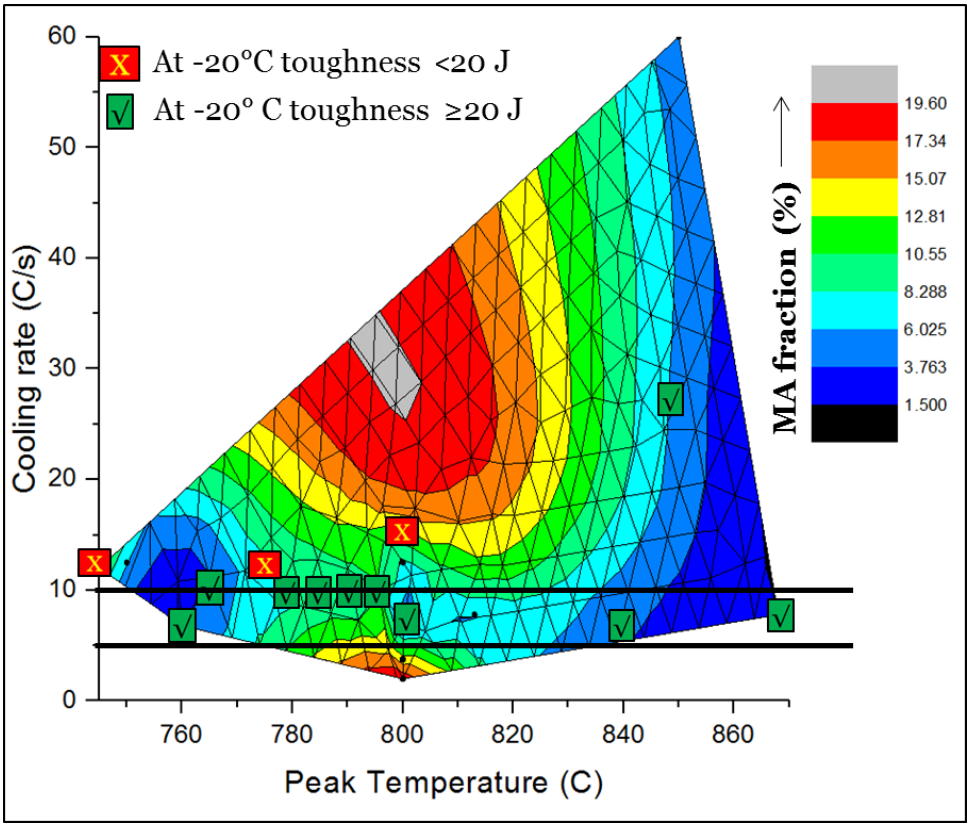

Figure 7-16 : Peak temperature, cooling rate and MA fraction correlation to toughness properties (at -20°C) [12, 73, 126, 128, 171-173]

The Y-axis in Figure 7-16 represents the represents second thermal cycle cooling rate while the X-axis is peak temperature in the second thermal cycle. The contour provides the fraction of MA formed in different second thermal cycle peak temperatures and cooling rates. The box with green and red colours represents the data collected from different research which reported toughness test at -20°C. The "black" dots in Figure 7-16 represent the data for which toughness tests were not performed.

The graph suggests that a 740-810°C (which is typically austenite transformation start temperature) temperature range with critical cooling rate of 10°C/s is detrimental to toughness properties. In this range of thermal conditions, a 6 to 12% fraction of MA can occur, however cooling rates between 5 to 10°C/s are not detrimental while lower cooling rates lead to poor toughness properties.

It has can be observed that an intermediate cooling (18-42°C/s) rate may lead to the formation of highest fraction of MA with peak temperature 775-825°C; although it is a extrapolation of the data. In addition, it can be observed that a higher fraction of MA also associated with very slow cooling rate between 2-3°C/s when peak temperature is between775-825°C.

A general conclusion can be reached to correlate peak temperature, cooling rate, and MA fraction to toughness properties. The MA distribution for the cooling rates 5-10°C/s containing 1 to 8% MA may produce better toughness properties for intercritical temperatures between 760-860°C.

Chapter 8 : Conclusions

In conclusion, this work was focused to study MA constituents internal structure, size, fraction, morphology and distribution effect on tensile strength, ductility and toughness. It was observed that variation of MA constituent fraction, size morphology and distribution, control the mechanical properties.

The MA constituent internal structure (Martensite-Austenite relative position) vary in the studied X80 material, however they are dominant in martensite structure while contain only a small percentage of austenite. Untempered MA constituent hardness is significantly higher than ferrite matrix. However, tempered MA constituents hardness is lower than untempered MA. The difference in hardness was attributed to the carbon content of MA constituents. Dislocation activity is observed inside and around MA.

A higher fraction with a coarser size usually leads to higher strength, while a higher MA fraction causes a loss in ductility. A more uniform and finer size MA distribution is more beneficial to strength and ductility by providing dispersion strengthening of the structure. Given similar fraction of MA in two structures, the one with coarser MA structure will provide inferior tensile properties.

The MA/ferrite interface was prone to void formation. A higher fraction of MA lead to higher fraction of void formation and coalescence of those voids lead to loss in ductility. Coarser MA produces more stress concentration in surrounding matrix, hence more prone to void formation. Void initiation has been observed at the start of plastic deformation. It was confirmed by simulation that strength mismatch between MA and ferrite lead to higher stress concentration in MA/ferrite interface which is the primary cause of void formation. The stress concentration has been also observed in sharper edges of MA/ferrite interface. It was also observed from experimental and simulation results that coarser MA is more prone to form premature void in comparison to small size MA.

An optimum tempering cycle has been observed to temper detrimental coarser MA and may reduce the dislocation around MA. Optimum temper cycle prevents the formation of premature void formation from MA/ferrite interface and there was improvement in strength and ductility. The fracture shift from HAZ to base metal after specimen was subjected to tempering

cycle. That suggests that tempering cycle can be used to get rid of detrimental MA and thereby improve mechanical properties.

MA constituents have a deleterious effect on toughness. A higher fraction of MA and coarser MA causes a loss in toughness. Based on the observations of fractured impact test specimens, it could be observed that MA constituents initiate cracks, debond frequently from the structure which accounts for the significant influence on toughness.

Recommendations and opportunities for future research

The toughness tests performed in the current study are not representative of actual welds since the tests were performed in furnace where a very slow heating is performed. Toughness specimens should be produced using Gleeble simulator and the role of MA constituents and their distribution on toughness should be studied. This would provide a study of more localized properties and would be more representative of an actual weld.

The intercritical peak temperature potentially can effect austenite transformation and prior austenite grain size which may have influence on MA formation; hence different intercritical temperature can be used for future study to observe the intercritical temperature effect on toughness.

It has been observed in current study that grain boundary and tri junction is potential location for MA nucleation, which essentially weaken the grain boundary or tri-junction. The reason for MA nucleation in those location can be explored. It will open the research to control the welding parameter to obtain different MA structure and formation location thereby improve the toughness properties

The effect of MA fraction, size, distribution and morphology effect should be confirmed in another pipeline alloy which potentially produce a different MA structure (dominant in austenite). These microstructural characteristics are closely controlled by the thermodynamic driving force for MA formation, and this is closely coupled to the chemistry of the material. Conducting a sensitivity study relative to the alloy chemistry has the potential to reveal possible trends in alloying elements versus MA formation rate, thus can potentially provide some guidelines regarding future pipeline alloy development for better toughness.

References

[1] A. Liessem, J. Schröder, M. Pant, M. Erdelen-Peppler, M. Liedtke, S. Höhler, C. Stallybrass, Manufacturing challenges of high strength line pipes, New Developments on Metallurgy and Applications of High Strength Steels (2008) 543-555.

[2] G. Demofonti, G. Mannucci, A critical review of the developed and available know how devoted to a safe use of X100 grade steel in large diameter pipelines, New Developments on Metallurgy and Applications of High Strength Steels, Buenos Aires 2008-Proceedings of the International Conference on New Developments on Metallurgy and Applications of High Strength steels, 2008, p. 625.

[3] U.S.E.I. Administration, Annual Energy Review 2008 (Aer), D. o. Energy, Ed. (2009).

[4] W. Bose-Filho, A. Carvalho, M. Strangwood, Effects of alloying elements on the microstructure and inclusion formation in HSLA multipass welds, Materials characterization 58(1) (2007) 29-39.

[5] S.K. Das, S. Sivaprasad, S. Das, S. Chatterjee, S. Tarafder, The effect of variation of microstructure on fracture mechanics parameters of HSLA-100 steel, Materials Science and Engineering: A 431(1-2) (2006) 68-79.

[6] A. Lambert-Perlade, A.-F. Gourgues, A. Pineau, Austenite to bainite phase transformation in the heat-affected zone of a high strength low alloy steel, Acta Materialia 52(8) (2004) 2337-2348.

[7] O. Akselsen, J. Solberg, O. Grong, Effect of Martensite-Austenite (MA) Islands on Intercritical Heat-Affected Zone Toughness of Low-Carbon Microalloyed Steels, Scandinavian journal of Metallurgy 17(5) (1988) 194-200.

[8] C. Davis, J. King, Cleavage initiation in the intercritically reheated coarse-grained heat-affected zone: Part I. Fractographic evidence, Metallurgical and materials transactions A 25(3) (1994) 563-573.

[9] S. Shanmugam, N. Ramisetti, R. Misra, J. Hartmann, S. Jansto, Microstructure and high strength–toughness combination of a new 700MPa Nb-microalloyed pipeline steel, Materials Science and Engineering: A 478(1) (2008) 26-37.

[10] J. Bauer, P. Flu¨ ss, E. Amoris, V. Schwinn, Microstructure and properties of thermomechanical controlled processing steels for linepipe applications, Ironmaking & steelmaking 32(4) (2005) 325-330.

[11] C.S. Association, CSA Z662. Oil & Gas Pipeline Systems, Mississauga, Canada: Author (2007).

[12] S.Y. Han, S.Y. Shin, S. Lee, N.J. Kim, J.-H. Bae, K. Kim, Effects of cooling conditions on tensile and charpy impact properties of API X80 linepipe steels, Metallurgical and Materials Transactions A 41(2) (2010) 329.

[13] H. Okada, K. Ikeuchi, F. Matsuda, I. Hrivnak, Effects of M-A constituent on fracture behaviour of weld HAZs: Deterioration and improvement of HAZ toughness in 780 and 980 MPa class HSLA steels welded with high heat input (5th report), (1995).

[14] S.A. Blackman, An economic assessment of mechanized welding of high-strength linepipe for the Australian pipeline industry, Pipes & pipelines international 48(2) (2003) 27-37.

[15] Y. Terada, H. Tamehiro, H. Morimoto, T. Hara, E. Tsuru, H. Asahi, M. Sugiyama, N. Doi, M. Murata, N. Ayukawa, X100 Linepipe with excellent HAZ toughness and deformability, ASME 2003 22nd International Conference on Offshore Mechanics and Arctic Engineering, American Society of Mechanical Engineers, 2003, pp. 287-294.

[16] J.K. Solberg, Teknologiske metaller og legeringer, NTNU, Editor (2010).

[17] H. Bhadeshia, R. Honeycombe, Steels: Microstructure and Properties, (2006), BH Pub 42-44.

[18] L. Collins, R. Klein, D. Bai, Development of high strength line pipe for Arctic applications, Canadian Metallurgical Quarterly 48(3) (2009) 261-270.

[19] D. Belato Rosado, W. De Waele, D. Vanderschueren, S. Hertelé, Latest developments in mechanical properties and metallurgical features of high strength line pipe steels, 5th International Conference on Sustainable Construction and Design, Ghent University, Laboratory Soete, 2013.

[20] J. Wang, A. Atrens, D. Cousens, N. Kinaev, Microstructure of X52 and X65 pipeline steels, Journal of Materials Science 34(8) (1999) 1721-1728.

[21] N. Tao, Y.-L. Kang, H.-W. Gu, Y.-Q. Yin, M.-L. Qiao, Precipitation behavior and its strengthening effect of X100 pipeline steel, Journal of Iron and Steel Research, International 17(11) (2010) 73-78.

[22] S. Dittrich, Welding of high yield strength X80-state of the art 1991, Welding in the World 30 (1992) 33-36.

[23] J. Gray, M. Pontremoly, Metallurgical options for grades X70 and X80 line pipe, International Conference on Pipe Technology, Rome, 1987, pp. 171-191.

[24] K. Banerjee, M. Militzer, M. Perez, X. Wang, Nonisothermal austenite grain growth kinetics in a microalloyed X80 linepipe steel, Metallurgical and Materials Transactions A 41(12) (2010) 3161-3172.

[25] M. Okatsu, F. Kawabata, K. Amano, Metallurgical and mechanical features of X100 linepipe steel, Proceedings of the International Conference on Offshore Mechanics and Arctic Engineering, AMERICAN SOCIETY OF MECHANICAL ENGINEERS, 1997, pp. 119-124.

[26] J.-m. Zhang, W.-H. Sun, S. Hao, Mechanical properties and microstructure of X120 grade high strength pipeline steel, Journal of iron and steel research, international 17(10) (2010) 63-67.

[27] S. Nafisi, M. Arafin, L. Collins, J. Szpunar, Texture and mechanical properties of API X100 steel manufactured under various thermomechanical cycles, Materials Science and Engineering: A 531 (2012) 2-11.

[28] P. Mohseni, Brittle and ductile fracture of X80 arctic steel,[dissertation]. Norwegian University of Science and Technology; 2012.
, (2012).

[29] B. Graville, Cold cracking in welds in HSLA steels, Welding of HSLA(Microalloyed) Structural Steels (1976) 85-101.

[30] L. Collins, J. Boyd, J. Jackman, L. Bayley, Microalloyed HSLA steels, American Society for Metals, Chicago (1988) 607.

[31] E. Hamre, A. Gilroy-Scott, Microalloying'75 Proceedings, Union Carbide (1977) 375-81.

[32] W. Morrison, Relationship Between ThermoMechanical Treatment and Properties of HSLA Steels, Scandinavian Journal of Metallurgy 9(2) (1980) 83-90.

[33] A. Ghosh, B. Mishra, S. Das, S. Chatterjee, Structure and properties of a low carbon Cu bearing high strength steel, Materials Science and Engineering: A 396(1) (2005) 320-332.

[34] E. Østby, C. Thaulow, O. Akselsen, Fracture Toughness Scatter and Effect of Constraint in Weld Thermal Simulated HAZ Microstructures at-60 C, The Twenty-first International Offshore and Polar Engineering Conference, International Society of Offshore and Polar Engineers, 2011.

[35] K. Easterling, Introduction to the physical metallurgy of welding, Elsevier2013.

[36] M. Toyoda, Significance of procedure/evaluation of CTOD test of weldments, IIW Doc. X-1192-89, International Institute of Welding (1989).

[37] U. Zerbst, R. Ainsworth, H.T. Beier, H. Pisarski, Z. Zhang, K. Nikbin, T. Nitschke-Pagel, S. Münstermann, P. Kucharczyk, D. Klingbeil, Review on fracture and crack propagation in weldments–A fracture mechanics perspective, Engineering fracture mechanics 132 (2014) 200-276.

[38] A. Lambert-Perlade, A.-F. Gourgues, J. Besson, T. Sturel, A. Pineau, Mechanisms and modeling of cleavage fracture in simulated heat-affected zone microstructures of a high-strength low alloy steel, Metallurgical and Materials Transactions A 35(13) (2004) 1039-1053.

[39] S. Moeinifar, A. Kokabi, H.M. Hosseini, Influence of peak temperature during simulation and real thermal cycles on microstructure and fracture properties of the reheated zones, Materials & design 31(6) (2010) 2948-2955.

[40] M. Warmuzek, G. Vander Voort, Metallography and Microstructures, ASM Handbook, (2004).

[41] G. Krauss, S.W. Thompson, Ferritic Microstructures in Continuously Cooled Low-and Ultralow-carbon Steels, ISIJ international 35(8) (1995) 937-945.

[42] M. Hillert, Thermodynamics of the massive transformation, Metallurgical and Materials Transactions A 15(3) (1984) 411-419.

[43] P. Cizek, B. Wynne, C. Davies, B. Muddle, P. Hodgson, Effect of composition and austenite deformation on the transformation characteristics of low-carbon and ultralow-carbon microalloyed steels, Metallurgical and Materials Transactions A 33(5) (2002) 1331-1349.

[44] N. Isasti, D. Jorge-Badiola, M. Taheri, B. López, P. Uranga, Effect of composition and deformation on coarse-grained austenite transformation in Nb-Mo microalloyed steels, Metallurgical and Materials Transactions A 42(12) (2011) 3729-3742.

[45] W.C. Jeong, Microstructural aspects of quasi-polygonal and granular bainitic ferrites in an ultra-low-carbon interstitial-free high-strength steel, Metallurgical and Materials Transactions A 34(9) (2003) 2025-2026.

[46] C. Wayman, Solid-state phase transformations, Annual Review of Materials Science 1(1) (1971) 185-218.

[47] E. Davenport, E. BAIN, Transformation of austenite at constant subcritical temperatures, Metallurgical and materials transactions. A, Physical metallurgy and materials science 41(6) (2010) 1353-1390.

[48] C. Zener, Kinetics of the decomposition of austenite, Trans. Aime 167(1946) (1946) 550-595.

[49] T. Ko, S. Cottrell, The formation of bainite, Journal of the Iron and Steel Institute 172(3) (1952) 307-&.

[50] L. Kaufmann, S. Radcliffe, M. Cohen, Decomposition of Austenite by Diffusional Processes, Interscience, New York (1962) 313.

[51] R. Hehemann, K. Kinsman, H. Aaronson, A debate on the bainite reaction, Metallurgical Transactions 3(5) (1972) 1077-1094.

[52] H. Bhadeshia, D. Edmonds, The mechanism of bainite formation in steels, Acta Metallurgica 28(9) (1980) 1265-1273.

[53] W.S.f.S.u.P. W. Bleck, 2nd ed. Aachen: VerlagMainz, Wissenschaftsverlag, (2004).

[54] A. Stormvinter, A. Borgenstam, P. Hedström, Investigation of lath and plate martensite in a carbon steel, Solid State Phenomena, Trans Tech Publ, 2011, pp. 61-66.

[55] S.-C. Wang, J.-R. Yang, Effects of chemical composition, rolling and cooling conditions on the amount of martensite/austenite (M/A) constituent formation in low carbon bainitic steels, Materials Science and Engineering: A 154(1) (1992) 43-49.

[56] C. Davis, J. King, Effect of cooling rate on intercritically reheated microstructure and toughness in high strength low alloy steel, Materials Science and technology 9(1) (1993) 8-15.

[57] I.K. Nuruddin, Effect of welding thermal cycles on the heat affected zone microstructure and toughness of multi-pass welded pipeline steels, (2012).

[58] Y. Li, T. Baker, Effect of morphology of martensite–austenite phase on fracture of weld heat affected zone in vanadium and niobium microalloyed steels, Materials Science and Technology 26(9) (2010) 1029-1040.

[59] B. Kim, S. Lee, N. Kim, D. Lee, Microstructure and local brittle zone phenomena in high-strength low-alloy steel welds, Metallurgical Transactions A 22(1) (1991) 139-149.

[60] F. Matsuda, K. Ikeuchi, Y. Fukada, Y. Horii, H. OKADA, T. SHIWAKU, C. SHIGA, S. Suzuki, Review of mechanical and metallurgical investigations of MA constituent in welded joint in Japan, TRANSACTIONS-JWRI 24 (1995) 1-1.

[61] Y. Nakao, H. Oshige, S. Noi, Y. Nishi, Distribution of toughness in HAZ of multi-pass welded high strength steel, Quarterly Journal of the Japan Welding Society 3(4) (1985) 773-781.

[62] Y. Nakao, Distribution of Microstructure in HAZ of Multi-Pass Welded High Strength Steel, Quar. J. JWS 3 (1985) 766-781.

[63] F. Matsuda, Y. Fukada, H. Okada, C. Shiga, K. Ikeuchi, Y. Horii, T. Shiwaku, S. Suzuki, Review of mechanical and metallurgical investigations of martensite-austenite constituent in welded joints in Japan, Welding in the World/Le Soudage dans le Monde 3(37) (1996) 134-154.

[64] H. Ikawa, H. Oshige, T. Tanoue, Effect of martensite-austenite constituent on HAZ toughness of a high strength steel, Transactions of the Japan Welding society 11(2) (1980) 87-96.

[65] C. Zhongxiao, C. Zigang, X. Shaoshan, L. Zhaoqi, D. Jiaxiang, D.J.H. Machine, B. Factory, The effect of MA constituent on toughness in the HAZ of low temperature 12Ni3MoV steel, Welding research: the state of the art: proceedings of the JDC University Research Symposium, 1985 International Welding Congress held in conjunction with ASM Materials Week, 1986, pp. 113-122.

[66] P. Mohseni, Brittle and ductile fracture of X80 arctic steel, (2012).

[67] N. Takayama, G. Miyamoto, T. Furuhara, Chemistry and three-dimensional morphology of martensite-austenite constituent in the bainite structure of low-carbon low-alloy steels, Acta Materialia 145 (2018) 154-164.

[68] C. Qiu, L. Lan, D. Zhao, X. Gao, L. Du, Microstructural evolution and toughness in the HAZ of submerged arc welded low welding crack susceptibility steel, Acta Metallurgica Sinica (English Letters) 26(1) (2013) 49-55.

[69] X. Luo, X. Chen, T. Wang, S. Pan, Z. Wang, Effect of morphologies of martensite–austenite constituents on impact toughness in intercritically reheated coarse-grained heat-affected zone of HSLA steel, Materials Science and Engineering: A 710 (2018) 192-199.

[70] H. Terasaki, Y.-i. Komizo, Correlation between the microstructural development of bainitic ferrite and the characteristics of martensite-austenite constituent, Metallurgical and Materials Transactions A 44(12) (2013) 5289-5293.

[71] P. Mohseni, J.K. Solberg, M. Karlsen, O.M. Akselsen, E. Østby, Cleavage fracture initiation at M–A constituents in intercritically coarse-grained heat-affected zone of a HSLA steel, Metallurgical and Materials Transactions A 45(1) (2014) 384-394.

[72] A.K. De, J.G. Speer, D.K. Matlock, Color tint-etching for multiphase steels, Advanced materials & processes 161(2) (2003) 27-30.

[73] X. Li, X. Ma, S. Subramanian, C. Shang, R. Misra, Influence of prior austenite grain size on martensite–austenite constituent and toughness in the heat affected zone of 700MPa high strength linepipe steel, Materials Science and Engineering: A 616 (2014) 141-147.

[74] J.M. Reichert, Structure and properties of complex transformation products in Nb/Mo-microalloyed steels, University of British Columbia, 2016.

[75] A. Lambert, A. Lambert, J. Drillet, A. Gourgues, T. Sturel, A. Pineau, Microstructure of martensite–austenite constituents in heat affected zones of high strength low alloy steel welds in relation to toughness properties, Science and technology of welding and joining 5(3) (2000) 168-173.

[76] S. Shanmugam, N. Ramisetti, R. Misra, J. Hartmann, S. Jansto, Microstructure and high strength–toughness combination of a new 700 MPa Nb-microalloyed pipeline steel, Materials Science and Engineering: A 478(1-2) (2008) 26-37.

[77] C. Wang, X. Wu, J. Liu, N.a. Xu, Transmission electron microscopy of martensite/austenite islands in pipeline steel X70, Materials Science and Engineering: A 438 (2006) 267-271.

[78] I. Hrivnak, F. MATSUDA, K. IKEUCHI, Investigation of MA constituent in high strength steel welds, Transactions of JWRI 21(2) (1992) 149-171.

[79] F. Matsuda, Z. Li, P. Bernasovsky, K. Ishihara, H. Okada, An Investigation on the Behaviour of the M-A Constituent in Simulated HAZ or HSLA Steels, Welding in the World(UK) 29(9) (1991) 307-313.

[80] I. Hrivnak, F. Matsuda, Z. Li, K. IKEUCHI, H. OKADA, Investigation of Metallography and Behavior of MA Constituent in Weld HAZ of HSLA Steels (Materials, Metallurgy & Weldability), Transactions of JWRI 21(2) (1992) 241-250.

[81] D. Tian, Microstructure, cleavage fracture and toughness of granular bainite in simulated coarse-grained heat-affected zones of low-carbon high-strength steels, Oulun yliopisto1998.

[82] T. Haze, S. Aihara, Influence of toughness and size of local brittle zone on HAZ toughness of HSLA steels, 7th International Conference on Offshore Mechanics and Arctic Engineering, Houston, 1988, pp. 515-523.

[83] P. Harrison, S. Webster, HAZ microstructure and toughness in single pass welds, 36 th Mechanical Working and Steel Processing Conference, 1994, pp. 551-559.

[84] M.X. S V Subramanian, and Laurie Collins, Structure-property studies on HAZ toughness of niobium microalloyed
linepipe steels, 6th International Pipeline Technology Conference, Belgium (2013).

[85] X. Li, C. Shang, X. Ma, B. Gault, S. Subramanian, J. Sun, R.D.K. Misra, Elemental distribution in the martensite–austenite constituent in intercritically reheated coarse-grained heat-affected zone of a high-strength pipeline steel, Scripta Materialia 139 (2017) 67-70.

[86] S.G. Lee, S.S. Sohn, B. Kim, W.G. Kim, K.-K. Um, S. Lee, Effects of martensite-austenite constituent on crack initiation and propagation in inter-critical heat-affected zone of high-strength low-alloy (HSLA) steel, Materials Science and Engineering: A (2018).

[87] A.J. DeArdo, G. Ratz, P. Wray, Thermomechanical processing of microalloyed austenite: Proceedings of the International Conference on the Thermomechanical Processing of Microalloyed Austenite, Metallurgical Society of AIME1982.

[88] O. Grong, O. Akselsen, HAZ toughness of microalloyed steels for offshore, (1986).

[89] H. MABUCHI, H. NAKAO, The effects of excess aluminum on mechanical properties of Mn-Mo, Mn-Mo-Ni and Mn-Mo-Ni-Cr Steels with regard to solute interactions, Transactions of the Iron and Steel Institute of Japan 23(6) (1983) 504-512.

[90] D. FARICHILD, N. Bangaru, J. Koo, P. Harrison, A. Ozekcin, A study concerning intercritical HAZ microstructure and toughness in HSLA steels, Welding Journal 70(12) (1991) 321. s-329. s.

[91] L. Lan, C. Qiu, D. Zhao, X. Gao, L. Du, Analysis of martensite–austenite constituent and its effect on toughness in submerged arc welded joint of low carbon bainitic steel, Journal of Materials Science 47(11) (2012) 4732-4742.

[92] C. Shiga, T. Hatomura, K. Amano, T. Enami, Effect of cooling rate and finishing-cooling temperature on properties of the plates controlledrolled and accelerated-cooled, Tetsu-to-Hagané 68 (1982) A227-A230.

[93] P. Bufalini, M. Pontremoli, M. Ghersi, A. Aprile, C. Jannone, A. DeArdo, Accelerated Cooling of Steel, Proc. Intl. Conf., TMS-AIME, Pittsburg, PA, 1985, p. 387.

[94] S. Moeinifar, A.H. Kokabi, H.R.M. Hosseini, Effect of tandem submerged arc welding process and parameters of Gleeble simulator thermal cycles on properties of the intercritically reheated heat affected zone, Materials & Design 32(2) (2011) 869-876.

[95] M. González, F. Landgraf, H. Goldenstein, A. Gorni, Curva TRC e sua Caracterização Microestrutural para um Aço Microligado para Tubos API 5LX80, Anais do 18º Congresso Brasileiro de Engenharia e Ciência dos Materiais-CBECiMat, 2008.

[96] Y. Zhong, F. Xiao, J. Zhang, Y. Shan, W. Wang, K. Yang, In situ TEM study of the effect of M/A films at grain boundaries on crack propagation in an ultra-fine acicular ferrite pipeline steel, Acta Materialia 54(2) (2006) 435-443.

[97] I.R.V. Pedrosa, R.S.d. Castro, Y.P. Yadava, R.A.S. Ferreira, Study of phase transformations In API 5L X80 Steel in order to increase its fracture toughness, Materials Research 16(2) (2013) 489-496.

[98] A. Lambert, X. Garat, T. Sturel, A. Gourgues, A. Gingell, Application of acoustic emission to the study of cleavage fracture mechanism in a HSLA steel, Scripta materialia 43(2) (2000) 161-166.

[99] J.H. Chen, Y. Kikuta, T. Araki, M. Yoneda, Y. Matsuda, Micro-fracture behaviour induced by M-A constituent (Island Martensite) in simulated welding heat affected zone of HT80 high strength low alloyed steel, Acta Metallurgica 32(10) (1984) 1779-1788.

[100] C. Lanzillotto, F. Pickering, Structure–property relationships in dual-phase steels, Metal Science 16(8) (1982) 371-382.

[101] P. Magnusen, E. Dubensky, D. Koss, The effect of void arrays on void linking during ductile fracture, Acta Metallurgica 36(6) (1988) 1503-1509.

[102] R.O. Laitinen, Improvement of weld HAZ toughness at low heat input by controlling the distribution of M-A constituents, 2006.

[103] K. Kweon, J. Kim, J. Hong, C. Lee, Microstructure and toughness of intercritically reheated heat affected zone in reactor pressure vessel steel weld, Science and technology of welding and joining 5(3) (2000) 161-167.

[104] J.-m. Zhang, W.-h. Sun, H. Sun, Mechanical Properties and Microstructure of X120 Grade High Strength Pipeline Steel, Journal of Iron and Steel Research, International 17(10) (2010) 63-67.

[105] S.M. Far, Influence of Thermal Simulated and Real Tandem Submerged Arc Welding Process on the Microstructure and Mechanical Properties of the Coarse-Grained Heat-Affected Zone, Materials and Manufacturing Processes 26(11) (2011) 1423-1429.

[106] D.W.G.X.Q. Xiaomei, Z.D.D.L.W. Guodong, Impact fracture behavior of X80 pipeline steel, Acta Metall Sin 46(5) (2010) 533-540.

[107] Y. Tian, Q. Li, Z.-d. Wang, G.-d. Wang, Effects of Ultra Fast Cooling on Microstructure and Mechanical Properties of Pipeline Steels, J. of Materi Eng and Perform 24(9) (2015) 3307-3314.

[108] J. Liao, K. Ikeuchi, F. Matsuda, Toughness investigation on simulated weld HAZs of SQV-2A pressure vessel steel, Nuclear engineering and design 183(1) (1998) 9-20.

[109] J. Liao, K. Ikeuchi, F. Matsuda, Weld HAZ Toughness and Its Improvement in Low Alloy Steel SQV-2A for Pressure Vessels (Report 3): Toughness Improvement by PWHT (Materials, Metallurgy & Weldability), Transactions of JWRI 23(2) (1994) 223-230.

[110] K. Ikeuchi, J. Liao, H. Tanabe, F. Matsuda, Effect of Temper-bead Thermal Cycle on Toughness of Weld ICCGHAZ of Low Alloy Steel SQV-2A, ISIJ international 35(10) (1995) 1203-1212.

[111] V. Magula, Z. Li, H. Okada, M. Fukuhisa, Microstructural Investigations on Decomposition Behaviour of MA Constituent and Recovery of Ductility due to PWHT in Simulated HAZ of HSLA Steels (Materials, Metallugy & Weldability), Transactions of JWRI 20(1) (1991) 69-75.

[112] C. Zhuang, N. Li, S. Wang, W. Lin, J. Ren, Microstructure and properties of heat-affected zones in X100 steel grade line pipes, ASME 2009 Pressure Vessels and Piping Conference, American Society of Mechanical Engineers, 2009, pp. 1311-1319.

[113] J. Janovec, M. Takahashi, T. Kuroda, K. Ikeuchi, Microstructural and mechanical aspects of tempered ICCGHAZ of SQV-2A low alloy steel weld, ISIJ International 40(Suppl) (2000) S44-S48.

[114] P. Mohseni, J.K. Solberg, M. Karlsen, O.M. Akselsen, E. Østby, Investigation of mechanism of cleavage fracture initiation in intercritically coarse grained heat affected zone of HSLA steel, Materials Science and Technology 28(11) (2012) 1261-1268.

[115] Z. Zhu, L. Kuzmikova, H. Li, F. Barbaro, The effect of chemical composition on microstructure and properties of intercritically reheated coarse-grained heat-affected zone in X70 steels, Metallurgical and Materials Transactions B 45(1) (2014) 229-235.

[116] Y. Ito, K. Bessyo, Weldability formula of high strength steels related to heataffected zone cracking", IIW-Doc, No: IX-467-68 (1968).

[117] T. Tagawa, T. Miyata, S. Aihara, K. Okamoto, Influence of martensitic islands on fracture toughness and strength of weld heat-affected zone, JOURNAL-IRON AND STEEL INSTITUTE OF JAPAN JAPANESE EDITION 79 (1993) 1176-1176.

[118] A. Coldren, R. Cryderman, M. Semchysen, Steel Strengthening Mechanisms, Climax Molybdenum, Ann Arbor, MI 17 (1969).

[119] A. Midawi, E. Santos, N. Huda, A. Sinha, R. Lazor, A. Gerlich, Microstructures and mechanical properties in two X80 weld metals produced using similar heat input, Journal of Materials Processing Technology 226 (2015) 272-279.

[120] O. Akselsen, Ø. Grong, J. Solberg, Structure–property relationships in intercritical heat affected zone of low-carbon microalloyed steels, Materials science and technology 3(8) (1987) 649-655.

[121] F. Matsuda, K. Ikeuchi, J. Liao, Weld HAZ Toughness and Its Improvement of Low Alloy Steel SQV-2A for Pressure Vessels (Report 1): Effect of cooling time on microstructure and Charpy impact value in single thermal cycle (Materials, Metallurgy & Weldability), Transactions of JWRI 22(2) (1993) 271-279.

[122] T. Araki, I. Kozasu, H. Tankechi, K. Shibata, M. Enomoto, H. Tamehiro, Atlas for Bainitic microstructures, ISIJ, Tokyo, Japan (1992) 1-100.

[123] H. Okada, K. Ikeuchi, F. Matsuda, I. Hrivnak, Effects of M-A constituent on fracture behaviour of weld HAZs: Deterioration and improvement of HAZ toughness in 780 and 980 MPa class HSLA steels welded with high heat input (5th report), (1995) 621-628.

[124] W. Xu, Q. Wang, T. Pan, H. Su, C. Yang, Effect of welding heat input on simulated HAZ microstructure and toughness of a VN microalloyed steel, Journal of Iron and Steel Research, International 14(5) (2007) 234-239.

[125] W. Process, The Procedure Handbook of Arc Welding, Cleveland: The James F. Lincoln Arc Welding Foundation, 2000.

[126] Z. Zhu, J. Han, H. Li, Influence of Heat Input on Microstructure and Toughness Properties in Simulated CGHAZ of X80 Steel Manufactured Using High-Temperature Processing, Metall and Mat Trans A 46(11) (2015) 5467-5475.

[127] A. Coldren, V.B.A. DeArdo, Thermomechanical Processing of Microalloyed Austenite, AIME, Pittsburgh, PA (1981) 591.

[128] S.Y. Han, S.Y. Shin, C.-H. Seo, H. Lee, J.-H. Bae, K. Kim, S. Lee, N.J. Kim, Effects of Mo, Cr, and V Additions on Tensile and Charpy Impact Properties of API X80 Pipeline Steels, Metallurgical and Materials Transactions A 40(8) (2009) 1851.

[129] Y. Li, D. Crowther, M. Green, P. Mitchell, T. Baker, The effect of vanadium and niobium on the properties and microstructure of the intercritically reheated coarse grained heat affected zone in low carbon microalloyed steels, ISIJ international 41(1) (2001) 46-55.

[130] S. Subramanian, M. Xiaoping, L. Collins, Structure-property studies on HAZ toughness of niobium microalloyed linepipe steels, 6th Int. Pipeline Technology Conf., Ostend, Belgium, Paper, 2013, pp. 1-24.

[131] V. Biss, R. Cryderman, Martensite and retained austenite in hot-rolled, low-carbon bainitic steels, Metallurgical and Materials Transactions B 2(8) (1971) 2267-2276.

[132] S. Barnard, G. Smith, M. Sarikaya, G. Thomas, Carbon atom distribution in a dual phase steel: An atom probe study, Scripta Metallurgica 15(4) (1981) 387-392.

[133] N. Huda, A.R. Midawi, J. Gianetto, R. Lazor, A.P. Gerlich, Influence of Martensite-Austenite (MA) on Impact Toughness of X80 Line Pipe Steels, Materials Science and Engineering: A (2016).

[134] F. Matsuda, L. Zhonglin, P. Bernasovsky, K. Ishihara, H. Okada, An investigation on the behaviour of the ma constituent in simulated haz of hsla steels, Welding Research Abroad 39(4) (1993) 24-30.

[135] A. Davenport, Formable HSLA and dual-phase steels, The Metallurgical Sociey of AIME, (1979).

[136] J. Rigsbee, P. VanderArend, A. Davenport, Formable HSLA and dual-phase steels, TMS-AIME, Warrendale, PA 56 (1979).

[137] S.A. Kim, W.L. Johnson, Elastic constants and internal friction of martensitic steel, ferritic-pearlitic steel, and a-iron, Mater Sci Eng A (2007) 452-453.

[138] A.R.H. Midawi, E.B.F. Santos, N. Huda, A.K. Sinha, R. Lazor, A.P. Gerlich, Microstructures and mechanical properties in two X80 weld metals produced using similar heat input, Journal of Materials Processing Technology 226 (2015) 272-279.

[139] P. Poruks, I. Yakubtsov, J. Boyd, Martensite–ferrite interface strength in a low-carbon bainitic steel, Scripta materialia 54(1) (2006) 41-45.

[140] M. Kamaya, A.J. Wilkinson, J.M. Titchmarsh, Quantification of plastic strain of stainless steel and nickel alloy by electron backscatter diffraction, Acta Materialia 54(2) (2006) 539-548.

[141] J. Kang, Y. Ososkov, J.D. Embury, D.S. Wilkinson, Digital image correlation studies for microscopic strain distribution and damage in dual phase steels, Scripta Materialia 56(11) (2007) 999-1002.

[142] J. Kadkhodapour, A. Butz, S.Z. Rad, Mechanisms of void formation during tensile testing in a commercial, dual-phase steel, Acta Materialia 59(7) (2011) 2575-2588.

[143] K. Andrews, Empirical formulae for the calculation of some transformation temperatures, J. Iron Steel Inst 203(7) (1965) 721-727.

[144] K. Ishida, Calculation of the effect of alloying elements on the M s temperature in steels, Journal of Alloys and Compounds 220(1) (1995) 126-131.

[145] Z. Zhu, L. Kuzmikova, H. Li, F. Barbaro, Effect of inter-critically reheating temperature on microstructure and properties of simulated inter-critically reheated coarse grained heat affected zone in X70 steel, Materials Science and Engineering: A 605 (2014) 8-13.

[146] X. Di, X. An, F. Cheng, D. Wang, X. Guo, Z. Xue, Effect of martensite–austenite constituent on toughness of simulated inter-critically reheated coarse-grained heat-affected zone in X70 pipeline steel, Science and Technology of Welding and Joining 21(5) (2016) 366-373.

[147] Y. Zhou, G. Wu, Materials analysis and testing technology—X-ray diffraction and electron microanalysis of materials, Harbin: Harbin institute of technology press, 2000.

[148] H.-y. Li, J.-d. Hu, J. Li, G. Chen, X.-j. Sun, Effect of tempering temperature on microstructure and mechanical properties of AISI 6150 steel, Journal of Central South University 20 (2013) 866-870.

[149] H. Okada, F. Matsuda, K. Ikeuchi, Z. Li, Toughness recovery for weld HAZ by post weld heat treatment, Quarterly Journal of Japan Welding Society 12(4) (1994) 521-527.

[150] D.-n. Zou, H. Ying, W. Zhang, X.-d. Fang, Influence of tempering process on mechanical properties of 00Cr13Ni4Mo supermartensitic stainless steel, Journal of Iron and Steel Research, International 17(8) (2010) 50-54.

[151] S. Tsuyama, H. Nakamichi, K. Yamada, S. Endo, Effects of Distribution and the Formation Process of MA on Deformation and Toughness of High Strength Linepipe Steel, ISIJ international 53(2) (2013) 317-322.

[152] B. Josefsson, H. Andren, S. David, J. Vitek, Recent Trends in Welding Science and Technology, ASM Inst., OH 243 (1989).

[153] T. Ohmura, K. Tsuzaki, S. Matsuoka, Evaluation of the matrix strength of Fe-0.4 wt% C tempered martensite using nanoindentation techniques, Philosophical Magazine A 82(10) (2002) 1903-1910.

[154] A. Gouldstone, H.-J. Koh, K.-Y. Zeng, A. Giannakopoulos, S. Suresh, Discrete and continuous deformation during nanoindentation of thin films, Acta Materialia 48(9) (2000) 2277-2295.

[155] S. Zhao, X. Cheng, S. Li, Y. Zhang, Effect of tempering temperatures on mechanical properties of a novel ultrahigh strength steel, Materials Research Innovations 18(sup4) (2014) S4-260-S4-264.

[156] H. Ikawa, H. Oshige, S. Noi, Study on the Grain Growth in Weld-Heat Affected Zone, Transactions of the Japan Welding Society 46 (1977) 713-720.

[157] E. Bayraktar, D. Kaplan, Mechanical and metallurgical investigation of martensite–austenite constituents in simulated welding conditions, Journal of materials processing technology 153 (2004) 87-92.

[158] D. Fairchild, N. Bangaru, J. Koo, P. Harrison, A. Ozekcin, Welding Research.

[159] H.K. Bhadeshia, Local Brittle Zones and the Role of Niobium, Materials Science Forum, Trans Tech Publ, 2014, pp. 2129-2135.

[160] N.-R.V. Bangaru, A.K. Sachdev, Influence of cooling rate on the microstructure and retained austenite in an intercritically annealed vanadium containing HSLA steel, Metallurgical Transactions A 13(11) (1982) 1899-1906.

[161] T. Haze, S. Aihara, Y. Hagiwara, K. Uchino, Y. Kawashima, S. Tomita, R. Chijiiwa, A study on factors controlling critical COD value of welded joints of high-tensile strength steels, Journal of the Society of Naval Architects of Japan 1987(162) (1987) 424-432.

[162] N. Balliger, T. Gladman, Work hardening of dual-phase steels, Metal Science 15(3) (1981) 95-108.

[163] R. Thomson, M. Miller, An atom probe study of carbon distribution in martensite in 214Cr1Mo steel, Scripta metallurgica et materialia 32(2) (1995) 149-154.

[164] D. Abson, R. Pargeter, Factors influencing as-deposited strength, microstructure, and toughness of manual metal arc welds suitable for C-Mn steel fabrications, International Metals Reviews 31(1) (1986) 141-196.

[165] D. Edmonds, R. Cochrane, Structure-property relationships in bainitic steels, Metallurgical Transactions A 21(6) (1990) 1527-1540.

[166] X. Zhang, H. Gao, A Study of Impact Toughness of Intercritically Reheated Coarse Grain Heat Affected Zone of Two Type X80 Grade Pipeline Steel, Transaction of JWRI, Special Issue WSE 2011 (2011) 101-104.

[167] F. Matsuda, K. Ikeuchi, H. Okada, I. Hrivnak, H.-S. Park, Effect of M-A Constituent on Fracture Behavior of 780 and 980MPa Class HSLA Steels Subjected to Weld HAZ Thermal Cycles(Materials, Metallurgy & Weldability), Transactions of JWRI 23(2) (1994) 231-238.

[168] N.J. Kim, A.H. Nakagawa, A.H. Nakagawa, Effective grain size of dual-phase steel, Materials Science and Engineering 83(1) (1986) 145-149.

[169] F. Matsuda, Investigation on the Behavior of MA Constituent in Simulated HAZ of HSLA steels, Doc, IIW-IX-1591-90.

[170] T. Montemarano, B. Sack, J. Gudas, High strength low alloy steels in naval construction, Journal of Ship Production 2(3) (1986).

[171] A. Lambert, J. Drillet, A.F. Gourgues, T. Sturel, A. Pineau, Microstructure of martensite–austenite constituents in heat affected zones of high strength low alloy steel welds in relation to toughness properties, Science and Technology of Welding and Joining 5(3) (2000) 168-173.

[172] X. Zhang, H. Gao, A study of impact toughness of intercritically reheated coarse-grain heat effected zone of two type X80 grade pipeline steel, Transactions of JWRI (2012) 101-104.

[173] X. Li, Y. Fan, X. Ma, S. Subramanian, C. Shang, Influence of martensite–austenite constituents formed at different intercritical temperatures on toughness, Materials & Design 67 (2015) 457-463.

SPRINGER NATURE

Title:	Study of MA Effect on Yield Strength and Ductility of X80 Linepipe Steels Weld
Author:	Nazmul Huda, Robert Lazor, Adrian P. Gerlich
Publication:	Metallurgical and Materials Transactions A
Publisher:	Springer Nature
Date:	Jan 1, 2017

Order Completed

Thank you for your order.

This Agreement between Nazmul Huda ("You") and Springer Nature ("Springer Nature") consists of your license details and the terms and conditions provided by Springer Nature and Copyright Clearance Center.

Your confirmation email will contain your order number for future reference.

printable details

License Number	4394921456526
License date	Jul 23, 2018
Licensed Content Publisher	Springer Nature
Licensed Content Publication	Metallurgical and Materials Transactions A
Licensed Content Title	Study of MA Effect on Yield Strength and Ductility of X80 Linepipe Steels Weld
Licensed Content Author	Nazmul Huda, Robert Lazor, Adrian P. Gerlich
Licensed Content Date	Jan 1, 2017
Licensed Content Volume	48
Licensed Content Issue	9
Type of Use	Thesis/Dissertation
Requestor type	academic/university or research institute
Format	print and electronic
Portion	full article/chapter
Will you be translating?	no
Circulation/distribution	5,001 to 10,000
Author of this Springer Nature content	yes
Title	PhD Candidate
Instructor name	Adrian Gerlich
Institution name	University of waterloo
Expected presentation date	Sep 2018
Order reference number	E-TP-17-155-AR
Requestor Location	Nazmul Huda 573 westvale drive waterloo, ON N2T1G5

	Canada Attn: Nazmul Huda
Billing Type	Invoice
Billing address	Nazmul Huda 573 westvale drive waterloo, ON N2T1G5 Canada Attn: Nazmul Huda
Total	0.00 USD

ORDER MORE CLOSE WINDOW

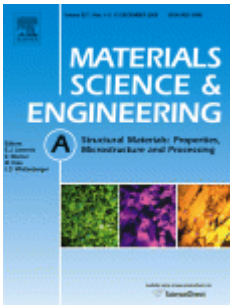

Title: Influence of martensite-austenite (MA) on impact toughness of X80 line pipe steels

Author: Nazmul Huda,Abdelbaset R.H. Midawi,James Gianetto,Robert Lazor,Adrian P. Gerlich

Publication: Materials Science and Engineering: A

Publisher: Elsevier

Date: 26 April 2016

Title:	ASME 2003 22nd International Conference on Offshore Mechanics and Arctic Engineering: Volume 3: Materials Technology; Ocean Engineering; Polar and Arctic Sciences and Technology; Workshops
Article ID:	978-0-7918-3683-5
Publication:	Publication1
Publisher:	CCC Republication
Date:	Jan 1, 2003

Order Completed

Thank you for your order.

This Agreement between Nazmul Huda ("You") and American Society of Mechanical Engineers ASME ("American Society of Mechanical Engineers ASME") consists of your order details and the terms and conditions provided by American Society of Mechanical Engineers ASME and Copyright Clearance Center.

License number	Reference confirmation email for license number
License date	Dec, 18 2018
Licensed content publisher	American Society of Mechanical Engineers ASME
Licensed content title	ASME 2003 22nd International Conference on Offshore Mechanics and Arctic Engineering: Volume 3: Materials Technology; Ocean Engineering; Polar and Arctic Sciences and Technology; Workshops
Licensed content date	Jan 1, 2003
Type of use	Thesis/Dissertation
Requestor type	Academic institution
Format	Print, Electronic
Portion	image/photo
Number of images/photos requested	1
The requesting person/organization	Nazmul Huda, University of waterloo
Title or numeric reference of the portion(s)	Figure 1
Title of the article or chapter the portion is from	X100 LINEPIPE WITH EXCELLENT HAZ TOUGHNESS AND DEFORMABILITY
Editor of portion(s)	N/A
Author of portion(s)	N/A
Volume of serial or monograph	OMAE2003-37392
Page range of portion	Page 5
Publication date of portion	June 8-13
Rights for	Main product
Duration of use	Life of current edition
Creation of copies for the disabled	no
With minor editing privileges	no

For distribution to	Worldwide
In the following language(s)	Original language of publication
With incidental promotional use	no
Lifetime unit quantity of new product	Up to 999
Title	Effect of Martensite-Austenite (MA) on Mechanical Properties of X80 Linepipe Steel
Institution name	n/a
Expected presentation date	Dec 2018
Requestor Location	Nazmul Huda 573 westvale drive waterloo, ON N2T1G5 Canada Attn: Nazmul Huda
Billing Type	Invoice
Billing address	Nazmul Huda 573 westvale drive waterloo, ON N2T1G5 Canada Attn: Nazmul Huda
Total (may include CCC user fee)	0.00 USD
Total	0.00 USD

CLOSE WINDOW

permission

Compose

Inbox 236
Starred
Snoozed
Important
Sent
Drafts 288
Categories
Social 1,588
Updates 22

Nazmul

Make a call

Also try our mobile apps for Android and iOS

permission to reprint image in thesis

Inbo

Nazmul Huda <nazmulbuet@gmail.com>
to Patrick.DeBaets

Hello Sir

I am Nazmul Huda, a PhD student from university of Waterloo, Canada. I paper that has the copyright by SOETE LABORATROY.

I would like to use Figure 2 (see attached) of paper titled " Latest develop

Can i have your permission to reprint his image in my thesis?

Thank you

--

Best Regards

Nazmul Huda
PhD Candidate
Department of Mechanical and Mechatronics Engineering
University of Waterloo
E3-2103, 200 University Avenue West
Waterloo, Ontario, Canada N2L 3G1

permission

Compose

Inbox 236
Starred
Snoozed
Important
Sent
Drafts 288
Categories
Social 1,588
Updates 22

Nazmul

Make a call

Also try our mobile apps for Android and iOS

<latest developments in mechanical properties.pdf>

Dear Nazmul Huda,

Herewith I grant permission to reprint the image in your thesis.

Kind regards,

Wim De Waele

Thanks a lot. Thank you. Thank you for your help.

Reply Reply to all Forward

ELSEVIER LICENSE
TERMS AND CONDITIONS

Dec 07, 2018

This Agreement between Nazmul Huda ("You") and Elsevier ("Elsevier") consists of your license details and the terms and conditions provided by Elsevier and Copyright Clearance Center.

License Number	4483881208093
License date	Dec 07, 2018
Licensed Content Publisher	Elsevier
Licensed Content Publication	Engineering Fracture Mechanics
Licensed Content Title	Review on fracture and crack propagation in weldments – A fracture mechanics perspective
Licensed Content Author	U. Zerbst,R.A. Ainsworth,H.Th. Beier,H. Pisarski,Z.L. Zhang,K. Nikbin,T. Nitschke-Pagel,S. Münstermann,P. Kucharczyk,D. Klingbeil
Licensed Content Date	Dec 1, 2014
Licensed Content Volume	132
Licensed Content Issue	n/a
Licensed Content Pages	77
Start Page	200
End Page	276
Type of Use	reuse in a thesis/dissertation
Intended publisher of new work	other
Portion	figures/tables/illustrations
Number of figures/tables/illustrations	1
Format	both print and electronic
Are you the author of this Elsevier article?	No
Will you be translating?	No
Original figure numbers	Figure 1
Title of your thesis/dissertation	Effect of Martensite-Austenite (MA) on Mechanical Properties of X80 Linepipe Steel
Expected completion date	Dec 2018
Estimated size (number of pages)	174
Requestor Location	Nazmul Huda 573 westvale drive waterloo, ON N2T1G5 Canada Attn: Nazmul Huda
Publisher Tax ID	GB 494 6272 12

Total 0.00 USD

Terms and Conditions

INTRODUCTION

1. The publisher for this copyrighted material is Elsevier. By clicking "accept" in connection with completing this licensing transaction, you agree that the following terms and conditions apply to this transaction (along with the Billing and Payment terms and conditions established by Copyright Clearance Center, Inc. ("CCC"), at the time that you opened your Rightslink account and that are available at any time at http://myaccount.copyright.com).

GENERAL TERMS

2. Elsevier hereby grants you permission to reproduce the aforementioned material subject to the terms and conditions indicated.
3. Acknowledgement: If any part of the material to be used (for example, figures) has appeared in our publication with credit or acknowledgement to another source, permission must also be sought from that source. If such permission is not obtained then that material may not be included in your publication/copies. Suitable acknowledgement to the source must be made, either as a footnote or in a reference list at the end of your publication, as follows:
"Reprinted from Publication title, Vol /edition number, Author(s), Title of article / title of chapter, Pages No., Copyright (Year), with permission from Elsevier [OR APPLICABLE SOCIETY COPYRIGHT OWNER]." Also Lancet special credit - "Reprinted from The Lancet, Vol. number, Author(s), Title of article, Pages No., Copyright (Year), with permission from Elsevier."
4. Reproduction of this material is confined to the purpose and/or media for which permission is hereby given.
5. Altering/Modifying Material: Not Permitted. However figures and illustrations may be altered/adapted minimally to serve your work. Any other abbreviations, additions, deletions and/or any other alterations shall be made only with prior written authorization of Elsevier Ltd. (Please contact Elsevier at permissions@elsevier.com). No modifications can be made to any Lancet figures/tables and they must be reproduced in full.
6. If the permission fee for the requested use of our material is waived in this instance, please be advised that your future requests for Elsevier materials may attract a fee.
7. Reservation of Rights: Publisher reserves all rights not specifically granted in the combination of (i) the license details provided by you and accepted in the course of this licensing transaction, (ii) these terms and conditions and (iii) CCC's Billing and Payment terms and conditions.
8. License Contingent Upon Payment: While you may exercise the rights licensed immediately upon issuance of the license at the end of the licensing process for the transaction, provided that you have disclosed complete and accurate details of your proposed use, no license is finally effective unless and until full payment is received from you (either by publisher or by CCC) as provided in CCC's Billing and Payment terms and conditions. If full payment is not received on a timely basis, then any license preliminarily granted shall be deemed automatically revoked and shall be void as if never granted. Further, in the event that you breach any of these terms and conditions or any of CCC's Billing and Payment terms and conditions, the license is automatically revoked and shall be void as if never granted. Use of materials as described in a revoked license, as well as any use of the materials beyond the scope of an unrevoked license, may constitute copyright infringement and publisher reserves the right to take any and all action to protect its copyright in the materials.
9. Warranties: Publisher makes no representations or warranties with respect to the licensed material.
10. Indemnity: You hereby indemnify and agree to hold harmless publisher and CCC, and their respective officers, directors, employees and agents, from and against any and all

claims arising out of your use of the licensed material other than as specifically authorized pursuant to this license.
11. No Transfer of License: This license is personal to you and may not be sublicensed, assigned, or transferred by you to any other person without publisher's written permission.
12. No Amendment Except in Writing: This license may not be amended except in a writing signed by both parties (or, in the case of publisher, by CCC on publisher's behalf).
13. Objection to Contrary Terms: Publisher hereby objects to any terms contained in any purchase order, acknowledgment, check endorsement or other writing prepared by you, which terms are inconsistent with these terms and conditions or CCC's Billing and Payment terms and conditions. These terms and conditions, together with CCC's Billing and Payment terms and conditions (which are incorporated herein), comprise the entire agreement between you and publisher (and CCC) concerning this licensing transaction. In the event of any conflict between your obligations established by these terms and conditions and those established by CCC's Billing and Payment terms and conditions, these terms and conditions shall control.
14. Revocation: Elsevier or Copyright Clearance Center may deny the permissions described in this License at their sole discretion, for any reason or no reason, with a full refund payable to you. Notice of such denial will be made using the contact information provided by you. Failure to receive such notice will not alter or invalidate the denial. In no event will Elsevier or Copyright Clearance Center be responsible or liable for any costs, expenses or damage incurred by you as a result of a denial of your permission request, other than a refund of the amount(s) paid by you to Elsevier and/or Copyright Clearance Center for denied permissions.

LIMITED LICENSE

The following terms and conditions apply only to specific license types:
15. **Translation**: This permission is granted for non-exclusive world **English** rights only unless your license was granted for translation rights. If you licensed translation rights you may only translate this content into the languages you requested. A professional translator must perform all translations and reproduce the content word for word preserving the integrity of the article.
16. **Posting licensed content on any Website**: The following terms and conditions apply as follows: Licensing material from an Elsevier journal: All content posted to the web site must maintain the copyright information line on the bottom of each image; A hyper-text must be included to the Homepage of the journal from which you are licensing at http://www.sciencedirect.com/science/journal/xxxxx or the Elsevier homepage for books at http://www.elsevier.com; Central Storage: This license does not include permission for a scanned version of the material to be stored in a central repository such as that provided by Heron/XanEdu.
Licensing material from an Elsevier book: A hyper-text link must be included to the Elsevier homepage at http://www.elsevier.com . All content posted to the web site must maintain the copyright information line on the bottom of each image.

Posting licensed content on Electronic reserve: In addition to the above the following clauses are applicable: The web site must be password-protected and made available only to bona fide students registered on a relevant course. This permission is granted for 1 year only. You may obtain a new license for future website posting.
17. **For journal authors:** the following clauses are applicable in addition to the above:
Preprints:
A preprint is an author's own write-up of research results and analysis, it has not been peer-reviewed, nor has it had any other value added to it by a publisher (such as formatting, copyright, technical enhancement etc.).
Authors can share their preprints anywhere at any time. Preprints should not be added to or enhanced in any way in order to appear more like, or to substitute for, the final versions of

articles however authors can update their preprints on arXiv or RePEc with their Accepted Author Manuscript (see below).
If accepted for publication, we encourage authors to link from the preprint to their formal publication via its DOI. Millions of researchers have access to the formal publications on ScienceDirect, and so links will help users to find, access, cite and use the best available version. Please note that Cell Press, The Lancet and some society-owned have different preprint policies. Information on these policies is available on the journal homepage.
Accepted Author Manuscripts: An accepted author manuscript is the manuscript of an article that has been accepted for publication and which typically includes author-incorporated changes suggested during submission, peer review and editor-author communications.
Authors can share their accepted author manuscript:

- immediately
  - via their non-commercial person homepage or blog
  - by updating a preprint in arXiv or RePEc with the accepted manuscript
  - via their research institute or institutional repository for internal institutional uses or as part of an invitation-only research collaboration work-group
  - directly by providing copies to their students or to research collaborators for their personal use
  - for private scholarly sharing as part of an invitation-only work group on commercial sites with which Elsevier has an agreement
- After the embargo period
  - via non-commercial hosting platforms such as their institutional repository
  - via commercial sites with which Elsevier has an agreement

In all cases accepted manuscripts should:

- link to the formal publication via its DOI
- bear a CC-BY-NC-ND license - this is easy to do
- if aggregated with other manuscripts, for example in a repository or other site, be shared in alignment with our hosting policy not be added to or enhanced in any way to appear more like, or to substitute for, the published journal article.

Published journal article (JPA): A published journal article (PJA) is the definitive final record of published research that appears or will appear in the journal and embodies all value-adding publishing activities including peer review co-ordination, copy-editing, formatting, (if relevant) pagination and online enrichment.
Policies for sharing publishing journal articles differ for subscription and gold open access articles:
Subscription Articles: If you are an author, please share a link to your article rather than the full-text. Millions of researchers have access to the formal publications on ScienceDirect, and so links will help your users to find, access, cite, and use the best available version.
Theses and dissertations which contain embedded PJAs as part of the formal submission can be posted publicly by the awarding institution with DOI links back to the formal publications on ScienceDirect.
If you are affiliated with a library that subscribes to ScienceDirect you have additional private sharing rights for others' research accessed under that agreement. This includes use for classroom teaching and internal training at the institution (including use in course packs and courseware programs), and inclusion of the article for grant funding purposes.
Gold Open Access Articles: May be shared according to the author-selected end-user license and should contain a CrossMark logo, the end user license, and a DOI link to the formal publication on ScienceDirect.
Please refer to Elsevier's posting policy for further information.

18. **For book authors** the following clauses are applicable in addition to the above: Authors are permitted to place a brief summary of their work online only. You are not allowed to download and post the published electronic version of your chapter, nor may you scan the printed edition to create an electronic version. **Posting to a repository:** Authors are permitted to post a summary of their chapter only in their institution's repository.
19. **Thesis/Dissertation**: If your license is for use in a thesis/dissertation your thesis may be submitted to your institution in either print or electronic form. Should your thesis be published commercially, please reapply for permission. These requirements include permission for the Library and Archives of Canada to supply single copies, on demand, of the complete thesis and include permission for Proquest/UMI to supply single copies, on demand, of the complete thesis. Should your thesis be published commercially, please reapply for permission. Theses and dissertations which contain embedded PJAs as part of the formal submission can be posted publicly by the awarding institution with DOI links back to the formal publications on ScienceDirect.

Elsevier Open Access Terms and Conditions

You can publish open access with Elsevier in hundreds of open access journals or in nearly 2000 established subscription journals that support open access publishing. Permitted third party re-use of these open access articles is defined by the author's choice of Creative Commons user license. See our open access license policy for more information.

Terms & Conditions applicable to all Open Access articles published with Elsevier:

Any reuse of the article must not represent the author as endorsing the adaptation of the article nor should the article be modified in such a way as to damage the author's honour or reputation. If any changes have been made, such changes must be clearly indicated.

The author(s) must be appropriately credited and we ask that you include the end user license and a DOI link to the formal publication on ScienceDirect.

If any part of the material to be used (for example, figures) has appeared in our publication with credit or acknowledgement to another source it is the responsibility of the user to ensure their reuse complies with the terms and conditions determined by the rights holder.

Additional Terms & Conditions applicable to each Creative Commons user license:

CC BY: The CC-BY license allows users to copy, to create extracts, abstracts and new works from the Article, to alter and revise the Article and to make commercial use of the Article (including reuse and/or resale of the Article by commercial entities), provided the user gives appropriate credit (with a link to the formal publication through the relevant DOI), provides a link to the license, indicates if changes were made and the licensor is not represented as endorsing the use made of the work. The full details of the license are available at http://creativecommons.org/licenses/by/4.0.

CC BY NC SA: The CC BY-NC-SA license allows users to copy, to create extracts, abstracts and new works from the Article, to alter and revise the Article, provided this is not done for commercial purposes, and that the user gives appropriate credit (with a link to the formal publication through the relevant DOI), provides a link to the license, indicates if changes were made and the licensor is not represented as endorsing the use made of the work. Further, any new works must be made available on the same conditions. The full details of the license are available at http://creativecommons.org/licenses/by-nc-sa/4.0.

CC BY NC ND: The CC BY-NC-ND license allows users to copy and distribute the Article, provided this is not done for commercial purposes and further does not permit distribution of the Article if it is changed or edited in any way, and provided the user gives appropriate credit (with a link to the formal publication through the relevant DOI), provides a link to the license, and that the licensor is not represented as endorsing the use made of the work. The full details of the license are available at http://creativecommons.org/licenses/by-nc-nd/4.0.

Any commercial reuse of Open Access articles published with a CC BY NC SA or CC BY NC ND license requires permission from Elsevier and will be subject to a fee.

Commercial reuse includes:

- Associating advertising with the full text of the Article
- Charging fees for document delivery or access
- Article aggregation
- Systematic distribution via e-mail lists or share buttons

Posting or linking by commercial companies for use by customers of those companies.

20. **Other Conditions**:

v1.9

Questions? customercare@copyright.com or +1-855-239-3415 (toll free in the US) or +1-978-646-2777.

SPRINGER NATURE LICENSE TERMS AND CONDITIONS

Dec 06, 2018

This Agreement between Nazmul Huda ("You") and Springer Nature ("Springer Nature") consists of your license details and the terms and conditions provided by Springer Nature and Copyright Clearance Center.

License Number	4483090724632
License date	Dec 06, 2018
Licensed Content Publisher	Springer Nature
Licensed Content Publication	Metallurgical and Materials Transactions A
Licensed Content Title	Cleavage initiation in the intercritically reheated coarse-grained heat-affected zone: Part I. Fractographic evidence
Licensed Content Author	C. L. Davis, J. E. King
Licensed Content Date	Jan 1, 1994
Licensed Content Volume	25
Licensed Content Issue	3
Type of Use	Thesis/Dissertation
Requestor type	academic/university or research institute
Format	print and electronic
Portion	figures/tables/illustrations
Number of figures/tables/illustrations	1
Will you be translating?	no
Circulation/distribution	1,001 to 2,000
Author of this Springer Nature content	no
Title	Effect of Martensite-Austenite (MA) on Mechanical Properties of X80 Linepipe Steel
Institution name	n/a
Expected presentation date	Dec 2018
Portions	Fig 1
Requestor Location	Nazmul Huda 573 westvale drive waterloo, ON N2T1G5 Canada Attn: Nazmul Huda
Billing Type	Invoice
Billing Address	Nazmul Huda 573 westvale drive waterloo, ON N2T1G5

Canada
Attn: Nazmul Huda

Total 0.00 USD

Terms and Conditions

Springer Nature Terms and Conditions for RightsLink Permissions

Springer Nature Customer Service Centre GmbH (the Licensor) hereby grants you a non-exclusive, world-wide licence to reproduce the material and for the purpose and requirements specified in the attached copy of your order form, and for no other use, subject to the conditions below:

1. The Licensor warrants that it has, to the best of its knowledge, the rights to license reuse of this material. However, you should ensure that the material you are requesting is original to the Licensor and does not carry the copyright of another entity (as credited in the published version).

   If the credit line on any part of the material you have requested indicates that it was reprinted or adapted with permission from another source, then you should also seek permission from that source to reuse the material.

2. Where **print only** permission has been granted for a fee, separate permission must be obtained for any additional electronic re-use.

3. Permission granted **free of charge** for material in print is also usually granted for any electronic version of that work, provided that the material is incidental to your work as a whole and that the electronic version is essentially equivalent to, or substitutes for, the print version.

4. A licence for 'post on a website' is valid for 12 months from the licence date. This licence does not cover use of full text articles on websites.

5. Where **'reuse in a dissertation/thesis'** has been selected the following terms apply: Print rights of the final author's accepted manuscript (for clarity, NOT the published version) for up to 100 copies, electronic rights for use only on a personal website or institutional repository as defined by the Sherpa guideline (www.sherpa.ac.uk/romeo/).

6. Permission granted for books and journals is granted for the lifetime of the first edition and does not apply to second and subsequent editions (except where the first edition permission was granted free of charge or for signatories to the STM Permissions Guidelines http://www.stm-assoc.org/copyright-legal-affairs/permissions/permissions-guidelines/), and does not apply for editions in other languages unless additional translation rights have been granted separately in the licence.

7. Rights for additional components such as custom editions and derivatives require additional permission and may be subject to an additional fee. Please apply to Journalpermissions@springernature.com/bookpermissions@springernature.com for these rights.

8. The Licensor's permission must be acknowledged next to the licensed material in print. In electronic form, this acknowledgement must be visible at the same time as the figures/tables/illustrations or abstract, and must be hyperlinked to the journal/book's homepage. Our required acknowledgement format is in the Appendix below.

9. Use of the material for incidental promotional use, minor editing privileges (this does not include cropping, adapting, omitting material or any other changes that affect the meaning, intention or moral rights of the author) and copies for the disabled are permitted under this licence.

10. Minor adaptations of single figures (changes of format, colour and style) do not require the Licensor's approval. However, the adaptation should be credited as shown in Appendix below.

Appendix — Acknowledgements:

For Journal Content:
Reprinted by permission from [**the Licensor**]: [**Journal Publisher** (e.g. Nature/Springer/Palgrave)] [**JOURNAL NAME**] [**REFERENCE CITATION** (Article name, Author(s) Name), [**COPYRIGHT**] (year of publication)

For **Advance Online Publication papers:**
Reprinted by permission from [**the Licensor**]: [**Journal Publisher** (e.g. Nature/Springer/Palgrave)] [**JOURNAL NAME**] [**REFERENCE CITATION** (Article name, Author(s) Name), [**COPYRIGHT**] (year of publication), advance online publication, day month year (doi: 10.1038/sj.[JOURNAL ACRONYM].)

For Adaptations/Translations:
Adapted/Translated by permission from [**the Licensor**]: [**Journal Publisher** (e.g. Nature/Springer/Palgrave)] [**JOURNAL NAME**] [**REFERENCE CITATION** (Article name, Author(s) Name), [**COPYRIGHT**] (year of publication)

Note: For any republication from the British Journal of Cancer, the following credit line style applies:

Reprinted/adapted/translated by permission from [**the Licensor**]: on behalf of Cancer Research UK: : [**Journal Publisher** (e.g. Nature/Springer/Palgrave)] [**JOURNAL NAME**] [**REFERENCE CITATION** (Article name, Author(s) Name), [**COPYRIGHT]** (year of publication)

For **Advance Online Publication** papers:
Reprinted by permission from The [**the Licensor**]: on behalf of Cancer Research UK: [**Journal Publisher** (e.g. Nature/Springer/Palgrave)] [**JOURNAL NAME**] [**REFERENCE CITATION** (Article name, Author(s) Name), [**COPYRIGHT**] (year of publication), advance online publication, day month year (doi: 10.1038/sj.[JOURNAL ACRONYM])

For Book content:
Reprinted/adapted by permission from [**the Licensor**]: [**Book Publisher** (e.g. Palgrave Macmillan, Springer etc) [**Book Title**] by [**Book author**(s)] [**COPYRIGHT**] (year of publication)

Other Conditions:

Version 1.1

SPRINGER NATURE LICENSE TERMS AND CONDITIONS

Dec 07, 2018

This Agreement between Nazmul Huda ("You") and Springer Nature ("Springer Nature") consists of your license details and the terms and conditions provided by Springer Nature and Copyright Clearance Center.

License Number	4483850169587
License date	Dec 07, 2018
Licensed Content Publisher	Springer Nature
Licensed Content Publication	Metallurgical and Materials Transactions A
Licensed Content Title	Cleavage Fracture Initiation at M–A Constituents in Intercritically Coarse-Grained Heat-Affected Zone of a HSLA Steel
Licensed Content Author	Peyman Mohseni, Jan Ketil Solberg, Morten Karlsen et al
Licensed Content Date	Jan 1, 2013
Licensed Content Volume	45
Licensed Content Issue	1
Type of Use	Thesis/Dissertation
Requestor type	academic/university or research institute
Format	print and electronic
Portion	figures/tables/illustrations
Number of figures/tables/illustrations	1
Will you be translating?	no
Circulation/distribution	1,001 to 2,000
Author of this Springer Nature content	no
Title	Effect of Martensite-Austenite (MA) on Mechanical Properties of X80 Linepipe Steel
Institution name	n/a
Expected presentation date	Dec 2018
Portions	Figure 1
Requestor Location	Nazmul Huda 573 westvale drive waterloo, ON N2T1G5 Canada Attn: Nazmul Huda
Billing Type	Invoice
Billing Address	Nazmul Huda 573 westvale drive

Print This Page

ELSEVIER LICENSE
TERMS AND CONDITIONS

Dec 07, 2018

This Agreement between Nazmul Huda ("You") and Elsevier ("Elsevier") consists of your license details and the terms and conditions provided by Elsevier and Copyright Clearance Center.

License Number	4483850456382
License date	Dec 07, 2018
Licensed Content Publisher	Elsevier
Licensed Content Publication	Materials Science and Engineering: A
Licensed Content Title	Influence of prior austenite grain size on martensite–austenite constituent and toughness in the heat affected zone of 700MPa high strength linepipe steel
Licensed Content Author	Xueda Li,Xiaoping Ma,S.V. Subramanian,Chengjia Shang,R.D.K. Misra
Licensed Content Date	Oct 20, 2014
Licensed Content Volume	616
Licensed Content Issue	n/a
Licensed Content Pages	7
Start Page	141
End Page	147
Type of Use	reuse in a thesis/dissertation
Intended publisher of new work	other
Portion	figures/tables/illustrations
Number of figures/tables/illustrations	1
Format	both print and electronic
Are you the author of this Elsevier article?	No
Will you be translating?	No
Original figure numbers	Figure 8a
Title of your thesis/dissertation	Effect of Martensite-Austenite (MA) on Mechanical Properties of X80 Linepipe Steel
Expected completion date	Dec 2018
Estimated size (number of pages)	174
Requestor Location	Nazmul Huda 573 westvale drive waterloo, ON N2T1G5 Canada Attn: Nazmul Huda

Publisher Tax ID	GB 494 6272 12
Total	0.00 USD

Terms and Conditions

INTRODUCTION

1. The publisher for this copyrighted material is Elsevier. By clicking "accept" in connection with completing this licensing transaction, you agree that the following terms and conditions apply to this transaction (along with the Billing and Payment terms and conditions established by Copyright Clearance Center, Inc. ("CCC"), at the time that you opened your Rightslink account and that are available at any time at http://myaccount.copyright.com).

GENERAL TERMS

2. Elsevier hereby grants you permission to reproduce the aforementioned material subject to the terms and conditions indicated.
3. Acknowledgement: If any part of the material to be used (for example, figures) has appeared in our publication with credit or acknowledgement to another source, permission must also be sought from that source. If such permission is not obtained then that material may not be included in your publication/copies. Suitable acknowledgement to the source must be made, either as a footnote or in a reference list at the end of your publication, as follows:
"Reprinted from Publication title, Vol /edition number, Author(s), Title of article / title of chapter, Pages No., Copyright (Year), with permission from Elsevier [OR APPLICABLE SOCIETY COPYRIGHT OWNER]." Also Lancet special credit - "Reprinted from The Lancet, Vol. number, Author(s), Title of article, Pages No., Copyright (Year), with permission from Elsevier."
4. Reproduction of this material is confined to the purpose and/or media for which permission is hereby given.
5. Altering/Modifying Material: Not Permitted. However figures and illustrations may be altered/adapted minimally to serve your work. Any other abbreviations, additions, deletions and/or any other alterations shall be made only with prior written authorization of Elsevier Ltd. (Please contact Elsevier at permissions@elsevier.com). No modifications can be made to any Lancet figures/tables and they must be reproduced in full.
6. If the permission fee for the requested use of our material is waived in this instance, please be advised that your future requests for Elsevier materials may attract a fee.
7. Reservation of Rights: Publisher reserves all rights not specifically granted in the combination of (i) the license details provided by you and accepted in the course of this licensing transaction, (ii) these terms and conditions and (iii) CCC's Billing and Payment terms and conditions.
8. License Contingent Upon Payment: While you may exercise the rights licensed immediately upon issuance of the license at the end of the licensing process for the transaction, provided that you have disclosed complete and accurate details of your proposed use, no license is finally effective unless and until full payment is received from you (either by publisher or by CCC) as provided in CCC's Billing and Payment terms and conditions. If full payment is not received on a timely basis, then any license preliminarily granted shall be deemed automatically revoked and shall be void as if never granted. Further, in the event that you breach any of these terms and conditions or any of CCC's Billing and Payment terms and conditions, the license is automatically revoked and shall be void as if never granted. Use of materials as described in a revoked license, as well as any use of the materials beyond the scope of an unrevoked license, may constitute copyright infringement and publisher reserves the right to take any and all action to protect its copyright in the materials.
9. Warranties: Publisher makes no representations or warranties with respect to the licensed material.
10. Indemnity: You hereby indemnify and agree to hold harmless publisher and CCC, and their respective officers, directors, employees and agents, from and against any and all

claims arising out of your use of the licensed material other than as specifically authorized pursuant to this license.
11. No Transfer of License: This license is personal to you and may not be sublicensed, assigned, or transferred by you to any other person without publisher's written permission.
12. No Amendment Except in Writing: This license may not be amended except in a writing signed by both parties (or, in the case of publisher, by CCC on publisher's behalf).
13. Objection to Contrary Terms: Publisher hereby objects to any terms contained in any purchase order, acknowledgment, check endorsement or other writing prepared by you, which terms are inconsistent with these terms and conditions or CCC's Billing and Payment terms and conditions. These terms and conditions, together with CCC's Billing and Payment terms and conditions (which are incorporated herein), comprise the entire agreement between you and publisher (and CCC) concerning this licensing transaction. In the event of any conflict between your obligations established by these terms and conditions and those established by CCC's Billing and Payment terms and conditions, these terms and conditions shall control.
14. Revocation: Elsevier or Copyright Clearance Center may deny the permissions described in this License at their sole discretion, for any reason or no reason, with a full refund payable to you. Notice of such denial will be made using the contact information provided by you. Failure to receive such notice will not alter or invalidate the denial. In no event will Elsevier or Copyright Clearance Center be responsible or liable for any costs, expenses or damage incurred by you as a result of a denial of your permission request, other than a refund of the amount(s) paid by you to Elsevier and/or Copyright Clearance Center for denied permissions.

LIMITED LICENSE

The following terms and conditions apply only to specific license types:
15. **Translation**: This permission is granted for non-exclusive world **English** rights only unless your license was granted for translation rights. If you licensed translation rights you may only translate this content into the languages you requested. A professional translator must perform all translations and reproduce the content word for word preserving the integrity of the article.
16. **Posting licensed content on any Website**: The following terms and conditions apply as follows: Licensing material from an Elsevier journal: All content posted to the web site must maintain the copyright information line on the bottom of each image; A hyper-text must be included to the Homepage of the journal from which you are licensing at http://www.sciencedirect.com/science/journal/xxxxx or the Elsevier homepage for books at http://www.elsevier.com; Central Storage: This license does not include permission for a scanned version of the material to be stored in a central repository such as that provided by Heron/XanEdu.
Licensing material from an Elsevier book: A hyper-text link must be included to the Elsevier homepage at http://www.elsevier.com . All content posted to the web site must maintain the copyright information line on the bottom of each image.

Posting licensed content on Electronic reserve: In addition to the above the following clauses are applicable: The web site must be password-protected and made available only to bona fide students registered on a relevant course. This permission is granted for 1 year only. You may obtain a new license for future website posting.
17. **For journal authors:** the following clauses are applicable in addition to the above:
Preprints:
A preprint is an author's own write-up of research results and analysis, it has not been peer-reviewed, nor has it had any other value added to it by a publisher (such as formatting, copyright, technical enhancement etc.).
Authors can share their preprints anywhere at any time. Preprints should not be added to or enhanced in any way in order to appear more like, or to substitute for, the final versions of

articles however authors can update their preprints on arXiv or RePEc with their Accepted Author Manuscript (see below).
If accepted for publication, we encourage authors to link from the preprint to their formal publication via its DOI. Millions of researchers have access to the formal publications on ScienceDirect, and so links will help users to find, access, cite and use the best available version. Please note that Cell Press, The Lancet and some society-owned have different preprint policies. Information on these policies is available on the journal homepage.
Accepted Author Manuscripts: An accepted author manuscript is the manuscript of an article that has been accepted for publication and which typically includes author-incorporated changes suggested during submission, peer review and editor-author communications.
Authors can share their accepted author manuscript:

- immediately
  - via their non-commercial person homepage or blog
  - by updating a preprint in arXiv or RePEc with the accepted manuscript
  - via their research institute or institutional repository for internal institutional uses or as part of an invitation-only research collaboration work-group
  - directly by providing copies to their students or to research collaborators for their personal use
  - for private scholarly sharing as part of an invitation-only work group on commercial sites with which Elsevier has an agreement
- After the embargo period
  - via non-commercial hosting platforms such as their institutional repository
  - via commercial sites with which Elsevier has an agreement

In all cases accepted manuscripts should:

- link to the formal publication via its DOI
- bear a CC-BY-NC-ND license - this is easy to do
- if aggregated with other manuscripts, for example in a repository or other site, be shared in alignment with our hosting policy not be added to or enhanced in any way to appear more like, or to substitute for, the published journal article.

Published journal article (JPA): A published journal article (PJA) is the definitive final record of published research that appears or will appear in the journal and embodies all value-adding publishing activities including peer review co-ordination, copy-editing, formatting, (if relevant) pagination and online enrichment.
Policies for sharing publishing journal articles differ for subscription and gold open access articles:
Subscription Articles: If you are an author, please share a link to your article rather than the full-text. Millions of researchers have access to the formal publications on ScienceDirect, and so links will help your users to find, access, cite, and use the best available version.
Theses and dissertations which contain embedded PJAs as part of the formal submission can be posted publicly by the awarding institution with DOI links back to the formal publications on ScienceDirect.
If you are affiliated with a library that subscribes to ScienceDirect you have additional private sharing rights for others' research accessed under that agreement. This includes use for classroom teaching and internal training at the institution (including use in course packs and courseware programs), and inclusion of the article for grant funding purposes.
Gold Open Access Articles: May be shared according to the author-selected end-user license and should contain a CrossMark logo, the end user license, and a DOI link to the formal publication on ScienceDirect.
Please refer to Elsevier's posting policy for further information.

18. **For book authors** the following clauses are applicable in addition to the above: Authors are permitted to place a brief summary of their work online only. You are not allowed to download and post the published electronic version of your chapter, nor may you scan the printed edition to create an electronic version. **Posting to a repository:** Authors are permitted to post a summary of their chapter only in their institution's repository.
19. **Thesis/Dissertation**: If your license is for use in a thesis/dissertation your thesis may be submitted to your institution in either print or electronic form. Should your thesis be published commercially, please reapply for permission. These requirements include permission for the Library and Archives of Canada to supply single copies, on demand, of the complete thesis and include permission for Proquest/UMI to supply single copies, on demand, of the complete thesis. Should your thesis be published commercially, please reapply for permission. Theses and dissertations which contain embedded PJAs as part of the formal submission can be posted publicly by the awarding institution with DOI links back to the formal publications on ScienceDirect.

Elsevier Open Access Terms and Conditions

You can publish open access with Elsevier in hundreds of open access journals or in nearly 2000 established subscription journals that support open access publishing. Permitted third party re-use of these open access articles is defined by the author's choice of Creative Commons user license. See our open access license policy for more information.

Terms & Conditions applicable to all Open Access articles published with Elsevier:

Any reuse of the article must not represent the author as endorsing the adaptation of the article nor should the article be modified in such a way as to damage the author's honour or reputation. If any changes have been made, such changes must be clearly indicated.

The author(s) must be appropriately credited and we ask that you include the end user license and a DOI link to the formal publication on ScienceDirect.

If any part of the material to be used (for example, figures) has appeared in our publication with credit or acknowledgement to another source it is the responsibility of the user to ensure their reuse complies with the terms and conditions determined by the rights holder.

Additional Terms & Conditions applicable to each Creative Commons user license:

CC BY: The CC-BY license allows users to copy, to create extracts, abstracts and new works from the Article, to alter and revise the Article and to make commercial use of the Article (including reuse and/or resale of the Article by commercial entities), provided the user gives appropriate credit (with a link to the formal publication through the relevant DOI), provides a link to the license, indicates if changes were made and the licensor is not represented as endorsing the use made of the work. The full details of the license are available at http://creativecommons.org/licenses/by/4.0.

CC BY NC SA: The CC BY-NC-SA license allows users to copy, to create extracts, abstracts and new works from the Article, to alter and revise the Article, provided this is not done for commercial purposes, and that the user gives appropriate credit (with a link to the formal publication through the relevant DOI), provides a link to the license, indicates if changes were made and the licensor is not represented as endorsing the use made of the work. Further, any new works must be made available on the same conditions. The full details of the license are available at http://creativecommons.org/licenses/by-nc-sa/4.0.

CC BY NC ND: The CC BY-NC-ND license allows users to copy and distribute the Article, provided this is not done for commercial purposes and further does not permit distribution of the Article if it is changed or edited in any way, and provided the user gives appropriate credit (with a link to the formal publication through the relevant DOI), provides a link to the license, and that the licensor is not represented as endorsing the use made of the work. The full details of the license are available at http://creativecommons.org/licenses/by-nc-nd/4.0.

Any commercial reuse of Open Access articles published with a CC BY NC SA or CC BY NC ND license requires permission from Elsevier and will be subject to a fee.

Commercial reuse includes:

- Associating advertising with the full text of the Article
- Charging fees for document delivery or access
- Article aggregation
- Systematic distribution via e-mail lists or share buttons

Posting or linking by commercial companies for use by customers of those companies.

20. **Other Conditions**:

v1.9

Questions? customercare@copyright.com or +1-855-239-3415 (toll free in the US) or +1-978-646-2777.

ELSEVIER LICENSE
TERMS AND CONDITIONS

Nov 23, 2018

This Agreement between Nazmul Huda ("You") and Elsevier ("Elsevier") consists of your license details and the terms and conditions provided by Elsevier and Copyright Clearance Center.

License Number	4474901271115
License date	Nov 23, 2018
Licensed Content Publisher	Elsevier
Licensed Content Publication	Materials Science and Engineering: A
Licensed Content Title	Microstructure and high strength–toughness combination of a new 700MPa Nb-microalloyed pipeline steel
Licensed Content Author	S. Shanmugam,N.K. Ramisetti,R.D.K. Misra,J. Hartmann,S.G. Jansto
Licensed Content Date	Apr 15, 2008
Licensed Content Volume	478
Licensed Content Issue	1-2
Licensed Content Pages	12
Start Page	26
End Page	37
Type of Use	reuse in a thesis/dissertation
Intended publisher of new work	other
Portion	figures/tables/illustrations
Number of figures/tables/illustrations	1
Format	both print and electronic
Are you the author of this Elsevier article?	No
Will you be translating?	No
Original figure numbers	Figure 11 d
Title of your thesis/dissertation	Effect of Martensite-Austenite (MA) on Mechanical Properties of X80 Linepipe Steel
Expected completion date	Dec 2018
Estimated size (number of pages)	174
Requestor Location	Nazmul Huda 573 westvale drive waterloo, ON N2T1G5 Canada Attn: Nazmul Huda
Publisher Tax ID	GB 494 6272 12
Total	0.00 CAD

Terms and Conditions

INTRODUCTION

1. The publisher for this copyrighted material is Elsevier. By clicking "accept" in connection with completing this licensing transaction, you agree that the following terms and conditions apply to this transaction (along with the Billing and Payment terms and conditions established by Copyright Clearance Center, Inc. ("CCC"), at the time that you opened your Rightslink account and that are available at any time at http://myaccount.copyright.com).

GENERAL TERMS

2. Elsevier hereby grants you permission to reproduce the aforementioned material subject to the terms and conditions indicated.
3. Acknowledgement: If any part of the material to be used (for example, figures) has appeared in our publication with credit or acknowledgement to another source, permission must also be sought from that source. If such permission is not obtained then that material may not be included in your publication/copies. Suitable acknowledgement to the source must be made, either as a footnote or in a reference list at the end of your publication, as follows:
"Reprinted from Publication title, Vol /edition number, Author(s), Title of article / title of chapter, Pages No., Copyright (Year), with permission from Elsevier [OR APPLICABLE SOCIETY COPYRIGHT OWNER]." Also Lancet special credit - "Reprinted from The Lancet, Vol. number, Author(s), Title of article, Pages No., Copyright (Year), with permission from Elsevier."
4. Reproduction of this material is confined to the purpose and/or media for which permission is hereby given.
5. Altering/Modifying Material: Not Permitted. However figures and illustrations may be altered/adapted minimally to serve your work. Any other abbreviations, additions, deletions and/or any other alterations shall be made only with prior written authorization of Elsevier Ltd. (Please contact Elsevier at permissions@elsevier.com). No modifications can be made to any Lancet figures/tables and they must be reproduced in full.
6. If the permission fee for the requested use of our material is waived in this instance, please be advised that your future requests for Elsevier materials may attract a fee.
7. Reservation of Rights: Publisher reserves all rights not specifically granted in the combination of (i) the license details provided by you and accepted in the course of this licensing transaction, (ii) these terms and conditions and (iii) CCC's Billing and Payment terms and conditions.
8. License Contingent Upon Payment: While you may exercise the rights licensed immediately upon issuance of the license at the end of the licensing process for the transaction, provided that you have disclosed complete and accurate details of your proposed use, no license is finally effective unless and until full payment is received from you (either by publisher or by CCC) as provided in CCC's Billing and Payment terms and conditions. If full payment is not received on a timely basis, then any license preliminarily granted shall be deemed automatically revoked and shall be void as if never granted. Further, in the event that you breach any of these terms and conditions or any of CCC's Billing and Payment terms and conditions, the license is automatically revoked and shall be void as if never granted. Use of materials as described in a revoked license, as well as any use of the materials beyond the scope of an unrevoked license, may constitute copyright infringement and publisher reserves the right to take any and all action to protect its copyright in the materials.
9. Warranties: Publisher makes no representations or warranties with respect to the licensed material.
10. Indemnity: You hereby indemnify and agree to hold harmless publisher and CCC, and their respective officers, directors, employees and agents, from and against any and all claims arising out of your use of the licensed material other than as specifically authorized pursuant to this license.

11. No Transfer of License: This license is personal to you and may not be sublicensed, assigned, or transferred by you to any other person without publisher's written permission.
12. No Amendment Except in Writing: This license may not be amended except in a writing signed by both parties (or, in the case of publisher, by CCC on publisher's behalf).
13. Objection to Contrary Terms: Publisher hereby objects to any terms contained in any purchase order, acknowledgment, check endorsement or other writing prepared by you, which terms are inconsistent with these terms and conditions or CCC's Billing and Payment terms and conditions. These terms and conditions, together with CCC's Billing and Payment terms and conditions (which are incorporated herein), comprise the entire agreement between you and publisher (and CCC) concerning this licensing transaction. In the event of any conflict between your obligations established by these terms and conditions and those established by CCC's Billing and Payment terms and conditions, these terms and conditions shall control.
14. Revocation: Elsevier or Copyright Clearance Center may deny the permissions described in this License at their sole discretion, for any reason or no reason, with a full refund payable to you. Notice of such denial will be made using the contact information provided by you. Failure to receive such notice will not alter or invalidate the denial. In no event will Elsevier or Copyright Clearance Center be responsible or liable for any costs, expenses or damage incurred by you as a result of a denial of your permission request, other than a refund of the amount(s) paid by you to Elsevier and/or Copyright Clearance Center for denied permissions.

LIMITED LICENSE

The following terms and conditions apply only to specific license types:
15. **Translation**: This permission is granted for non-exclusive world **English** rights only unless your license was granted for translation rights. If you licensed translation rights you may only translate this content into the languages you requested. A professional translator must perform all translations and reproduce the content word for word preserving the integrity of the article.
16. **Posting licensed content on any Website**: The following terms and conditions apply as follows: Licensing material from an Elsevier journal: All content posted to the web site must maintain the copyright information line on the bottom of each image; A hyper-text must be included to the Homepage of the journal from which you are licensing at http://www.sciencedirect.com/science/journal/xxxxx or the Elsevier homepage for books at http://www.elsevier.com; Central Storage: This license does not include permission for a scanned version of the material to be stored in a central repository such as that provided by Heron/XanEdu.
Licensing material from an Elsevier book: A hyper-text link must be included to the Elsevier homepage at http://www.elsevier.com . All content posted to the web site must maintain the copyright information line on the bottom of each image.

Posting licensed content on Electronic reserve: In addition to the above the following clauses are applicable: The web site must be password-protected and made available only to bona fide students registered on a relevant course. This permission is granted for 1 year only. You may obtain a new license for future website posting.
17. **For journal authors:** the following clauses are applicable in addition to the above:
Preprints:
A preprint is an author's own write-up of research results and analysis, it has not been peer-reviewed, nor has it had any other value added to it by a publisher (such as formatting, copyright, technical enhancement etc.).
Authors can share their preprints anywhere at any time. Preprints should not be added to or enhanced in any way in order to appear more like, or to substitute for, the final versions of articles however authors can update their preprints on arXiv or RePEc with their Accepted Author Manuscript (see below).

If accepted for publication, we encourage authors to link from the preprint to their formal publication via its DOI. Millions of researchers have access to the formal publications on ScienceDirect, and so links will help users to find, access, cite and use the best available version. Please note that Cell Press, The Lancet and some society-owned have different preprint policies. Information on these policies is available on the journal homepage.
Accepted Author Manuscripts: An accepted author manuscript is the manuscript of an article that has been accepted for publication and which typically includes author-incorporated changes suggested during submission, peer review and editor-author communications.
Authors can share their accepted author manuscript:

- immediately
  - via their non-commercial person homepage or blog
  - by updating a preprint in arXiv or RePEc with the accepted manuscript
  - via their research institute or institutional repository for internal institutional uses or as part of an invitation-only research collaboration work-group
  - directly by providing copies to their students or to research collaborators for their personal use
  - for private scholarly sharing as part of an invitation-only work group on commercial sites with which Elsevier has an agreement
- After the embargo period
  - via non-commercial hosting platforms such as their institutional repository
  - via commercial sites with which Elsevier has an agreement

In all cases accepted manuscripts should:

- link to the formal publication via its DOI
- bear a CC-BY-NC-ND license - this is easy to do
- if aggregated with other manuscripts, for example in a repository or other site, be shared in alignment with our hosting policy not be added to or enhanced in any way to appear more like, or to substitute for, the published journal article.

Published journal article (JPA): A published journal article (PJA) is the definitive final record of published research that appears or will appear in the journal and embodies all value-adding publishing activities including peer review co-ordination, copy-editing, formatting, (if relevant) pagination and online enrichment.
Policies for sharing publishing journal articles differ for subscription and gold open access articles:
Subscription Articles: If you are an author, please share a link to your article rather than the full-text. Millions of researchers have access to the formal publications on ScienceDirect, and so links will help your users to find, access, cite, and use the best available version.
Theses and dissertations which contain embedded PJAs as part of the formal submission can be posted publicly by the awarding institution with DOI links back to the formal publications on ScienceDirect.
If you are affiliated with a library that subscribes to ScienceDirect you have additional private sharing rights for others' research accessed under that agreement. This includes use for classroom teaching and internal training at the institution (including use in course packs and courseware programs), and inclusion of the article for grant funding purposes.
Gold Open Access Articles: May be shared according to the author-selected end-user license and should contain a CrossMark logo, the end user license, and a DOI link to the formal publication on ScienceDirect.
Please refer to Elsevier's posting policy for further information.
18. **For book authors** the following clauses are applicable in addition to the above:
Authors are permitted to place a brief summary of their work online only. You are not

allowed to download and post the published electronic version of your chapter, nor may you scan the printed edition to create an electronic version. **Posting to a repository:** Authors are permitted to post a summary of their chapter only in their institution's repository.
19. **Thesis/Dissertation**: If your license is for use in a thesis/dissertation your thesis may be submitted to your institution in either print or electronic form. Should your thesis be published commercially, please reapply for permission. These requirements include permission for the Library and Archives of Canada to supply single copies, on demand, of the complete thesis and include permission for Proquest/UMI to supply single copies, on demand, of the complete thesis. Should your thesis be published commercially, please reapply for permission. Theses and dissertations which contain embedded PJAs as part of the formal submission can be posted publicly by the awarding institution with DOI links back to the formal publications on ScienceDirect.

Elsevier Open Access Terms and Conditions

You can publish open access with Elsevier in hundreds of open access journals or in nearly 2000 established subscription journals that support open access publishing. Permitted third party re-use of these open access articles is defined by the author's choice of Creative Commons user license. See our open access license policy for more information.
Terms & Conditions applicable to all Open Access articles published with Elsevier:
Any reuse of the article must not represent the author as endorsing the adaptation of the article nor should the article be modified in such a way as to damage the author's honour or reputation. If any changes have been made, such changes must be clearly indicated.
The author(s) must be appropriately credited and we ask that you include the end user license and a DOI link to the formal publication on ScienceDirect.
If any part of the material to be used (for example, figures) has appeared in our publication with credit or acknowledgement to another source it is the responsibility of the user to ensure their reuse complies with the terms and conditions determined by the rights holder.
Additional Terms & Conditions applicable to each Creative Commons user license:
CC BY: The CC-BY license allows users to copy, to create extracts, abstracts and new works from the Article, to alter and revise the Article and to make commercial use of the Article (including reuse and/or resale of the Article by commercial entities), provided the user gives appropriate credit (with a link to the formal publication through the relevant DOI), provides a link to the license, indicates if changes were made and the licensor is not represented as endorsing the use made of the work. The full details of the license are available at http://creativecommons.org/licenses/by/4.0.
CC BY NC SA: The CC BY-NC-SA license allows users to copy, to create extracts, abstracts and new works from the Article, to alter and revise the Article, provided this is not done for commercial purposes, and that the user gives appropriate credit (with a link to the formal publication through the relevant DOI), provides a link to the license, indicates if changes were made and the licensor is not represented as endorsing the use made of the work. Further, any new works must be made available on the same conditions. The full details of the license are available at http://creativecommons.org/licenses/by-nc-sa/4.0.
CC BY NC ND: The CC BY-NC-ND license allows users to copy and distribute the Article, provided this is not done for commercial purposes and further does not permit distribution of the Article if it is changed or edited in any way, and provided the user gives appropriate credit (with a link to the formal publication through the relevant DOI), provides a link to the license, and that the licensor is not represented as endorsing the use made of the work. The full details of the license are available at http://creativecommons.org/licenses/by-nc-nd/4.0.
Any commercial reuse of Open Access articles published with a CC BY NC SA or CC BY NC ND license requires permission from Elsevier and will be subject to a fee.
Commercial reuse includes:

- Associating advertising with the full text of the Article
- Charging fees for document delivery or access

- Article aggregation
- Systematic distribution via e-mail lists or share buttons

Posting or linking by commercial companies for use by customers of those companies.

20. **Other Conditions**:

v1.9

Questions? customercare@copyright.com or +1-855-239-3415 (toll free in the US) or +1-978-646-2777.

ELSEVIER LICENSE
TERMS AND CONDITIONS

Nov 23, 2018

This Agreement between Nazmul Huda ("You") and Elsevier ("Elsevier") consists of your license details and the terms and conditions provided by Elsevier and Copyright Clearance Center.

License Number	4474900885807
License date	Nov 23, 2018
Licensed Content Publisher	Elsevier
Licensed Content Publication	Materials Science and Engineering: A
Licensed Content Title	Transmission electron microscopy of martensite/austenite islands in pipeline steel X70
Licensed Content Author	Chunming Wang,Xingfang Wu,Jie Liu,Ning'an Xu
Licensed Content Date	Nov 25, 2006
Licensed Content Volume	438
Licensed Content Issue	n/a
Licensed Content Pages	5
Start Page	267
End Page	271
Type of Use	reuse in a thesis/dissertation
Portion	figures/tables/illustrations
Number of figures/tables/illustrations	2
Format	both print and electronic
Are you the author of this Elsevier article?	No
Will you be translating?	No
Original figure numbers	Figure 1 a and 1 i
Title of your thesis/dissertation	Effect of Martensite-Austenite (MA) on Mechanical Properties of X80 Linepipe Steel
Expected completion date	Dec 2018
Estimated size (number of pages)	174
Requestor Location	Nazmul Huda 573 westvale drive waterloo, ON N2T1G5 Canada Attn: Nazmul Huda
Publisher Tax ID	GB 494 6272 12

Print This Page

ELSEVIER LICENSE
TERMS AND CONDITIONS

Nov 23, 2018

This Agreement between Nazmul Huda ("You") and Elsevier ("Elsevier") consists of your license details and the terms and conditions provided by Elsevier and Copyright Clearance Center.

License Number	4474901496717
License date	Nov 23, 2018
Licensed Content Publisher	Elsevier
Licensed Content Publication	Materials Science and Engineering: A
Licensed Content Title	Effect of morphologies of martensite–austenite constituents on impact toughness in intercritically reheated coarse-grained heat-affected zone of HSLA steel
Licensed Content Author	Xiang Luo,Xiaohua Chen,Tao Wang,Shiwei Pan,Zidong Wang
Licensed Content Date	Jan 5, 2018
Licensed Content Volume	710
Licensed Content Issue	n/a
Licensed Content Pages	8
Start Page	192
End Page	199
Type of Use	reuse in a thesis/dissertation
Intended publisher of new work	other
Portion	figures/tables/illustrations
Number of figures/tables/illustrations	1
Format	both print and electronic
Are you the author of this Elsevier article?	No
Will you be translating?	No
Original figure numbers	Figure 8
Title of your thesis/dissertation	Effect of Martensite-Austenite (MA) on Mechanical Properties of X80 Linepipe Steel
Expected completion date	Dec 2018
Estimated size (number of pages)	174
Requestor Location	Nazmul Huda 573 westvale drive waterloo, ON N2T1G5 Canada

Print This Page

ELSEVIER LICENSE
TERMS AND CONDITIONS

Nov 23, 2018

This Agreement between Nazmul Huda ("You") and Elsevier ("Elsevier") consists of your license details and the terms and conditions provided by Elsevier and Copyright Clearance Center.

License Number	4474910175492
License date	Nov 23, 2018
Licensed Content Publisher	Elsevier
Licensed Content Publication	Scripta Materialia
Licensed Content Title	Elemental distribution in the martensite–austenite constituent in intercritically reheated coarse-grained heat-affected zone of a high-strength pipeline steel
Licensed Content Author	Xueda Li,Chengjia Shang,Xiaoping Ma,Baptiste Gault,S.V. Subramanian,Jianbo Sun,R.D.K. Misra
Licensed Content Date	Oct 1, 2017
Licensed Content Volume	139
Licensed Content Issue	n/a
Licensed Content Pages	4
Start Page	67
End Page	70
Type of Use	reuse in a thesis/dissertation
Intended publisher of new work	other
Portion	figures/tables/illustrations
Number of figures/tables/illustrations	1
Format	both print and electronic
Are you the author of this Elsevier article?	No
Will you be translating?	No
Original figure numbers	Figure 2 (a-f)
Title of your thesis/dissertation	Effect of Martensite-Austenite (MA) on Mechanical Properties of X80 Linepipe Steel
Expected completion date	Dec 2018
Estimated size (number of pages)	174
Requestor Location	Nazmul Huda 573 westvale drive waterloo, ON N2T1G5 Canada Attn: Nazmul Huda

Publisher Tax ID	GB 494 6272 12
Total	0.00 USD

Terms and Conditions

INTRODUCTION

1. The publisher for this copyrighted material is Elsevier. By clicking "accept" in connection with completing this licensing transaction, you agree that the following terms and conditions apply to this transaction (along with the Billing and Payment terms and conditions established by Copyright Clearance Center, Inc. ("CCC"), at the time that you opened your Rightslink account and that are available at any time at http://myaccount.copyright.com).

GENERAL TERMS

2. Elsevier hereby grants you permission to reproduce the aforementioned material subject to the terms and conditions indicated.
3. Acknowledgement: If any part of the material to be used (for example, figures) has appeared in our publication with credit or acknowledgement to another source, permission must also be sought from that source. If such permission is not obtained then that material may not be included in your publication/copies. Suitable acknowledgement to the source must be made, either as a footnote or in a reference list at the end of your publication, as follows:
"Reprinted from Publication title, Vol /edition number, Author(s), Title of article / title of chapter, Pages No., Copyright (Year), with permission from Elsevier [OR APPLICABLE SOCIETY COPYRIGHT OWNER]." Also Lancet special credit - "Reprinted from The Lancet, Vol. number, Author(s), Title of article, Pages No., Copyright (Year), with permission from Elsevier."
4. Reproduction of this material is confined to the purpose and/or media for which permission is hereby given.
5. Altering/Modifying Material: Not Permitted. However figures and illustrations may be altered/adapted minimally to serve your work. Any other abbreviations, additions, deletions and/or any other alterations shall be made only with prior written authorization of Elsevier Ltd. (Please contact Elsevier at permissions@elsevier.com). No modifications can be made to any Lancet figures/tables and they must be reproduced in full.
6. If the permission fee for the requested use of our material is waived in this instance, please be advised that your future requests for Elsevier materials may attract a fee.
7. Reservation of Rights: Publisher reserves all rights not specifically granted in the combination of (i) the license details provided by you and accepted in the course of this licensing transaction, (ii) these terms and conditions and (iii) CCC's Billing and Payment terms and conditions.
8. License Contingent Upon Payment: While you may exercise the rights licensed immediately upon issuance of the license at the end of the licensing process for the transaction, provided that you have disclosed complete and accurate details of your proposed use, no license is finally effective unless and until full payment is received from you (either by publisher or by CCC) as provided in CCC's Billing and Payment terms and conditions. If full payment is not received on a timely basis, then any license preliminarily granted shall be deemed automatically revoked and shall be void as if never granted. Further, in the event that you breach any of these terms and conditions or any of CCC's Billing and Payment terms and conditions, the license is automatically revoked and shall be void as if never granted. Use of materials as described in a revoked license, as well as any use of the materials beyond the scope of an unrevoked license, may constitute copyright infringement and publisher reserves the right to take any and all action to protect its copyright in the materials.
9. Warranties: Publisher makes no representations or warranties with respect to the licensed material.
10. Indemnity: You hereby indemnify and agree to hold harmless publisher and CCC, and their respective officers, directors, employees and agents, from and against any and all

claims arising out of your use of the licensed material other than as specifically authorized pursuant to this license.
11. No Transfer of License: This license is personal to you and may not be sublicensed, assigned, or transferred by you to any other person without publisher's written permission.
12. No Amendment Except in Writing: This license may not be amended except in a writing signed by both parties (or, in the case of publisher, by CCC on publisher's behalf).
13. Objection to Contrary Terms: Publisher hereby objects to any terms contained in any purchase order, acknowledgment, check endorsement or other writing prepared by you, which terms are inconsistent with these terms and conditions or CCC's Billing and Payment terms and conditions. These terms and conditions, together with CCC's Billing and Payment terms and conditions (which are incorporated herein), comprise the entire agreement between you and publisher (and CCC) concerning this licensing transaction. In the event of any conflict between your obligations established by these terms and conditions and those established by CCC's Billing and Payment terms and conditions, these terms and conditions shall control.
14. Revocation: Elsevier or Copyright Clearance Center may deny the permissions described in this License at their sole discretion, for any reason or no reason, with a full refund payable to you. Notice of such denial will be made using the contact information provided by you. Failure to receive such notice will not alter or invalidate the denial. In no event will Elsevier or Copyright Clearance Center be responsible or liable for any costs, expenses or damage incurred by you as a result of a denial of your permission request, other than a refund of the amount(s) paid by you to Elsevier and/or Copyright Clearance Center for denied permissions.

LIMITED LICENSE

The following terms and conditions apply only to specific license types:
15. **Translation**: This permission is granted for non-exclusive world **English** rights only unless your license was granted for translation rights. If you licensed translation rights you may only translate this content into the languages you requested. A professional translator must perform all translations and reproduce the content word for word preserving the integrity of the article.
16. **Posting licensed content on any Website**: The following terms and conditions apply as follows: Licensing material from an Elsevier journal: All content posted to the web site must maintain the copyright information line on the bottom of each image; A hyper-text must be included to the Homepage of the journal from which you are licensing at http://www.sciencedirect.com/science/journal/xxxxx or the Elsevier homepage for books at http://www.elsevier.com; Central Storage: This license does not include permission for a scanned version of the material to be stored in a central repository such as that provided by Heron/XanEdu.
Licensing material from an Elsevier book: A hyper-text link must be included to the Elsevier homepage at http://www.elsevier.com . All content posted to the web site must maintain the copyright information line on the bottom of each image.

Posting licensed content on Electronic reserve: In addition to the above the following clauses are applicable: The web site must be password-protected and made available only to bona fide students registered on a relevant course. This permission is granted for 1 year only. You may obtain a new license for future website posting.
17. **For journal authors:** the following clauses are applicable in addition to the above:
Preprints:
A preprint is an author's own write-up of research results and analysis, it has not been peer-reviewed, nor has it had any other value added to it by a publisher (such as formatting, copyright, technical enhancement etc.).
Authors can share their preprints anywhere at any time. Preprints should not be added to or enhanced in any way in order to appear more like, or to substitute for, the final versions of

articles however authors can update their preprints on arXiv or RePEc with their Accepted Author Manuscript (see below).
If accepted for publication, we encourage authors to link from the preprint to their formal publication via its DOI. Millions of researchers have access to the formal publications on ScienceDirect, and so links will help users to find, access, cite and use the best available version. Please note that Cell Press, The Lancet and some society-owned have different preprint policies. Information on these policies is available on the journal homepage.
Accepted Author Manuscripts: An accepted author manuscript is the manuscript of an article that has been accepted for publication and which typically includes author-incorporated changes suggested during submission, peer review and editor-author communications.
Authors can share their accepted author manuscript:

- immediately
  - via their non-commercial person homepage or blog
  - by updating a preprint in arXiv or RePEc with the accepted manuscript
  - via their research institute or institutional repository for internal institutional uses or as part of an invitation-only research collaboration work-group
  - directly by providing copies to their students or to research collaborators for their personal use
  - for private scholarly sharing as part of an invitation-only work group on commercial sites with which Elsevier has an agreement
- After the embargo period
  - via non-commercial hosting platforms such as their institutional repository
  - via commercial sites with which Elsevier has an agreement

In all cases accepted manuscripts should:

- link to the formal publication via its DOI
- bear a CC-BY-NC-ND license - this is easy to do
- if aggregated with other manuscripts, for example in a repository or other site, be shared in alignment with our hosting policy not be added to or enhanced in any way to appear more like, or to substitute for, the published journal article.

Published journal article (JPA): A published journal article (PJA) is the definitive final record of published research that appears or will appear in the journal and embodies all value-adding publishing activities including peer review co-ordination, copy-editing, formatting, (if relevant) pagination and online enrichment.
Policies for sharing publishing journal articles differ for subscription and gold open access articles:
Subscription Articles: If you are an author, please share a link to your article rather than the full-text. Millions of researchers have access to the formal publications on ScienceDirect, and so links will help your users to find, access, cite, and use the best available version.
Theses and dissertations which contain embedded PJAs as part of the formal submission can be posted publicly by the awarding institution with DOI links back to the formal publications on ScienceDirect.
If you are affiliated with a library that subscribes to ScienceDirect you have additional private sharing rights for others' research accessed under that agreement. This includes use for classroom teaching and internal training at the institution (including use in course packs and courseware programs), and inclusion of the article for grant funding purposes.
Gold Open Access Articles: May be shared according to the author-selected end-user license and should contain a CrossMark logo, the end user license, and a DOI link to the formal publication on ScienceDirect.
Please refer to Elsevier's posting policy for further information.

18. **For book authors** the following clauses are applicable in addition to the above: Authors are permitted to place a brief summary of their work online only. You are not allowed to download and post the published electronic version of your chapter, nor may you scan the printed edition to create an electronic version. **Posting to a repository:** Authors are permitted to post a summary of their chapter only in their institution's repository.
19. **Thesis/Dissertation**: If your license is for use in a thesis/dissertation your thesis may be submitted to your institution in either print or electronic form. Should your thesis be published commercially, please reapply for permission. These requirements include permission for the Library and Archives of Canada to supply single copies, on demand, of the complete thesis and include permission for Proquest/UMI to supply single copies, on demand, of the complete thesis. Should your thesis be published commercially, please reapply for permission. Theses and dissertations which contain embedded PJAs as part of the formal submission can be posted publicly by the awarding institution with DOI links back to the formal publications on ScienceDirect.

Elsevier Open Access Terms and Conditions

You can publish open access with Elsevier in hundreds of open access journals or in nearly 2000 established subscription journals that support open access publishing. Permitted third party re-use of these open access articles is defined by the author's choice of Creative Commons user license. See our open access license policy for more information.

Terms & Conditions applicable to all Open Access articles published with Elsevier:

Any reuse of the article must not represent the author as endorsing the adaptation of the article nor should the article be modified in such a way as to damage the author's honour or reputation. If any changes have been made, such changes must be clearly indicated.

The author(s) must be appropriately credited and we ask that you include the end user license and a DOI link to the formal publication on ScienceDirect.

If any part of the material to be used (for example, figures) has appeared in our publication with credit or acknowledgement to another source it is the responsibility of the user to ensure their reuse complies with the terms and conditions determined by the rights holder.

Additional Terms & Conditions applicable to each Creative Commons user license:

CC BY: The CC-BY license allows users to copy, to create extracts, abstracts and new works from the Article, to alter and revise the Article and to make commercial use of the Article (including reuse and/or resale of the Article by commercial entities), provided the user gives appropriate credit (with a link to the formal publication through the relevant DOI), provides a link to the license, indicates if changes were made and the licensor is not represented as endorsing the use made of the work. The full details of the license are available at http://creativecommons.org/licenses/by/4.0.

CC BY NC SA: The CC BY-NC-SA license allows users to copy, to create extracts, abstracts and new works from the Article, to alter and revise the Article, provided this is not done for commercial purposes, and that the user gives appropriate credit (with a link to the formal publication through the relevant DOI), provides a link to the license, indicates if changes were made and the licensor is not represented as endorsing the use made of the work. Further, any new works must be made available on the same conditions. The full details of the license are available at http://creativecommons.org/licenses/by-nc-sa/4.0.

CC BY NC ND: The CC BY-NC-ND license allows users to copy and distribute the Article, provided this is not done for commercial purposes and further does not permit distribution of the Article if it is changed or edited in any way, and provided the user gives appropriate credit (with a link to the formal publication through the relevant DOI), provides a link to the license, and that the licensor is not represented as endorsing the use made of the work. The full details of the license are available at http://creativecommons.org/licenses/by-nc-nd/4.0.

Any commercial reuse of Open Access articles published with a CC BY NC SA or CC BY NC ND license requires permission from Elsevier and will be subject to a fee.

Commercial reuse includes:

- Associating advertising with the full text of the Article
- Charging fees for document delivery or access
- Article aggregation
- Systematic distribution via e-mail lists or share buttons

Posting or linking by commercial companies for use by customers of those companies.

20. **Other Conditions**:

v1.9

Questions? customercare@copyright.com or +1-855-239-3415 (toll free in the US) or +1-978-646-2777.

SPRINGER NATURE LICENSE TERMS AND CONDITIONS

Nov 23, 2018

This Agreement between Nazmul Huda ("You") and Springer Nature ("Springer Nature") consists of your license details and the terms and conditions provided by Springer Nature and Copyright Clearance Center.

License Number	4474910373338
License date	Nov 23, 2018
Licensed Content Publisher	Springer Nature
Licensed Content Publication	Metallurgical and Materials Transactions A
Licensed Content Title	Effects of Cooling Conditions on Tensile and Charpy Impact Properties of API X80 Linepipe Steels
Licensed Content Author	Seung Youb Han, Sang Yong Shin, Sunghak Lee et al
Licensed Content Date	Jan 1, 2009
Licensed Content Volume	41
Licensed Content Issue	2
Type of Use	Thesis/Dissertation
Requestor type	academic/university or research institute
Format	print and electronic
Portion	figures/tables/illustrations
Number of figures/tables/illustrations	1
Will you be translating?	no
Circulation/distribution	2,001 to 5,000
Author of this Springer Nature content	no
Title	Effect of Martensite-Austenite (MA) on Mechanical Properties of X80 Linepipe Steel
Institution name	n/a
Expected presentation date	Dec 2018
Portions	Figure 8a
Requestor Location	Nazmul Huda 573 westvale drive waterloo, ON N2T1G5 Canada Attn: Nazmul Huda
Billing Type	Invoice
Billing Address	Nazmul Huda 573 westvale drive waterloo, ON N2T1G5

Canada
Attn: Nazmul Huda

Total 0.00 USD

Terms and Conditions

Springer Nature Terms and Conditions for RightsLink Permissions

Springer Nature Customer Service Centre GmbH (the Licensor) hereby grants you a non-exclusive, world-wide licence to reproduce the material and for the purpose and requirements specified in the attached copy of your order form, and for no other use, subject to the conditions below:

1. The Licensor warrants that it has, to the best of its knowledge, the rights to license reuse of this material. However, you should ensure that the material you are requesting is original to the Licensor and does not carry the copyright of another entity (as credited in the published version).

   If the credit line on any part of the material you have requested indicates that it was reprinted or adapted with permission from another source, then you should also seek permission from that source to reuse the material.

2. Where **print only** permission has been granted for a fee, separate permission must be obtained for any additional electronic re-use.

3. Permission granted **free of charge** for material in print is also usually granted for any electronic version of that work, provided that the material is incidental to your work as a whole and that the electronic version is essentially equivalent to, or substitutes for, the print version.

4. A licence for 'post on a website' is valid for 12 months from the licence date. This licence does not cover use of full text articles on websites.

5. Where **'reuse in a dissertation/thesis'** has been selected the following terms apply: Print rights of the final author's accepted manuscript (for clarity, NOT the published version) for up to 100 copies, electronic rights for use only on a personal website or institutional repository as defined by the Sherpa guideline (www.sherpa.ac.uk/romeo/).

6. Permission granted for books and journals is granted for the lifetime of the first edition and does not apply to second and subsequent editions (except where the first edition permission was granted free of charge or for signatories to the STM Permissions Guidelines http://www.stm-assoc.org/copyright-legal-affairs/permissions/permissions-guidelines/), and does not apply for editions in other languages unless additional translation rights have been granted separately in the licence.

7. Rights for additional components such as custom editions and derivatives require additional permission and may be subject to an additional fee. Please apply to Journalpermissions@springernature.com/bookpermissions@springernature.com for these rights.

8. The Licensor's permission must be acknowledged next to the licensed material in print. In electronic form, this acknowledgement must be visible at the same time as the figures/tables/illustrations or abstract, and must be hyperlinked to the journal/book's homepage. Our required acknowledgement format is in the Appendix below.

9. Use of the material for incidental promotional use, minor editing privileges (this does not include cropping, adapting, omitting material or any other changes that affect the meaning, intention or moral rights of the author) and copies for the disabled are permitted under this licence.

10. Minor adaptations of single figures (changes of format, colour and style) do not require the Licensor's approval. However, the adaptation should be credited as shown in Appendix below.

Appendix — Acknowledgements:

For Journal Content:
Reprinted by permission from [**the Licensor**]: [**Journal Publisher** (e.g. Nature/Springer/Palgrave)] [**JOURNAL NAME**] [**REFERENCE CITATION** (Article name, Author(s) Name), [**COPYRIGHT**] (year of publication)

For **Advance Online Publication papers:**
Reprinted by permission from [**the Licensor**]: [**Journal Publisher** (e.g. Nature/Springer/Palgrave)] [**JOURNAL NAME**] [**REFERENCE CITATION** (Article name, Author(s) Name), [**COPYRIGHT**] (year of publication), advance online publication, day month year (doi: 10.1038/sj.[JOURNAL ACRONYM].)

For Adaptations/Translations:
Adapted/Translated by permission from [**the Licensor**]: [**Journal Publisher** (e.g. Nature/Springer/Palgrave)] [**JOURNAL NAME**] [**REFERENCE CITATION** (Article name, Author(s) Name), [**COPYRIGHT**] (year of publication)

Note: For any republication from the British Journal of Cancer, the following credit line style applies:

Reprinted/adapted/translated by permission from [**the Licensor**]: on behalf of Cancer Research UK: : [**Journal Publisher** (e.g. Nature/Springer/Palgrave)] [**JOURNAL NAME**] [**REFERENCE CITATION** (Article name, Author(s) Name), [**COPYRIGHT]** (year of publication)

For **Advance Online Publication** papers:
Reprinted by permission from The [**the Licensor**]: on behalf of Cancer Research UK: [**Journal Publisher** (e.g. Nature/Springer/Palgrave)] [**JOURNAL NAME**] [**REFERENCE CITATION** (Article name, Author(s) Name), [**COPYRIGHT**] (year of publication), advance online publication, day month year (doi: 10.1038/sj.[JOURNAL ACRONYM])

For Book content:
Reprinted/adapted by permission from [**the Licensor**]: [**Book Publisher** (e.g. Palgrave Macmillan, Springer etc) [**Book Title**] by [**Book author**(s)] [**COPYRIGHT**] (year of publication)

Other Conditions:

Version 1.1

SPRINGER NATURE LICENSE TERMS AND CONDITIONS

Nov 23, 2018

This Agreement between Nazmul Huda ("You") and Springer Nature ("Springer Nature") consists of your license details and the terms and conditions provided by Springer Nature and Copyright Clearance Center.

License Number	4474910657867
License date	Nov 23, 2018
Licensed Content Publisher	Springer Nature
Licensed Content Publication	Metallurgical and Materials Transactions A
Licensed Content Title	Microstructure and local brittle zone phenomena in high-strength low-alloy steel welds
Licensed Content Author	B. C. Kim, S. Lee, N. J. Kim et al
Licensed Content Date	Jan 1, 1975
Licensed Content Volume	22
Licensed Content Issue	1
Type of Use	Thesis/Dissertation
Requestor type	academic/university or research institute
Format	print and electronic
Portion	figures/tables/illustrations
Number of figures/tables/illustrations	2
Will you be translating?	no
Circulation/distribution	501 to 1000
Author of this Springer Nature content	no
Title	Effect of Martensite-Austenite (MA) on Mechanical Properties of X80 Linepipe Steel
Institution name	n/a
Expected presentation date	Dec 2018
Portions	Figure 19 and Figure 20
Requestor Location	Nazmul Huda 573 westvale drive waterloo, ON N2T1G5 Canada Attn: Nazmul Huda
Billing Type	Invoice
Billing Address	Nazmul Huda 573 westvale drive waterloo, ON N2T1G5

Canada
Attn: Nazmul Huda

Total 0.00 USD

Terms and Conditions

Springer Nature Terms and Conditions for RightsLink Permissions

Springer Nature Customer Service Centre GmbH (the Licensor) hereby grants you a non-exclusive, world-wide licence to reproduce the material and for the purpose and requirements specified in the attached copy of your order form, and for no other use, subject to the conditions below:

1. The Licensor warrants that it has, to the best of its knowledge, the rights to license reuse of this material. However, you should ensure that the material you are requesting is original to the Licensor and does not carry the copyright of another entity (as credited in the published version).

   If the credit line on any part of the material you have requested indicates that it was reprinted or adapted with permission from another source, then you should also seek permission from that source to reuse the material.

2. Where **print only** permission has been granted for a fee, separate permission must be obtained for any additional electronic re-use.

3. Permission granted **free of charge** for material in print is also usually granted for any electronic version of that work, provided that the material is incidental to your work as a whole and that the electronic version is essentially equivalent to, or substitutes for, the print version.

4. A licence for 'post on a website' is valid for 12 months from the licence date. This licence does not cover use of full text articles on websites.

5. Where **'reuse in a dissertation/thesis'** has been selected the following terms apply: Print rights of the final author's accepted manuscript (for clarity, NOT the published version) for up to 100 copies, electronic rights for use only on a personal website or institutional repository as defined by the Sherpa guideline (www.sherpa.ac.uk/romeo/).

6. Permission granted for books and journals is granted for the lifetime of the first edition and does not apply to second and subsequent editions (except where the first edition permission was granted free of charge or for signatories to the STM Permissions Guidelines http://www.stm-assoc.org/copyright-legal-affairs/permissions/permissions-guidelines/), and does not apply for editions in other languages unless additional translation rights have been granted separately in the licence.

7. Rights for additional components such as custom editions and derivatives require additional permission and may be subject to an additional fee. Please apply to Journalpermissions@springernature.com/bookpermissions@springernature.com for these rights.

8. The Licensor's permission must be acknowledged next to the licensed material in print. In electronic form, this acknowledgement must be visible at the same time as the figures/tables/illustrations or abstract, and must be hyperlinked to the journal/book's homepage. Our required acknowledgement format is in the Appendix below.

9. Use of the material for incidental promotional use, minor editing privileges (this does not include cropping, adapting, omitting material or any other changes that affect the meaning, intention or moral rights of the author) and copies for the disabled are permitted under this licence.

10. Minor adaptations of single figures (changes of format, colour and style) do not require the Licensor's approval. However, the adaptation should be credited as shown in Appendix below.

Appendix — Acknowledgements:

For Journal Content:
Reprinted by permission from [**the Licensor**]: [**Journal Publisher** (e.g. Nature/Springer/Palgrave)] [**JOURNAL NAME**] [**REFERENCE CITATION** (Article name, Author(s) Name), [**COPYRIGHT**] (year of publication)

For **Advance Online Publication papers:**
Reprinted by permission from [**the Licensor**]: [**Journal Publisher** (e.g. Nature/Springer/Palgrave)] [**JOURNAL NAME**] [**REFERENCE CITATION** (Article name, Author(s) Name), [**COPYRIGHT**] (year of publication), advance online publication, day month year (doi: 10.1038/sj.[JOURNAL ACRONYM].)

For Adaptations/Translations:
Adapted/Translated by permission from [**the Licensor**]: [**Journal Publisher** (e.g. Nature/Springer/Palgrave)] [**JOURNAL NAME**] [**REFERENCE CITATION** (Article name, Author(s) Name), [**COPYRIGHT**] (year of publication)

Note: For any republication from the British Journal of Cancer, the following credit line style applies:

Reprinted/adapted/translated by permission from [**the Licensor**]: on behalf of Cancer Research UK: : [**Journal Publisher** (e.g. Nature/Springer/Palgrave)] [**JOURNAL NAME**] [**REFERENCE CITATION** (Article name, Author(s) Name), [**COPYRIGHT]** (year of publication)

For **Advance Online Publication** papers:
Reprinted by permission from The [**the Licensor**]: on behalf of Cancer Research UK: [**Journal Publisher** (e.g. Nature/Springer/Palgrave)] [**JOURNAL NAME**] [**REFERENCE CITATION** (Article name, Author(s) Name), [**COPYRIGHT**] (year of publication), advance online publication, day month year (doi: 10.1038/sj.[JOURNAL ACRONYM])

For Book content:
Reprinted/adapted by permission from [**the Licensor**]: [**Book Publisher** (e.g. Palgrave Macmillan, Springer etc) [**Book Title**] by [**Book author**(s)] [**COPYRIGHT**] (year of publication)

Other Conditions:

Version 1.1

ELSEVIER LICENSE
TERMS AND CONDITIONS

Nov 23, 2018

This Agreement between Nazmul Huda ("You") and Elsevier ("Elsevier") consists of your license details and the terms and conditions provided by Elsevier and Copyright Clearance Center.

License Number	4474910870448
License date	Nov 23, 2018
Licensed Content Publisher	Elsevier
Licensed Content Publication	Acta Metallurgica
Licensed Content Title	The effect of void arrays on void linking during ductile fracture
Licensed Content Author	P.E. Magnusen,E.M. Dubensky,D.A. Koss
Licensed Content Date	Jun 1, 1988
Licensed Content Volume	36
Licensed Content Issue	6
Licensed Content Pages	7
Start Page	1503
End Page	1509
Type of Use	reuse in a thesis/dissertation
Intended publisher of new work	other
Portion	figures/tables/illustrations
Number of figures/tables/illustrations	2
Format	both print and electronic
Are you the author of this Elsevier article?	No
Will you be translating?	No
Original figure numbers	Figure 5 and Figure 6
Title of your thesis/dissertation	Effect of Martensite-Austenite (MA) on Mechanical Properties of X80 Linepipe Steel
Expected completion date	Dec 2018
Estimated size (number of pages)	174
Requestor Location	Nazmul Huda 573 westvale drive waterloo, ON N2T1G5 Canada Attn: Nazmul Huda
Publisher Tax ID	GB 494 6272 12
Total	0.00 USD

Terms and Conditions

INTRODUCTION

1. The publisher for this copyrighted material is Elsevier. By clicking "accept" in connection with completing this licensing transaction, you agree that the following terms and conditions apply to this transaction (along with the Billing and Payment terms and conditions established by Copyright Clearance Center, Inc. ("CCC"), at the time that you opened your Rightslink account and that are available at any time at http://myaccount.copyright.com).

GENERAL TERMS

2. Elsevier hereby grants you permission to reproduce the aforementioned material subject to the terms and conditions indicated.
3. Acknowledgement: If any part of the material to be used (for example, figures) has appeared in our publication with credit or acknowledgement to another source, permission must also be sought from that source. If such permission is not obtained then that material may not be included in your publication/copies. Suitable acknowledgement to the source must be made, either as a footnote or in a reference list at the end of your publication, as follows:
"Reprinted from Publication title, Vol /edition number, Author(s), Title of article / title of chapter, Pages No., Copyright (Year), with permission from Elsevier [OR APPLICABLE SOCIETY COPYRIGHT OWNER]." Also Lancet special credit - "Reprinted from The Lancet, Vol. number, Author(s), Title of article, Pages No., Copyright (Year), with permission from Elsevier."
4. Reproduction of this material is confined to the purpose and/or media for which permission is hereby given.
5. Altering/Modifying Material: Not Permitted. However figures and illustrations may be altered/adapted minimally to serve your work. Any other abbreviations, additions, deletions and/or any other alterations shall be made only with prior written authorization of Elsevier Ltd. (Please contact Elsevier at permissions@elsevier.com). No modifications can be made to any Lancet figures/tables and they must be reproduced in full.
6. If the permission fee for the requested use of our material is waived in this instance, please be advised that your future requests for Elsevier materials may attract a fee.
7. Reservation of Rights: Publisher reserves all rights not specifically granted in the combination of (i) the license details provided by you and accepted in the course of this licensing transaction, (ii) these terms and conditions and (iii) CCC's Billing and Payment terms and conditions.
8. License Contingent Upon Payment: While you may exercise the rights licensed immediately upon issuance of the license at the end of the licensing process for the transaction, provided that you have disclosed complete and accurate details of your proposed use, no license is finally effective unless and until full payment is received from you (either by publisher or by CCC) as provided in CCC's Billing and Payment terms and conditions. If full payment is not received on a timely basis, then any license preliminarily granted shall be deemed automatically revoked and shall be void as if never granted. Further, in the event that you breach any of these terms and conditions or any of CCC's Billing and Payment terms and conditions, the license is automatically revoked and shall be void as if never granted. Use of materials as described in a revoked license, as well as any use of the materials beyond the scope of an unrevoked license, may constitute copyright infringement and publisher reserves the right to take any and all action to protect its copyright in the materials.
9. Warranties: Publisher makes no representations or warranties with respect to the licensed material.
10. Indemnity: You hereby indemnify and agree to hold harmless publisher and CCC, and their respective officers, directors, employees and agents, from and against any and all claims arising out of your use of the licensed material other than as specifically authorized pursuant to this license.

11. No Transfer of License: This license is personal to you and may not be sublicensed, assigned, or transferred by you to any other person without publisher's written permission.
12. No Amendment Except in Writing: This license may not be amended except in a writing signed by both parties (or, in the case of publisher, by CCC on publisher's behalf).
13. Objection to Contrary Terms: Publisher hereby objects to any terms contained in any purchase order, acknowledgment, check endorsement or other writing prepared by you, which terms are inconsistent with these terms and conditions or CCC's Billing and Payment terms and conditions. These terms and conditions, together with CCC's Billing and Payment terms and conditions (which are incorporated herein), comprise the entire agreement between you and publisher (and CCC) concerning this licensing transaction. In the event of any conflict between your obligations established by these terms and conditions and those established by CCC's Billing and Payment terms and conditions, these terms and conditions shall control.
14. Revocation: Elsevier or Copyright Clearance Center may deny the permissions described in this License at their sole discretion, for any reason or no reason, with a full refund payable to you. Notice of such denial will be made using the contact information provided by you. Failure to receive such notice will not alter or invalidate the denial. In no event will Elsevier or Copyright Clearance Center be responsible or liable for any costs, expenses or damage incurred by you as a result of a denial of your permission request, other than a refund of the amount(s) paid by you to Elsevier and/or Copyright Clearance Center for denied permissions.

LIMITED LICENSE

The following terms and conditions apply only to specific license types:
15. **Translation**: This permission is granted for non-exclusive world **English** rights only unless your license was granted for translation rights. If you licensed translation rights you may only translate this content into the languages you requested. A professional translator must perform all translations and reproduce the content word for word preserving the integrity of the article.
16. **Posting licensed content on any Website**: The following terms and conditions apply as follows: Licensing material from an Elsevier journal: All content posted to the web site must maintain the copyright information line on the bottom of each image; A hyper-text must be included to the Homepage of the journal from which you are licensing at http://www.sciencedirect.com/science/journal/xxxxx or the Elsevier homepage for books at http://www.elsevier.com; Central Storage: This license does not include permission for a scanned version of the material to be stored in a central repository such as that provided by Heron/XanEdu.
Licensing material from an Elsevier book: A hyper-text link must be included to the Elsevier homepage at http://www.elsevier.com . All content posted to the web site must maintain the copyright information line on the bottom of each image.

Posting licensed content on Electronic reserve: In addition to the above the following clauses are applicable: The web site must be password-protected and made available only to bona fide students registered on a relevant course. This permission is granted for 1 year only. You may obtain a new license for future website posting.
17. **For journal authors:** the following clauses are applicable in addition to the above:
Preprints:
A preprint is an author's own write-up of research results and analysis, it has not been peer-reviewed, nor has it had any other value added to it by a publisher (such as formatting, copyright, technical enhancement etc.).
Authors can share their preprints anywhere at any time. Preprints should not be added to or enhanced in any way in order to appear more like, or to substitute for, the final versions of articles however authors can update their preprints on arXiv or RePEc with their Accepted Author Manuscript (see below).

If accepted for publication, we encourage authors to link from the preprint to their formal publication via its DOI. Millions of researchers have access to the formal publications on ScienceDirect, and so links will help users to find, access, cite and use the best available version. Please note that Cell Press, The Lancet and some society-owned have different preprint policies. Information on these policies is available on the journal homepage.
Accepted Author Manuscripts: An accepted author manuscript is the manuscript of an article that has been accepted for publication and which typically includes author-incorporated changes suggested during submission, peer review and editor-author communications.
Authors can share their accepted author manuscript:

- immediately
  - via their non-commercial person homepage or blog
  - by updating a preprint in arXiv or RePEc with the accepted manuscript
  - via their research institute or institutional repository for internal institutional uses or as part of an invitation-only research collaboration work-group
  - directly by providing copies to their students or to research collaborators for their personal use
  - for private scholarly sharing as part of an invitation-only work group on commercial sites with which Elsevier has an agreement
- After the embargo period
  - via non-commercial hosting platforms such as their institutional repository
  - via commercial sites with which Elsevier has an agreement

In all cases accepted manuscripts should:

- link to the formal publication via its DOI
- bear a CC-BY-NC-ND license - this is easy to do
- if aggregated with other manuscripts, for example in a repository or other site, be shared in alignment with our hosting policy not be added to or enhanced in any way to appear more like, or to substitute for, the published journal article.

Published journal article (JPA): A published journal article (PJA) is the definitive final record of published research that appears or will appear in the journal and embodies all value-adding publishing activities including peer review co-ordination, copy-editing, formatting, (if relevant) pagination and online enrichment.
Policies for sharing publishing journal articles differ for subscription and gold open access articles:
Subscription Articles: If you are an author, please share a link to your article rather than the full-text. Millions of researchers have access to the formal publications on ScienceDirect, and so links will help your users to find, access, cite, and use the best available version.
Theses and dissertations which contain embedded PJAs as part of the formal submission can be posted publicly by the awarding institution with DOI links back to the formal publications on ScienceDirect.
If you are affiliated with a library that subscribes to ScienceDirect you have additional private sharing rights for others' research accessed under that agreement. This includes use for classroom teaching and internal training at the institution (including use in course packs and courseware programs), and inclusion of the article for grant funding purposes.
Gold Open Access Articles: May be shared according to the author-selected end-user license and should contain a CrossMark logo, the end user license, and a DOI link to the formal publication on ScienceDirect.
Please refer to Elsevier's posting policy for further information.
18. **For book authors** the following clauses are applicable in addition to the above:
Authors are permitted to place a brief summary of their work online only. You are not

allowed to download and post the published electronic version of your chapter, nor may you scan the printed edition to create an electronic version. **Posting to a repository:** Authors are permitted to post a summary of their chapter only in their institution's repository.
19. **Thesis/Dissertation**: If your license is for use in a thesis/dissertation your thesis may be submitted to your institution in either print or electronic form. Should your thesis be published commercially, please reapply for permission. These requirements include permission for the Library and Archives of Canada to supply single copies, on demand, of the complete thesis and include permission for Proquest/UMI to supply single copies, on demand, of the complete thesis. Should your thesis be published commercially, please reapply for permission. Theses and dissertations which contain embedded PJAs as part of the formal submission can be posted publicly by the awarding institution with DOI links back to the formal publications on ScienceDirect.

Elsevier Open Access Terms and Conditions

You can publish open access with Elsevier in hundreds of open access journals or in nearly 2000 established subscription journals that support open access publishing. Permitted third party re-use of these open access articles is defined by the author's choice of Creative Commons user license. See our open access license policy for more information.
Terms & Conditions applicable to all Open Access articles published with Elsevier:
Any reuse of the article must not represent the author as endorsing the adaptation of the article nor should the article be modified in such a way as to damage the author's honour or reputation. If any changes have been made, such changes must be clearly indicated.
The author(s) must be appropriately credited and we ask that you include the end user license and a DOI link to the formal publication on ScienceDirect.
If any part of the material to be used (for example, figures) has appeared in our publication with credit or acknowledgement to another source it is the responsibility of the user to ensure their reuse complies with the terms and conditions determined by the rights holder.
Additional Terms & Conditions applicable to each Creative Commons user license:
CC BY: The CC-BY license allows users to copy, to create extracts, abstracts and new works from the Article, to alter and revise the Article and to make commercial use of the Article (including reuse and/or resale of the Article by commercial entities), provided the user gives appropriate credit (with a link to the formal publication through the relevant DOI), provides a link to the license, indicates if changes were made and the licensor is not represented as endorsing the use made of the work. The full details of the license are available at http://creativecommons.org/licenses/by/4.0.
CC BY NC SA: The CC BY-NC-SA license allows users to copy, to create extracts, abstracts and new works from the Article, to alter and revise the Article, provided this is not done for commercial purposes, and that the user gives appropriate credit (with a link to the formal publication through the relevant DOI), provides a link to the license, indicates if changes were made and the licensor is not represented as endorsing the use made of the work. Further, any new works must be made available on the same conditions. The full details of the license are available at http://creativecommons.org/licenses/by-nc-sa/4.0.
CC BY NC ND: The CC BY-NC-ND license allows users to copy and distribute the Article, provided this is not done for commercial purposes and further does not permit distribution of the Article if it is changed or edited in any way, and provided the user gives appropriate credit (with a link to the formal publication through the relevant DOI), provides a link to the license, and that the licensor is not represented as endorsing the use made of the work. The full details of the license are available at http://creativecommons.org/licenses/by-nc-nd/4.0.
Any commercial reuse of Open Access articles published with a CC BY NC SA or CC BY NC ND license requires permission from Elsevier and will be subject to a fee.
Commercial reuse includes:

- Associating advertising with the full text of the Article
- Charging fees for document delivery or access

- Article aggregation
- Systematic distribution via e-mail lists or share buttons

Posting or linking by commercial companies for use by customers of those companies.

20. **Other Conditions**:

v1.9

Questions? customercare@copyright.com or +1-855-239-3415 (toll free in the US) or +1-978-646-2777.

Thesis/Dissertation Reuse Request

Taylor & Francis is pleased to offer reuses of its content for a thesis or dissertation free of charge contingent on resubmission of permission request if work is published.

BACK | CLOSE WINDOW

SPRINGER NATURE LICENSE TERMS AND CONDITIONS

Nov 23, 2018

This Agreement between Nazmul Huda ("You") and Springer Nature ("Springer Nature") consists of your license details and the terms and conditions provided by Springer Nature and Copyright Clearance Center.

License Number	4474911197390
License date	Nov 23, 2018
Licensed Content Publisher	Springer Nature
Licensed Content Publication	Metallurgical and Materials Transactions A
Licensed Content Title	Cleavage initiation in the intercritically reheated coarse-grained heat-affected zone: Part I. Fractographic evidence
Licensed Content Author	C. L. Davis, J. E. King
Licensed Content Date	Jan 1, 1994
Licensed Content Volume	25
Licensed Content Issue	3
Type of Use	Thesis/Dissertation
Requestor type	academic/university or research institute
Format	print and electronic
Portion	figures/tables/illustrations
Number of figures/tables/illustrations	1
Will you be translating?	no
Circulation/distribution	2,001 to 5,000
Author of this Springer Nature content	no
Title	Effect of Martensite-Austenite (MA) on Mechanical Properties of X80 Linepipe Steel
Institution name	n/a
Expected presentation date	Dec 2018
Portions	Figure 18
Requestor Location	Nazmul Huda 573 westvale drive waterloo, ON N2T1G5 Canada Attn: Nazmul Huda
Billing Type	Invoice
Billing Address	Nazmul Huda 573 westvale drive waterloo, ON N2T1G5

Canada
Attn: Nazmul Huda

Total 0.00 USD

Terms and Conditions

Springer Nature Terms and Conditions for RightsLink Permissions

Springer Nature Customer Service Centre GmbH (the Licensor) hereby grants you a non-exclusive, world-wide licence to reproduce the material and for the purpose and requirements specified in the attached copy of your order form, and for no other use, subject to the conditions below:

1. The Licensor warrants that it has, to the best of its knowledge, the rights to license reuse of this material. However, you should ensure that the material you are requesting is original to the Licensor and does not carry the copyright of another entity (as credited in the published version).

   If the credit line on any part of the material you have requested indicates that it was reprinted or adapted with permission from another source, then you should also seek permission from that source to reuse the material.

2. Where **print only** permission has been granted for a fee, separate permission must be obtained for any additional electronic re-use.

3. Permission granted **free of charge** for material in print is also usually granted for any electronic version of that work, provided that the material is incidental to your work as a whole and that the electronic version is essentially equivalent to, or substitutes for, the print version.

4. A licence for 'post on a website' is valid for 12 months from the licence date. This licence does not cover use of full text articles on websites.

5. Where **'reuse in a dissertation/thesis'** has been selected the following terms apply: Print rights of the final author's accepted manuscript (for clarity, NOT the published version) for up to 100 copies, electronic rights for use only on a personal website or institutional repository as defined by the Sherpa guideline (www.sherpa.ac.uk/romeo/).

6. Permission granted for books and journals is granted for the lifetime of the first edition and does not apply to second and subsequent editions (except where the first edition permission was granted free of charge or for signatories to the STM Permissions Guidelines http://www.stm-assoc.org/copyright-legal-affairs/permissions/permissions-guidelines/), and does not apply for editions in other languages unless additional translation rights have been granted separately in the licence.

7. Rights for additional components such as custom editions and derivatives require additional permission and may be subject to an additional fee. Please apply to Journalpermissions@springernature.com/bookpermissions@springernature.com for these rights.

8. The Licensor's permission must be acknowledged next to the licensed material in print. In electronic form, this acknowledgement must be visible at the same time as the figures/tables/illustrations or abstract, and must be hyperlinked to the journal/book's homepage. Our required acknowledgement format is in the Appendix below.

9. Use of the material for incidental promotional use, minor editing privileges (this does not include cropping, adapting, omitting material or any other changes that affect the meaning, intention or moral rights of the author) and copies for the disabled are permitted under this licence.

10. Minor adaptations of single figures (changes of format, colour and style) do not require the Licensor's approval. However, the adaptation should be credited as shown in Appendix below.

Appendix — Acknowledgements:

For Journal Content:
Reprinted by permission from [**the Licensor**]: [**Journal Publisher** (e.g. Nature/Springer/Palgrave)] [**JOURNAL NAME**] [**REFERENCE CITATION** (Article name, Author(s) Name), [**COPYRIGHT**] (year of publication)

For **Advance Online Publication papers:**
Reprinted by permission from [**the Licensor**]: [**Journal Publisher** (e.g. Nature/Springer/Palgrave)] [**JOURNAL NAME**] [**REFERENCE CITATION** (Article name, Author(s) Name), [**COPYRIGHT**] (year of publication), advance online publication, day month year (doi: 10.1038/sj.[JOURNAL ACRONYM].)

For Adaptations/Translations:
Adapted/Translated by permission from [**the Licensor**]: [**Journal Publisher** (e.g. Nature/Springer/Palgrave)] [**JOURNAL NAME**] [**REFERENCE CITATION** (Article name, Author(s) Name), [**COPYRIGHT**] (year of publication)

Note: For any republication from the British Journal of Cancer, the following credit line style applies:

Reprinted/adapted/translated by permission from [**the Licensor**]: on behalf of Cancer Research UK: : [**Journal Publisher** (e.g. Nature/Springer/Palgrave)] [**JOURNAL NAME**] [**REFERENCE CITATION** (Article name, Author(s) Name), [**COPYRIGHT]** (year of publication)

For **Advance Online Publication** papers:
Reprinted by permission from The [**the Licensor**]: on behalf of Cancer Research UK: [**Journal Publisher** (e.g. Nature/Springer/Palgrave)] [**JOURNAL NAME**] [**REFERENCE CITATION** (Article name, Author(s) Name), [**COPYRIGHT**] (year of publication), advance online publication, day month year (doi: 10.1038/sj.[JOURNAL ACRONYM])

For Book content:
Reprinted/adapted by permission from [**the Licensor**]: [**Book Publisher** (e.g. Palgrave Macmillan, Springer etc) [**Book Title**] by [**Book author**(s)] [**COPYRIGHT**] (year of publication)

Other Conditions:

Version 1.1

SPRINGER NATURE LICENSE TERMS AND CONDITIONS

Nov 23, 2018

This Agreement between Nazmul Huda ("You") and Springer Nature ("Springer Nature") consists of your license details and the terms and conditions provided by Springer Nature and Copyright Clearance Center.

License Number	4474911338696
License date	Nov 23, 2018
Licensed Content Publisher	Springer Nature
Licensed Content Publication	Metallurgical and Materials Transactions A
Licensed Content Title	Effects of Cooling Conditions on Tensile and Charpy Impact Properties of API X80 Linepipe Steels
Licensed Content Author	Seung Youb Han, Sang Yong Shin, Sunghak Lee et al
Licensed Content Date	Jan 1, 2009
Licensed Content Volume	41
Licensed Content Issue	2
Type of Use	Thesis/Dissertation
Requestor type	academic/university or research institute
Format	print and electronic
Portion	figures/tables/illustrations
Number of figures/tables/illustrations	1
Will you be translating?	no
Circulation/distribution	501 to 1000
Author of this Springer Nature content	no
Title	Effect of Martensite-Austenite (MA) on Mechanical Properties of X80 Linepipe Steel
Institution name	n/a
Expected presentation date	Dec 2018
Portions	Figure 14
Requestor Location	Nazmul Huda 573 westvale drive waterloo, ON N2T1G5 Canada Attn: Nazmul Huda
Billing Type	Invoice
Billing Address	Nazmul Huda 573 westvale drive waterloo, ON N2T1G5

Canada
Attn: Nazmul Huda

Total 0.00 USD

Terms and Conditions

Springer Nature Terms and Conditions for RightsLink Permissions

Springer Nature Customer Service Centre GmbH (the Licensor) hereby grants you a non-exclusive, world-wide licence to reproduce the material and for the purpose and requirements specified in the attached copy of your order form, and for no other use, subject to the conditions below:

1. The Licensor warrants that it has, to the best of its knowledge, the rights to license reuse of this material. However, you should ensure that the material you are requesting is original to the Licensor and does not carry the copyright of another entity (as credited in the published version).

   If the credit line on any part of the material you have requested indicates that it was reprinted or adapted with permission from another source, then you should also seek permission from that source to reuse the material.

2. Where **print only** permission has been granted for a fee, separate permission must be obtained for any additional electronic re-use.

3. Permission granted **free of charge** for material in print is also usually granted for any electronic version of that work, provided that the material is incidental to your work as a whole and that the electronic version is essentially equivalent to, or substitutes for, the print version.

4. A licence for 'post on a website' is valid for 12 months from the licence date. This licence does not cover use of full text articles on websites.

5. Where **'reuse in a dissertation/thesis'** has been selected the following terms apply: Print rights of the final author's accepted manuscript (for clarity, NOT the published version) for up to 100 copies, electronic rights for use only on a personal website or institutional repository as defined by the Sherpa guideline (www.sherpa.ac.uk/romeo/).

6. Permission granted for books and journals is granted for the lifetime of the first edition and does not apply to second and subsequent editions (except where the first edition permission was granted free of charge or for signatories to the STM Permissions Guidelines http://www.stm-assoc.org/copyright-legal-affairs/permissions/permissions-guidelines/), and does not apply for editions in other languages unless additional translation rights have been granted separately in the licence.

7. Rights for additional components such as custom editions and derivatives require additional permission and may be subject to an additional fee. Please apply to Journalpermissions@springernature.com/bookpermissions@springernature.com for these rights.

8. The Licensor's permission must be acknowledged next to the licensed material in print. In electronic form, this acknowledgement must be visible at the same time as the figures/tables/illustrations or abstract, and must be hyperlinked to the journal/book's homepage. Our required acknowledgement format is in the Appendix below.

9. Use of the material for incidental promotional use, minor editing privileges (this does not include cropping, adapting, omitting material or any other changes that affect the meaning, intention or moral rights of the author) and copies for the disabled are permitted under this licence.

10. Minor adaptations of single figures (changes of format, colour and style) do not require the Licensor's approval. However, the adaptation should be credited as shown in Appendix below.

Appendix — Acknowledgements:

For Journal Content:
Reprinted by permission from [**the Licensor**]: [**Journal Publisher** (e.g. Nature/Springer/Palgrave)] [**JOURNAL NAME**] [**REFERENCE CITATION** (Article name, Author(s) Name), [**COPYRIGHT**] (year of publication)

For **Advance Online Publication papers:**
Reprinted by permission from [**the Licensor**]: [**Journal Publisher** (e.g. Nature/Springer/Palgrave)] [**JOURNAL NAME**] [**REFERENCE CITATION** (Article name, Author(s) Name), [**COPYRIGHT**] (year of publication), advance online publication, day month year (doi: 10.1038/sj.[JOURNAL ACRONYM].)

For Adaptations/Translations:
Adapted/Translated by permission from [**the Licensor**]: [**Journal Publisher** (e.g. Nature/Springer/Palgrave)] [**JOURNAL NAME**] [**REFERENCE CITATION** (Article name, Author(s) Name), [**COPYRIGHT**] (year of publication)

Note: For any republication from the British Journal of Cancer, the following credit line style applies:

Reprinted/adapted/translated by permission from [**the Licensor**]: on behalf of Cancer Research UK: : [**Journal Publisher** (e.g. Nature/Springer/Palgrave)] [**JOURNAL NAME**] [**REFERENCE CITATION** (Article name, Author(s) Name), [**COPYRIGHT]** (year of publication)

For **Advance Online Publication** papers:
Reprinted by permission from The [**the Licensor**]: on behalf of Cancer Research UK: [**Journal Publisher** (e.g. Nature/Springer/Palgrave)] [**JOURNAL NAME**] [**REFERENCE CITATION** (Article name, Author(s) Name), [**COPYRIGHT**] (year of publication), advance online publication, day month year (doi: 10.1038/sj.[JOURNAL ACRONYM])

For Book content:
Reprinted/adapted by permission from [**the Licensor**]: [**Book Publisher** (e.g. Palgrave Macmillan, Springer etc) [**Book Title**] by [**Book author**(s)] [**COPYRIGHT**] (year of publication)

Other Conditions:

Version 1.1

Thesis/Dissertation Reuse Request

Taylor & Francis is pleased to offer reuses of its content for a thesis or dissertation free of charge contingent on resubmission of permission request if work is published.

BACK | CLOSE WINDOW